
University of Glasgow

# Modulating the Local Innate Immune Response in the Central Nervous System to Protect Against Progressive Multifocal Leukoencephalopathy

**Alistair James Gamble**

BSc (Hons); MSc (Res)

Submitted in fulfilment of the requirements for the degree of Doctor of Philosophy

School of Infection and Immunity

College of Medical, Veterinary, and Life Sciences

University of Glasgow

**January 2024**

# Abstract

Multiple sclerosis (MS) is a chronic disease of the central nervous system (CNS) characterised by inflammation and demyelination. As a leading cause of disability in adults, several disease modifying therapies are now available. Many of these work by suppressing the immune system which, while effective, can leave people with MS susceptible to opportunistic infections. One of the most severe of these is progressive multifocal leukoencephalopathy (PML), a rare but often fatal infection of oligodendrocytes by Human Polyomavirus 2, more commonly known as John Cunningham virus. There currently are no antivirals or vaccines for PML, therefore the only treatment option involves stopping immunosuppressive treatments, leaving patients at risk of further MS-related inflammatory events. As a result, there is a need to develop antivirals that work in conjunction with immunosuppressive treatments.

A subset of MS patients synthesise intrathecal lipid-reactive IgM, the presence of which has been associated with a reduced incidence of PML. This is compatible with our lab's recent observation that the murine lipid-reactive IgM antibody clone O4, when added to murine myelinating cell cultures, induces the expression of interferon beta (IFN-β). As IFN-β is produced in response to viral infection, these data could explain why individuals with lipid-reactive IgM seem protected from PML.

These findings prompted our investigation into the effect of IFN-β treatment on the major cell types of the CNS; the oligodendrocytes, microglia, neurons, and astrocytes. Using murine CNS cell cultures, we utilised fluorescence activated cell sorting (FACS) to separate out the individual cell types of the CNS for RNAseq analysis. This way we characterised the unique transcriptional profile of each individual cell-type following IFN-β treatment. Importantly, several oligodendrocyte-unique genes were upregulated including *Il10ra*, the gene encoding IL-10R. It was deduced through RT-qPCR, plaque assays, and fluorescence microscopy that treatment with IFN-β or blocking IL-10R was able to decrease infectivity of a model neurotropic virus both *in vitro* and *in vivo*.

The data presented in this thesis provides evidence of innate antiviral activity of oligodendrocytes which can be manipulated pharmacologically to protect against viral infection. This research will aid in the development of future therapeutics to decrease the

infectivity of JCV in the CNS. This would allow MS patients to remain on their effective therapeutics without being at increased risk. Further investigation of the IFN-β response of the CNS could lead to the development of an antiviral therapy that can be used as a co-treatment in MS or as a broad-spectrum antiviral for viral encephalitis.

# Table of Contents

# List of Tables

# List of Figures:

# Acknowledgments

First and foremost, I would like to thank my two invaluable supervisors who have guided me through to the completion of this PhD. Dr Marieke Pingen, the hostess with the mostess, the killer of the patriarchy, and the god of viruses and statistics, thank you for sticking by me through thick and thin and making most of this possible. Prof. Julia Edgar, the god of neuroscience and multiple sclerosis studies, thank you for being there with a bit of level-headedness, especially when my ideas started to get a bit out of control or weren't written down particularly well (even if I had to clutch those pearls on many an occasion!). Thanks to you both I am a much better scientist, researcher, and person. The PhD would have likely been much shorter without both of you.

Secondly, I would like to thank all the other people who have had a guiding hand in helping me get to where I am now. To my funders the MS Society, and by extension the Lorna and Yuti Chernajovsky Foundation go my undying gratitude. Not only did you fund my PhD and allow me to pursue a career in what I enjoy, you gave me multiple opportunities to further advance my scientific abilities with presentation and networking opportunities. Prof. Chris Linington, thank you for being there with some big ideas on my research, and having an accompanying wine recommendation to mellow the pain. Diane Vaughan, Alana Hamilton, and the flow core facility for assisting with those gruelling 6 months of cell sorting, thanks for always being there and having some good chat to boot. To all the wonderful people at the CRF and WRF, thank you for your assistance with matings and making dissection days a bit better by not judging the Disney music blasting from the rooms.

Clearly massive thanks have to go to both Janice and Malcolm Gamble, or as I call them "mum" and "dad". Look at me now, bare minimum Alistair has submitted a PhD. Thank you for keeping on at me to not just quit when the going gets tough, and for being a sympathetic ear when I needed to rant about absolutely anything – this definitely helped with keeping me sane during PhD turmoil.

To everyone else who had a helping hand in this journey, a special thank you it all so fantastic with all the assistance – be that with experiments or emotional support. Thank you, Lina, for being a wee ray of sunshine, even if your face didn't show it a lot of the time aha. Becky, you were right, my fingers really didn't survive to the end, we truly did trauma bond through this hellish thing. Lily, bin rat, piss factory, you're going to need someone else to gaslight, gatekeep, girlboss you a bit ;). Ben, for having to suffer many a PhD related rant about people you have never met, being there with a bottle of wine (or a few more), some crappy hallmarks to kind words to calm me down. Campbell, the geriatric at (currently) 7290 years old, for being a constant source of joy, absolutely insane one liners, and general hilarity. Peter, yes I gave you your full name, for always bringing a smile with some verbose remark and some class chat over Indian food, maybe a Ting Thai. Ron, our favourite ~edgy~ man, for being there for a chill night in Catty, some pints that always turns into more, and reassuring words. Finally, Haley, H-Dawg for short, we've came quite far haven't we. COVID Masters' in that flat, to now trans-continental PhDs, look at us now. Thanks for being there for far too many wines, at least five (5) full watches of the twilight saga, and just general insanity when we're trapped in a room together. Honestly couldn't have done this all without you.

# Authors Declaration

I declare that, except where referenced to others, this thesis is the product of my own work and has not been submitted for any other degree at the University of Glasgow or any other institution.

Signature:

Printed name: ALISTAIR JAMES GAMBLE

# List of Abbreviations

| Abbreviation | Full Name |
|---|---|
| 5-HT2R | 5-hydroxytryptamine 2 receptor |
| ACSA | Astrocyte cell specific antigen |
| AIM | Apoptosis inhibitor of macrophages |
| ANOVA | Analysis of variance |
| AP | Action potential |
| APC | Antigen presenting cells |
| ATP | Adenosine triphosphate |
| BBB | Blood brain barrier |
| BHK | Baby hamster kidney cells |
| BLAST | Basic Local Alignment Search Tool |
| bp | Base pair |
| BSA | Bovine serum albumin |
| Cb | Cerebellum |
| CCL | C-C ligand |
| CCR | C-C motif receptor |
| CD | Cluster differentiation |
| cDNA | Complementary deoxyribose nucleic acid |
| cGAS | Cyclic GMP-AMP synthase |
| CIS | Clinically isolated syndrome |
| CM | Culture medium |
| CNS | Central nervous system |
| CO | Carbon monoxide |
| Co | Cortex |
| CTLA | Cytotoxic T-lymphocyte associated protein |
| CT | Copy number at threshold |
| CXCL | C-X-C motif ligand |
| CXCR | C-X-C motif receptor |
| DAI | DNA-dependent activator of IFN regulatory factors |
| DAMP | Danger associated molecular pattern |
| DAPI | 4',6-diamidino-2-phenylindole |
| DC | Dendritic cells |
| DEG | Differentially expressed gene |
| DIV | Day in vitro |
| DM | Differentiation medium |
| DMEM | Dulbeccos modified eagle medium |
| DMSO | Dimethyl sulfoxide |
| DMT | Disease modifying therapy |
| DNA | Deoxyribose nucleic acid |
| dPBS | Dulbeccos phosphate buffered saline |
| dsDNA | Double stranded DNA |
| | ***Continued overleaf*** |

| | |
|---|---|
| E# | Embryonic day |
| $EC_{50}$ | Half maximal effective concentration |
| EDTA | Ethylenediaminetetraacetic acid |
| eGFP | Enhanced green fluorescent protein |
| ELISA | Enzyme linked immunosorbent assay |
| FACS | Fluorescence activated/assisted cell sorting |
| FCS | Foetal calf serum |
| FMO | Fluorescence minus one |
| FSC-A | Forward scatter area |
| FSC-H | Forward scatterr height |
| GA | Glatiramer acetate |
| GFAP | Glial fibrillary acid protein |
| GM-CSF | Granulocyte-macrophage colony-stimulating factor |
| GMEM | Glasgow modified eagle medium |
| GMEMcult | GMEM culture medium for BMDMs |
| GO | Gene ontology |
| HBSS | Hanks' balanced salt solution |
| HIV | Human immunodeficiency virus |
| HLA | Human leukocyte antigen |
| HSC | Hematopoeitic stem cells |
| HSV | Herpes simplex virus |
| Iba1 | Ionised calcium binding adapter molecule 1 |
| IFN-α | Interferon alpha |
| IFN-β | Interferon beta |
| IFN-γ | Interferon gamma |
| IFN-κ | Interferon kappa |
| IFN-λ | Interferon lambda |
| IFN-ω | Interferon omega |
| IFN-τ | Interferon tau |
| IgA | Immunoglobulin A |
| IGFBP | Insulin like growth factor binding protein |
| IgG | Immunoglobulin G |
| IgM | Immunoglobulin M |
| IKK | IkB Kinase |
| IL | Interleukin |
| IN | Intranasal |
| IP | Intraperitoneal |
| iPSC | Induced pluripotent stem cell |
| IRF | IFN regulator factors |
| IRIS | Immune reconstitution inflammation syndrome |
| ISG | Interferon stimulated gene |
| ISGF3 | IFN-stimulated gene factor 3 |
| ISRE | Interferon stimulated response elements |
| | ***Continued overleaf*** |

| | |
|---|---|
| JAK | Janus kinase |
| JCV | John Cunningham Virus |
| KEGG | Kyoto encyclopaedia of genes and genomes |
| L-15 | Leibovitz's L-15 medium |
| LAL | Limulus amebocyte lysate |
| LCMV | Lymphocytic choriomeningitis virus |
| LPS | Lipopolysaccharide |
| LTSc | Lactoseries tetrasaccharide C |
| M-CSF | Macrophage colony stimulating factor |
| mAb | Monoclonal antibody |
| MAP2 | Microtubule associated glycoprotein 2 |
| MBP | Myelin basic protein |
| MCMV | Mouse cytomegalovirus |
| MEM | Modified eagle medium |
| MHC-I | Major histocombatibility complex, type I |
| MHC-II | Major histocombatibility complex, type II |
| MOI | Multiplicity of infection |
| mRNA | Messenger RNA |
| MS | Multiple sclerosis |
| Mx1 | MX dynamin-like GTPase 1 |
| NCCR | Non-coding control region |
| NeuN | Neuronal specific nuclear protein |
| NFkB | Nuclear factor kappa-light-chain enhancer of activated B cells |
| NG2 | Neuro / glial antigen 2 |
| NK | Natural killer |
| NO | Nitrous oxide |
| NPC | Neural progenitor cell |
| NT | Neurotransmitter |
| O4 | Mouse anti-sulfatide IgM clone O4 |
| OAS | Oligoadenylate synthase |
| OB | Olfactory bulb |
| OPC | Oligodendrocyte progenitor cell |
| PAMP | Pathogen associated molecular pattenr |
| PCR | Polymerase chain reaction |
| PE | Phycoerythrin |
| PFA | Paraformaldehyde |
| PFU | Plaque forming units |
| pHrodo | pH Rhodamine |
| PLL | Poly-L-lysine |
| PML | Progressive multifocal leukoencephalopathy |
| Poly(I:C) | Polyinosinic:polycytidylic acid |
| PPMS | Primary progressive multiple sclerosis |
| | ***Continued overleaf*** |

| | |
|---|---|
| PRR | Pattern recognition receptors |
| RABV | Rabies virus |
| rhIgM22 | Recombinant human IgM antibody 22 |
| RIG-I | Retinoic acid-inducible gene I |
| RIS | Radiologically isolated syndrome |
| RNA | Ribonucleic acid |
| RNAseq | RNA sequencing |
| rpm | Rotations per minute |
| RRMS | Relapsing remitting multiple sclerosis |
| Rsad2 | Radical S-adenosyl methionine domain-containing protein 2 |
| RT | Room temperature |
| RT-qPCR | Reverse transcription quantitative polymerase chain reaction |
| S1P | Sphingosine-1-phosphate |
| SDS-PAGE | Sodium dodecyl sulphate polyacrylamide gel electrophoresis |
| SFV | Semliki forest virus |
| siRNA | Small interfering RNA |
| SMI31 | Neurofilament H, Clone SMI-31 |
| SPMS | Secondary progressive multiple sclerosis |
| SSC-A | Side scatter area |
| SSC-H | Side scatter height |
| ssRNA | Single stranded RNA |
| STAT | Signal transducer and activator of transcription |
| STING | Stimulator of interferon genes |
| T-150 | 150cm^2 tissue culture flask |
| T-75 | 75cm^2 tissue culture flask |
| TAE | Tris-acetate EDTA buffer |
| TANK | TRAF family member associated NF-kB activator |
| TBK | TANK-binding kinase |
| TCR | T cell receptor |
| Th | T helper cell |
| TLR | Toll like receptor |
| TMEV | Theiler's murine encephalomelitis virus |
| TNF-a | Tumor necrosis factor alpha |
| TRAF | Tumor necrosis factor receptor-associated factor |
| Treg | Regulatory T cells |
| TYK | Tyrosine kinase |
| VSV | Vesicular stomatitis virus |
| WT | Wild type |
| ZsGreen | Zoanthus derived green fluorescent protein |

# Chapter 1

## Introduction

# 1.0 Introduction

## 1.1 Central nervous system

### 1.1.1 General overview

The central nervous system (CNS) is the connected tissue that is responsible for receiving, processing, and responding to information from the environment and our own bodies. The CNS consists of the brain, spinal cord, and optic nerve (Payne *et al.*, 2018). The brain is primarily involved in responses, movement, sensation, emotions, thought processing, communication, and memory (Ackerman, 1992). Comparatively, the spinal cord is primarily involved in sending motor commands to the brain and controlling rhythmic motion such as walking or breathing (McDonald, Belegu and Becker, 2013). The CNS consists of a plethora of cells, with the major cell types being microglia, oligodendrocytes, astrocytes, and neurons (Kovacs, 2018). These cells form an extremely complex and fragile environment and even small amounts of force or changes in the homeostasis of the constituent cells can result in wide ranging effects and issues (Upadhyay, 2014).

### 1.1.2 Oligodendrocytes

Oligodendrocytes are the myelinating cells of the CNS. Originally differentiating from neural precursor cells into oligodendrocyte precursor cells (OPCs) (Mathews and Appel, 2016). Mature oligodendrocytes differentiate from oligodendrocyte precursor cells (OPCs) in three distinct waves in different regions of the brain. The first in the forebrain, the second in the dorsal ventricular zone, and a third postnatal wave in the cortex (van Tilborg *et al.*, 2018; Nishiyama *et al.*, 2021). These waves produce an overabundance of cells that compete for limited space and resources. Almost all the first wave OPCs mostly die off and are replaced by second wave OPCs, however a small number survive and have key roles in synaptic connectivity and cell interactions (Orduz *et al.*, 2019). These OPCs differentiate into oligodendrocytes depending on distinct cues, such as neuronal electrical activity (Wheeler and Fuss, 2016).

The processes of the oligodendrocytes wrap around the axons multiple times forming a tight spiral of myelin (Edgar *et al.*, 2021; Osanai *et al.*, 2022). The tight, compact layers of

the myelin act as insulator, and increase the speed of the action potentials (APs), the electrical signal of neurons, down the axon. The mature oligodendrocyte will wrap uniform ~1mm long sections of axon leaving small ~1µm gaps called nodes of Ranvier (Simons and Nave, 2016; Villalón *et al.*, 2018). Through these gaps sodium ions can flow into the axon allowing action potential propagation (Rasband and Peles, 2021). Since myelin insulates, the AP "jumps" between the nodes of Ranvier, and this rapidly increases the rate of propagation along the axon (Seidl, 2014).

Deficiencies in myelination can result in both neurological and neuropsychological disorders. Myelination requires the proliferation and maturation of OPCs into mature oligodendrocytes. However, in response to a pro-inflammatory environment, such as that caused by injury or viral infection, oligodendrocytes are known to upregulate chemokines and cytokines which can block this maturation and result in demyelination (Kirby and Castelo-Branco, 2021). In the context of mouse hepatitis virus infections of the CNS, oligodendrocytes upregulate expression of major histocompatibility complex I, interferon stimulated genes, and have increased antigen presentation (Pan *et al.*, 2020). It is proposed this is through the activity of the type-II interferon, interferon gamma (IFN-γ) (Turnley, Miller and Bartlett, 1991). However, IFN-γ has been noted to both result in oligodendrocyte cell death as well as decreased maturation and differentiation. Increased expression of MHC-I has been linked with apoptosis through increasing endoplasmic reticulum (ER) stress as the overexpression of these proteins accumulate in the ER, ultimately reducing the proportion of myelination in the developing CNS (Turnley, Miller and Bartlett, 1991; Power, Kong and Trapp, 1996; Horiuchi *et al.*, 2006, 2011; Boccazzi *et al.*, 2021). Additionally, OPCs can express CCL2 and interleukin 1-b, both potent modulaters of the peripheral immune system (Moyon *et al.*, 2015). CCL2 can recruit monocytes to the site of injury which can result in increased damage caused to the central nervous system (Mildner *et al.*, 2009).

### 1.1.3 Neurons

Neurons are the central cell of the CNS which are electrically excitable and transfer information between and within the CNS, peripheral nervous system, and tissues and organs of the body (Sidiropoulou, Pissadaki and Poirazi, 2006). The neuron is classically composed of the cell body (soma), dendrites, axon, and the synapses (Goaillard *et al.*,

2020). The axons can range from ~1mm to ~1m long and can be wrapped in an insulating myelin layer. Neurons generate and propagate electrical signals known as action potentials down axons, and release neurotransmitters (NT) at the axon termini to communicate with other neurons (Kress and Mennerick, 2009).

In the formation of an action potential the dendrites detect NTs from other neurons through the respective neurotransmitter receptor (Kress and Mennerick, 2009). Once the NT binds to its receptor, the neuron opens ion channels resulting in a rapid change in ion concentration on either side of the membrane (Smart and Paoletti, 2012). Neurons can be either excitatory or inhibitory, meaning they either stimulate or inhibit the next neuron. For the neuron to transmit the information to the next cell, there must be an influx of positive ions (for example sodium, Na) into the cell. This moves the membrane potential of the neuron, which rests at approximately -70mV (Kadir, Stacey and Barrett-Jolley, 2018), towards the threshold potential ~-55mV (Azouz and Gray, 1999; Yu, Shu and McCormick, 2008). If enough ions enter the neuron the cell to cross the threshold potential the neuron will open additional sodium channels and “fire” an action potential (AP), a rapid depolarisation towards +30mV (Kress and Mennerick, 2009). This signal propagates from the cell body and down the axon opening more sodium channels as it passes subsequent nodes of Ranvier until it reaches the presynapse. Here, the electrical signal results in the secretion of NTs into the synaptic gap where they can bind to the subsequent neuron and repeat the process (Rusakov *et al.*, 2011).

### 1.1.4 Astrocytes

Astrocytes are the most abundant of the non-neuronal cells in the CNS (Miller, 2018) Astrocytes can be classed into two distinct morphological subtypes, protoplasmic in the grey matter, and fibrous in the white matter (Batiuk et al., 2020). Differentiating from neural precursor cells, astrocytes originally derive from the subventricular zone and migrate along radial glia processes to populate the whole CNS (Gengatharan, Bammann and Saghatelyan, 2016). Astrocytes contribute to the blood brain barrier (BBB) by forming a thin barrier around endothelial cells of the vascular system separating the CNS from the blood circulation (Abbott, Rönnbäck and Hansson, 2006).

Mature astrocytes have many distinct roles in maintaining CNS homeostasis, including, neurotransmitter recycling (Weber and Barros, 2015), modulating synaptic transmission and synaptogenesis (Ota, Zanetti and Hallock, 2013), and, as mentioned, maintenance of the blood brain barrier (BBB) (Cabezas *et al.*, 2014). Passage of molecules across the BBB is controlled by multiple cell types, including astrocytes. Interestingly, approximately 97% of all astrocytes have contact with the blood supply, signifying the importance of these cells to maintaining homeostasis of the CNS (Abbott, 2002; C. Y. Liu *et al.*, 2018).

While astrocytes are essential to maintaining homeostasis in the CNS, they also assist with inflammation (Colombo and Farina, 2016; Giovannoni and Quintana, 2020). CNS inflammation or injury is increasingly associated with astrogliosis, a cellular response to injury and disease characterised by morphological, molecular, and functional remodelling(Sofroniew, 2015). Reactive astrocytes express pattern recognition receptors (PRRs) and cytokine receptors. As a result, astrocytes can respond to both pro- and anti-inflammatory cues implying a strong role in the innate immune response of the CNS (Kigerl *et al.*, 2014; Li *et al.*, 2021; Szpakowski *et al.*, 2022). Similarly, reactive astrocytes release a broad spectrum of pro-inflammatory molecules that promote the migration of infiltrating immune cells into the CNS environment (Linnerbauer, Wheeler and Quintana, 2020).

### 1.1.5 Microglia

Microglia are the resident macrophages of the CNS and are essential to maintaining the homeostatic environment and responding to any damage caused from both physical stress and invading pathogens (Thompson and Tsirka, 2017). Whilst the other key CNS cell types arise from the neural tube, microglia are derived from the yolk sac (Ginhoux and Prinz, 2015). Microglia represent approximately 20% of all glial cells, however, can rapidly proliferate in response to infection, injury, or toxic proteins (Lawson *et al.*, 1990; Gómez-Nicola *et al.*, 2013). Microglia have been implicated to have critical roles in neurogenesis in the developing brain, both promoting and inhibiting cell death (Gemma and Bachstetter, 2013). When microglia are removed from the embryonic CNS wide ranges of issues arise such as retinal dysfunction (Li, Jiang and Samuel, 2019), neuronal apoptosis (Dixon *et al.*, 2021), impaired oligodendrocyte maturation (McNamara *et al.*, 2023), and eventually severe motor dysfunction and death (Pereira *et al.*, 2023), showing microglia are essential to the establishment of the homeostatic CNS.

In the healthy CNS, microglia are constantly surveying the local environment by reorganising their processes to check for injury or infection, and have also been linked to modulating neuronal activity, pruning synapses amongst other roles (Shih and Dulla, 2018; Geloso and D'ambrosi, 2021). The processes have been shown to respond to neurotransmitters such as glutamate (Liu, Leak and Hu, 2016), danger-associated molecular patterns (DAMPs) such as adenosine triphosphate (ATP) (Lin *et al.*, 2022), pathogen associated molecular patterns (PAMPs) such as lipopolysaccharide (LPS) and viral genetic material (Lively and Schlichter, 2018; Chhatbar and Prinz, 2021), and chemokines and cytokines (Shields, Haque and Banik, 2020).

Microglia are classically known for their roles in responding to inflammation, damage, and combatting infection in the CNS. As mentioned, microglia can respond to varied stimuli, for example chemokines and cytokines released by other cells, in response to inflammation which alters the gene expression towards a more "activated" phenotype (Lively and Schlichter, 2018; Shields, Haque and Banik, 2020; Woodburn, Bollinger and Wohleb, 2021). During viral infections these activated microglia are critical for clearing viral load and preventing disease progression. This neuroprotection is mediated through phagocytosis of viral debris and damaged cells and the release of proinflammatory cytokines such as CXCL10, CCL2, CCL, and IL-6 (Chhatbar and Prinz, 2021). These proinflammatory cytokines lead to infiltration of the CNS by macrophages to help clear any infection, however these can contribute to neurotoxicity and neurodegeneration through non-specific damage (Wang *et al.*, 2015; Shields, Haque and Banik, 2020).

### 1.1.6 Invading immune cells

The CNS, sometimes controversially, is considered an immune privileged site. However, the immune cells of the peripheral system can infiltrate the BBB and mediate inflammation in the CNS. The breakdown of the BBB is critical to the pathogenesis of many diseases in the CNS, both infectious and autoimmune (Yang and Rosenberg, 2011; Spindler and Hsu, 2012; Galea, 2021; Patabendige and Janigro, 2023). For example, the presence of $CD8^+$ T-cells ad B cells in the CNS are found in MS (van Langelaar *et al.*, 2020). The immune system can be split into three functionally distinct systems, cell intrinsic, innate and adaptive immunity.

The cell intrinsic response will be discussed later in this introduction. Innate immune system forms the first line of defence against invading pathogens and initiates the inflammatory response (Newton and Dixit, 2012; Hato and Dagher, 2015). Meanwhile, the adaptive immune system is the second line of defence that forms antibodies and orchestrates chemokines and cytokines to protect the host (Alberts *et al.*, 2002; Chaplin, 2010). While having a role in neurogenesis and spatial learning (Ziv *et al.*, 2006), the adaptive and innate immune systems are more classically linked with the immune response to injury. Both adaptive and innate immune cells are found to infiltrate the CNS under inflammatory conditions with substantial populations of macrophages, monocytes, T cells, and B cells found (Nevalainen, Autio and Hurme, 2022).

### 1.1.7 Innate immune cells

The innate immune system is the first line of defence. Here, the cells initiate the immune response by rapidly acting upon infection or tissue damage (Hato and Dagher, 2015). The cells of the innate immune system can create physical barriers (Marshall *et al.*, 2018), chemical barriers such as low pH (Kalló *et al.*, 2022), release pro-inflammatory compounds such as cytokines (Lacy and Stow, 2011), and also actively phagocytose pathogens and debris to eliminate the damage immediately (Lim, Grinstein and Roth, 2017). These multiple different functions are orchestrated by many different cell types. Here a small introduction to the main cell types of the innate immune system.

#### *1.1.7.1 Neutrophils*

Neutrophils are the most abundant immune cell type found in the periphery (Rosales, 2018). After differentiation and maturation in the bone marrow, neutrophils migrate into the blood where they primarily phagocytose small invading pathogens (Lee, Harrison and Grinstein, 2003). Since they are primarily involved in actively eliminating the source of infection, they are the first cell type recruited to the site of infection and help drive the inflammation response (Kim and Luster, 2015; Fine *et al.*, 2020). Neutrophils also orchestrate the subsequent immune response through secreting several cytokines and inflammatory factors to recruit additional immune cells to the site of infection (Nauseef and Borregaard, 2014; Scapini and Cassatella, 2014; Tecchio and Cassatella, 2016).

During tissue damage, such as that caused by viral infections, damage associated molecular patterns (DAMPs) are released, for example extracellular DNA (Pittman and Kubes, 2013; Broggi and Granucci, 2015). These are likely to be the first signals neutrophils recognise (Cordeiro and Jacinto, 2013) through a variety of pattern recognition receptors (PRRs), such as toll-like receptors (TLRs)(Broggi and Granucci, 2015). Additionally, the expression of chemokines for example the C-X-C motif ligand CXCL1 and CXCL2, are linked with neutrophil recruitment (Russo *et al.*, 2014). The expression of DAMPs and CXCL1/2 create a gradient of signals that neutrophils recognise to recruit them to the site of injury to mediate their protective effect.

#### *1.1.7.2 Monocytes*

Monocytes are innate immune cells that are capable of phagocytosis. They are distributed throughout the body and are linked with clearing debris, phagocytosing pathogens, and antigen presentation to T cells (Steigbigel, Lambert and Remington, 1974; Pugliese *et al.*, 2005; Chiu and Bharat, 2016; Austermann, Roth and Barczyk-Kahlert, 2022). Monocytes differentiate in the bone marrow in the presence of macrophage colony-stimulating factor (M-CSF) (Aronson, 2016). Monocytes go through additional differentiation once they infiltrate a tissue, for example the CNS. When exposed to interleukin 4 and GM-CSF monocytes differentiate into macrophages, or when exposed to IL-6 and M-CSF monocytes differentiate into dendritic cells. (DCs) (Sallusto and Lanzavecchia, 1994; Zhou, Tedder and Amos, 1996; Chomarat *et al.*, 2000; Boulakirba *et al.*, 2018). Classical, or patrolling monocytes scan for signs of inflammation or infection, and activate when an inflammatory response is detected, such as the presence of amyloid beta in the brains of people with Alzheimer's disease (Koronyo-Hamaoui *et al.*, 2009; Kapellos *et al.*, 2019).

In relation to the brain, there is increased infiltration of monocytes following brain-derived inflammatory cues. Once across the BBB, monocytes differentiate into activated macrophages which produce a variety of pro-inflammatory molecules, such as interleukin-1b and tumour necrosis factor alpha (TNF-a) (Garré and Yang, 2018). It is interesting to note that once monocytes differentiate in the brain they are morphologically indistinguishable from microglia, but are more phagocytic (Jung and Schwartz, 2012).

*1.1.7.3 Natural killer cells*

Natural killer (NK) cells recognise and kill cells that have been infected or are mutated such as cancer cells (Björkström, Strunz and Ljunggren, 2022; Chan and Ewald, 2022). The exact site where NK cells differentiate is currently open to speculation, however it is known that NK cells differentiate from hematopoietic stem cells (HSCs) (Godin and Cumano, 2002; Colucci, Caligiuri and Di Santo, 2003). To differentiate between healthy cells and cells in distress, the cell recognises stress-induced ligands such as NKG2D and toll like receptor (TLR) ligands (Wensveen, Jelenčić and Polić, 2018; Noh *et al.*, 2020). These ligands can activate NK cells and induce expression of interferon gamma (Mah and Cooper, 2016). It is also thought that the cells can recognise the absence of certain cell receptors, such as the constitutively expressed MHC I receptor (Kumar and McNerney, 2005). In relation to viruses, NK cells have been linked to actively controlling the course of infection. Deficiencies in the NK cell population have been linked with increased infectivity of certain viruses such as mouse cytomegalovirus (MCMV) (Mitrović *et al.*, 2012). NK cells can actively interact with the virus itself, such as receptors recognising viral surface molecules (Van Erp *et al.*, 2019; Björkström, Strunz and Ljunggren, 2022). Following exposure to IL-12 and IFN-γ expressed by DCs, the cells actively proliferate and follow a cytokine gradient towards the site of infection (Shemesh *et al.*, 2022).

*1.1.7.4 Dendritic cells are on the interface of innate and adaptive immune system*

Dendritic cells are a class of antigen presenting cells (APCs) (Yao, Platell and Hall, 2002). These cells present degraded cellular debris from invading pathogens to cells of the adaptive immune system to help drive that response (Théry and Amigorena, 2001). Dendritic cells (DCs) identify pattern associated molecular patterns (PAMPs) or DAMPs) which drive their maturation and activation (Iwasaki and Medzhitov, 2004; Martin, Henry and Cullen, 2012). Activated DCs then promote the differentiation of effector T cells, which in turn control the response of regulatory T cells (Tang *et al.*, 2020). These cells express major histocompatibility complex (MHC) II, which are important proteins for antigen presentation to CD8+ T cells (ten Broeke, Wubbolts and Stoorvogel, 2013), but also have been known to express pro-inflammatory cytokines such as IL-12 and IFN-γ (Heufler *et al.*, 1996; Pan *et al.*, 2004). DCs also are known to express type-I IFNs in response to infection (Hornung *et al.*, 2004; Wang, Peters and Schwarze, 2006). The role of type-I IFNs is discussed later in this introduction.

### 1.1.8 Adaptive immune system

The adaptive immune system is defined by specificity and memory (Marshall *et al.*, 2018). Here, the cells are collectively referred to as lymphocytes and can be split into two distinctive types – T cells which orchestrate the cytokine and chemokine response (Bromley, Mempel and Luster, 2008; Kenway-Lynch *et al.*, 2014; Eberlein *et al.*, 2020), and B cells which produce antibodies against the pathogens (Häusser-Kinzel and Weber, 2019). The adaptive immune system allows the immune system to form immunological memory, where the antibodies produced by B cells and memory T cells remain following infection and if the same pathogen is encountered a stronger, more rapid, immune response is mounted (Ratajczak *et al.*, 2018; Palm and Henry, 2019; Barnaba, 2022).

#### *1.1.8.1 T cells*

T cells are produced in the bone marrow and mature in the thymus (Thapa and Farber, 2019). To ensure self-reactive T cells do not cause pathology, the cells undergo autoreactive elimination where self-reactive cells undergo apoptosis (Boehncke and Brembilla, 2019). The presence of certain cytokines secreted by cells in the innate immune system determine the cell fate during differentiation, such as CD4+ T helper Th1 cells differentiating in the presence of DC derived IL-12 (Yoo *et al.*, 2002). T cells can be broken down into two distinctive classes, effector T cells which eliminate pathogens (Sun *et al.*, 2023), and memory T cells which help the immune system retain a memory of previous infections (Barnaba, 2022). A subset of CD4+ T cells, Th1 cells, secrete IFN-γ which activates macrophages to kill intracellular microbes (Sallusto, 2016). Another subset, Th17, secrete IL-17A and IL-21, which macrophages and endothelial cells to produce cytokines to recruit neutrophils (Kolls and Lindé, 2004; Korn *et al.*, 2009; Pelletier *et al.*, 2010). Both Th1 and Th17 have been particularly implicated in the development of the neurological disease multiple sclerosis, discussed in **1.2**.

To activate, T cells need to interact with a peptide or MHC protein bound to the T cell receptor (TCR), react with co-stimulatory molecule, and be exposed to cytokines released from APCs (Frauwirth and Thompson, 2002; Courtney, Lo and Weiss, 2018; Dong, 2021). Antigen presenting cells, such as DCs, phagocytose debris or pathogens and present these to T cells using MHC-I or MHC-II molecules (Nussenzweig *et al*. 1980; Zinkernagel and Doherty 1975; Steinman *et al.* 1979). The APCs identify and process these proteins in either

the periphery or CNS before migrating into lymphoid tissue through following chemokine and cytokine gradients (Steinman *et al*. 1979; Szakal, Holmes, and Tew 1983; Cumberbatch and Kimber 1992; Morikawa *et al.* 1995) . In the lymphoid tissue, the APCs interact with CD4+ and CD8+ T cells to facilitate their activation. CD4+ T cells are activated following binding with antigen presented on MHC class II, while CD8+ T cells are activated after MHC-I binding. CD4+ T cells primarily act as helper T cells which can facilitate the activity of B Cells and CD8 T cells (Creemers *et al.*, 1986; Buller R M L *et al.*, 1987). CD8+ T cells can also directly remove infected cells by a variety of methods including inducing apoptosis (Daniels *et al.*, 2001). Due to this strong role, they regularly need co-stimulatory factors such as the presence of CD4+ T cells (Daniels *et al.*, 2001; Shedlock *et al.*, 2003).

#### *1.1.8.2 B cells*

B cells are the main moderators of the creation and production of antibodies. They are bone marrow derived and differentiate from pluripotent haematopoietic stem cells (Takatsu', 1997). When first leaving the bone marrow the cells are referred to as "naïve" as they have not been exposed to antigens. These cells follow chemoattractant signals, such as CXCL13, towards secondary lymphoid organs, for example the lymph nodes or spleen, where they are exposed to antigens by APCs which stimulate antibody production (Kowarik *et al.*, 2012; Rubio, Porter and Zhong, 2020; Bekele Feyissa *et al.*, 2021). B cells have membrane bound IgD and IgM molecules that are specific for antigens for a particular pathogen (Geisberger, Lamers and Achatz, 2006). Activated B cells undergo somatic mutation of the variable portion of the genes encoding these antibodies which increases the binding affinity for the antigen to these antibodies (Pilzecker and Jacobs, 2019). B cells which have successful binding to these receptors, along with costimulatory signals from Th cells, are induced to proliferate and additionally differentiate into either antibody secreting B cells, known as plasma cells, or memory B cells (Nemazee, 2017; Tsai *et al.*, 2019). Memory B cells are involved in maintaining the immune memory to the pathogen (Ratajczak *et al.*, 2018; Palm and Henry, 2019). B cells can also induce a positive feedback loop of antibody production by presenting antigens directly to T cells, which stimulate cytokine production, which in turn stimulates activation of more B cells (Crotty, 2015).

## 1.2 Multiple sclerosis

### 1.2.1 General overview

Multiple sclerosis (MS) is a demyelinating disease of the CNS characterised by regions of inflammation and demyelination of the axon which leads to axon degeneration, decreased neuronal activity and eventually neuronal cell death (Ghasemi, Razavi and Nikzad, 2017). Symptoms range from problems with mobility and vision in the early disease stages, to irreversible disability and death in the later stages (Ghasemi, Razavi and Nikzad, 2017). The cause of MS is unknown, and there is currently no cure (Hauser and Cree, 2020). However, there are many disease modifying therapies (DMTs) which reduce disease progression and prevent additional neurological deficits for people with MS (Polman and Uitdehaag, 2000; Hauser and Cree, 2020).

### 1.2.2 Disease development

In the UK, there are approximately 130,000 people living with MS and ~7000 new diagnoses each year (Mackenzie *et al.*, 2014). Globally, this equates to an estimated 2.8 million (Walton *et al.*, 2020). As mentioned, the cause of the disease is unknown, however, it is considered there are some genetic and environmental factors which initiate disease development.

There are multiple environmental factors that have been linked with the onset of MS. Exposure to viruses such as Epstein Barr Virus and herpes simplex virus 6, along with smoking, diet, UV radiation, and vitamin D and B12 deficiencies have all been associated with the onset of MS (Orton *et al.*, 2011; Najafi *et al.*, 2012; Wingerchuk, 2012; Katz Sand, 2018; Sintzel, Rametta and Reder, 2018; Lundström and Gustafsson, 2022; Soldan and Lieberman, 2023). It is thought that the viruses have similar surface proteins to proteins found in the myelin sheath which, when presented to the adaptive immune system, result in these cells attacking the myelin sheath (Kuchroo and Weiner, 2022; Lundström and Gustafsson, 2022; Soldan and Lieberman, 2023). In smoking, there is the production of both nitrous oxide (NO) and carbon monoxide (CO). NO is a toxic soluble gas that has been shown to damage both neurons and oligodendrocytes, and CO leads to a decrease in tissue

oxygenation and activation in the inflammatory response – both combined resulting in demyelination (Mitrovic *et al.*, 1995; Molina-Holgado *et al.*, 2001; Guo, Hu and Pan, 2020). Vitamin D has roles in controlling cell proliferation and differentiation, along with gene expression and a host of immune regulatory roles ranging from synthesis of cytokines and induction of B cell apoptosis (Veldman, Cantorna and DeLuca, 2000; Orton *et al.*, 2011; Cui and Eyles, 2022). The vitamin D deficiency can be linked to low-level exposure to UV radiation. A link has been described between low-levels of UV radiation and decreased incidence of MS pathology, likely due to sun light being a principle source of vitamin D3 synthesis (Orton *et al.*, 2011).

In combination with environmental factors, a genetic predisposition might be involved in MS development. In humans, over 200 loci have been associated with disease susceptibility, with 10.5% of these appearing in the human leukocyte antigen (HLA) region of chromosome 6 (Hollenbach and Oksenberg, 2015; Baranzini and Oksenberg, 2017). Examples of these are HLA-DR2+, HLA-DQ6, DRB1*1501, and DRB1*1503. In addition to these, mutations in IL7RA, IL2RA, and TNFRSF1A have been linked to minor susceptibility to MS disease progression (Ottoboni *et al.*, 2013; H. Liu *et al.*, 2017; Buhelt *et al.*, 2019).

### 1.2.3 Symptoms

Disease symptoms are very varied and depend on the MS phenotype. Relapsing remitting MS (RRMS) is characterised by periods of acute disease pathology followed by a functional recovery, or remission (Goldenberg, 2012; Cunill *et al.*, 2018). Associated symptoms include visual impairments, numbness, fatigue, and incontinence along with general neurological deficits. Approximately 87% of people present with RRMS, with a typical age of onset between 20 to 40 years old (Goldenberg, 2012). Of these, ~65% will subsequently develop SPMS within 10-20 years of RRMS diagnosis (Rovaris *et al.*, 2006; Tremlett, Zhao and Devonshire, 2008). People with SPMS experience progressively more severe symptoms of RRMS. Approximately 10-15% of people are diagnosed with PPMS, which largely affects nerves in the spinal cord and has a later age of onset than RRMS at ~50 years old (Macaron and Ontaneda, 2019).

Initial disease diagnoses can be found during a CIS episode. Differing from MS, there is a single isolated demyelinating lesion in the CNS with symptoms lasting longer than 24 hours and peaking 2-3 weeks after onset of symptoms (Efendi, 2015). These symptoms include visual impairment, ataxia, and possibly weakness depending on location of the lesion (Efendi, 2015). To rule out MS, the incident must only occur once, and must occur in the absence of fever or symptoms of general encephalopathy (Hou, Jia and Hou, 2018). CIS is often the first presentation of RRMS with 10-85% of CIS cases converting, depending on other MS risk factors (Efendi, 2015; Hou, Jia and Hou, 2018; Klineova and Lublin, 2018).

### 1.2.4 Relapsing Remitting MS Pathogenesis

Initial disease progression is associated with inflammation in the CNS (Koudriavtseva and Mainero, 2016; Vavasour *et al.*, 2022). This inflammation is characterised by the penetration of T and B cells into the CNS and is most pronounced at disease onset and decreases during disease progression (van Langelaar *et al.*, 2020; Comi *et al.*, 2021). It is generally believed that the inflammatory response in the CNS is initiated by autoantigen-specific CD4+ T cells which enter the CNS and initiate a chronic inflammatory response (Fletcher *et al.*, 2010; Kaskow and Baecher-Allan, 2018). The exact mechanism of autoimmune activation in MS is unclear, however there has been a link to myelin-based proteins MOG, myelin oligodendrocyte glycoprotein, and MBP, myelin basic protein, reactive T cells in both the blood and CSF of MS patients (Meinl and Hohlfeld, 2002; Bettini, Rosenthal and Evavold, 2009; Fletcher *et al.*, 2010). These auto-reactive T cells are primed to CNS autoantigens in the periphery and then cross the BBB and enter the CNS.

At the onset of MS, T helper 1 (Th1) and Th17 subsets of CD4+ cells are increased in the CNS of people with MS compared to “healthy” individuals. It is thought that antigen presenting cells (APCs) such as microglia present degraded myelin which trigger activation and differentiation of Th1 and Th17 cells(Prajeeth et al., 2017; Moser et al., 2020) if it was just microglia presenting, how would these T cells get into the CNS? There has to be earlier inflammation or so?. These two subsets regulate the production of pro-inflammatory cytokines such as interferon-gamma, TNF-alpha, IL-17, and IL-6. Th17 cells could contribute to chronic CNS inflammation (Arellano *et al.*, 2017), with high levels of *IL17* mRNA correlated with MS disease severity (Gold and Lühder, 2008; Omidian *et al.*, 2019). Th17 cells are also implicated in activating the endothelial cells of the blood-brain barrier (BBB)

by secreting IL-17 and IL-22. This activated BBB results in additional recruitment of immune cells into the CNS (Kebir *et al.*, 2007).

Similarly, the activity of regulatory T (Treg) cells are implicated in MS pathology. Tregs inhibit the inflammatory response by decreasing expression of the pro-inflammatory cytokines of Th1 and Th17 cells, and promoting T cell apoptosis by expressing cytotoxic T-lymphocyte associated protein 4 (CTLA-4) (Luan *et al.*, 2015; Wang *et al.*, 2023). Myelin-reactive T cells are found in healthy individuals, and therefore MS pathogenesis could be associated with insufficient immune regulation by Tregs (Stephens, Malpass and Anderton, 2009; Tapia-Maltos *et al.*, 2021).

Originally, MS was believed to be primarily T-cell mediated disease, however B cells are now recognised to play a crucial role in pathogenesis. Underlying mechanisms are not fully clear, but both antibody dependent and independent mechanisms are implicated in mediating CNS injury in MS (Wilson, 2012; Häusser-Kinzel and Weber, 2019). Intrathecal synthesis of immunoglobulin antibodies that bind myelin and axons, known as oligoclonal bands, have long been associated with MS disease severity (Arrambide *et al.*, 2018). B cell infiltration is often found along the vasculature of the meninges at the sites of myelin degradation, implying a sustained proliferation of mature B cells in the CNS (Torres Iglesias *et al.*, 2023). These B cells are likely to be producing further anti-myelin antibodies which could exacerbate MS disease pathology (Torres Iglesias *et al.*, 2023). Additionally, these B cells could produce pro-inflammatory cytokines such as IL-6 further contributing to MS pathogenesis (Barr *et al.*, 2012). B cell depleting therapies, such as treatments with anti-CD20 monoclonal antibodies (mAbs) are highly effective in all forms of MS by supressing inflammation and reducing MS relapses (Greenfield and Hauser, 2018; de Sèze *et al.*, 2023)., suggesting that B cells play a core role in the pathogenesis of MS.

### 1.2.5 Progressive MS Pathogenesis

Meanwhile, the pathogenesis of primary progressive MS (PPMS) and secondary progressive MS (SPMS) differs. Progressive MS differs as it lacks a large quantity of the infiltration of perivascular immune cells seen in RRMS (Ontaneda and Fox, 2015; Havla and Hohlfeld,

2022). While peripheral immune cells are present in the CNS, they are at a much lesser extent than seen in RRMS, and this presents significant problems to DMTs as these primarily focus on modifying the infiltration of immune cells into the CNS (Ontaneda and Fox, 2015; Hollen *et al.*, 2020; Kamma *et al.*, 2022). This leads to the concept that disease progression in progressive MS is due to axonal degeneration caused by inflammatory activity inside the CNS without the activity of the peripheral immune system (Ontaneda and Fox, 2015). While new lesions can develop, the main drivers of the disease are lesion expansion and diffuse white matter pathology (Arnold *et al.*, 2021).

The lesions in PMS can be separated into two phenotypes, chronic-active and chronic-inactive lesions (Lassmann, 2018). Chronic-active lesions are characterised by an inactive lesion core surrounded by an active rim. This rim is composed of activated microglia and macrophages that slowly expand outwards phagocytosing myelin breakdown products (Eisele *et al.*, 2021). The core is hypocellular comprising mainly of reactive astrocytes and myeloid cells with few if any oligos (Lassmann, 2018). These oligodendrocytes have been known to remyelinate, however this is rarer in PMS than RRMS (Prineas and Connell, 1978; Raine and Wu, 1993). Inactive lesions, or burnt-out lesions, are primarily comprised of reactive astrocytes that form a fibrotic scar, where axons are reduced by up to 80% (Kolb *et al.*, 2022). Unlike the active lesions, these lesions do not remyelinate and inflammation has decreased.

Interestingly, approximately 40-70% of people with SPMS have meningeal B-cell follicular structures, which are areas that contain proliferating B cells and T cells (Magliozzi *et al.*, 2007; Haugen, Frederiksen and Degn, 2014). These are not found in PPMS, and are normally found near grey-matter pathology. These structures are linked with more severe MS pathology – suggesting they promote the production of cytokines, auto-antibodies, and other pro-inflammatory molecules (Magliozzi *et al.*, 2007; Haugen, Frederiksen and Degn, 2014; Holloman *et al.*, 2021). This is supported by findings such as B-cell depletion therapies such as those discussed previously have positive therapeutic outcomes, something not seen with T-cell therapies.

### 1.2.6 Treatment

Primarily, therapeutics are aimed at increasing recovery following a relapse, delay disease progression to PMS, and alleviate the symptoms (Robertson and Moreo, 2016). Most therapeutics are immunomodulatory in nature and primarily act to reduce inflammation in the CNS (Hauser and Cree, 2020). Among the first DMTs prescribed to MS patients were treatments such as interferon beta (IFN-β) and glatiramer acetate (GA) (Gajofatto and Benedetti, 2015; Coerver *et al.*, 2023). They were linked with a 30% reduction in relapse rate and a 50% reduction in new lesions (Filipi and Jack, 2020). While efficacious, these drugs have been linked with side effects such as flu-like symptoms, injection site reactions and dyspnoea which have decreased their popularity with MS patients (Coerver *et al.*, 2023). These drugs worked by decreasing pro-inflammatory cytokine production and inhibiting immune cell activation by decreasing antigen presentation through downregulation of HLA expression (Brod *et al.*, 1633; Kasper and Reder, 2014).

Following the development of these first agents, the focus turned to modifying the aberrant immune response and the infiltration of immune cells into the CNS. Fingolimod, a sphingosine-1-phosphate (S1P) inhibitor, prevents T cells migrating to the CNS by degrading the S1P receptor on lymphocytes (Chun and Hartung, 2010). Natalizumab, an alpha4beta1 integren inhibitor blocks lymphocyte adhesion to VCAM on the endothelium and thus prevents migration across the BBB (Brandstadter and Sand, 2017). Rituximab and ocrelizumab target CD20 thus depleting the B cell population (Gelfand, Cree and Hauser, 2017; Chisari *et al.*, 2021). All these therapeutics are associated with decreased relapse rates of 50-70%, and new lesions by 80-90%. Ocrelizumab has also been shown to influence PMS progression, with up to an ~25% decrease in clinical disability progression seen (Mulero, Midaglia and Montalban, 2018).

However, while these second-line agents have increased efficacy, they also come with an increased risk of serious, sometimes fatal, side effects. One of these is progressive multifocal leukoencephalopathy (PML), caused by the lytic infection of oligodendrocytes in the CNS by human polyomavirus 2, formerly known as JCV (Berger, 2017).

## 1.3 Progressive multifocal leukoencephalopathy

### 1.3.1 General Overview

Progressive multifocal leukoencephalopathy (PML) is a rapidly progressive neurodegenerative disease characterised by large regions of demyelination and necrosis in the CNS (Berger and Major, 1999; Adang and Berger, 2015). The disease is primarily found in people who are immunocompromised or immunosuppressed, such as people with late stage HIV-AIDS or certain MS patients (Berger and Major, 1999; Sharma *et al.*, 2013). Often fatal if untreated, the disease is caused by infection of oligodendrocytes by human polyomavirus 2, commonly known as john Cunningham virus (JCV), eventually leading to the death of the oligodendrocyte (Saribaş *et al.*, 2010). Due to the infection being able to infect virtually any region of the brain, there are a wide range of symptoms and signs and can be challenging to distinguish from an MS relapse making diagnosis difficult (Lopes *et al.*, 2019; De Mercanti *et al.*, 2020). Some of the commonly reported symptoms are muscle weakness, cognitive impairment, and sensory symptoms (Berger *et al.*, 2013; Adang and Berger, 2015). First-line treatments are immediate drug cessation and supportive care, leaving patients open to their original diseases (Williamson and Berger, 2017). There are no antiviral therapeutics available, and this is an active area of investigation.

### 1.3.2 Human polyomavirus 2

Human polyomavirus 2, or John Cunningham Virus (JCV, as it will be referred to from now on) is a strain of polyomavirus that is extremely prevalent in the human population with ~50% seropositive for the virus (Lambrianides *et al.*, 2019; Hanaei *et al.*, 2020). First identified in 1971, the virus was one of the first polyomaviruses discovered and isolated (Padgett *et al.*, 1971). It is a non-enveloped virus with a circular dsDNA genome (Meneguzzi *et al.*, 1978). In the context of infection, the virus interacts with alpha2,6-linked sialic acid in an L shape, found on lactoseries tetrasaccharide C (LSTc) receptors (Liu, Wei and Atwood, 1998; Elphick, 2004). It also transiently interacts with 5-hydroxytryptamine 2 receptors (5-HT2R) before entering the cell through endocytosis (Elphick, 2004).

It is thought that 10-20% of people are infected during childhood, and this number increases over the following years (Knowles *et al.*, 2003). Initial infection is thought to occur in a faecal-oral route, as the virus is routinely shed in urine (Booll-Mas and Girones, 2001). This infectious form of the virus is not generally pathogenic and establishes an asymptomatic persistent infection of the kidneys (Dorries and Ter Meulen, 1983; Kato *et al.*, 2004). This form is thought to be held in control by the immune system until immunosuppression by either disease or treatment with immunomodulatory drugs. When the immune system is suppressed, JCV can increasingly replicate which can result in genomic rearrangement of the non-coding control region (NCCR) (Gosert *et al.*, 2010). If this occurs, there can be an increase in the JCV infectivity of glial cells, and it is only this pathogenic form, termed the PML-type, that is found in the CNS and CSF of patients with active disease (Wharton *et al.*, 2016; Lauver and Lukacher, 2020).

How the virus moves from the sites of latent infection to the CNS is not well understood. However, potential routes have been suggested such as through infecting B cells which migrate into the CNS or through the choroid plexus. As already discussed, B cells can infiltrate the CNS which would provide a direct route of infection for the virus to enter the CNS. The choroid plexus however is a membranous structure known for the production of CSF (Lun, Monuki and Lehtinen, 2015). The endothelial cells of the choroid plexus have all the required receptors for JCV infection and been shown both *in vitro* and *in vivo* to be capable of supporting the viral life cycle (Haley *et al.*, 2015; O'Hara *et al.*, 2020). Once the virus is into the CNS, it is proposed the virus can spread along myelin sheaths between neighbouring cells (Wharton *et al.*, 2016).

### 1.3.4 Pathogenesis

The most obvious factor for PML pathogenesis is the underlying disease or treatments causing the immunosuppression. Several transcription factors that are downstream of pro-inflammatory cytokines have been implicated in JCV replication, such as those that are found to be expressed during RRMS (Wollebo *et al.*, 2011; Fresegna *et al.*, 2020). Similarly, the proliferation of B cells during MS could contribute to disease pathogenesis, as this would increase the production of the B cell recombinase enzymes RAG1 and RAG2 which have been proposed to facilitate the NCCR rearrangement required for the neurotropic form of JCV to emerge (Marzocchetti *et al.*, 2008; Bellizzi *et al.*, 2011; Durali *et al.*, 2015).

However, PML does not occur uniformly across the immunosuppressed patient populations, implying there must be additional factors contributing to disease progression. Deficiencies in CD4 T cells are linked with a prognosis in PML (Pavlovic *et al.*, 2018), and CD8 T cell reactivity is associated with disease prevention and resolution(Du Pasquier *et al.*, 2004; Gheuens *et al.*, 2011). Other factors which have been linked with an increase in viral infectivity are polymorphisms of the tumour suppressor protein p53 and mutations in HLA-DRB*0401 (Ariza *et al.*, 1992; Jelčić *et al.*, 2013). The latter has been linked with a decreased ability to mount robust antiviral responses.

### 1.3.5 Treatments

Treatments for PML can be categorised into two broad groups, direct antiviral therapies and indirect strategies designed to reconstitute the innate antiviral response. Multiple antiviral therapies have been investigated such as targeting viral replication (cytarabine and cidofovir) and viral entry into cells (mirtazapine) (Jiang *et al.*, 2010; Matsudaira *et al.*, 2014; Mullins *et al.*, 2017). However, these strategies failed to decrease neurological disability or prolong survival in clinical trials while being attributed to having excessive toxicity (All *et al.*, 1998; Marra *et al.*, 2002; Pavlovic *et al.*, 2015). Therefore, immune reconstitution is the primary method of treating PML (Pavlovic *et al.*, 2015). In MS, this occurs following discontinuation of immunosuppressive drugs. The reconstitution of the immune system can result in Immune Reconstitution Inflammation Syndrome (IRIS) which can lead to a worsened PML disease pathology (Clifford, 2015; Fournier *et al.*, 2017; Frattaroli *et al.*, 2021). If PML is caught within the first 6 months of natalizumab use and the immune system reconstituted rapidly there is a high survival rate. However, this is not always the case and some people do die from IRIS itself (Clifford, 2015). A current trend of research into possible therapeutics for PML have been looking into “checkpoint inhibitors”, or methods of decreasing T cell efficacy at clearing infection. These checkpoint inhibitors allow reconstitution of the immune system (Beck and Cortese, 2020). However, these inhibitors still rely on ending treatment with immunomodulatory drugs.

### 1.3.6 Animal models of human polyomavirus 2

As JCV is a human obligate virus, meaning it does not replicate in non-human cells, this disease is challenging to investigate. Complete animal models of JCV infections are not available which makes studying the virus challenging. One mouse model developed engrafts human glial cell progenitors into immunodeficient neonatal mice, however this is limited in its scope and a complicated methodology (Tan *et al.*, 2013). Other studies have tried replicating JCV in animal models, however these have ultimately failed as they did not mirror PML pathology (Kondo *et al.*, 2014).

An alternative approach is to utilise a substitute virus to facilitate animal research (Dalianis and Hirsch, 2013). Semliki forest virus (SFV) is a mouse-adapted positive sense ssRNA Alphavirus (Kujala *et al.*, 2001). Originally isolated in 1961 from *Aedes argenteopunctatus* in East Africa, the virus is neurotropic infecting oligodendrocytes resulting in demyelination in the CNS (Atkins, Sheahan and Liljestro, 1999). Therefore, the virus is functionally similar, even if it lacks human relevance. The virus has also been well characterised both *in vivo* and *in vitro*, meaning well-informed conclusions can be drawn through comparing any results obtained to existing literature (Fazakerley and Webb, 1987; Fazakerley *et al.*, 2006; Fragkoudis *et al.*, 2009). Conveniently, this virus is easily genetically manipulated allowing development of highly trackable models *in vivo* and *in vitro*.

## 1.4 Immune responses to virus

### 1.4.1 General overview

Viruses are obligate intracellular parasites that require a host cell to replicate and facilitate the spread to others. While most viruses are rarely lethal in humans due to our efficient immune systems immunocompromised individuals are at risk of severe disease pathology (Rouse and Sehrawat, 2010). Therefore, advances in understanding the immune response of healthy individuals can identify therapeutic targets to decrease viral infectivity. The immune responses to virus can be separated into the cell intrinsic immune response, which blocks viral infection (Takeuchi and Akira, 2009), the cellular innate immunity, and adaptive immunity, which takes longer but provides more specific protection against virus and virus infected cells with the capacity to form memory (Libbey and Fujinami, 2014).

As previously mentioned, the innate immune response is initiated by the neutrophils, monocytes, dendritic cells and natural killer cells, while the adaptive immune response derives from the T cells and B cells. In the context of MS of particular interest are the antibodies produced by B cells (Greenfield and Hauser, 2018; Comi *et al.*, 2021; Holloman *et al.*, 2021).

### 1.4.2 Antibody response

B-cell derived antibodies have many distinct functions in viral infectivity including binding and neutralising the viral particle, enhancing phagocytosis, antibody-dependent cytotoxicity, and complement fixation (Forthal, 2014; Mielke *et al.*, 2019; Reiling *et al.*, 2019; Tay, Wiehe and Pollara, 2019; Morales-Núñez *et al.*, 2021). Neutralisation of infectivity occurs through the antibodies, specifically immunoglobulin A (IgA) or immunoglobulin M (IgM) binding to the surface of the pathogen causing them to aggregate together which results in decreased infectivity, probably through decreasing the number of free virus in the host (Lu *et al.*, 2018; Sterlin *et al.*, 2020). Antibodies can also neutralise the pathogen though binding to surface ligands that are essential for virus-cell interactions and internalisation (Forthal, 2014). A well characterised example are antibodies against HIV-1 gp120 which when bound interfere with the virus binding to CD4 (Ferrari *et al.*, 2011). Antibodies can also inhibit viral fusion or entry using a similar mechanism. For certain viruses such as Influenza A virus, after binding to the surface of the cell, anti-influenza haemagglutinin antibodies, can alter the conditions and inhibit the structural changes to allow for the fusion of the viral and cell membranes (Krammer, 2019; C.-J. Li *et al.*, 2022).

Antibodies can also activate the complement system, which can induce the lysis of the pathogen or infected cell, and increased phagocytosis resulting in clearance of the pathogen (Janeway, Travers and Walport, 2001; Gavin *et al.*, 2019). Complement associated phagocytosis can result in increased T-cell recruitment through antigen presentation on major histocompatibility complexes (MHCs), and as mentioned this can feed into a positive feedback loop of B-cell T-cell activation (Merle *et al.*, 2015; West, Kolev and Kemper, 2018).

B-cell derived antibodies also can induce antibody-dependent cytotoxicity. Here, the antibody increases binds both an immune cell and either the pathogen or an infected cell

(Raúl *et al.*, 2012). This activates the immune cell to lyse the pathogen or infected cell and can be effective against a wide variety of pathogens (Ahmad and Menezes, 1996; Vanderven *et al.*, 2017; Gauthier *et al.*, 2021).

#### *1.4.2.1 IgM*

One of the first antibodies to be secreted during infection are IgM antibodies. Immunoglobulin M (IgM) is the largest antibody produced in humans and largely appears after a primary infection (Kaveri, Silverman and Bayry, 2012; Keyt *et al.*, 2020). IgM can be expressed as a monomer on the surface of B-cells, but when secreted the antibody appears as a pentameric (rarely hexameric) antibody of 5+ IgM monomers (Burrell, Howard and Murphy, 2017; Hiramoto *et al.*, 2018). IgM has multiple different roles in immune defence against pathogens. Secreted IgM can directly bind the pathogen and form aggregations of viral particles, manipulate gene expression, and activate the adaptive immune system (Ma1 *et al.*, 1992; Atif *et al.*, 2018; Pradhan *et al.*, 2022). It is seen that is seen that C57BL/6J mice that have lost the ability to secrete IgM have an increase in proinflammatory cytokines, difficulties clearing pathogens as well as a decrease in recruitment of neutrophils to the sites of infection (Boes *et al.*, 1998).

#### *1.4.2.2 Lipid-specific IgM antibodies in multiple sclerosis*

In MS specifically, it has been proposed that if there is intrathecal synthesis of lipid-specific IgM antibodies this can be used as a prediction of a more severe MS disease pathology (Villar *et al.*, 2002). However, these exact same antibodies are also thought to be neuroprotective in PML. There is a 60-fold risk increase in patients which have anti-JCV antibodies developing PML if there is no intrathecal synthesis of IgM seen in the CNS (Villar *et al.*, 2015).

Recent research has identified that the lipid-reactive IgM antibody O4 can confer an antiviral effect *in vitro* (Hayden *et al.*, 2020). It was found that O4 induced a significant increase in IFN-β in rat microglia by a cGAS-STING dependent manner, and this in turn resulted in a marked increase in IFN-β in other neuronal cells by interaction of secreted IFN-β with IFNAR (Hayden *et al.*, 2020). This significant upregulation in IFN-β resulted in a protective antiviral effect in these cultures when challenged with multiple viruses. Similarly, previous studies have identified that IFN-β can stop infection of glial cells by JCV (O'Hara

and Atwood, 2008), and since these are the primary cells that JCV infects this would have a decrease in the progression of PML. However, as mentioned previously, these antibodies are implied to be a marker for more severe and aggressive MS disease progression (Villar *et al.*, 2002). As such, lipid-specific IgMs are not suitable for treatment of PML in MS patients (Villar *et al.*, 2005).

### 1.4.3 Interferons

#### *1.4.3.1 General overview*

Interferons are a broad class of cytokines induced following an infectious challenge and are essential for inducing the immune response (Levy and García-Sastre, 2001; Kopitar-Jerala, 2017). There are three distinct classes of interferons, type I, type II, and type III, all of which share the ability to elicit an antiviral response in the cells (Pestka *et al.*, 2004).

#### *1.4.3.2 Type I interferons*

Type I interferons are broadly expressed proteins that are produced by almost all cells in the body in response to stimulation by a microbial pathogen. There are many type-I interferons, the most well characterised are interferon alpha (IFN-α) and interferon beta (IFN-β) (Capobianchi *et al.*, 2015). There are other type-I IFNs, such as IFN-τ, IFN-κ, IFN-ω, however these are poorly defined (Capobianchi *et al.*, 2015). Type-I IFNs are best known for inducing an antiviral state through inducing interferon stimulated genes which can interfere with multiple stages of the viral replication cycle, either through direct activity or recruitment of additional cells to the site of infection (Schoggins, 2019).

##### 1.4.3.2.1 Induction of type I interferons

Initial induction of type-I IFNs is reliant on microbial products binding to pathogen recognition receptors (PRRs) on the cell membrane or in the cytosol (Mogensen, 2009; Li and Wu, 2021). These products are normally foreign nucleic acids or pathogen associated molecular patterns (PAMPs), with different products activating different PRRs (Mogensen, 2009). For example, RNA activates RNA helicases retinoic acid-inducible gene I (RIG-I), or DNA activates DNA-dependent activator of IFN regulatory factors (DAI) (Wang *et al.*, 2008; Matsumiya and Stafforini, 2010). These are particularly useful for sensing different genera of virus, and both lead to IFN-α/β production. Additionally, IFN-α/β production can be

induced by Toll-like receptors (TLRs) (Uematsu and Akira, 2007). Depending on the TLR, these can similar products to PRRs, or TLR4 can recognise lipopolysaccharide (LPS) from bacteria (Uematsu and Akira, 2007; Soares *et al.*, 2010). TLR4 is a strong inducer of IFN-β by signalling through TIR-domain-containing adaptor protein inducing IFN-β (TRIF) (Soares *et al.*, 2010; Zhu *et al.*, 2019).

All these signals converge on a few key pathways or molecules, beginning with the kinases IkB kinase-e (IKKe) and TANK-binding kinase 1 (TBK1) (Fitzgerald, McWhirter, *et al.*, 2003; Balka *et al.*, 2020). These activate IFN regulatory factors (IRFs), which are transcription factors that activate the transcription of the genes encoding IFN-α/β (Yanai, Negishi and Taniguchi, 2012). The best characterised IRFs are IRF3 and IRF7, however, additional IRFs are known to induce gene transcription (Yanai, Negishi and Taniguchi, 2012). TLR4 induces TRIF to associate with TBK1 inducing the activation of IRF3 (Fitzgerald, Rowe, *et al.*, 2003). This pathway of activation has been visualised in **Figure 1.1**.

#### 1.4.3.2.2 Responses to type I interferons

Following expression of IFN-α/β, these molecules bind through the heterodimeric transmembrane receptor complex of IFNAR1 and IFNAR2 (De Weerd and Nguyen, 2012). The binding of IFN to the receptor activates the associated protein Janus kinase 1 (JAK1) and tyrosine kinase 2 (TYK2), which in turn activate signal transducer and activator of transcription 1 (STAT1) and STAT2 (Gauzzi *et al.*, 1996; Li *et al.*, 1996; Au-Yeung, Mandhana and Horvath, 2013; Majoros *et al.*, 2017). STAT1 and STAT2 dimerise and bind IRF9 in the nucleus to form IFN-stimulated gene factor 3 (ISGF3). ISGF3 then binds to IFN-stimulated response elements (ISREs) which activate the transcription of the interferon stimulated genes (ISGs) (Fu *et al.*, 1990; Yang *et al.*, 2005; Platanitis *et al.*, 2019; Leviyang, 2021). This pathway is visualised in **Figure 1.2.** The ISGs are described in **1.4.3.5**.

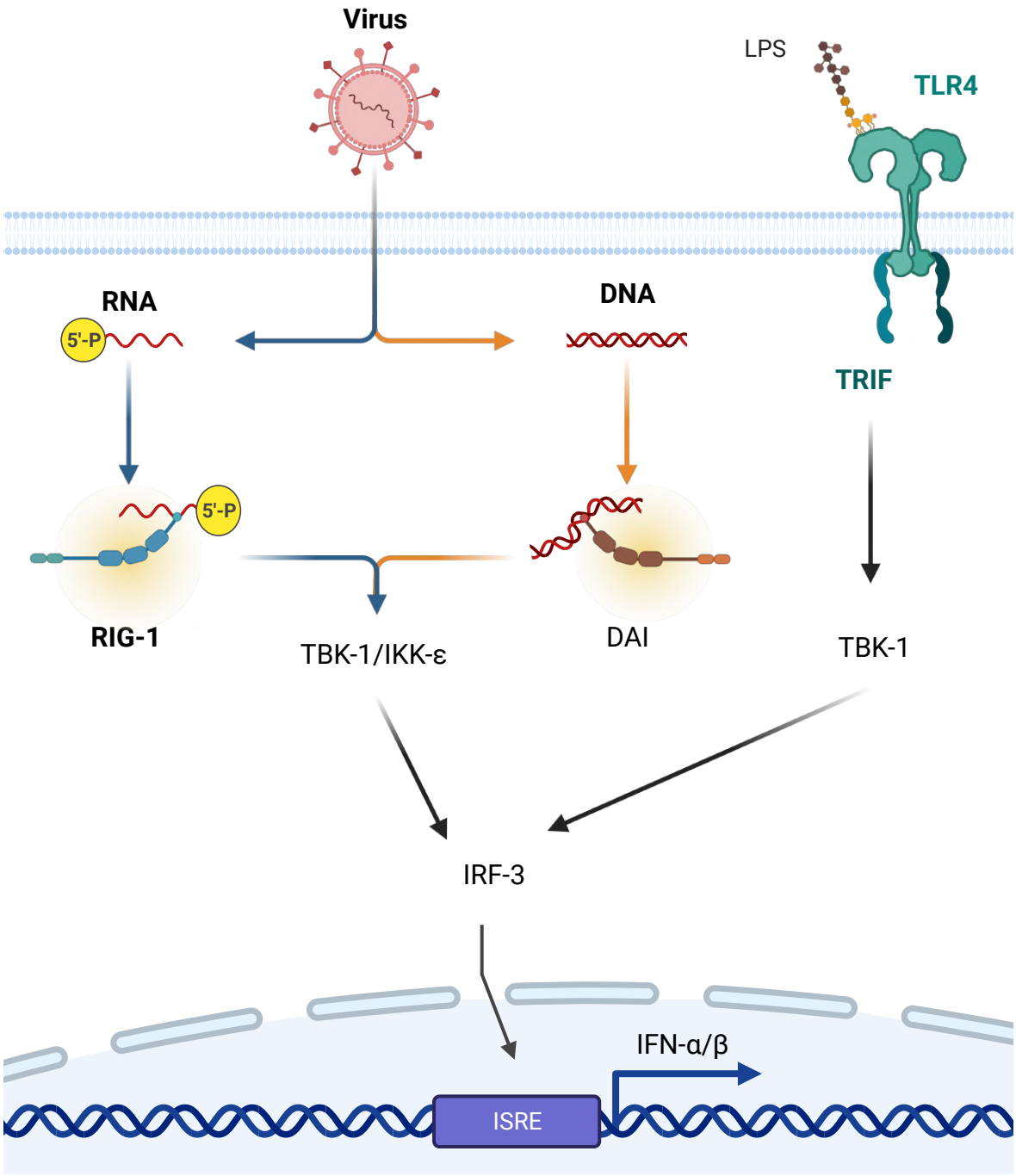


**Figure 1.1: Diagram of interferon-inducing pattern recognition receptors mentioned.** Figure created with BioRender.

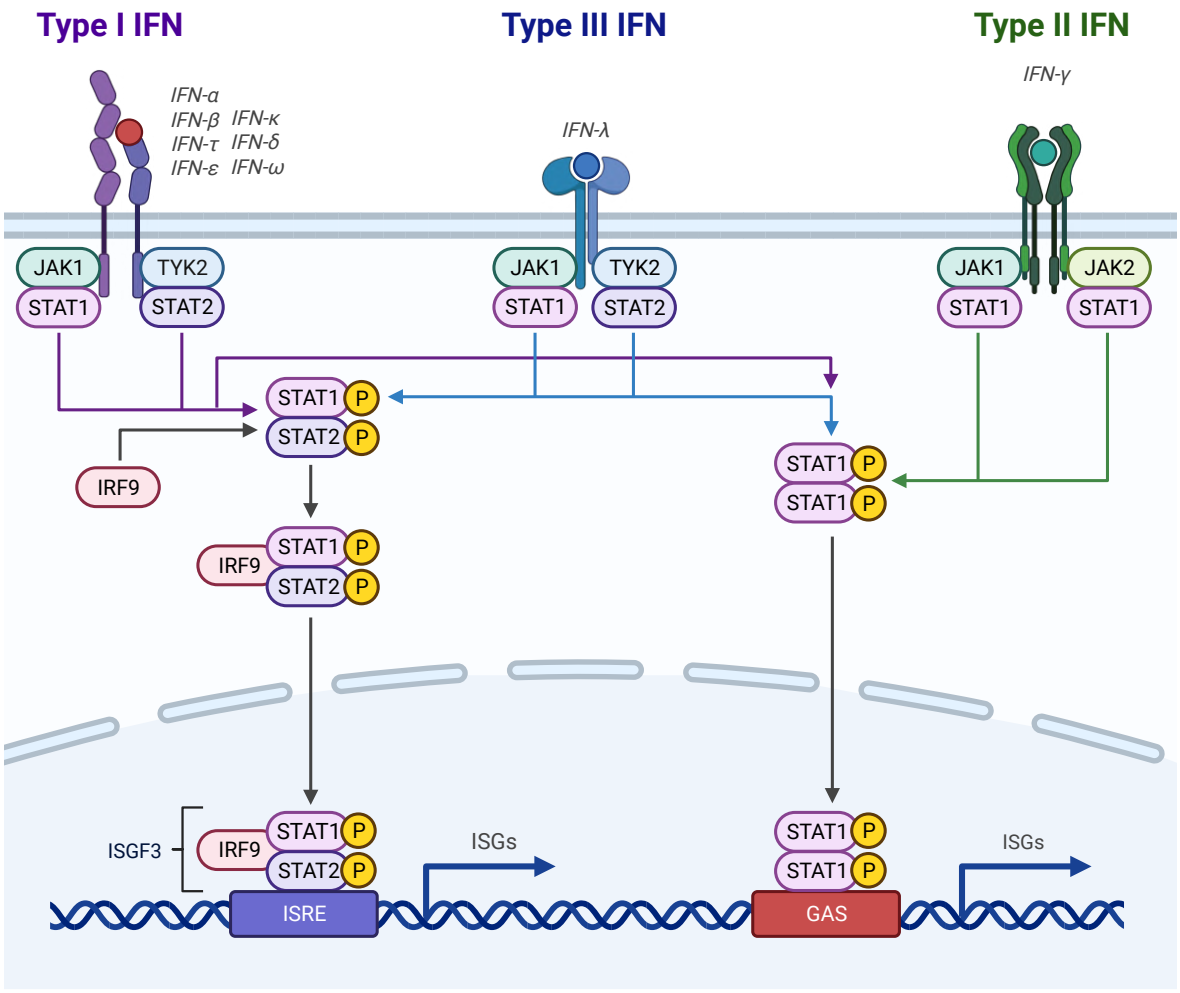


**Figure 1.2: Diagram of ISG upregulation following type I, II, and III IFN signalling.** Figure created with BioRender.

Type-I IFNs can convey a cell-intrinsic antiviral response, for example restricting viral replication. In studies of IFNAR KO mice there was increased susceptibility to viral infectivity, with this effect seen across genetically distinct viruses, for example Semliki Forest virus and lymphocytic choriomeningitis virus (LCMV) (Piersma *et al.*, 2020; Meyts and Casanova, 2021). In humans this antiviral effect can be harder to disseminate as contributions of the type-III IFN response can confound results as they share similar pathways (Lazear, Schoggins and Diamond, 2019).

Type-I IFNs do not solely induce cell-intrinsic antiviral responses, they can also affect the innate and adaptive immune systems. IFN-α/β can modify the response of B cells, T cells and NK cells to enhance their response to more efficiently clear viral infection and improve the generation of the immune memory response to allow a faster response to viral challenge (Kiefer *et al.*, 2012; Gangaplara *et al.*, 2018; Barnes *et al.*, 2022). Depending on the context, IFN-α/β can either induce or inhibit the differentiation of DCs, which as mentioned produce IL-12 which is crucial for driving the Th1 response (Müller, Aigner and Stoiber, 2017; Barnes *et al.*, 2022).

The production of antibodies by B cells can be modulated by IFN-α/β. In committed B cells, IFN-α/β promotes B cell activation and antibody production during viral infection (Kiefer *et al.*, 2012; Bénard *et al.*, 2018).

IFN-α/β can also act enhance the effect of CD4 and CD8 T cells. IFN-α/β can modulate CD4 survival to viral challenge, however this role has been reported to both assist and have a detrimental effect in viral and bacterial clearance (Havenar-Daughton, Kolumam and Murali-Krishna, 2006; Teijaro *et al.*, 2013; Gangaplara *et al.*, 2018). Type-I signalling can also inhibit CD4 cell migration from the lymph nodes (Huber and David Farrar, 2011). In CD8 T cells IFN-α/β can inhibit growth by decreasing STAT1 signalling (LCMV), while contrarily also promoting the expansion of CD8 T cells (Nguyen *et al.*, 2002; Kolumam *et al.*, 2005; Welsh *et al.*, 2012). These contradictory findings are not well characterised, however could be due to differences in STAT signalling. In STAT1 deficient cells IFN-α/β induces a proliferative signal possibly through STAT3 or STAT5, rather than STAT1 which is known to be anti-proliferative (Bromberg *et al.*, 1996; Tanabe *et al.*, 2005; Sherry *et al.*, 2009; Bitar *et al.*, 2019). IFN-α/β can also contribute to the memory T cell response by promoting cytokine

production during viral infections to recruit memory T cells to the sites of infection (Huber and David Farrar, 2011).

Similarly to both T and B cells, IFN-α/β increases the activity and proliferation of NK cells. During influenza, IFN-α/β signalling is essential for their activation and expression of IFN-γ (Gill *et al.*, 2011; Pegram *et al.*, 2011). The activation of IFN-γ expression seems to be influenced by differential STAT signalling, similar to CD8 cell proliferation (Gill *et al.*, 2011; Pegram *et al.*, 2011). High STAT1 inhibits IFN-γ production, while high levels of STAT4 increases IFN-γ expression (Miyagi *et al.*, 2007). Thereby showing how IFN-α/β can have dual activation or inhibition roles depending on the cell acted upon.

#### *1.4.3.3 Type II Interferons*

There is only a single type-II interferon, interferon gamma (IFN-γ). Structurally unrelated to type-I IFN, IFN-γ is secreted mainly by activated NK and T cells, however additional cell types for example NK T (NKT) cells are known to secrete type-II IFN (Fujii *et al.*, 2002). IFN-γ binds to IFNGR1 and IFNGR2 which in turn associated with JAK1 and JAK2 respectively (Platanias, 2005). This activates a STAT1 homodimer referred to as GAF to translocate to the nucleus and activates GAS DNA sequences (Au-Yeung, Mandhana and Horvath, 2013; Begitt *et al.*, 2014). Visualised in **Figure 1.2**.

#### *1.4.3.4 Type III Interferons*

Type III, or interferon lambda (IFN-λ) are the least characterised. While structurally similar to type-I IFNs, these bind to the heterodimeric receptor of IL-28R and IL-10R2 (Manivasagam and Klein, 2021). These induce the activation of the JAK-STAT pathway to form the ISGF3 transcription factor that activates downstream ISGs (Wack, Terczyńska-Dyla and Hartmann, 2015; Stanifer, Pervolaraki and Boulant, 2019). Visualised in **Figure 1.2**.

#### *1.4.3.5 Interferon stimulated genes*

The simplest definition of an interferon stimulated gene (ISG) is any gene induced by an interferon response across the three classes of IFNs. Over 450 individual genes have been described as induced by Type-I IFNs in mammals, however up to 10% of the human genome could be subject to IFN regulation (Shaw *et al.*, 2017). When specifically looking at genes with over 4-fold upregulation by Type-I IFN, only 62 common genes are upregulated

suggesting a core group of ISGs that are critical to the IFN response (Schneider, Chevillotte and Rice, 2014). These genes can have many varied, distinct antiviral roles therefore categorising them can prove difficult. One method of simplifying ISGs is to categorise them by their mechanisms of action in the viral replication cycle, these being entry, nuclear import, mRNA synthesis, protein synthesis, replication, and assembly/egress (Schoggins, 2014; Li, MacDonald and Rice, 2015; Yang and Li, 2020; Betancor *et al.*, 2021). For example, IFITM3 inhibits viral entry to the cell by blocking membrane fusion through endocytosis (Guo *et al.*, 2021). ISGs have a broad spectrum of activity and can influence the infectivity of both DNA and RNA viruses (Schneider, Chevillotte and Rice, 2014; Schoggins, 2014; Yang and Li, 2020).

### 1.4.4 Antiviral response in CNS

The CNS is sometimes referred to as an immune privileged site. While this is a controversial topic, the BBB is effective at ensuring most blood-borne pathogens are not able to enter the central nervous system (Chen and Li, 2021). However, there are exceptions. Viruses with a neuronal tropism can enter the CNS through multiple routes, including infecting infiltrating leukocytes, infection of the neuroepithelial cells allowing passage across the BBB, and retrograde transmission along axons (Kaul, Garden and Lipton, 2001; McGavern and Kang, 2011; Koyuncu, Hogue and Enquist, 2013; Taylor and Enquist, 2015; Ayala-Nunez and Gaudin, 2020). For most viruses, the initial site of infection is in the periphery before invading the CNS. PRRs are expressed by all neural cells including both the DNA/RNA sensors and TLRs mentioned previously (Hanamsagar, Hanke and Kielian, 2012). However, the expression differs throughout the CNS. Detection of PAMPs and DAMPs activate the antiviral signalling which induce the expression of antiviral chemokines and cytokines, for example type-I IFNs and their associated ISGs (Nair and Diamond, 2015).

In general, the glial cells are the major CNS population involved in protection against viral infection, in particular astrocytes and microglia (Meyding-Lamadé, Craemer and Schnitzler, 2019). However, both neurons and oligodendrocytes do have a distinct response and contribute to the CNS antiviral response. The expression of multiple PRRs have been described in microglia, oligodendrocytes, and neurons. For example, TLRs, which recognise viral RNAs, have been described in the CNS (Hanamsagar, Hanke and Kielian, 2012), with different proportions in the different cell types. Neurons express TLRs 3, 7, 8, and 9, which

are primarily involved with detection of dsRNA and ssRNA; while astrocytes express TLRs 1-7, 9 and 10 (Jack *et al.*, 2005; Hanamsagar, Hanke and Kielian, 2012). These differences in the expression of TLRs indicates niche roles for each cell type that act constructively together to protect the CNS from viral infections.

Astrocytes and microglia are considered the primary source of IFN-β in many viral infections, for example rabies virus (RABV), vesicular stomatitis virus (VSV), and Theiler's murine encephalomyelitis virus (TMEV) (Kallfass *et al.*, 2012; Pfefferkorn *et al.*, 2016; Li *et al.*, 2018). IFN-β expression has been shown to be dependent on the activity of TLR3 during MHV infection (Costello and Lynch, 2013). Astrocytes and microglia have also been shown to be particularly sensitive to type-I IFNs and induce a robust upregulation of ISGs, while the response in solo cultures of primary neurons is inefficient to protect against viral infections (Kreit *et al.*, 2014). This adds further evidence that the CNS acts as a unit to protect against viral infections where individual cell types, for example neurons, are unable to protect against a broad spectrum of viral infections.

## 1.6 Aims and hypotheses

The overarching aim of this thesis was to investigate whether IFN-β, and IFN-β derived therapeutics, could elicit a protective antiviral response in CNS cultures and *in vivo*. I aimed to improve our understanding of the innate antiviral response in the major cell types of the CNS to allow MS patients access to high efficacy drugs without risk of development of PML. To address this, four main avenues were investigated:

1) Determine the optimal dose of IFN-β to induce a significant upregulation in ISGs

2) Characterise a method to isolate individual cell-types from a mixed-neuronal cell culture

3) Investigate the oligodendrocyte specific response to IFN-β and identify candidates for future investigation as an antiviral therapeutic

4) Ascertain whether IFN-β or an oligodendrocyte specific candidate can evoke an antiviral response *in vitro* and *in vivo*.

To investigate these, I utilised my novel CNS culture (Gamble *et al.*, 2023) with a well-described neurotropic virus to model the effect of IFN-β in the context of MS and viral encephalitis.

I built on previous findings in the lab that IFN-β is upregulated by microglia following treatment with the lipid-reactive IgM O4. As synthesis of lipid-reactive IgM in MS patients is associated with a decrease in JCV infectivity (Villar *et al.*, 2015), I hypothesised that this IFN-β upregulation is at contributing to this antiviral effect.

As mentioned in **1.3.6**, SFV is an appropriate model virus for JCV as they have a similar pathogenesis. JCV, and other polyomaviruses, could not be used as these are human obligate pathogens which do not replicate in murine cells.

The above aims were achieved using real-time quantitative PCR (RT-qPCR), enzyme linked immunosorbent assay (ELISA) and Luminex to identify an optimal dose of IFN-β. To ascertain the transcriptional profile of individual cell types in the CNS cultures, I optimised a fluorescence assisted cell sorting (FACS) protocol to separate the major CNS cell types grown in the cultures. Single cell-type populations were analysed using RNAseq and pathway analysis performed on the differentially expressed genes. Efficacy of IFN-β and oligodendrocyte specific candidates was assessed using flow cytometry and immunocytochemistry for virus positive cells, alongside plaque assays for viral titre, and RT-qPCR for quantity of viral RNA.

Together, these aims identified that IFN-β and blocking IL-10R have antiviral properties, and therefore identified avenues for future drug development against neurotropic viruses.

# Chapter 2

## Materials and Methods

# 2.0 Materials and Methods

## 2.1 Cell culture

All cell culture procedures were performed in sterilised laminar flow cabinets, except for animal dissections. All materials required were sterilised with 70% methylated spirits before entering the cabinet. Cells were maintained in a humidified incubator at 37°C with 7% $CO_2$ unless otherwise stated.

### 2.1.1 Animal sources

Primary cultures were generated from C57BL/6 or CD45.1 C57BL/6 wildtype (WT) mice (Charles River and Envigo). All animal experiments conformed to the animal care and welfare protocols approved by University of Glasgow, carried out under the UK Home Office Project License PP6655603. Mice were maintained at the University of Glasgow Central Research Facility and the Wolfson Research Facility under a 12-hour light/dark cycle with food and water *ad libitum*.

### 2.1.2 Myelinating cultures

Mice were time-mated and pregnant females culled at E13.5 by rising $CO_2$ concentration, after which death was confirmed by severing the femoral artery. Embryos were excised from the amniotic sac and the spinal cords were extracted. The meninges were removed from each spinal cord and discarded, and the cords were placed in 1 mL Hank's Balanced Salt Solution without calcium ($Ca^{2+}$) or magnesium ($Mg^{2+}$) ($HBSS^{-/-}$, Sigma), with no more than 6 cords per mL. The cords were enzymatically digested with 200µL 10x trypsin (porcine pancreas, Sigma) for 15 minutes at 37°C. Enzyme activity was inhibited with 2mL SD inhibitor (Leibovitz's L-15 medium (Gibco™), 0.52mg/ml soybean trypsin inhibitor, 40 µg/ml DNase I from bovine pancreas, and 3mg/mL BSA (all Sigma)). The cords were triturated by increasing gauge needles, centrifuged at 200 x *g* for 5 minutes and resuspended in plating media (50% high glucose DMEM (Gibco™), 25% horse serum (Gibco™), 25% $HBSS^{+/+}$ (Sigma)) at a concentration of $1.8x10^6$ cells/ml, cell counts obtained using Luna cell counter. 100µL cell suspension was placed onto 14mm coverslips coated with boric-acid containing poly-l-lysine (13.2µg/mL in boric acid buffer, pH 8.4). Three

coverslips were contained in a 35mm petri dish, and incubated 2-4 hours to allow cells to adhere. Dishes were topped up with 300 µL plating media and 600 µL differentiation media containing 10µg/mL insulin (high glucose DMEM with L-glutamine and sodium pyruvate (Gibco$^{TM}$), 10ng/mL biotin, 50nM hydrocortisone, 0.005x N1 media supplement). Cells were fed every 2-3 days by removing 500µL old media and replacing with 600µL of fresh differentiation media containing insulin. From Day *in vitro* (DIV) 12, cells were fed with differentiation media without the additional insulin (DM-). These cultures were used initially to investigate the effect of different antibodies on the lipid-reactive IgM response.

### 2.1.3 CNS cultures

Mice were time-mated and pregnant females culled at E17 by rising $CO_2$ concentration, death confirmed by femoral artery severing. Embryos were excised from the amniotic sac and immediately decapitated, with the heads being stored in HBSS$^{-/-}$ on ice. The brains were excised from the skull, the meninges removed and discarded, before being stored in 2mL HBSS$^{-/-}$, with no more than 4 brains per 2mL. The brains were processed in a similar manner as the myelinating cultures discussed above with some slight modifications. Brains were digested with 250µL 10x trypsin per 2mL HBSS$^{-/-}$, and inhibited with 2mL SD inhibitor. The brains were triturated, centrifuged at 250 x *g* for 5 mins before being resuspended in plating media at a concentration of 1.8x10$^6$ cells/mL, cell counts obtained using Luna cell counter. Cells were either plated on poly-l-lysine coated coverslips (same as above), in poly-l-lysine coated 6 well plates (1mL cells), or in poly-l-lysine coated 96 well plates (50µL cells per well) and incubated for 2-4 hours to allow cells to adhere. Once adhered, coverslips were topped up as above, 6 well plates had 400µL media removed and 600µL DM+ added, and 96 well plates had 60µL DM+ added to each well. Cells were fed and maintained as above for the myelinating culture protocol.

### 2.1.4 Microglial cultures

Postnatal day 1 CD45.1 C57BL6/J ice were euthanised by lethal intraperitoneal injection of euthatal, and death confirmed by femoral artery severing. Mice were decapitated, heads submerged in 70% ethanol on ice and immediately transferred to a 50mL centrifuge tube containing L-15 media (Gibco$^{tm}$, no supplements) and kept on ice until brain dissection. Brains were excised from the skull and meninges removed before being placed in 2mL L-15

on ice, with no more than 4 brains per 2mL L-15. Once all brains were dissected, the brains were gently triturated with a P5 stripette and transferred to a 50mL centrifuge tube and centrifuged at 2500 x *g* for 5 minutes. The supernatant was discarded and 10mL fresh L-15 media added. The cell suspension was lightly triturated with a P5 stripette before being centrifuged at 2500 x *g* for 5 mins. The supernatant was discarded and cells were resuspended in 10 mL pre-warmed glial media (DMEM, high glucose, L-glutamine (Gibco$^{TM}$), 10% FCS, 1% Pen/Strep). Cell suspension was added to a T-75 flask containing 20mL pre-warmed glial media supplanted with 5ng/mL GM-CSF and incubated for 7 days. Media was removed and replaced with 30mL pre-warmed glial media for another 7 days. The flasks were placed in a 37°C pre-warmed shaking incubator at 100rpm for 1 hour. The media containing the microglia was removed, placed in a 50mL centrifuge tube, and centrifuged at 2500 x *g* for 5 minutes and the supernatant discarded. Cells were resuspended in microglial pre-treatment media (DMEM (high glucose, L-glutamine) supplanted with 10% horse serum and 1% Pen/Strep) at a concentration of 1x10$^6$ cells/ml. Cells were plated either on uncoated glass coverslips (100µL per coverslip) for microscopy or into 6 well plates (1mL per well) for mRNA analysis, after which microglia were allowed to adhere overnight before treatments. Treatments were performed in fresh microglial treatment media (DMEM (high glucose, L-glutamine, supplemented with 1% Pen/Strep).

### 2.1.5 Bone marrow derived macrophages

Tibia and femurs were collected from culled mice and excess tissue removed. The cleaned bones were taken to a sterile laminar flow cabinet and dipped quickly in 70% ethanol. Both ends of the bones were cut and the bone marrow flushed out with 5mL DMEM (supplanted with 10% FCS (Gibco$^{TM}$)) by a 5mL syringe with a 23G needle. The cell suspension was lightly titrated before being filtered through a 70µL cell strainer into a 50mL centrifuge tube and centrifuged at 300 x *g* for 5 minutes. The supernatant was discarded and the pellet resuspended in 1mL ACK lysis buffer (Gibco$^{TM}$) to lyse the red blood cells. Cells were centrifuged at 300 x *g*, supernatant discarded, and resuspended at 5x10$^6$ cells/mL in GMEMcult (GMEM, 10% FBS, 1% non-essential amino acids, 2mL L-glutamine, 1mM sodium pyruvate, 0.1mM beta-mercaptoethanol, 15% L929 conditioned media (kindly donated by Robin Bartolini)). In a 90mm petridish 10mL of cells were were plated for 4 days. The cells were washed with 1x dPBS (dulbeccos phosphate buffered saline), and 10mL fresh GMEMcult was added. Differentiated macrophages were lifted between days 5-7 by TrypLe

Select (Gibco™) and plated out in 6 well plates at $1.8x10^6$ cells per well to study mRNA upregulation.

## 2.2 Virus production, purification, and infection

### 2.2.1 Semliki Forest virus (SFV) electroporation in BHK cells

Different strains of SFV plasmids were kindly generated and provided by Andres Merits, University of Tartu. One T150 flask of BHK cells was grown in GMEM culture media (GMEM CM, GMEM supplemented with 5% FCS, 10% tryptose phosphate broth, 1% Pen/Strep, Gibco™), before being lifted with Trypsin-EDTA (Gibco™). The cells were centrifuged at 400x g for 5 minutes before being resuspended 400µL ice cold dPBS. 3µg plasmid was electroporated using 2 pulses of 850V for 0.4ms into the BHK cells before being incubated in a fresh T150 flask containing 25mL GMEM CM until severe cytopathic effect was observed (3-4 days post electroporation). The virus-containing supernatant was centrifuged at 500 x *g* for 30 minutes to remove debris before purification via column exclusion. Add 23g/L NaCl and 70g/L PEG 8000 to the supernatant containing virus and incubate at 4°C for [[how long]] with gentle shaking. Centrifuge suspension at 4000 x *g* for 30 minutes and discard supernatant as the PEG-bound virus is found in the pellet. The pellet was resuspended in 12mL TNE ($dH_2O$ supplemented with 1mM EDTA, 500mM NaCl, 10mM Tris-Cl) before centrifuged through Amicon Ultra-15 100kDa filter device at 4000 x *g* for 30 minutes. If volume remaining is 500µL, store aliquot at -80°C, if volume remaining is more than 500µL, centrifuge for a further 15 minutes before storing at -80°C. The virus stocks were quantified by plaque assay (described below).

### 2.2.4 Quantification of virus plaque forming units by plaque assay

BHK cells were grown in multiple T150 flasks until confluent and subsequently seeded at a 1:3 dilution in a 24 well plate. To quantify the stocks, the virus was serially diluted in PBS-A (dPBS with 0.75% BSA added) from $x10^{-2}$ to $x10^{-8}$ and 100µL added to the cells in the 24 well plate for 1 hour on a shake plate under gentle agitation. The virus was removed and disposed into 2% Virkon (Antec™) The cells were covered with 50% 2.4% Avicel in dPBS and 50% 2x MEM (minimum essential medium, supplanted with 4% FCS and 2% PenStrep), and incubated at 37°C for 2 days. Cells were fixed with 4% formaldehyde for 1 hour, and stained

with 0.1% toluidine blue (Sigma) for one hour. The concentration of plaque-forming units (PFU) was calculated from the counted number of plaques as follows:

$$pfu/mL = ((count\ of\ plaques)/(10\text{^}(dilution\ factor)))/(inoculum\ in\ ml)$$

### 2.2.5 Infection of culture media by different viruses

Cells were pre-treated as and how the experiment needed. The media was removed and replaced with either 0.75% PBS-A or SFV6 in 0.75% PBS-A (MOI=0.03). Cells were placed on a shake plate for 1 hour under gentle agitation before inoculum was removed and fresh DM- added. Cells were returned to the incubator for 2-96 hours, after which supernatants were collected for plaque assays, ELISA or Luminex, cells were lysed with TRIzol for RNA analysis, or coverslips were washed with 0.75% PBS-A and fixed with 4% PFA for 15 minutes. Once fixative was removed, coverslips were stored in 0.75% PBS-A at 4°C until stained for immunocytochemistry.

### 2.2.6 *in vivo* infections

Mice were pre-treated as and how the experiment needed and infected using intranasal administration of virus. Briefly, mice were anaesthetised in a chamber with isoflurane gas. Once unresponsive, the mice were removed from the chamber and 30µL containing $1x10^5$ PFU was dropped onto the nostrils using a pipette, alternating droplets between nostrils. Once the full volume was administered, mice were returned to their cage and monitored until recovered from anaesthesia. Mice were culled 48 hours post infection by rising $CO_2$ concentration. Olfactory bulb, cortex, cerebellum, spinal cord, and pancreas were removed to quantify viral titre by plaque assay and viral RNA by RT-qPCR, both described below.

## 2.3 Treatments

### 2.3.1 Antibody treatments

Preparations of antibodies were tested for antiviral activity in DIV24 myelinating cultures, DIV24 CNS cultures, or DIV14 solo microglial cultures. The cultures were treated with 20µg/mL Pentaglobin (negative control IgM, supplied kindly by Lorna Hayden) or rhIgM22 (recombinant human IgM22, supplied kindly by Arthur Worthington and Moses Rodriguez)

for 4-24 hours to assess the upregulation of interferon stimulated genes (ISGs). As a positive control, high molecular weight polyinosinic:polycytidylic acid (poly I:C) was used at 5µg/mL in myelinating cultures, or 10µg/mL in CNS cultures or microglia. For a vehicle control either dPBS or DMSO was used depending on what the antibody was reconstituted in. Treatments were added directly to the dish or well the cultures were growing in.

### 2.3.2 pHrodo™ tagging of antibodies and proteins

pHrodo™ was reconstituted in DMSO at a concentration of 10.2mM and stored in 10µL aliquots at -20°C . The antibody was diluted to a concentration of 1mg/mL in endotoxin-free dPBS. 10µL pHrodo™ was added to 100µL antibody and mixed gently by pipetting. The mixture was incubated for 1 hour at RT in the dark. To purify the protein, the mixture was added to an Amicon® Ultracel® 50k centrifugal filter., before being diluted with 2mL endotoxin-free dPBS and centrifuged at 4000 x *g* for 10 minutes. The tagged-antibody was washed a further 2x with 4mL endotoxin-free dPBS, before the mixture being resuspended to a final volume of 100µL and stored at 4°C until needed for treatments.

### 2.3.3 Interferon beta treatments

The activity of Interferon beta (IFN-β) was tested for antiviral activity in DIV21 CNS cultures. The cultures were treated with concentrations ranging between 0.1pg/mL and 100ng/mL to determine an effective dose, which was found to be 50ng/mL. As a positive control high molecular weight polyinosinic:polycytidylic acid (poly I:C) was used at 5µg/mL in myelinating cultures, or 10µg/mL in CNS cultures or microglia. For a vehicle / negative control dPBS was used. The treatments were added directly to the dish or well the cultures were growing in.

### 2.3.4 Oligodendrocyte identified target treatments.

The activity of the oligodendrocyte RNAseq identified targets (*Drd4*, *Il10ra*, *Erap1*) were tested for antiviral activity in DIV 21 CNS cultures. These targets were tested using pharmacological manipulators as follows: 20µg/mL dopamine hydrochloride (*Drd4*, Sigma), 1µg/mL IL-10R blocking antibody (*Il10ra*, Absolute antibody, kindly supplied by Dr Georgia Perona-Wright), and 25µg/mL ERAP1-IN-1 (chemexpress). As a positive control poly(I:C)

was used at 10µg/mL. For a vehicle control for ERAP1-IN-1 DMSO was used at 0.1% in dPBS, and for the other two dPBS was used. The treatments were added directly to the dish or the well the cultures were growing in.

### 2.3.5 *in vivo* treatments

The efficacy of IFN-β and IL-10R blocking antibody as antiviral therapies were tested *in vivo*. Briefly, 24 hours pre-infection mice were anaesthetised in a chamber with isoflurane gas. Once unresponsive, the mice were removed from the chamber and 10µL of either 100µg/mL IFN-β in dPBS or 50mg/mL IL-10R blocking Ab in dPBS were dropped onto the nostrils using a pipette, alternating droplets between nostrils. For a vehicle control dPBS was administered. Once the full volume administered, mice were returned to their cage and monitored until recovered from anaesthesia. This process was repeated 24 hours post infection.

## 2.4 Molecular Biology

### 2.4.1 RNA isolation

RNA was extracted using one of two protocols. For all experiments aside from the FACS sorted cells, the RNA was isolated using the PureLink RNA mini kit (Invitrogen) as per manufacturers instructions. The first steps need to be performed in a chemical fume hood. The cells were lysed in a quantity of TRIzol reagent for 20 minutes at RT, and either stored at -80°C until use or immediately processed. 200µL chloroform (Fisher scientific) was added to 1mL TRIzol lysate, vigorously shaken and allowed to incubate for 1-2 mins at RT. The lysate was span at 12,000 x *g* for 15 mins at 4°C before the top clear layer was collected. This clear phase was mixed with an equal volume 70% ethanol before being transferred to the kit's spin columns. Samples were spun at 12,000 x *g* for 15 seconds and then washed with 500µL Wash Buffer I. To remove any contaminating genomic DNA (gDNA), samples were incubated with 80µL DNase I for 15 minutes at RT. Samples were subsequently washed with 500µL Wash Buffer I, and once with 750µL Wash Buffer II. The membrane was dried by spinning at 12,000 x *g* for 3 minutes, and the RNA eluted into a 1.5mL RNase free tube in 30µL RNase free water. RNA was immediately quantified and converted to cDNA, with any surplus RNA stored at -80°C.

For the FACS sorted cells, the RNA was isolated using the RNeasy® Plus Micro Kit (Qiagen) as per manufacturers instructions. Cells were centrifuged at 500 x *g* for 10 minutes, supernatant discarded, and the pellet resuspended in 600µL RLT buffer + 0.6µL beta-mercaptoethanol. The cells were disrupted by vortex mixing for 10 seconds before being mixed with an equal volume 70% ethanol. This mixture was transferred to the kit's spin columns and span at max speed for 15 seconds and then washed with 350µL Buffer RW1. Any contaminating gDNA was removed using the same procedure as above. The column was washed with 350µL Buffer RW1, and then once more with 500µL Buffer RPE. Finally, the column was washed with 500µL 80% ethanol and the membrane dried by spinning the column at max speed for 5 minutes with the lid open. The RNA was eluted in 14µL RNase free water into an RNase free 1.5mL collection tube and immediately stored at -80°C before being shipped for sequencing.

### 2.4.2 cDNA generation

cDNA was generated from up to 500ng RNA using the High Capacity cDNA Reverse Transcription Kit (Applied Biosciences) following manufacturer's instructions using a thermal cycler. To ensure consistency, each experiment used the same quantity of RNA for all conditions. A maximum of 10µL RNA was added to a 200µL PCR tube (Star Lab), the remaining volume up to 10µL was made up with RNase free water. 10µL RT mix (1µL reverse transcriptase, 0.8µL dNTPs, 2µL random primers, 2µL RT buffer, 4.2µL RNase free water) was added to each column before being incubated at 37°C for 1 hour. cDNA was diluted to an appropriate volume (1:20 for 500ng starting RNA, meaning 180µL RNase free water) before being stored at -20°C.

### 2.4.3 Primer design

For use in RT-qPCR gene target primers were designed. Briefly, primers are designed using Primer 3 (available online http://bioinfo.ut.ee/primer3-0.4.0/), and had to satisfy primer specification requirements: between 18 to 23 base pairs in length, between 40 and 65% GC content; Tm of primers within 59.5 and 61, maximum 3' self-complementarity of 1; amplicon (amplified region of genomic material) less than 150bp, and preferably no GC clamp at the 5' or 3' end, and preferably no more than 4 G or C bases in a row. Two primers

outside of this region are used to generate primers that are used to create standards, a positive control for your gene of interest. BLAST analysis is used on the primer sequences to ensure they are specific for the gene of interest alone and that no splice variants exist. To test for specificity, a standard PCR (described in 2.4.4) using cDNA known to contain the gene of interest is performed and visualised with ultraviolet light. If a single band exists, PCR specificity has been achieved. Primer sequences used for qPCR can be found in Table 2.1.

### 2.4.4 Polymerase Chain Reaction (PCR) and gel electrophoresis of primers

To amplify standards, test primer pairs before use in RT-qPCR, and for genotyping of genetically modified embryos, end point PCR was performed. For generating the PCR mixture, 2µL primer-mix (1:1 forward:reverse primers at 100µM), 3µL cDNA and 45µL REDTaq ReadyMix™ PCR reaction mix (sigma) were mixed in a 200µL PCR tube. The PCR tube was added to a 2720 Thermal Cycler (applied biosciences) with the following settings: 50°C for 5 minutes, 95°C for 5 minutes, followed by 40 cycles of 95°C for 15 seconds, 55°C for 1 minute, and 95°C for 15 seconds. To ensure the correct PCR fragment was amplified, the samples were ran on an agarose gel and imaged. 2g UltraPure™ Agarose (Invitrogen) was dissolved in 100mL 1x TAE buffer (40nM Tris Base, 20mM acetic acid, 1mM EDTA, in $dH_2O$ by heating. Once the agarose had dissolved, 6µL SYBR Safe™ was added and the solution was swirled to mix before poured into a gel tray and allowed to set for a minimum of 30 mins. Either 5µL amplified standard primers or 40µL genotyped samples and 5µL 100bp DNA ladder (Promega) were loaded into individual wells of the gel. Gels were subsequently ran at 120 V with fixed current for 1 hour and imaged with ultraviolet light.

### 2.4.5 Reverse Transcription quantitative PCR (RT-qPCR)

Quantitative real time-PCR was performed in triplicate in Starlab 384-well PCR plate . For each well, 3µL cDNA was added, along with 0.15µL primer mix (1:1 dilution of forward:reverse primers at 100µM), 4µL RNase free water, 5µL SYBR™ Green PCR Master Mix (Avantor). Plates were ran in an applied biosystems QuantStudio 7 Flex, and data quantified using either the comparative CT (ΔΔCT) method or using a standard curve to determine relative expression. Cycle settings for the machine were as follows: 50°C for 2 minutes, 95°C for 10 minutes, then 40 cycles of 95°C for 15 seconds, 60°C for 1 minute. To

end, a melt curve was generated using the following cycle settings, 95°C for 15 seconds, 60°C for 1 minute, then slowly increase temperature 0.05°C/s up to 95°C. Either *Gapdh* or *18S* were used as housekeeping genes.

### 2.4.6 Enzyme linked immunosorbent assay (ELISA)

The supernatant from CNS cultures were collected and 200µL stored in a 96 well plate at 80°C for further analysis. The following cytokines and interferons were analysed using BioTechne's DuoSet ELISA kits according to manufacturers instruction: CCL5, and IFN-β. Samples were measured in triplicate 1:10 dilution with dPBS. The wells of a 96 well plate were coated with a capture antibody overnight at RT. In between each step the wells were washed with wash buffer (dPBS with 0.05% Tween 20). The wells were then blocked for 2 hours with assay reagent diluent (1% dPBS with BSA). Following, the supernatant and a control standard that was serially diluted were added to the wells and incubated either for 2 hours at RT or overnight at 4°C. A monoclonal detection antibody specific to the protein in question was added and incubated for 1 hour. An antibody specific to the detection antibody containing HRP-peroxidase was added for 1 hour. A colour change solution containing TMB is added, with the colour developing in proportion to the quantity of protein bound in the first step. To stop the reaction, 1M $H_2SO_4$ was added. To read the concentration, an optical plate reader set to 450nm with compensation at 570nm was used. A best fit curve was plotted for the standard curve to extrapolate the concentration of total protein from the equation of the line of best fit.

### 2.4.7 Bicinchoninic Acid Assay (BCA)

A BCA assay can determine the concentration of protein for further analysis and quantification. A Pierce BCA protein assay (Thermofisher) was followed according to manufacturer's instructions. Samples were measured in duplicate. Prewarm a 96 well plate to 37°C in an incubator. Serially dilute 2mg/ml albumin down to 20µg/ml using dPBS (Gibco™). Add 25µL standard or supernatant into a 96 well plate, and add 200µL working reagent (1 part BCA reagent B, 50 parts BCA reagent A). Incubate at 37°C for 30 minutes. Cool plate to RT, and measure the absorbance at 562nm. Extrapolate concentration of the protein from the line of best fit equation of the standard curve.

### 2.4.8 Luminex

A Luminex assay can determine the concentration of multiple proteins simultaneously. The following chemokines, cytokines, and secreted proteins were analysed using Luminex® multiplex beads (RnD Biosciences): GMCSF, CXCL1, CCL2, CCL3, CCL4, CCL5, CCL7, CCL11, CCL19, CCL20, CCL21, CCL22 CXCL2, CXCL10, CXCL12, CXCl13, CXCL16, IL-1a, IL-3, IL-4, IL-5, IL-6, IL-7, IL-10, IL-13, IL-16, IL-17, IFN-γ, and IGBP3. Samples were measured using manufacturers' instructions. Begin by preparing all reagents as instructed. Add 50µL of either standard of a known concentration for all proteins to be measured or sample to each well. Subsequently add 50µL of diluted Microparticle Cocktail to each well and incubate for 2 hours at RT on shaker set to 800 rpm. From this point on between all steps the samples were washed 3x with wash buffer (dPBS with 0.05% Tween-20), and any incubation steps are on the shaker at RT at 800 rpm. Add 50µL diluted Biotin-Antibody cocktail to each well and incubate for 1 hour. Add 50µL diluted Steptavidin-PE to each well and incubate for 30 mins. Add 100µL wash buffer to each well and incubate 2 minutes. Read plate using Luminex analyser.

### 2.4.9 Endotoxin quantification

To determine endotoxin LPS contamination, a Pierce LAL Endotoxin Quant Kit (Thermofisher) was used according to manufacturer's instructions. First pre-warm a 96 well plate to 37°C in an incubator for 10 minutes. Add 50µL of LPS standard or sample to each well, with each sample measured in triplicate. Add 50µL LAL reagent to each well. Once samples were added the plate was gently tapped to mix and returned to the incubator for 10 minutes, measured from the time of adding the first sample. 100µL pre-warmed chromogenic substrate solution was added to each well, gently tap side, return to incubator for 6 minutes. Add 100µL stop reagent (25% acetic acid), gently tap, and measure the absorbance at 405nm on a plate reader. Extrapolate concentration of the LPS from the line of best fit equation of the standard curve.

## 2.5 Flow cytometry

Antibodies used for flow cytometry can be found in **Table 2.4**. All fluorescence minus one (FMO) staining controls received the full panel staining except for one antibody to allow for

the true population to be able to be gated. FMOs were generated from surplus, pooled cells. Controls and FMOs were stained in 96 well, round bottom plates (Corning), and depending on the analysis method the samples were either stained in a 96 well, round bottom plate (flow cytometric analysis on BD Fortessa) or in 1.5mL RNase-free tubes (FACS to isolate individual cell populations). Compensation beads were stained immediately before setting up the flow cytometer or FACS machine. Flow cytometry was performed at the Flow Core Facility (University of Glasgow) for sorting on the FACS Aria IIu, FACS Aria III, or the Sony MA-900, or flow cytometric analysis on BD fortessa. All analysis performed using FlowJo (v10.9).

### 2.5.1 Lifting and homogenising CNS cultures

The media was removed from the cultures, washed 2x with dPBS (Gibco$^{TM}$) before 1mL 0.05% Trypsin-EDTA (Gibco$^{TM}$) was added. As this is a different methodology from the usual Papain dissociation used for neural cells, 0.05% Trypsin-EDTA was confirmed to be a viable method for generating a single cell suspension through testing a range of conditions that is covered in **Chapter 4**. The cultures were incubated at 37°C for 20-30 minutes before the trypsinisation was inhibited by 1mL DM- media. The cells were very gently triturated with a wide bore pipette tip to lift from the bottom before being transferred to a 50mL centrifuge tube. The cells were span at 400 x *g* for 5 minutes and the supernatant discarded. The cells were resuspended in 400µL FACS buffer (dPBS, 0.5% FCS, 0.4% 0.5M EDTA) before the staining protocol.

### 2.5.2 Flow cytometry staining

CNS *in vitro* cultures were stained with the following protocol. The lifted cultures were added into either 96 well plates (100µL diluted surplus cells per control) or into a 1.5mL centrifuge tube (at least 400µL cells), and span down at 400 x *g* for 5 minutes at 4°C. The following steps were performed, with a wash with FACS buffer and centrifuge spin (400 x *g* for 5 mins at 4°C) unless stated otherwise, and all steps performed at 4°C; Live/dead stain in dPBS, 15 minutes; Fc block in FACS buffer, 5 minutes (no wash or centrifuge), conjugated antibodies in FACS buffer, 20 mins, extra wash step, resuspension in 200µL FACS buffer. Samples that were infected with virus were stained in a sterile laminar flow hood and fixed

using BD Cytofix™ Fixation Buffer (BD Biosciences) for 20 minutes before analysis on BD fortessa.

All samples were gated initially on forward scatter (FSC) and side scatter (SSC) to select cells, followed by FSC-height (FSC-H) and FSC-area (FSC-A) to exclude doublets, and Live/dead to exclude dead cells. Individual gating strategies shown for each individual experiment.

### 2.5.3 Fluorescence assisted cell sorting (FACS)

All samples were gated according to the cells to be sorted. The cell populations for microglia ($CD11b^+CD45^+$), oligodendrocytes ($CD11b^-CD45^-O4^+$), astrocytes ($CD11b^-CD45^-O4^+ACSA\text{-}2^+$), and neurons ($CD11b^-CD45^-O4^+ACSA\text{-}2^+$) were gated and the machine set to sort in a 4 way sort into 5mL FACS tubes. The cells were sorted on either an FACS Aria machine (BD) or the Sony MA-900 into 1mL 50% FCS/ 50% dPBS. The cells were immediately diluted with FACS buffer to a final volume of 5mL and centrifuged at 500 x *g* for 10 minutes, and the supernatant discarded.

## 2.6 Immunohistochemistry

Cells were fixed by removing all media and adding 4% paraformaldehyde (PFA) for 15-20 minutes at RT. Coverslips were then stored in 1x dPBS at 4°C until being processed. PFA-fixed cells were permeabilised with 0.5% Triton-X (Sigma) in dPBS for 15-20 minutes at RT. Coverslips were washed 3x in dPBS, before being blocked with blocking buffer (dPBS (Gibco™, 10% horse serum (Gibco™), 1% BSA (Sigma) for 1 hour at RT. Coverslips were then incubated in primary antibodies (Table 2.2) diluted in blocking buffer for 1 hour at RT. Coverslips were washed 3x in dPBS before being incubated in secondary antibodies (Table 2.3) for 20 mins at RT in the dark. Coverslips were washed 3x in dPBS and 1x in $dH_2O$ before being mounted onto glass slides with Mowiol 4-88 mounting medium (0.13M Tris, pH 8.5, 33% w/v Mowiol 4-88 (Sigma), 13.2% w/v glycterol (Sigma), 0.05% v/v DAPI (Invitrogen)). Mounted slides were stored at 4°C in the dark until analysed.

## 2.7 Image capture

All coverslips were imaged on an AxioImage M2 (Zeiss) fluorescent microscope. 10 images were taken per coverslip, and 3 coverslips were used per biological replicate. Slides were blinded by someone in the lab by obscuring the information, with the information of what each slide contains written down and put aside until all imaging and quantification has been completed. Cell counts for the different experimental conditions were all quantified using multiple CellProfiler pipelines (based on https://github.com/muecs/cp/tree/v1.1). Cell counts displayed as cells/$mm^2$ or percentage field of view.

## 2.8 RNAseq

RNA isolated from the FACS sorts were analysed by RNAseq. The samples were sent to Novogene on dry ice overnight. Results were returned for in-house analysis. Initial analysis was graciously provided by John Cole, which included the following steps. The fastQ files were quality control checked using FastQC (Andrews, GitHub, v0.11.7) and then aligned to the reference genome and transcriptome GRCm39 (release 108) using STAR (v2.6) (Dobin et al. 2013). Read counts were merged and genes with a mean of < 1 read per sample were excluded. We used the SVA (v4.3) function combat-seq to correct for mouse specific batch effects. Mouse was the batch covariate and cell type + treatment the protected. The expression and differential expression values were generated using DESeq2, under default settings (v1.24) (Love, Huber, and Anders 2014). All comparisons were performed pairwise, with no additional covariates. Initial graphs for analysis were also provided by John Cole using the DESeq2 data generated of differentially expressed genes.

Subsequent pathway enrichment analysis was performed using the Database for Annotation, Visualisation, and Integrated Discovery (DAVID). Pathways enrichment analysis performed includes gene ontology (GO), Kyoto encyclopaedia of genes and genomes (KEGG), and Reactome. When discussing RNAseq analysis the terms *p.adj* and log2fold are used frequently. The *p.adj* value stands for the adjusted *p*-value, which means the *p*-value has been adjusted to compensate for multiple statistical tests being performed simultaneously. The log2fold stands for the log2 manipulation of the fold-change in expression.

## 2.9 Statistics

Details of the individual statistics performed, including n-values are reported in the figure legends. All statistical analysis unless stated otherwise was performed with GraphPad Prism 9. Unless stated otherwise n represents biological replicates. For cell culture experiments, individual biological replicates are repeats from embryos from different pregnant dams, with one dam contributing 1 biological n. Statistical significance was determined using one of the following tests, depending on sample numbers and variable: two-tailed t-test, one-way ANOVA, or two-way ANOVA. Data was interpreted as significant when p-value was less than 0.05, and are shown in figures as *$p$<0.05, **$p$<0.01, ***$p$<0.005, ****$p$<0.001

**Table 2.1 – qPCR Primers**

| Gene Target | Species | Forward Primer Sequence | Reverse Primer Sequence |
|---|---|---|---|
| *18s* | Mouse | GACTCAACACGGGAAACCTC | TAACCAGACAAATCGCTCCAC |
| *Ifnb1* | Mouse | CACAGCCCTCTCCATCAACT | GCATCTTCTCCGTCATCTCC |
| *Cxcl10* | Mouse | GCTCAAGTGGCTGGGATG | GAGGACAAGGAGGGTGTGG |
| *Ccl5* | Mouse | ACACACTTGGCGGTTCCTT | CTGCTGCTTTGCCTACCTCT |
| *Oasl1* | Mouse | AGGGGGTGTGAGAAGTCGT | GATTGGTTAGGAAGATGGTTTGG |
| *Mx1* | Mouse | GGTCGGCTTCTGGTTTTGT | TGATGGGTGGTGGGCTAA |
| *Ifit2* | Mouse | CAATCCCTTCATCCCCACT | TCTCCCTACTCTGCCCTCCT |
| *Rsad2* | Mouse | AAATGTGGCTTCTGCTTCCA | CCAAGTATTCACCCCTGTCCT |
| *Isg15* | Mouse | CGCAGACTGGCACGCTTA | CTCGAAGCTCAGCCAGAACT |
| *Isg20* | Mouse | CGCCTGCTACACAAGAACAT | TGACCATTCCGACATAGAGC |
| *E1* | SFV Virus | CGCATCACCTTCTTTTGTG | CCAGACCACCCGAGATTTT |

**Table 2.2 - Primary antibodies for immunocytochemistry**

| Description | Manufacturer | Isotype | Dilution |
|---|---|---|---|
| Anti-Iba1 | Wacko | Rabbit IgG | 1:500 |
| Anti-CNP | Abcam | Mouse IgG1 | 1:800 |
| Anti-GFAP | Invitrogen | Rat IgG2a | 1:2000 |
| Anti-NeuN | Invitrogen | Rabbit IgG | 1:300 |
| Anti-Smi31 | BioLegend | Mouse IgG1 | 1:1000 |
| Anti-MBP | Bio-Rad | Rat IgG | 1:500 |
| Anti-Nestin | Millipore | Mouse IgG1 | 1:500 |
| Anti-NG2 | Sigma | Rabbit IgG | 1:500 |

**Table 2.3 – Secondary antibodies for immunocytochemistry**

| Description (clone) | Manufacturer | Isotype | Dilution |
|---|---|---|---|
| Anti-Mouse IgG, IgM (H+L) Secondary antibody, Alexa Fluor 488 | Invitrogen | Goat IgG | 1:1000 |
| Anti-Mouse IgG1, IgM (H+L) Cross-Adsorbed Secondary antibody, Alexa Fluor 488 | Invitrogen | Goat IgG | 1:1000 |
| Anti-Mouse IgG2a, IgM (H+L) Cross-Adsorbed Secondary antibody, Alexa Fluor 488 | Invitrogen | Goat IgG | 1:1000 |
| Anti-Mouse IgG, IgM (H+L) Secondary antibody, Alexa Fluor 568 | Invitrogen | Goat IgG | 1:1000 |
| Anti-Mouse IgG1, IgM (H+L) Cross-Adsorbed Secondary antibody, Alexa Fluor 568 | Invitrogen | Goat IgG | 1:1000 |
| Anti-Mouse IgG2a, IgM (H+L) Cross-Adsorbed Secondary antibody, Alexa Fluor 568 | Invitrogen | Goat IgG | 1:1000 |
| Anti-Mouse IgG, IgM (H+L) Secondary antibody, Alexa Fluor 647 | Invitrogen | Goat IgG | 1:1000 |
| Anti-Mouse IgG1, IgM (H+L) Cross-Adsorbed Secondary antibody, Alexa Fluor 647 | Invitrogen | Goat IgG | 1:1000 |
| Anti-Mouse IgG2a, IgM (H+L) Cross-Adsorbed Secondary antibody, Alexa Fluor 647 | Invitrogen | Goat IgG | 1:1000 |
| Anti-Rat IgG, IgM (H+L) Cross-Adsorbed Secondary antibody, Alexa Fluor 488 | Invitrogen | Goat IgG | 1:1000 |
| Anti-Rat IgG, IgM (H+L) Cross-Adsorbed Secondary antibody, Alexa Fluor 568 | Invitrogen | Goat IgG | 1:1000 |
| Anti-Rat IgG, IgM (H+L) Cross-Adsorbed Secondary antibody, Alexa Fluor 647 | Invitrogen | Goat IgG | 1:1000 |
| Anti-Rabbit IgG, IgM (H+L) Cross-Adsorbed Secondary antibody, Alexa Fluor 488 | Invitrogen | Goat IgG | 1:1000 |
| Anti-Rabbit IgG, IgM (H+L) Cross-Adsorbed Secondary antibody, Alexa Fluor 568 | Invitrogen | Goat IgG | 1:1000 |
| Anti-Rabbit IgG, IgM (H+L) Cross-Adsorbed Secondary antibody, Alexa Fluor 647 | Invitrogen | Goat IgG | 1:1000 |

**Table 2.4 – Antibodies for flow cytometry**

| Description | Fluorophore | Clone | Manufacturer | Target | Dilution |
|---|---|---|---|---|---|
| Viability Dye | APC-Cy7 | | BD Biosciences | Live/Dead | 1:1000 |
| CD45 | BV605 | 30-F11 | BD Biosciences | Microglia | 1:40 |
| CD45 | BUV395 | 30-F11 | BD Biosciences | Microglia | 1:40 |
| CD11b | PE-Cy7 | M1/70 | BD Biosciences | Microglia | 1:40 |
| CD11b | BV785 | M1/70 | BD Biosciences | Microglia | 1:40 |
| O4 | APC | O4 | Miltenyi | Oligodendrocytes | 1:40 |
| ACSA-2 | PE | REA969 | Miltenyi | Astrocytes | 1:67 |
| ACSA-2 | PE-Cy7 | REA969 | Miltenyi | Astrocytes | 1:40 |
| CD24 | BV421 | M1/69 | BD Biosciences | Astrocytes / Neurons | 1:40 |
| CD24 | BV605 | M1/69 | BD Biosciences | Astrocytes / Neurons | 1:40 |

# Chapter 3

## Strong immune response to rhIgM22 partially attributed to endotoxin contamination

# 3.0 Immune response to rhIgM22 can be partially attributed to endotoxin contamination

## 3.1 Introduction

Data generated in our laboratory indicated that the mouse IgM antibody O4 induced a strong antiviral immune response in murine spinal cord-derived cell cultures (Hayden *et al.*, 2020). The proposed mechanism of action (**Figure 3.1)** is through the antibody interacting with microglia and inducing the expression of IFN-β, which warns the other cells of the CNS to upregulate their own innate antiviral defences.

To facilitate translation to a human context, the recombinant human IgM antibody 22 (rhIgM22) was studied preliminarily (Hayden *et al.*, 2020). This human lipid-specific IgM was found to upregulate the expression of interferon stimulated genes (ISGs) both *in vitro* and *in vivo,* in mice (Hayden *et al.*, 2020). In humans, the antibody has been applied therapeutically and found to increase clearance of myelin debris and enhance remyelination in the CNS (Mullin *et al.*, 2017; Zorina *et al.*, 2018; Greenberg *et al.*, 2022).

In this chapter, I aimed to expand upon Hayden et al's observations to understand the antibody's anti-viral mechanism of action.

Therefore, the aims of this chapter were to:

1. Investigate the mechanism by which the lipid-specific IgM antibody rhIgM22 induces an antiviral response *in vitro*.
2. Identify the putative receptor(s) the antibody is binding to on microglia.

To address these aims, I used murine microglial cultures, to determine the cell intrinsic effects of IFN-β on microglia, and murine CNS cell cultures (**Appendix 8.5**) which yield more cells than spinal cord cultures used by Hayden et al. and provide a more *in vivo* like environment than microglial cultures.

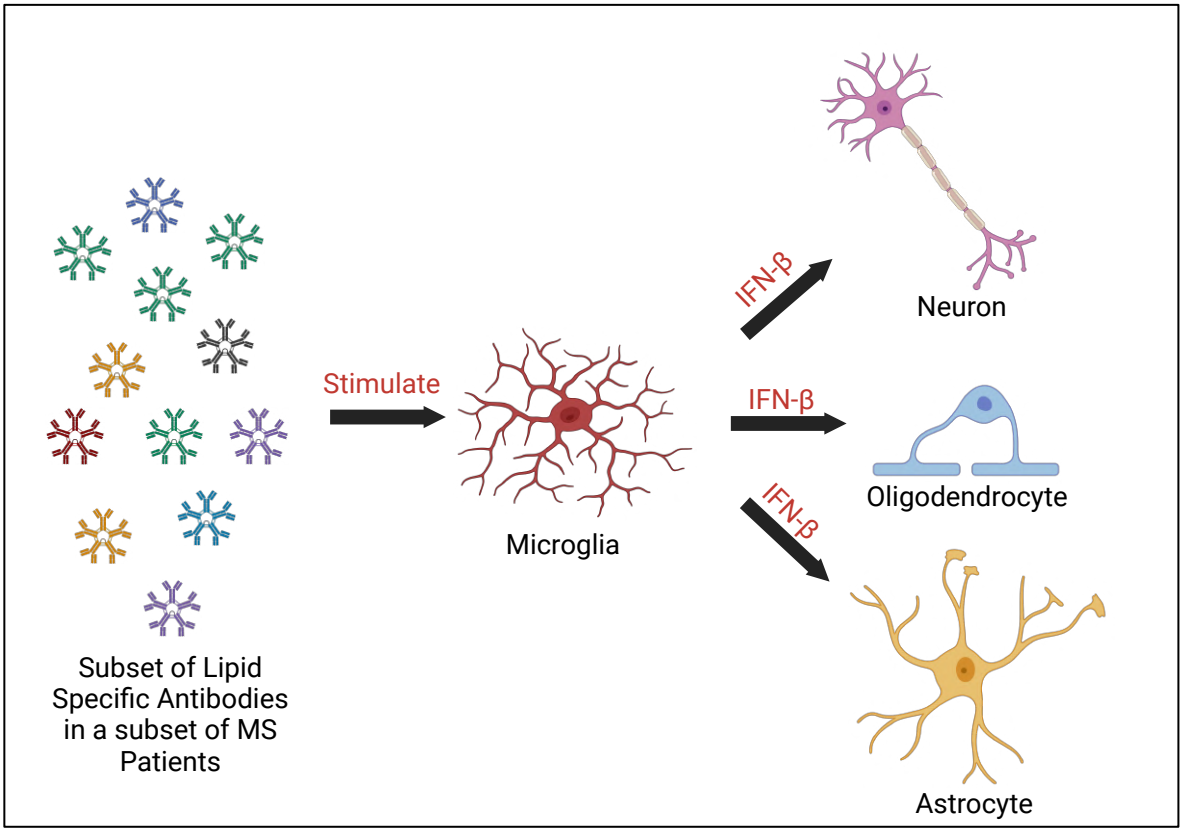


**Figure 3.1: Proposed mechanism of action of lipid-specific antibodies to induce an antiviral response.** The antibodies stimulate microglia to express IFN-β, which when secreted warns the other cells in the central nervous system to increase their innate antiviral defences. Diagram adapted from Hayden, L, et al. Acta Neuropathologica Communications (2020).

## 3.2 Microglial cultures are >95% pure

It was previously determined that microglia are essential to the antiviral response induced by rhIgM22 (Hayden *et al.*, 2020). Therefore, initial studies involving rhIgM22 were conducted on cultures of murine microglia. These were chosen due to the ease with which they can be established and maintained. As they were generated from mixed glial cultures, as described previously (Chen, Oyarzabal and Hong, 2013), it was important to confirm their purity.

Isolated microglia were grown for 24 hours before being fixed and visualised by immunofluorescence microscopy. By immunofluorescence staining of microglia (anti-Iba1, red, **Figure 3.2E**) and astrocytes (anti-GFAP, green, **Figure 3.2E**), only one GFAP-positive astrocyte was found across 12 coverslips; 100,000 cells per coverslip. Qualitatively, all other cells were Iba1 positive. Flow cytometry confirmed that 97.4% of live, single cells expressed the microglial markers $CD11b^+$ and $CD45^+$ (G. Kantzer *et al.*, 2017) (**Figure 3.2 A-D**). Together these data demonstrate that the cultures were practically pure (**Figure 3.2F**) and that the responses to any treatment could be attributed to this cell type.

## 3.3 rhIgM22 preparations induce a strong upregulation in interferon stimulated genes

### 3.3.1 Interferon stimulated gene panel

As shown previously, rhIgM22 can induce an antiviral response in murine spinal cord cell cultures as assessed by RT-qPCR of ISG mRNAs (Hayden *et al.*, 2020). I hypothesised that since rhIgM22 is a lipid-reactive IgM, like mouse O4, it will upregulate a similar panel of ISGs. Therefore, I designed an ISG panel for mRNA studies based on the data generated by Hayden *et al* that had a wide variety of antiviral functions (**Table 3.1).**

### 3.3.2 rhIgM22 has a similar effect on both microglial and mixed CNS cell cultures.

To confirm rhIgM22 can induce a similar antiviral effect to O4, the first three ISGs mentioned in **Table 3.1** (*Ifnb1, Cxcl10,* and *Ccl5*) were chosen due to their high level of upregulation in expression in E13 spinal cord cultures.

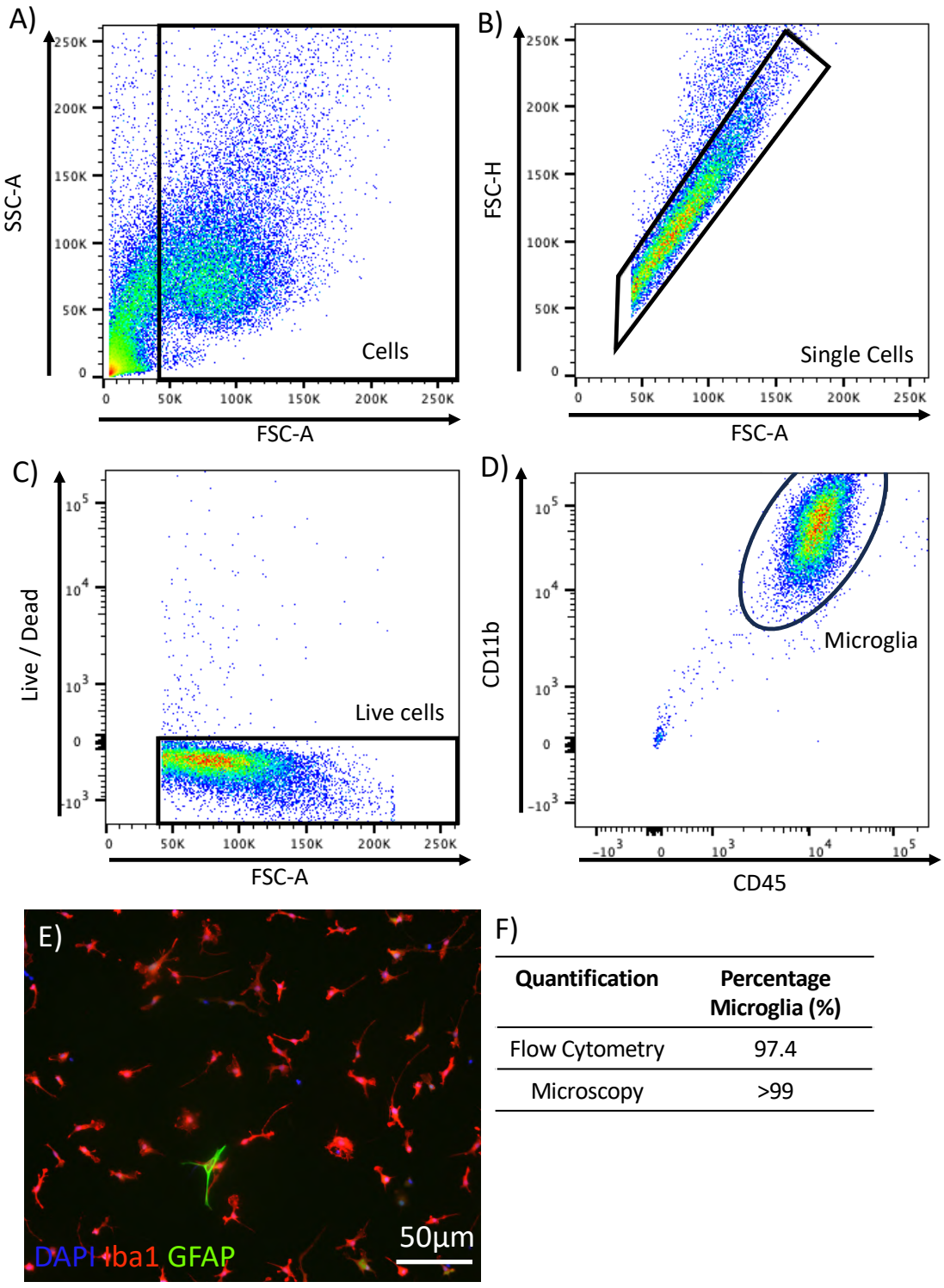


F)

| Quantification | Percentage Microglia (%) |
|---|---|
| Flow Cytometry | 97.4 |
| Microscopy | >99 |

**Figure 3.2. Microglial cultures are >95% pure.** When measured by flow cytometry and immunofluorescence microscopy both showed the solo cultures of microglia were >95% pure. A-D) Flow cytometry gating strategy for determining population of microglia. Gating strategy set as follows: A) FSC/SSC to exclude debris; B) FSC/Viability dye to exclude dead cells; C) SSC-H and SSC-A to exclude doublets; D) $CD45^{+}CD11b^{+}$ which represents microglia; E) Fluorescence microscopy image of untreated microglia (Iba1) and astrocytes (GFAP); F) Table showing proportion of microglia from flow cytometry as >95%. n=1

**Table 3.1: Interferon stimulated genes studied**

| Gene | Protein Encoded | Effect in Viral Infections | Reference |
|---|---|---|---|
| *Ifnb1* | IFN-β | Prevents viral infection, directs NK cells, activate antigen presenting DCs, expansion of virus specific T-cells, expansion of antibody producing B cells. | (Stanton et al., 1987; Katze, He and Gale, 2002; Seo and Hahm, 2010) |
| *Cxcl10* | CXCL10 | Lymphocyte activation, migration and infiltration of T cells, inflammation. | (Trifilo *et al.*, 2004; Lee, Lee and Song, 2009) |
| *Ccl5* | CCL5 | Promotes inflammation and viral clearance through attracted inflammatory cells, protection from viral induced apoptosis. | (Tyner *et al.*, 2004; Culley *et al.*, 2006; Silva *et al.*, 2021) |
| *Oasl1* | OASL | Trap viral RNAs, reduce IFN induction. | (Choi *et al.*, 2015; Kang *et al.*, 2018) |
| *Mx1* | MX1 | Block viral transcription. | (Verhelst *et al.*, 2012; Jung, Oh and Lee, 2019) |
| *Ifit2* | IFIT2 | Proposed to induce apoptosis in cells that are virus infected. | (Reich, 2013; Tran *et al.*, 2020) |
| *Rsad2* | RSAD2 | Decrease viral budding, inhibit viral replication. | (Helbig *et al.*, 2005; Wang, Hinson and Cresswell, 2007) |
| *Isg15* | ISG15 | Extracellular signalling, inhibits oligomerisation of viral proteins. | (Durfee *et al.*, 2010; Zhao *et al.*, 2016) |
| *Isg20* | ISG20 | RNase activity. | (Leong *et al.*, 2016; Y. Liu *et al.*, 2017) |

Both microglial and CNS cultures were treated with 20µg/mL rhIgM22 for 4 to 24 hours before cells were lysed and ISG mRNA levels quantified (RT-qPCR). As controls, PBS (vehicle) and poly(I:C) (positive) were employed. As shown in **Figure 3.3**, there was a high degree of variability in the data generated, and only *Ifnb1* was significantly upregulated at 4-hour of continuous treatment of CNS cultures. Nonetheless, I observed a clear trend in both cell culture types indicating that rhIgM22 induces a higher expression of all ISGs tested, compared to a control IgM antibody (**Figure 3.3**), when both are compared to PBS. Notably, similar levels of expression of all ISGs tested were seen across the two different culture methods. I concluded that the intra-group variability was likely due to inconsistency in culture quality, due to the experimenter's inexperience.

These data suggest that rhIgM22 upregulates ISGs in a similar manner to that of murine IgM O4, and likely does this through inducing IFN-β expression. I concluded that both the CNS cultures and microglial cultures could be used to investigate the mechanism of action of rhIgM22, with the caveat that more consistency in culture quality would be required to obtain meaningful data. I further conclude that for the ISGs tested, microglia alone are sufficient to express them, at least at the level of mRNA.

## 3.4 rhIgM22 did not cause an upregulation in ISGs in murine bone marrow derived macrophages

While rhIgM22 can induce a strong upregulation in ISGs in microglia, bone marrow derived macrophages (BMDMs) can be obtained easily from human blood samples, providing a more human relevant assay system. Consequently, I turned to murine BMDMs to test, in principle, if this cell type responds similarly to murine microglia. (Savarin, Dutta and Bergmann, 2018; Cuadros *et al.*, 2022a). BMDMs also differentiate faster than microglia, and consistently produce higher cell yields (Chen, Oyarzabal and Hong, 2013; Toda *et al.*, 2021).

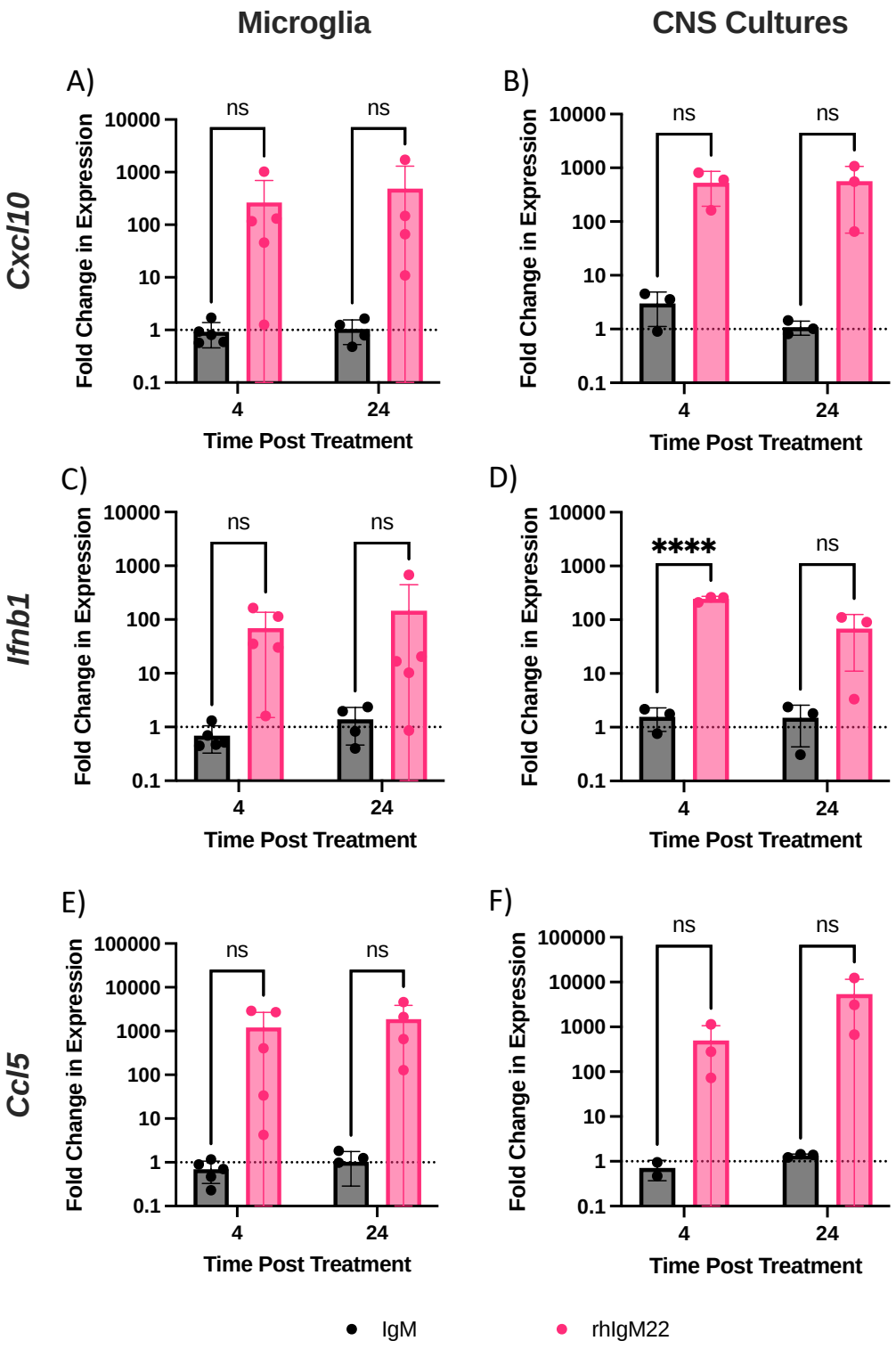


**Figure 3.3: Expression of ISGs in microglia and CNS cultures tends to increase in response to rHIgM22, in comparison to PBS**. Cultures were treated with either control antibody against pentaglobin (IgM) (black bars) or rhIgM22 (red bars) for 4 or 24 hours illustrated in comparison to PBS control. RNA levels were measured by RT-qPCR. Data presented as mean ± SEM, analysed by two-way ANOVA with Sidak's multiple comparisons test. n=5 for 4hr microglia, n=4 for 24 microglia, n=3 for all CNS conditions. $p$<0.001****.

Therefore, the expression of ISGs following rhIgM22 treatment was compared between microglial cultures and BMDMs. Primary microglia and BMDMs were treated with rhIgM22 for 4 or 24 hours before being lysed and ISG mRNA levels quantified (RT-qPCR). Additionally, the 2 culture systems were treated with PBS (vehicle control) and poly(I:C) (positive control).

In cultures of microglia, rhigM22 tended to increase expression of *Cxcl10* (~1000-fold, **Figure 3.4A**), *Ifnb1* (~100 fold, **Figure 3.4B**), and *Ccl5* (~1000 fold, **Figure 3.4C**) at both 4 and 24 hours post treatment, however only *Ccl5* upregulation after 4 hours continuous treatment reached statistical significance. In BMDMs, the average rhIgM22-induced upregulation was lower than in microglia, only increasing ~10 fold. Despite this small increase in expression levels, the differences for both *Cxcl10* and *Ccl5* between rhIgM22 treatment and PBS were significant at 24 hours. These results show that microglia mount a stronger response to IFN-β than non-CNS macrophages.

## 3.5 rhIgM22 is internalised by microglia within 1 hour

The first aim of this project was to elucidate the mechanism by which rhIgM22 induces the upregulation of ISGs. I aimed to explore whether the antibody was binding to an intracellular receptor or surface receptors. To study this, rhIgM22 was conjugated to a pH sensitive photoreactive dye, pHrodo, which in acidic environments, such as phagosomes, gains a fluorescent signal (Lukacs, Rotstein and Grinstein, 1991). Initially, I confirmed that the conjugation of pHrodo to rhIgM22 did not affect the antiviral activity of the antibody as measured by mRNA upregulation of ISGs. Once this was validated (data not shown as only n of 1, not verified further due to reasons given from **3.6** onwards), the solo microglia cultures were treated with rhIgM22-pHrodo for between 30 minutes to 4 hours before being fixed and analysed using immunofluorescence microscopy. Pentaglobin was also conjugated with pHrodo to act as a negative control (IgM-pHrodo).

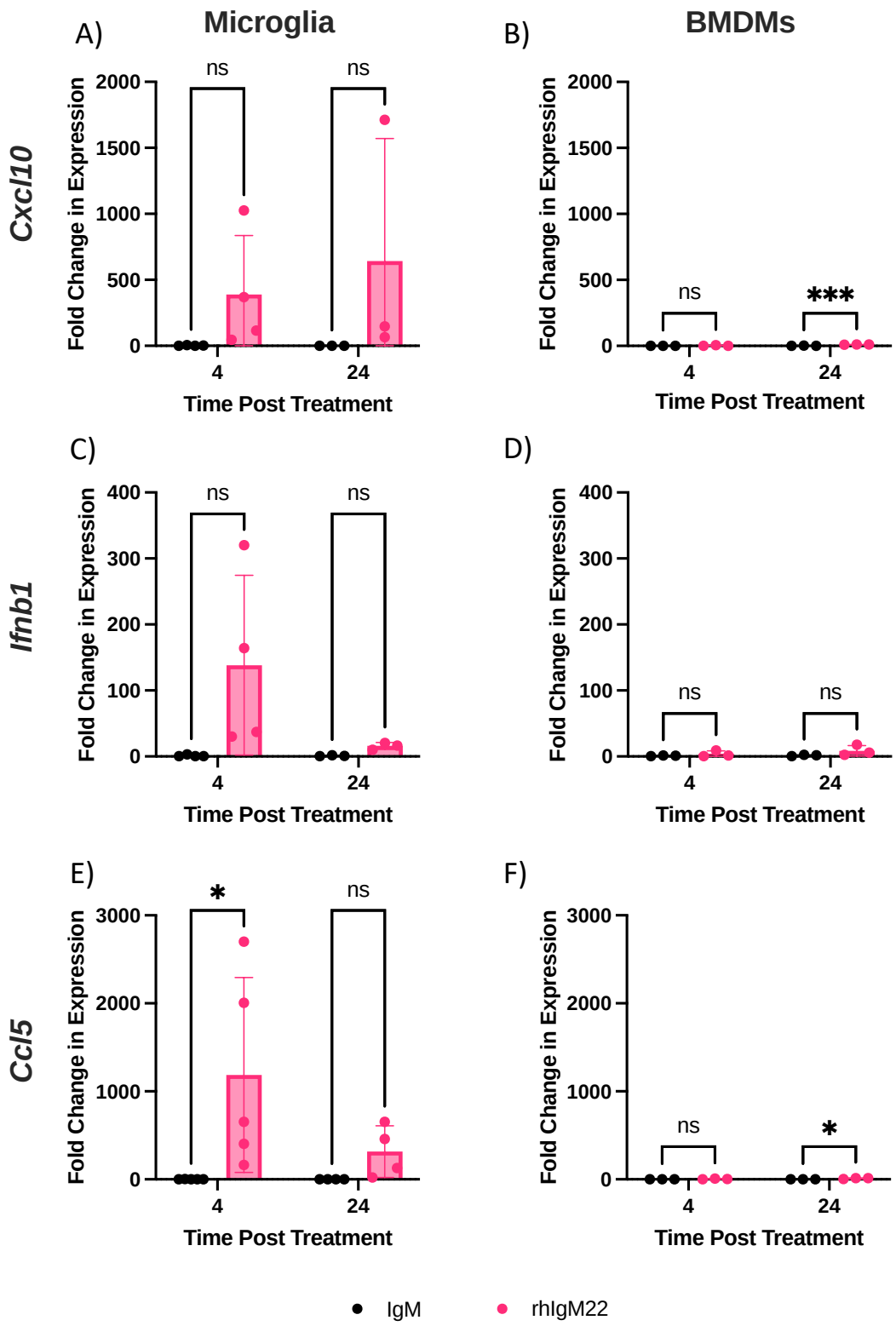


**Figure 3.4: Upregulation of ISGs following treatment with rhIgM22 in microglia and bone marrow derived macrophages.** Cultures were treated with pentaglobin (IgM) or rhIgM22 for either 4 or 24 hours. A,C,E) Microglial cultures, BD,F) Mature BMDMs. A,B) *Cxcl10*; C,D) *Cxcl10*; E,F) *Ccl5*. Upregulation compared to PBS vehicle control. Data presented as mean ± SEM, analysed by two-way ANOVA with Sidaks test. n=4 for 4hr microglia, n=3 for all other conditions. $p<0.05$ *, $p<0.001$ ****.

To confirm that any difference in pHrodo$^+$ cell proportions were not due to differences in the numbers of cells present in the two treatment conditions, DAPI$^+$ cells were quantified per field of view following treatment with pHrodo or antibody-conjugated pHrodo. No difference in cell density was observed (**Figure 3.5A**). The percentage of rhIgM22-pHrodo$^+$ cells (**Figure 3.5B**) increased until 1 hour post treatment and quickly decreased afterward. One hour post treatment 78.3±10.2% of the DAPI positive cells were rhIgM22-pHrodo positive (**Figure 3.5D**), while 0% of the cells treated with control IgM-pHrodo were positive (**Figure 3.5C**). These data support the possibility that rhIgM22 acts through an intracellular receptor but for the reasons given in the sections below, this was not examined further.

## 3.6 Antibody preparations are contaminated with LPS

As the rhIgM22 preparations were considered to be within GMP regulations, I had assumed until this stage they were free of endotoxin. However, I decided before undertaking further studies to confirm this.

### 3.6.1 rhIgM22 induces a similar expression profile to LPS

I set out to confirm the antibody was endotoxin free by determining the upregulation of *Ifnb1*, *Cxcl10*, and *Ccl5* in the CNS cultures treated with various concentrations of LPS. Unexpectedly, the upregulation of ISGs in the CNS cultures following LPS treatment was similar to those treated with rhIgM22 at all concentrations (**Figure 3.6B,C**). This raised concerns that the results may be due to possible endotoxin contamination.

### 3.6.2 High concentrations of LPS detected in rhIgM22 antibody preparations

To quantify levels of putative endotoxin contamination of rhIgM22, I used the Pierce$^{TM}$ LAL Endotoxin Quant Kit (per manufacturers' instructions). I found that rhIgM22 was contaminated with 5.2±0.9ng/mL LPS (**Table 3.2**). Since this was higher than the minimum concentration of LPS tested above (**Figure 3.6)**, it was impossible to determine if the anti-viral effect was due to the activity of rhIgM22 or contaminating LPS. I tested additional preparations of rhIgM22 for the presence of LPS, including shIgM22 previously tested by our lab. However, this preparation also had a higher concentration of LPS than the minimum concentration tested above **Figure 3.6** at 2.9±0.2ng/mL LPS (**Table 3.2**).

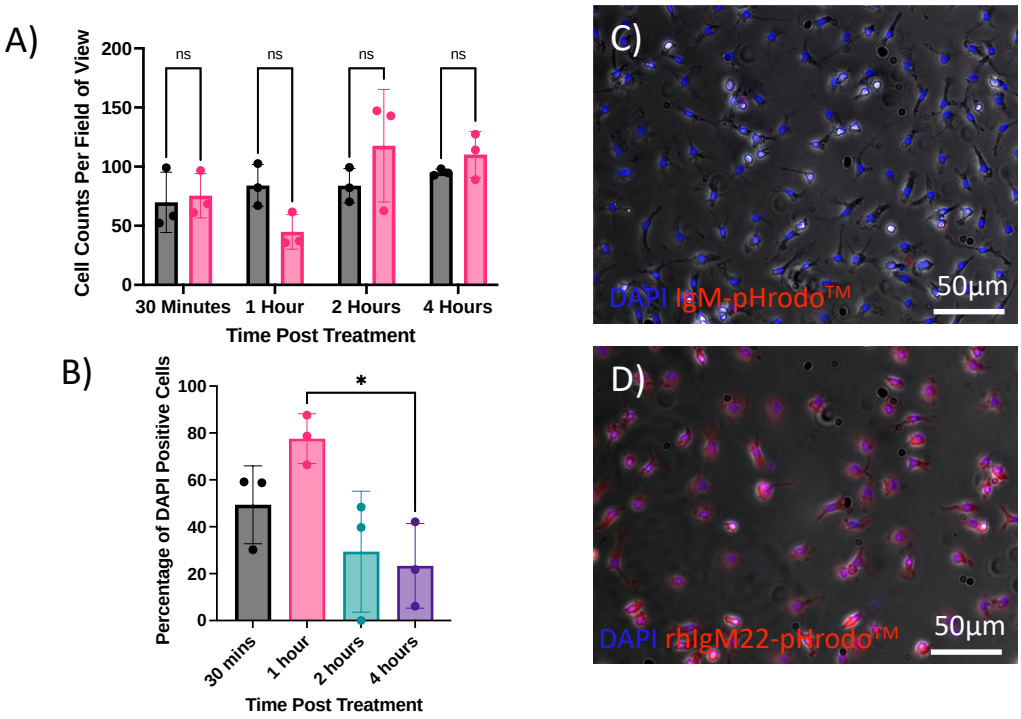


**Figure 3.5: Internalisation of rhIgM22-pHrodo into primary microglia.** rhIgM22 was conjugated to pHrodo and microglia were treated for 30 minutes to 4 hours. A) DAPI counts per field of view for timepoints; B) percentage rhIgM22-pHrodo positive cells, measured by percentage of DAPI positive cells per field of view; C-D) Representative immunofluorescence images of microglia 1 hour post treatment with a control antibody (C) or rhIgM22-pHroro (D). Microglia determined by morphology seen with phase-contrast microscopy. Data presented as mean ± SEM, analysed by two-way ANOVA with Sidák's multiple comparisons test (DAPI positive cells), or one-way ANOVA with Tukey's multiple comparisons test (Percentage rhIgM22-pHrodo positive). n=3 for all conditions.

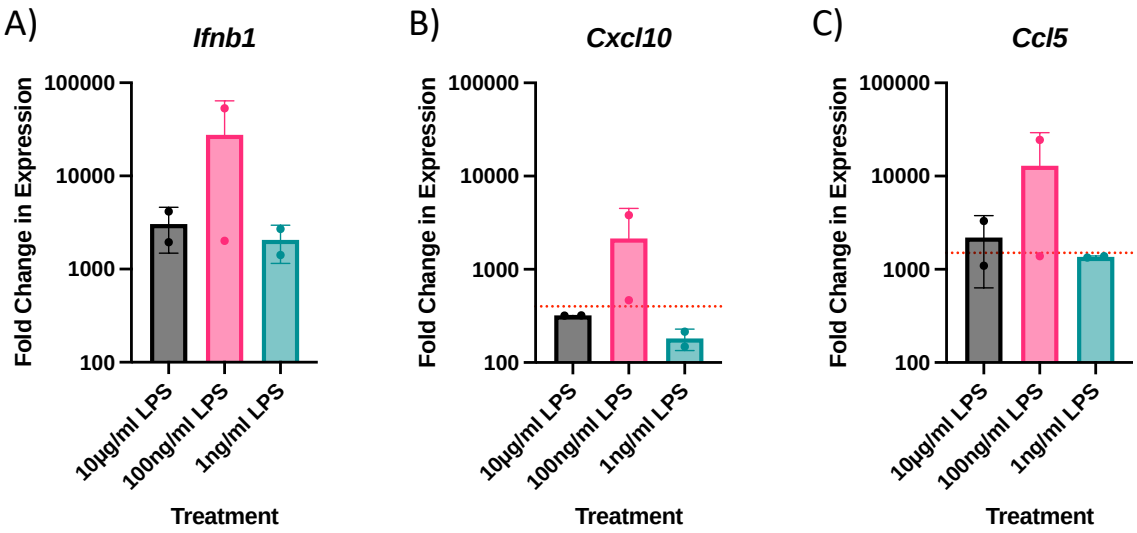


**Figure 3.6: Upregulation of ISGs in CNS cultures in response to various concentrations of LPS, in comparison to PBS.** CNS cultures were treated with PBS or various concentrations of LPS, and RNA isolated after 24 hours. Red dotted line indicates level of expression of associated genes following treatment with 20µg/mL rhIgM22. A) *Ifnb1*; B) *Cxcl10*; C) *Ccl5*. Data presented as mean ± SEM, analysed by two-tier *t*-test. n=2 for all conditions.

**Table 3.2 Quantification of LPS contamination of rhIgM22 and shIgM22**

| **Antibody** | **rhIgM22 (batch used so far)** | **shIgM22** |
|---|---|---|
| LPS (ng/mL ± SD) | 5.2±0.9 | 2.9±0.2 |

### 3.6.3 Endotoxin-free antibody preparations did not induce an ISG response

Additional preparations of rhIgM22 antibodies were tested for endotoxin contamination, aside from those described in **Table 3.2**. E17 CNS cultures were treated with 20µg/mL of these preparations and the cell culture supernatants analysed for CCL5 concentrations by ELISA. Many of these preparations could induce a strong expression in CCL5. However, when they were analysed for LPS contamination the preparations that induced a strong expression of CCL5 also had LPS contamination >1ng/mL (**Figure 3.7**).

### 3.6.4 Attempts to purify antibody preparations were unsuccessful.

Following the confirmation of substantial endotoxin levels in several batches of rhIgM22, an attempt was made to remove the contaminating LPS using Pierce™ High-capacity endotoxin removal columns (per manufacturer's instructions). LPS is bound to beaded cellulose, removing contaminating LPS. To assay the removal of the endotoxin, 1µg rhIgM22 protein from each step of the process was ran on a western blot.

To perform this, 100µL of rhIgM22 was attempted to be purified. Following the use of the endotoxin removal column, the concentration of antibody decreased (**Figure 3.8C** compared to **Figure 3.8A**). While this could have been due to non-specific binding of the antibody to the beads, it is much more likely that rhIgM22, which is lipid-specific, has bound to the LPS and was removed in the column at the same time. Therefore, I was unable to purify rhIgM22 of the endotoxin contamination. Data generated from rhIgM22 could be due to LPS and were subsequently excluded.

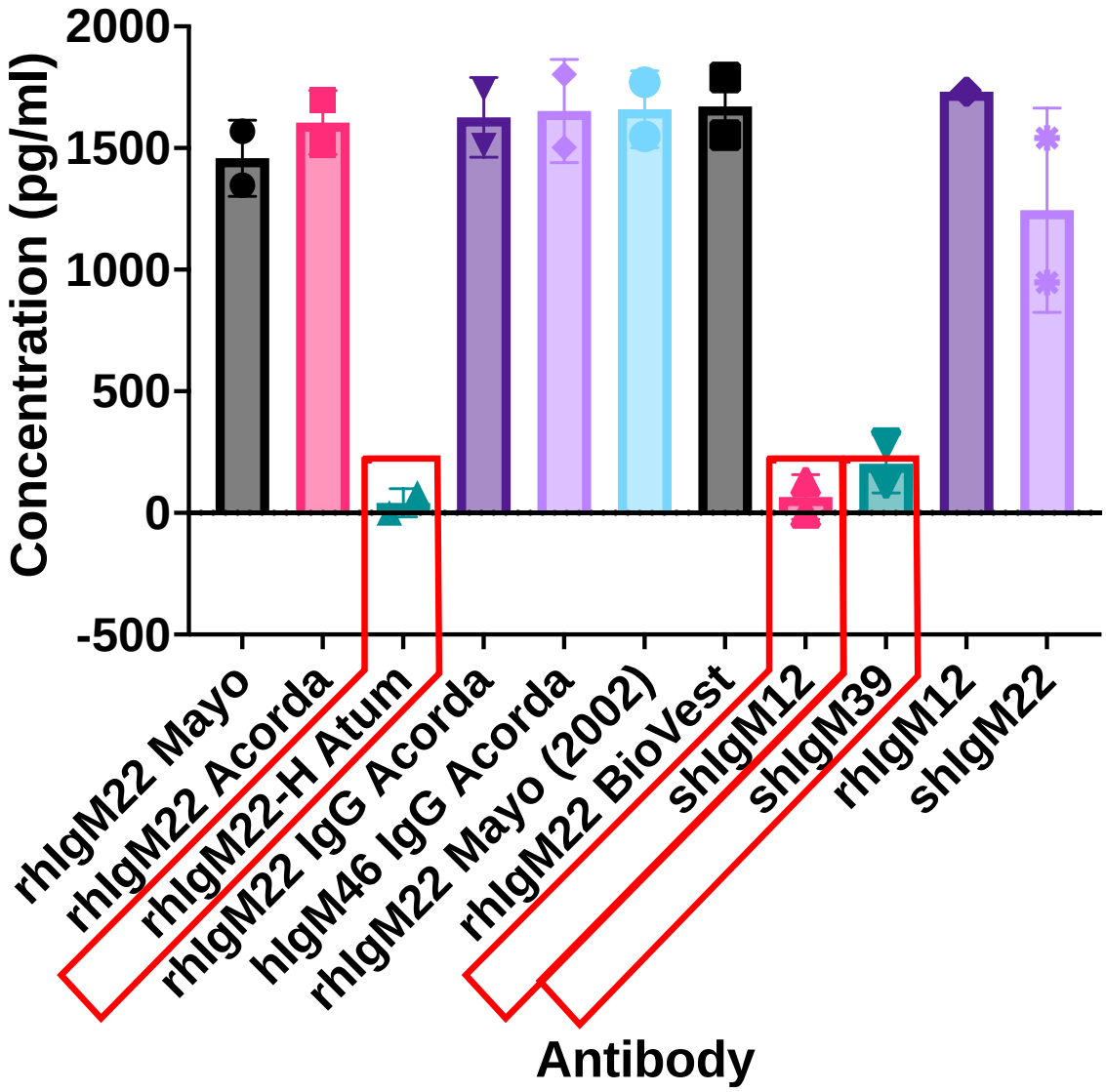


**Figure 3.7: CCL5 concentration following treatment with different preparations of IgM antibodies.** Cultures were treated with antibody for 24 hours before supernatants were analysed by ELISA. Antibodies surrounded in red had endotoxin levels below detection limit. Data presented as mean ± SEM. n=2

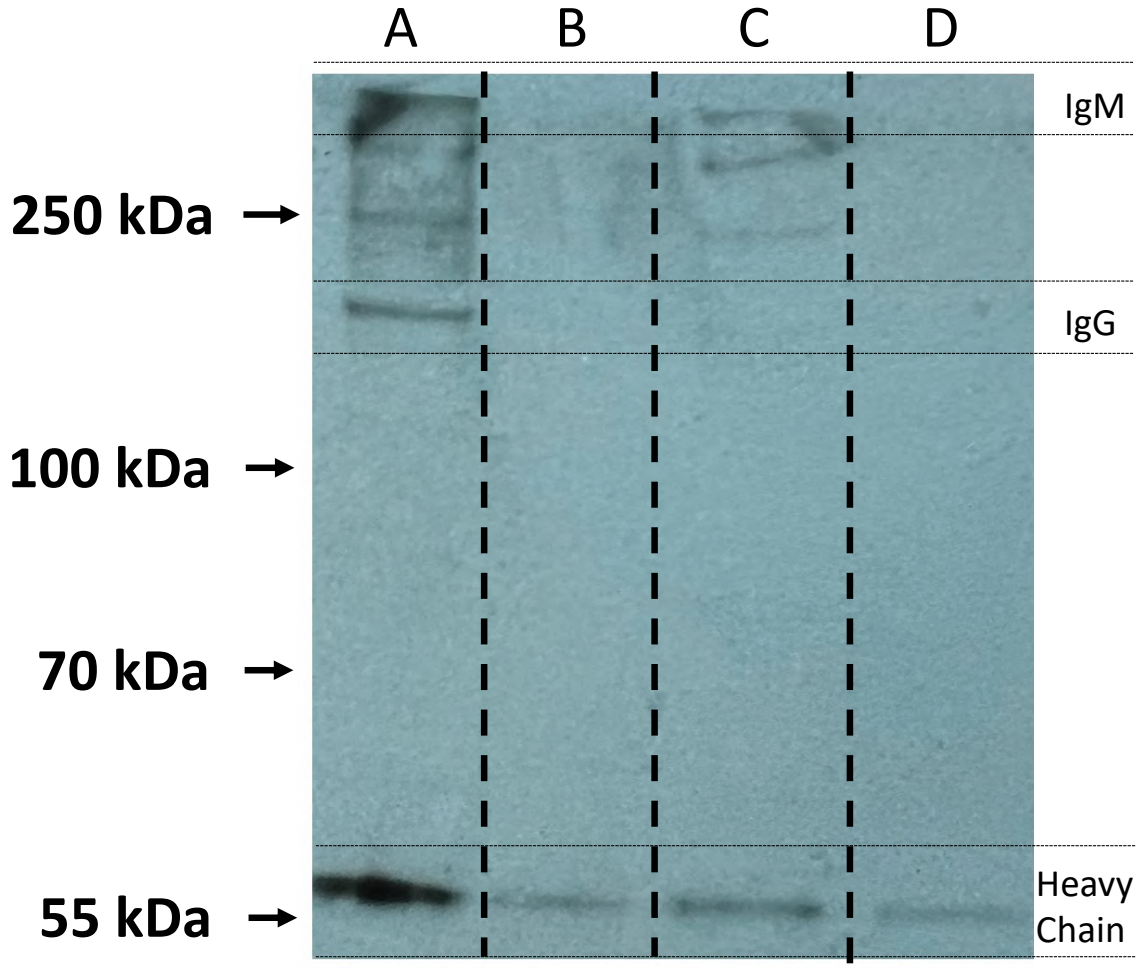


**Figure 3.8: Western blot analysis of rhIgM22 following attempt at purification.** A) 1µg unpurified rhIgM22; B) 0.2µg unpurified rhIgM22. C) 1µg rhIgM22 following purification with endotoxin removal column. D) 1µg rhIgM22 following concentration of antibody using Amicon Ultra spin column. Ladder from HiMark protein ladder indicated by arrows on left. Band identity indicated on right.

## 3.7 Discussion

The data presented in this chapter showed that rhIgM22 upregulated IFN-β, which in turn upregulated expression of ISGs, in both microglia and mixed CNS cultures. It has also been previously shown by our lab that all major cell types of the CNS upregulate ISGs in response to O4 (Hayden *et al*., 2020). Putatively, I concluded rhIgM22 would protect the major CNS cells from viral infection in a similar manner to murine IgM O4. However, these conclusions must be reconsidered in light of the fact that rhIgM22 was contaminated with LPS.

Initially, I researched the effect of treating CNS cells with lipid specific antibodies, following up on Hayden et al. Using human IgM22 for this purpose would allow us to translate my findings more easily to human in *in vitro* and *in vivo* studies. Currently, all therapeutic drugs must be tested in a rodent (mouse and rats) as required by UK law, before being trialled in another animal and eventually in humans (Prior *et al.*, 2020). While humans and mice share ~90% of their genomes, toxicity in humans against compounds found safe in mice has been reported (Bryda, 2013; Van Norman, 2019). Human cell derived studies likely decrease the chances of this toxicity and enable better selection of drug candidates (Van Norman, 2019). Therefore, rhIgM22-derived therapeutics are a very good avenue for research under the current legislation. The antibody rhIgM22, which has previously been shown to induce an antiviral effect in murine cell cultures (Hayden *et al.*, 2020), has been trialled in both humans and mice, and been shown to have a therapeutic benefit in increasing remyelination of the central nervous system when injected intrathecally (Mullin *et al.*, 2017; Zorina *et al.*, 2018; Greenberg *et al.*, 2022). Therefore, further studies to investigate the mechanism of activity of rhIgM22 as an antiviral has an increased chance of producing positive avenues for novel drug development compared to trialling a murine IgM antibody alone, such as O4.

Our lab observed that lipid-specific antibodies interact with microglia to induce their expression of interferon beta (IFN-β). I investigated cultures of microglia as these could be grown and differentiated in a shorter time than the E13 spinal cord cultures or the E17 CNS cultures, thereby increasing efficiency and decreasing the complexity of the cultures by removing possible confounding cell types. Microglial cultures were isolated from a co-culture with astrocytes and oligodendrocyte precursor cells (OPCs). IFNAR, the receptor for IFN-β is found expressed on all cells of the CNS (Okada *et al.*, 2005; Heine *et al.*, 2006), and

therefore in principle all these cells could respond to IFN-β. Two of the ISGs found upregulated previously in the E13 spinal cord cultures by lipid-reactive IgMs O4 and rhIgM22 were *Cxcl10* and *Ccl5*. The *Cxcl10* gene is significantly upregulated in reactive, or pro-inflammatory, astrocytes (Phares *et al.*, 2013; Hwang and Bergmann, 2018), as was *Ccl5* (Pittaluga, 2017). Our lab has also shown that *Cxcl10* is upregulated in astrocytes treated with O4 (Hayden *et al.*, 2020). Astrocytes have also been shown to increase the transcription of *Ifnb1* following viral infection (Kallfass *et al.*, 2012; Reinert *et al.*, 2012; Detje *et al.*, 2015). In combination, these results imply that astrocytes could confound the results if found in co-culture with microglia. There is little current literature stating that the oligodendrocyte precursor cells secrete IFN-β or upregulate the expression of *Cxcl10* or *Ccl5*. In fact, the expression of CXCL10 is linked with inducing apoptosis of OPCs (Michlmayr and McKimmie, 2014), while CCL5 is linked with inducing their proliferation (Lanfranco *et al.*, 2018), both of which would not cause an issue with the purity of the solo cultures of microglia. These cells also are unable to differentiate into mature oligodendrocytes (which do express CXCL10 and CCL5) due to the serum-rich media the microglia are grown (Suzuki *et al.*, 2017). Therefore, to be confident my results were due to microglia and not astrocytic contamination I focussed on ensuring microglial purity.

Of the 12 coverslips investigated, which includes 1.2 million cells, only one GFAP +ve astrocyte was discovered. To isolate the astrocytes from flask of mixed-glial cells trypsinisation is needed (Schildge *et al.*, 2013). Therefore, this method creates consistently pure cultures of solo microglia. When confirmed using flow cytometry the solo cultures were >97% pure for microglia (CD11b+CD45+, (G. Kantzer *et al.*, 2017)). While flow cytometry becomes more prevalent as a method later in this thesis, I did not at this time have the required antibodies or knowledge to conclusively determine what the remaining 3% are comprised of. However due to the position of the gates I feel confident that the majority of this 3% was cellular debris. Therefore, any results generated when discussing solo cultures of microglia were likely from a microglial transcriptional profile and not another cell type.

The ISGs discussed in this chapter were chosen due to being highly upregulated in previous analysis (Hayden *et al.*, 2020), and for having various functions in relation to viral infection (**Table 3.1**). However, only three of these were presented here: *Cxcl10*, *Ifnb1*, and *Ccl5*.

CXCL10 acts as a chemoattractant for peripheral immune cells such as monocytes, T cells, and NK cells. Expression of *Cxcl10*, and the subsequent immune cell migration, significantly decrease infection with a variety of viruses (Müller *et al.*, 2010). For example, mouse hepatitis virus (MHV) (Liu *et al.*, 2001; Stiles *et al.*, 2006), lymphocytic choriomeningitis virus (LCMV) (Christensen *et al.*, 2009), West Nile virus (WNV) (Zhang *et al.*, 2008), and Herpes simplex virus (HSV) (Wuest and Carr, 2009). CCL5 also acts as a chemoattractant primarily recruiting leukocytes to the site of infection and induces the proliferation of NK cells. The expression of CCL5 significantly protects neurons against HIV-1 infection (Silva *et al.*, 2023), while interestingly decreasing CCL5 increased survival of mice infected with rabies by decreasing pro-inflammatory cytokine production in the CNS (Huang *et al.*, 2014). Therefore, these three genes act as a good markers for the antiviral profile that has been previously discussed (Hayden *et al.*, 2020).

I observed a strong increase in the expression of these three ISGs in the microglial cultures, demonstrating that this cell type alone produces a large proportion of these 3 ISGs. However, in the CNS cultures, due to the large intra-group variation, most did not reach significance. This was likely due to the author's inexperience with cell culturing techniques. Uniformity in the dissected brains, number of cells plated, and the media preparations could all have been slightly different from one culture to the next.

Bone marrow derived macrophages were proposed as an alternative model. Microglia and BMDMs share a similar yolk-sac derived lineage and in mouse models where microglia have been depleted, cells from bone marrow transplanted directly into the brain of mice can proliferate and spread throughout the CNS and act like microglia (Cronk *et al.*, 2018; Lund *et al.*, 2018). At the same time, I was thinking towards the future. Primary human microglia are difficult to obtain only coming from post-mortem tissue, either adult or foetal, and biopsies for disease – all of which pose their own limitations and ethical issues (Durafourt et al., 2013; Melief et al., 2016; Rustenhoven et al., 2016; Mizee, van der Poel and Huitinga, 2018). Therefore, another model was desirable for mechanistic studies aimed at understanding the human CNS antiviral response. I first determined if murine BMDMs responded similarly to microglia when treated with IgM22. I found upregulation of ISGs was lower compared to that in primary murine microglia. This implies there could be a CNS macrophage-specific antiviral response to IgM22. Microglia differentiate in the yolk sac at

the same time as other immune cells in the yolk sac during the first wave of haematopoiesis around E7.5 in mice (Sheng, Ruedl and Karjalainen, 2015; Hoeffel and Ginhoux, 2018). Due to the blood-brain barrier (BBB) the microglia inside the CNS are isolated from transcriptional factors such as *Myb* (Schulz *et al.*, 2012) which drive the differentiation of the hematopoietic stem cells. Microglia have a distinct transcriptional profile compared to BMDMs (Cuadros *et al.*, 2022b), however, BMDMs which infiltrate the CNS become "microglial-like" cells (Shemer *et al.*, 2018). Genes expressed in mature microglia, such as *Tmem119* and *P2yr12* are expressed significantly lower in microglial-like cells compared to native microglia, while the two populations are only 90% similar when measuring the transcriptome (Shemer *et al.*, 2018).

Before identifying LPS contamination I aimed to determine the mechanism by which rhIgM22 induced the antiviral effect through investigating how rhIgM22 interacts with microglia. Whilst these studies became redundant for IgM22, I include them here because they could apply also to murine IgM O4. IFN-inducing autoantibodies bind to ds / ss DNA or other genetic structures in the external milieu. I hypothesised these would be internalised into the cell and release the genetic material to interact with cGAS or STING and activate this pathway (Li *et al.*, 2010; Decout *et al.*, 2021). Our lab previously showed murine IgM O4 and rHIgM22 antibodies act through the cGAS-STING pathways (Hayden *et al.*, 2020), therefore I hypothesised that rhIgM22 binds to microglia, possibly through Fc receptors, before being internalised. While no receptor has been confirmed for IgMs in microglia, it is likely the Fcα/μR as this is expressed on peripheral macrophages (Liu *et al.*, 2019). I found that rHIgM22 was internalised rapidly in cultured microglia. This would allow the IgM complex to interact with intracellular PRRs such as releasing the DNA for cGAS recognition, however this has not been adequately studied. There is also an intracellular receptor for IgMs, the cytosolic Fc receptor tripartite motif 21 (TRIM21), which can bind IgG, IgM, and IgA (Mallery *et al.*, 2010; Bidgood *et al.*, 2014). However, the expression of TRIM21 has not been adequately described in microglia, and is reliant on type-I expression itself therefore being unlikely to be part of the signalling pathway to induce type-I expression. Further studies on the mechanism of action, particularly the effect of blocking the Fc receptor and blocking phagocytosis to elucidate the receptor the antibody is interacting, were halted following my discovery of the preparations being contaminated with LPS.

As the IgM22 antibody had been used in clinical trials, and was allegedly produced under GMP regulations, I did not initially investigate for LPS contamination. However, similarities were seen between previously described macrophage responses to LPS and the antiviral responses rhIgM22 was inducing (Bandow *et al.*, 2012). Of particular note are the expression of *Cxcl10* and *Ccl5,* which were upregulated ~900 fold and ~200 fold respectively in microglia. While the *Ccl5* expression was much lower than in my solo-cultures of microglia, the upregulation of *Cxcl10* was similar. This further indicates that LPS might be a contributing factor to the results seen thus far, especially since the upregulation of these ISGs by both LPS and rhIgM22 were similar as measured by RT-qPCR. Therefore, once the contamination was identified, previous results by rhIgM22 were cast into doubt.

LPS induces the cGAS-STING pathway by dysregulating mitochondrial functions which results in mtDNA leaking into the cytoplasm to activate the cGAS-STING pathway (M. Z. Li *et al.*, 2022). LPS also induces *Ifnb1* transcription through the binding to TLR4 (Fitzgerald, Rowe, *et al.*, 2003). Previous data has linked different preparations of the same reagent, which have different cytokine responses to LPS contamination in both the CNS and in general macrophages (Glim *et al.*, 2010), where microglia in particular are of significant risk of LPS-related activity (Weinstein *et al.*, 2008). This group also state that any results where LPS contamination has not been considered be cautiously interpreted by readers, a view mirrored by the author. Therefore, following my discovery of significant LPS contamination any following reagents are either tested for LPS or ensured from the manufacturer to have low LPS detection rates, <0.1 EU/mL, or <10pg/mL. Finally, my samples were found to have 5.22ng/mL LPS. Working up from my 20µg/mL working concentration of rhIgM22, if a comparable dose was given to an average human of 60kg with 5L of blood there would be a total quantity of 26.1µg LPS. This is well above the lethal dose in humans, which is as low as ~1-2µg (Sauter and Wolfensberger, 1980).

When attempting to clear the antibody using the Pierce LAL columns the antibody itself ended up being removed from the preparation. This is likely due to the LPS binding to the antibody itself, which has been shown previously to occur against LPS purified from different bacterial strains (Hiyoshi *et al.*, 2018). These columns work through binding the LPS to poly-L-lysine coated cellulose beads (Takahashi *et al.*, 1992), however additionally IgM antibodies are polyreactive and have been shown to bind to multiple different antigens,

for example poly-l-lysine (Novick *et al.*, 1992), further contributing to the removal of the antibody instead of the LPS.

Therefore, a new direction needed to be chosen. The results thus far cannot be attributed to rhIgM22 due to contaminating LPS. I adapted my direction, using the same data previously generated with O4, to investigate the effect of IFN-β directly. This allowed us to continue to investigate the original pathway, but focussing on the downstream pathways of IFN-β.

# Chapter 4

## Characterising the effect of interferon beta on central nervous system cultures

# 4.0 Characterising the effect of interferon beta on central nervous system cultures

## 4.1 Introduction

In Chapter 3, I observed a high concentration of LPS in the antibody preparations being studied and a new avenue of research needed to be chosen. As our lab had shown previously that lipid-specific antibodies *per se* induced IFN-β expression in microglia to warn the other cells of the CNS to upregulate their innate antiviral defences (**Figure 3.1**), I chose to investigate the mechanism of activity of IFN-β directly for reason given below. The activity of IFN-β is well researched in the context of MS (Jakimovski *et al.*, 2018; Filipi and Jack, 2020) and has been directly linked with antiviral activity against viruses including Human Polyomavirus 2 (Katze, He and Gale, 2002; Co *et al.*, 2007; Mantlo *et al.*, 2020). However, the response of individual cell types in the CNS to IFN-β is not well investigated or characterised. I speculated that through researching the responses of the individual CNS cell types to IFN-β, cell-type specific downstream pathways could be identified and investigated for any antiviral activity, driving future therapeutic development that preclude the requirement for a global (whole CNS) approach. Therefore, the aims of this chapter were to:

1. Titrate IFN-β to identify the minimum concentration capable of inducing an anti-viral response *in vitro,* as assessed by ISG expression.
2. Characterise the antiviral response induced by IFN-β in the cultures by RT-qPCR analysis of ISGs.
3. Optimise a process to isolate the individual cell types of the CNS for cell type-specific investigations in the subsequent chapter.

## 4.2 Concentrations above 50ng/mL of interferon beta could induce strong expression of interferon stimulated genes

The response of murine CNS cultures to IFN-β has not been characterised previously, therefore for the purpose of developing a model system to test response to IFN-β, an optimal dose needed to be determined. CNS cultures were treated with a range of doses of

IFN-β (10pg/mL to 100ng/mL) for 24 hours, at which point cells were lysed and ISG mRNA levels quantified (RT-qPCR), and supernatants were quantified for CCL5 expression (ELISA). Additionally, CNS cultures were treated with PBS (vehicle control) and poly(I:C) (positive control).

Using RT-qPCR, I found that ~25ng/mL IFN-β was sufficient for strong upregulation of *Cxcl10*, *Oasl1*, *Mx1*, and *Rsad2*. Using non-linear regression analysis, the IFN-β $EC_{50}$ of *Oasl1* and *Rsad2* was 12.3±5.1ng/mL ($R^2$=0.7680, **Figure 4.1B**) and 17.8±9.1ng/mL ($R^2$=0.7431 **Figure 4.1D**), respectively. In this series of titrations, the upregulation of the *Cxcl10* and *Mx1* had likely not reached maximum and therefore no $EC_{50}$ was calculated (**Figure 4.1A,C**). These results indicate that 25ng/mL IFN-β is sufficient to induce a strong upregulation of ISGs. However, as protein levels cannot be assumed based on mRNA expression, it was crucial to investigate protein levels. 96-well plate grown CNS cultures were used due to them being amenable to high through-put testing. Non-linear regression analysis indicated that the IFN-β $EC_{50}$ for CCL5 was 61.7±29.4ng/mL ($R^2$=0.8410, **Figure 4.1E**).

The combined results of the qPCR and ELISA analysis led us to conclude that 50ng/mL of IFN-β was sufficient to induce upregulation of ISG mRNA and protein as even though insignificant there was a >30fold increase in mRNA expression and ~100pg/mL increase in CCL5 concentration in the supernatant found following 24 hours of IFN-β treatment.

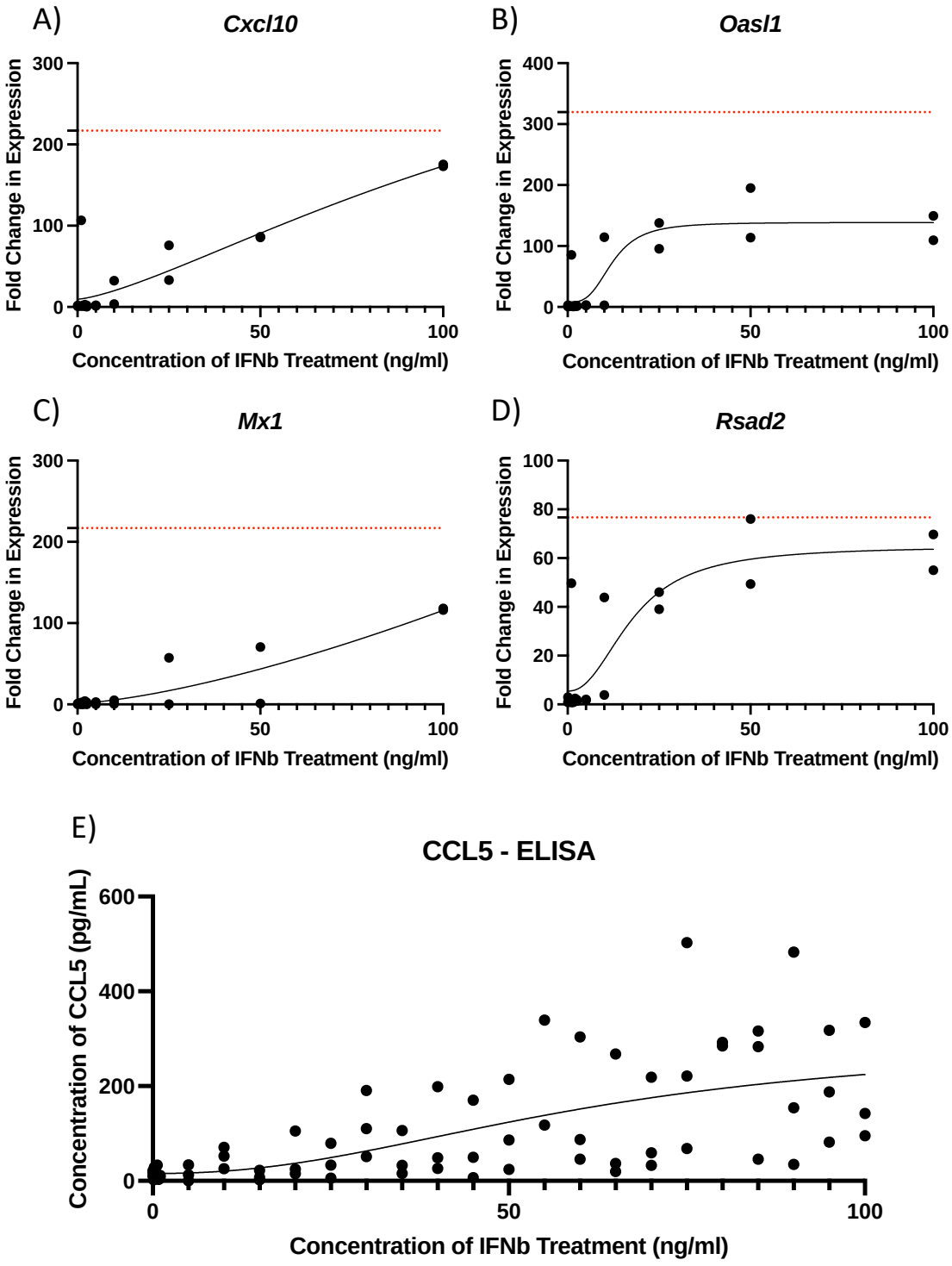


**Figure 4.1: Upregulation and expression of ISGs following treatment with different doses of IFN-β.** Coverslip (A-D) or 96 well plate (E) grown CNS cultures were treated with between 0-100ng/mL IFN-β before analysing *Cxcl10* (A), *Oasl1* (B), *Mx1* (C), and *Rsad2* (D) upregulation by qPCR, and CCL5 expression by ELISA (E). Non-linear fit trendlines added. Expression of poly(I:C) treated cultures (positive control) indicated by dashed red line. Data presented as mean ± SEM. (RT-qPCR n=2, ELISA n=3).

## 4.3 Interferon beta induces strong upregulation in interferon stimulated genes from 4 hours to 48 hours post treatment

To determine if exogenous IFN-β induces expression of ISGs in my CNS cell cultures, I used RT-qPCR following treatment with 50ng/mL IFN-β between 4hr to 96hr post treatment CNS cultures were additionally treated with PBS (vehicle control) or poly(I:C) (positive control), data not shown as comparisons were made between each timepoint and t=0. Of the ISGs analysed, 3 were significantly upregulated at 4 hours post treatment with IFN-β (*Cxcl10,* ($p$<0.01), *Oasl1* ($p$<0.05), and *Rsad2* ($p$<0.05)) (**Figure 4.2A,B,D**). On average, *Mx1* was upregulated by ~150 fold compared to vehicle control, however due to variability in the data, this did not reach the threshold for significance ($p$<0.05) (**Figure 4.2C**). All investigated ISGs reached a peak in mRNA expression after 4 hours, after which the expression gradually decreased back down to baseline. There was still some mRNA upregulation at 24 hours, however this did not reach significance. These data show that IFN-β increases expression of ISGs for at least 24 hours after treatment.

## 4.4 Interferon beta upregulates many cytokines in the CNS cultures

Next, I asked if protein levels were similarly altered. As ISG mRNAs were upregulated for at least 24 hours post treatment, supernatants from IFN-β treated cultures up to 48 hours post treatment were analysed. CNS cultures were treated with either PBS as a vehicle control or IFN-β for 4, 24, or 48 hours. Supernatants were collected at these time points and analysed by Luminex, which was graciously performed by Dr Fabian Schütte to analyse multiple cytokines released in the supernatant simultaneously, a list of which can be found in **Table 4.1**.

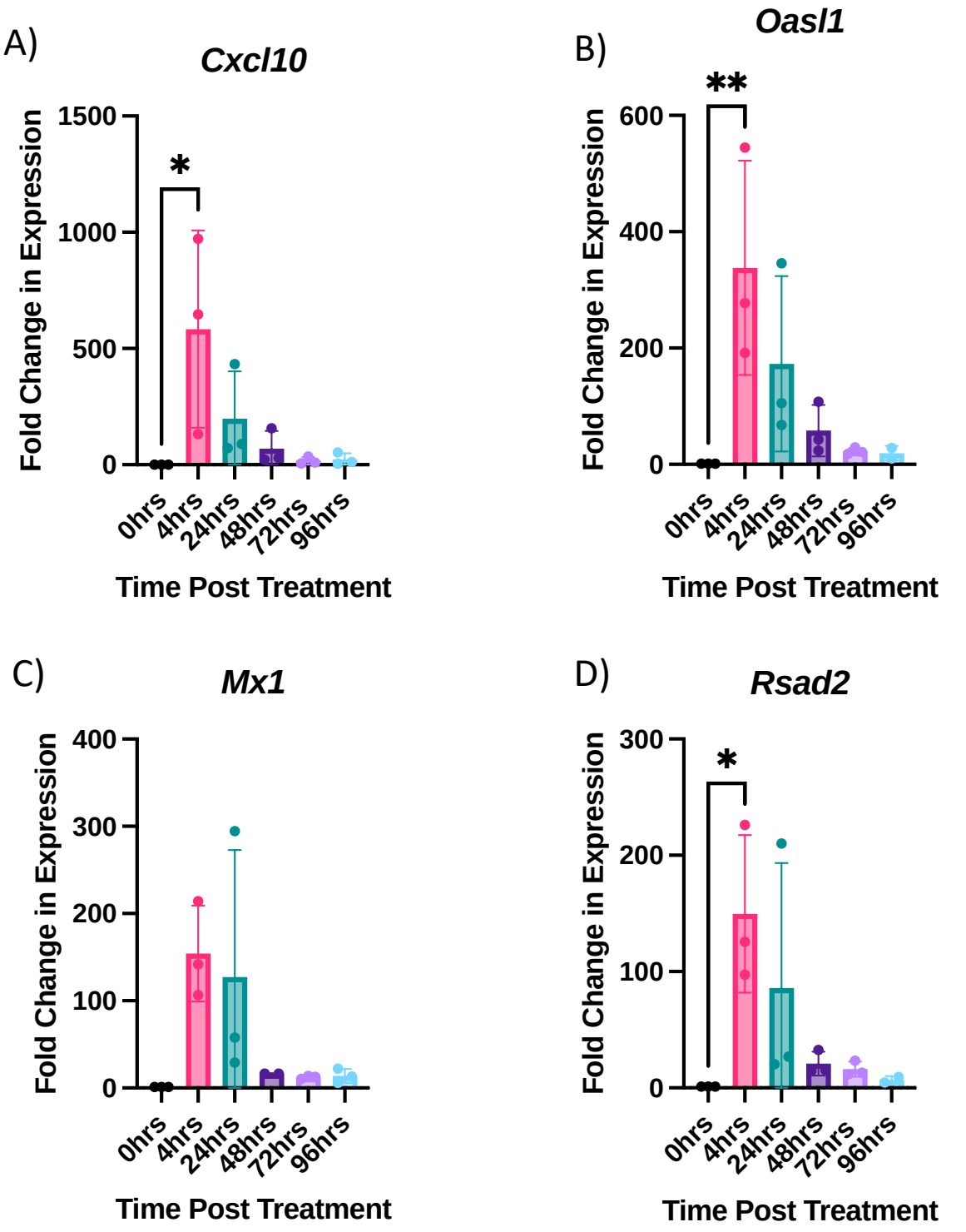


**Figure 4.2: Timecourse of upregulation in ISGs following treatment with IFN-β.** RT-qPCR analysis of the upregulation of ISGs in CNS cultures following IFN-β from 0-96 hours post IFN-β treatment. Expression of *Cxcl10* (A), *Oasl1* (B), *Mx1* (C), and *Rsad2* (D) presented as mean ± SD. Analysed by one-way ANOVA with Dunnett's multiple comparisons test, comparing all to t=0. $p<0.05$ *, $p<0.01$ ** (n=3).

**Table 4.1: Cell analytes analysed by Luminex with associated function.**

| Protein | Role | Reference |
|---|---|---|
| CCL2 | Attracts monocytes and macrophages | (Bose and Cho, 2013) |
| CCL3 | Neutrophil and eosinophil recruitment | (Domachowske *et al.*, 2000) |
| CCL4 | Attract monocytes and macrophages | (Abdulrahman *et al.*, 2022) |
| CCL5 | Attract monocytes and macrophages, recruit lymphocytes | (Marques *et al.*, 2013) |
| CCL7 | Attract eosinophils, Th2 response | (Shang *et al.*, 2002 |
| CCL11 | Attract eosinophils, Th2 Response | (Dixon *et al.*, 2006) |
| CCL12 | Attract eosinophils, monocytes, and macrophages | (Jia *et al.*, 1996) |
| CCL19 | T cell and DC recruitment to lymph nodes | (Shannon *et al.*, 2012) |
| CCL20 | Th17 immune response, GALT development | (Harper *et al.*, 2009) |
| CCL21 | T cell and DC recruitment to lymph nodes | (Shannon *et al.*, 2012) |
| CCL22 | Th2 response | (Nakayama *et al.*, 2004) |
| CXCL1 | Attract and activate neutrophils | (Sawant *et al.*, 2016) |
| CXCL2 | Attract and activate neutrophils | (Rouault *et al.*, 2013) |
| CXCL10 | Th1 response | (J. Li *et al.*, 2017) |
| CXCL12 | B cell Lymphopoiesis, myelopoiesis | (Nagasawa *et al.*, 1996) |
| CXCL13 | Regulate lymphocyte trafficking | (Pan *et al.*, 2022) |
| CXCL16 | NK and T cell trafficking | (Lesch *et al.*, 2021) |
| GMCSF | Promotes myeloid cell development and maturation | (Egea, Hirata and Kagnoff, 2010) |
| IFN-γ | Activation of macrophages, increase phagocytosis, stimulate immune response | (Jorgovanovic *et al.*, 2020) |
| IGBP3 | Inhibit cell proliferation | (Kim, 2013) |
| IL-1α | Attract neutrophils and macrophages, induce inflammation | (Boraschi, 2022) |

***Continues overleaf***

| | | |
|---|---|---|
| IL-3 | Regulate haematopoiesis | (Mangi and Newland, 1998) |
| IL-4 | Regulate haematopoiesis, antibody production, inflammation | (Gadani *et al.*, 2012) |
| IL-5 | Activate and differentiate eosinophils | (Greenfeder *et al.*, 2001) |
| IL-6 | Stimulate haematopoiesis | (Tanaka, Narazaki and Kishimoto, 2014) |
| IL-7 | Regulate homeostasis of lymphocytes and NK cells | (Chen *et al.*, 2021) |
| IL-10 | Regulate production of pro-inflammatory cytokines | (Subramanian Iyer and Cheng, 2012) |
| IL-13 | Induce leukocyte proliferation and activation, recruit eosinophils | (Marone *et al.*, 2019) |
| IL-16 | Attract CD4 T cells, activate T cells | (Mathy et al., no date) |
| IL-17 | Attract neutrophils, activate T cells | (Zenobia and Hajishengallis, 2015) |

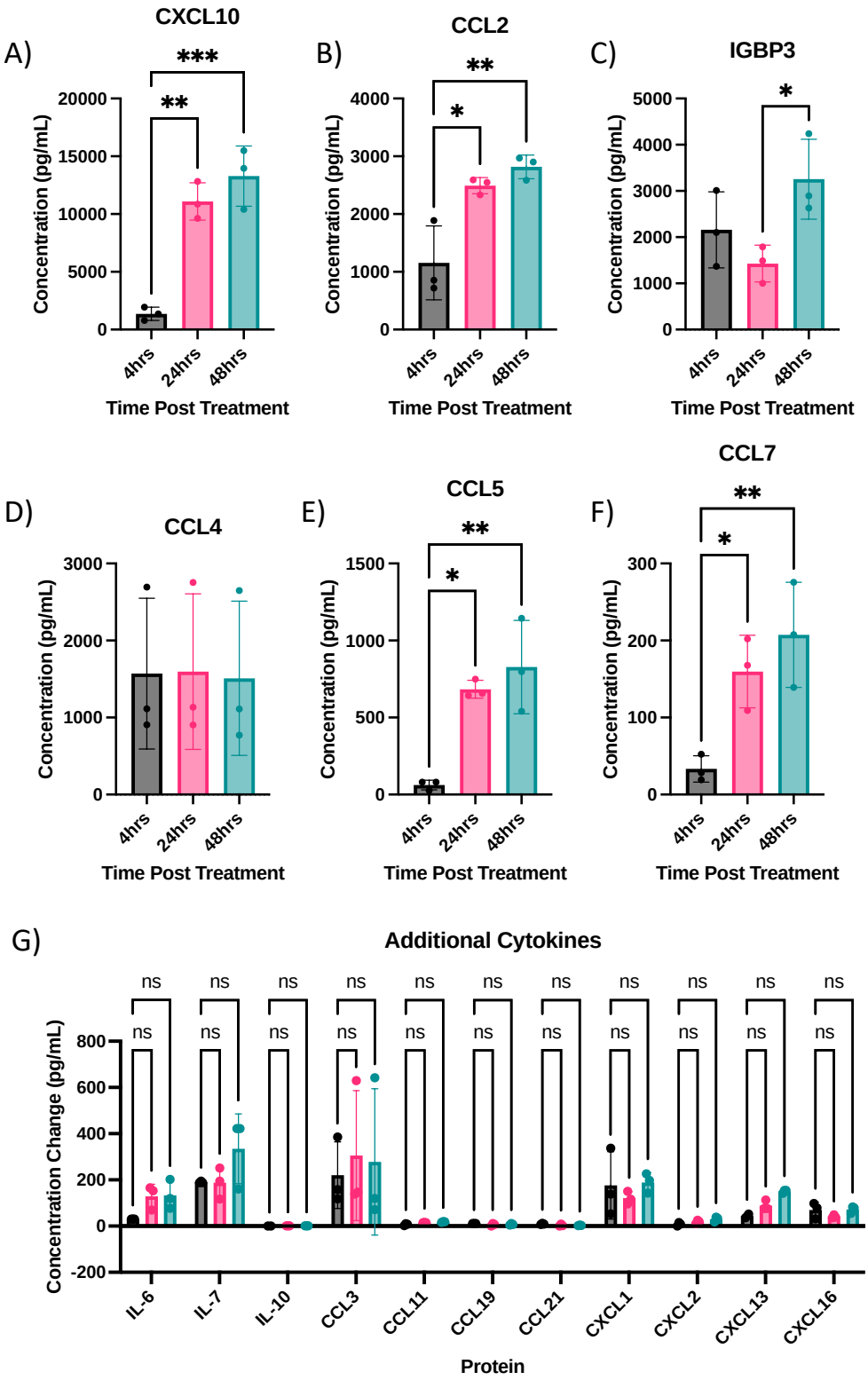


**Figure 4.3: Expression of cytokines following IFN-β treatment**. Expression of cytokines by the CNS cultures 4, 24, and 48 hours after treatment with IFN-β, analysed by Luminex. Expression of CXCL10 (A), CCL2 (B), IGFBP (C), CCL4 (D), CCL5 (E), CCL7 (F) and other cytokines (G) plotted as mean ± SD. A)-F) analysed by one-way ANOVA, F) analysed by two-way ANOVA with Dunnett's multiple comparisons test. All comparisons compared to t=4hr. $p$<0.05 *, $p$<0.01 **, $p$<0.005 ***. (n=3)

Of the 31 proteins investigated, 14 were undetectable. Of the remaining 17 (**Figure 4.3**), 5 had a significant change in their expression. The expression of the chemokine CXCL10 which is involved in T cell recruitment ($p$<0.01, **Figure 4.3A**), monocyte chemoattractant CCL2 ($p$<0.05, **Figure 4.3B**), chemoattractant CCL5 ($p$<0.05, **Figure 4.3E**), and chemoattractant CCL7 ($p$<0.05, **Figure 4.3F**) increased both by 24 hours post treatment and remained significantly higher at 48 hours. The concentration of antiproliferative IGFBP3 decreased between 4 and 24 hours post treatment, then increased significantly between 24 and 48 hours post treatment ($p$<0.05, **Figure 4.3B**). The expression of chemoattractant CCL4 was consistently high across all timepoints analysed (~1600pg/mL, **Figure 4.3D**). The expression of the remaining cytokines remained low, however the concentration IL-6 and IL-7 both tended to increase compared to baseline, albeit not statistically significantly (IL-6 at 24 hours, and IL-7 at 48 hours post treatment, **Figure 4.3F**).

This implied that 50ng/mL of IFN-β is sufficient to induce a significant expression of many varied proteins for up to 48 hours post treatment.

## 4.5 Optimising a gating strategy for individual cell types

To facilitate my investigation of the ISG expression profiles of the individual cell types following IFN-β treatment, I chose fluorescence assisted cell sorting (FACS) to separate out the four major individual cell populations comprising the CNS cell cultures. This method was chosen due to its perceived ease and its prevalent use in immunological studies. However, the multiple dissociation steps, combined with the fragility of neural cells, resulted in significant loss of mRNA from the sorted cells. Consequently, cell dissociation methods, cell markers, and the purity of the sorted cells had to be optimised.

### 4.5.1 0.05% Trypsin-EDTA dissociated cultures have greatest viability and yield

CNS cell cultures were grown on plastic 6 well plates and need to be lifted and dissociated gently to maintain sufficient cell viability for RNA isolation. Since these cultures are fragile, as the cells form numerous processes and connections with the surrounding cells (Michalski and Kothary, 2015; Babetto and Beirowski, 2022), multiple dissociation methods were compared to determine which method provided the optimal viability and cell yield. Untreated cultures were dissociated with different concentrations of trypsin, trypsin-EDTA,

and TrypLE, as detailed in **Table 4.2**. These methods were chosen due to availability, use in pre-established flow cytometry protocols (Kaur and Esau, 2015), and the perceived gentleness of TrypLE (Tsuji *et al.*, 2017). CNS cultures were grown in a 6 well plate, and 1 well (~$1.8x10^6$ cells) was dissociated with each of the selected methods. The resulting yield, viability, and ease of dissociation can be found in **Table 4.2**.

Based on cell viability and counts obtained using a Luna cell counter, and more subjective information such as ease of dissociation and no observed clumping of cells following dissociation, 0.05% Trypsin/EDTA was chosen for further studies. While 10x trypsin yielded a higher number of cells ($5.1x10^5$ vs $4.2x10^5$, **Table 4.2**), and 1x Trypsin had a higher cell viability (68% vs 67%, **Table 4.2**), trypsin/EDTA treated cultures were more easily detached and less likely to form cell clumps. This was the first time the author had dissociated the cultures, and subsequent attempts increased the viability to >85%.

This suggested that 0.05% trypsin-EDTA was the best for dissociating the cultures into a single cell suspension while maintaining sufficient cell viability.

### 4.5.2 Populations of individual cell types can be identified by cell surface immunostaining

As a starting point, cell surface markers for all the cell types in the CNS were identified. Limited use of flow cytometry in neuroimmunology made it challenging to find suitable antibodies. However, a panel was designed as follows. Markers were selected based on a literature search and their expression on the cell surface (G. Kantzer *et al.*, 2017):

- Microglia: $CD45^+CD11b^+$
- Oligodendrocytes: $CD45^-CD11b^-O4^+$
- Astrocytes: $CD45^-CD11b^-O4^-ACSA\text{-}2^+CD24^+$
- Neurons: $CD45^-CD11b^-O4^-ACSA\text{-}2^-CD24^+$

CNS cultures were grown in a 6 well plate and ~$10.8x10^6$ cells were dissociated using the chosen method in **4.5.1**. Using the cell markers above, individual populations of cells could be distinguished by flow cytometry (**Figure 4.4**).

**Table 4.2: Viability of CNS cultures after different dissociation methods**

| Dissociation Method | Live Cells (Total) | Dead Cells (Total) | % Viability | Ease of Dissociation | Clumping of cells observed |
|---|---|---|---|---|---|
| 10x Trypsin | $5.1x10^5$ | $2.54x10^5$ | 66 | No | Yes |
| 1x Trypsin | $3.54x10^5$ | $1.65x10^5$ | 68 | No | Yes |
| 10x Trypsin/EDTA (0.5%) | $3.1x10^5$ | $2.22x10^5$ | 60 | No | No |
| 0.25% Trypsin/EDTA | $2.32x10^5$ | $2.42x10^5$ | 49 | No | No |
| 0.05% Trypsin/EDTA | $4.2x10^5$ | $2.06x10^5$ | 67 | Yes | No |
| TrypLE Express | $2.16x10^5$ | $1.06x10^5$ | 67 | No | Yes |

**Table 4.2: Viability of CNS cultures after different dissociation methods.** Table of cell count data following dissociation of $1.8x10^6$ CNS culture cells indicating cell counts, cell viability, the ease of dissociation, and whether the cells clumped following dissociation. n=1.

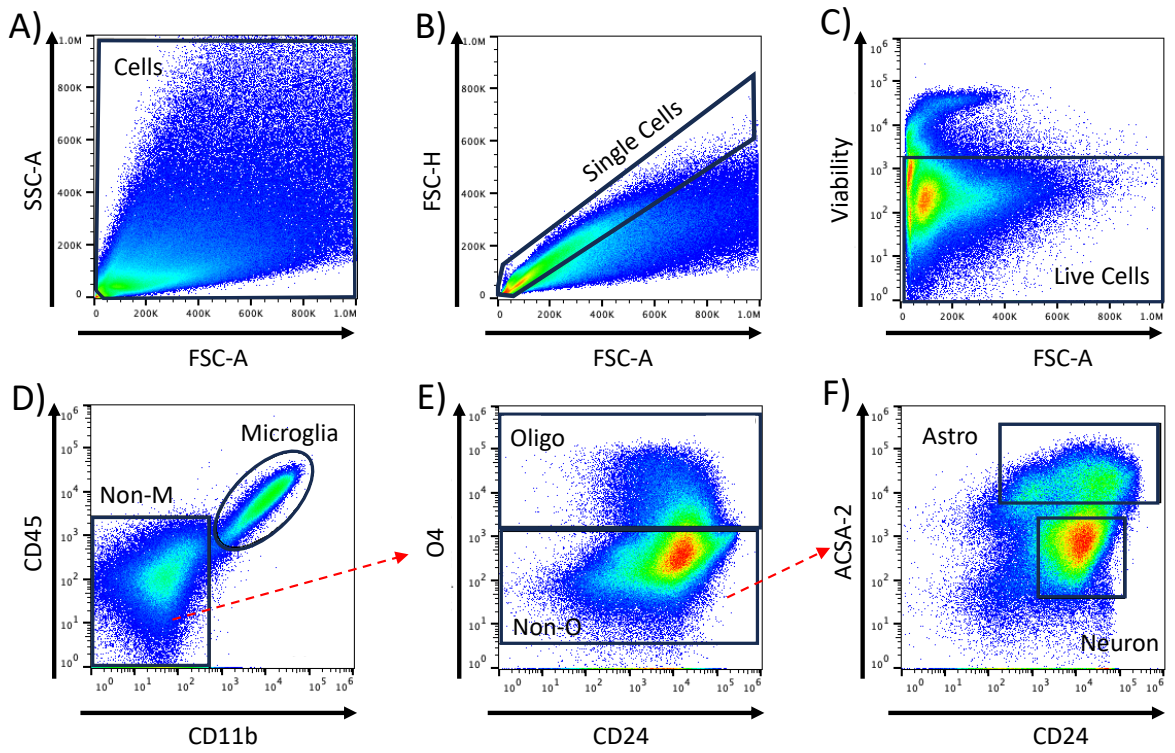


**Figure 4.4: Representative gating strategy for individual populations of cells from CNS cultures.** CNS cultures were grown to DIV21, dissociated into a single cell suspension, and stained with CD45, CD11b, O4, CD24, and ACSA-2 for flow cytometry analysis to confirm the gating strategy. Red arrows indicate subsequent gates between the sub-populations of cells. A) Gate for cells, excluding debris. B) Gate for single cells, excluding doublets or cell connections. C) Gate for live cells, excluding dead. D) Gate for microglia, $CD11b^{+}CD45^{+}$. E) Gate for oligodendrocytes, $CD11b^{-}CD45^{-}O4^{+}$. F) Gate for astrocytes, $CD11b^{-}CD45^{-}O4^{-}ACSA\text{-}2^{+}CD24^{+}$, gate for neurons, $CD11b^{-}CD45^{-}O4^{-}ACSA\text{-}2^{-}CD24^{+}$. Gates determined through use of FMOs. Representative gates established from n=15.

### 4.5.3 By flow cytometry the sorted cells are distinct, mostly uniform, and highly enriched

Following confirmation that the individual populations of cells were distinguishable using flow cytometry, FACS was attempted to confirm that the dissociated CNS cells could be sorted for RNAseq and were of sufficient purity and quantity that valid conclusions could be drawn from the data (**Figure 4.5**). CNS cultures grown in a 6 well plate (~$10.8x10^6$ cells) were dissociated using 0.05% Trypsin-EDTA and stained for FACS, before being sorted using a Sony MA-9000 cell sorter. The individual populations of cells (**Figure 4.5A-D**) appeared distinct and of a similar size, as measured by flow cytometry.

To ensure enrichment, 10,000 sorted cells of each cell-type, for example sorted microglia, were re-analysed using flow cytometry to ensure that the gating strategy selected for sorting was appropriate without contamination of other cell types. I found that >90% of the correct subpopulation of cells were sorted (**Figure 4.5E**), with only oligodendrocytes being less than 99% pure. At least 100,000 cells were sorted per cell type, up to approximately 450,000 microglial cells (**Figure 4.5F**). This experiment suggests that single cell populations of cells can be sorted with sufficient purity and viability for robust RNAseq analysis.

A schematic showing the experimental procedure of procuring single cell populations found in **Figure 4.6**.

### 4.5.4 Sorted cells express appropriate cell type specific markers

To further confirm the purity and viability of the sorted cells, the cell populations were plated on glass coverslips and maintained in cell culture for 4 hours. Subsequently, the cells were fixed visualised using immunofluorescence microscopy. As expected, the sorted cells expressed the cell surface markers of the relevant cell type (**Figure 4.7, red bordered images**). While there were few CNP stained oligodendrocytes, those that were $CNP^+$ had the expected stellate oligodendrocyte morphology (**Figure 4.7F**).

However, there appeared also positive staining of astrocytes by anti-Iba1 (**Figure 4.7C**) and anti-CNP (**Figure 4.7G**). This was likely a false positive due to the secondary AF488 antibody having a similar excitation spectrum to PE-Cy7, the fluorochrome conjugated to ACSA-2. False positives were not observed with anti-NeuN (**Figure 4.7O**) or any other cell type. Therefore, all the experiments performed thus far suggest the sorted cells are pure, viable, and of a sufficient number for robust RNAseq analysis.

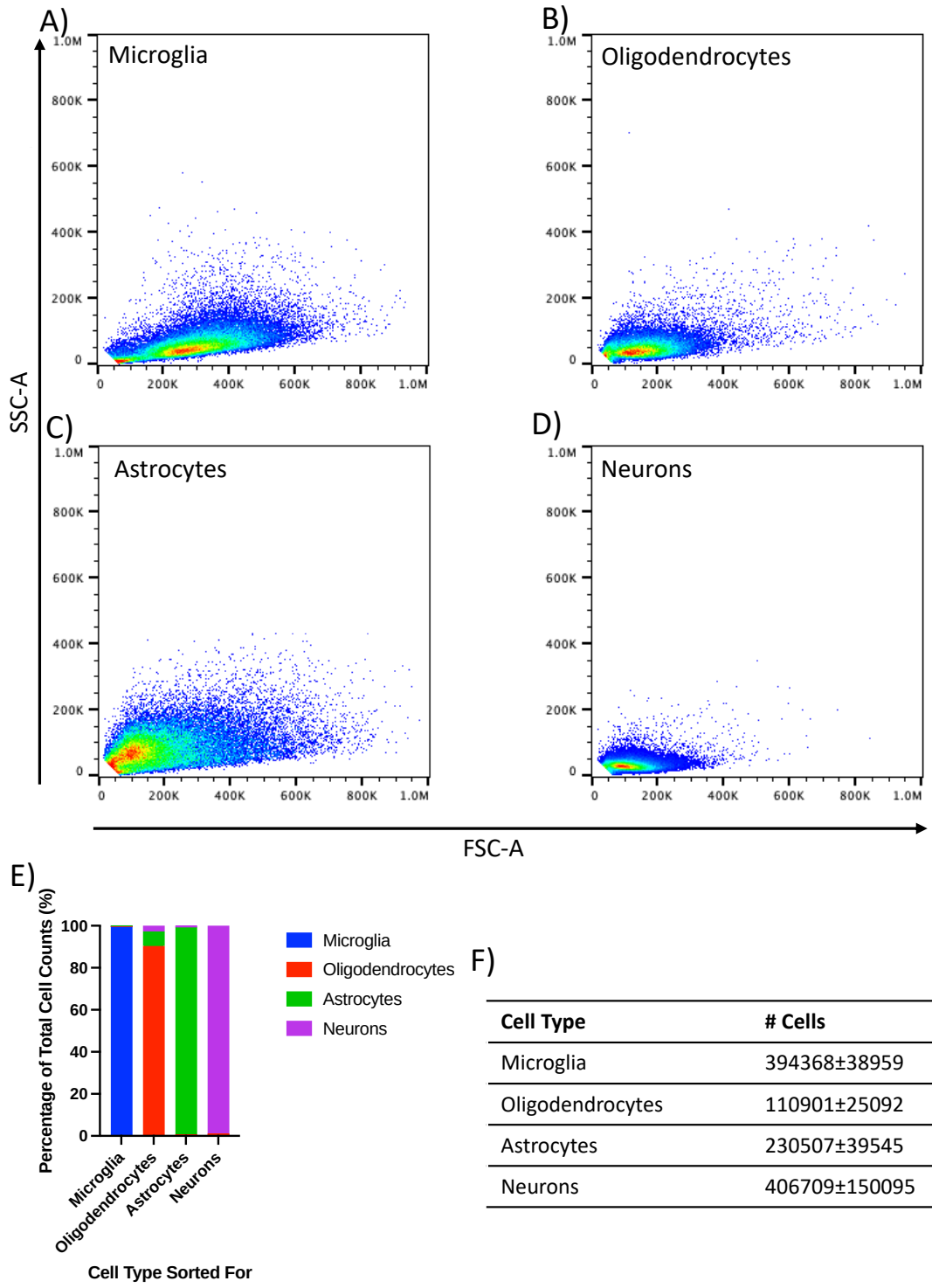


| Cell Type | # Cells |
|---|---|
| Microglia | 394368±38959 |
| Oligodendrocytes | 110901±25092 |
| Astrocytes | 230507±39545 |
| Neurons | 406709±150095 |

**Figure 4.5: Sorted cells are distinct, pure, and of sufficient quantity for RNAseq**. Cells sorted with 130µm nozzle into 50% FCS, 50% PBS before running through the sorter again to verify the populations were pure. Gates follow Figure 5.1. A) FSC-A/SSC-A plot of microglia, B) oligodendrocytes C) astrocyte or D) neurons. E) Stacked plot of sorted cells as a percentage of total cells sorted (n=1). F) Cell counts of sorted cells ± SEM, n=15 (±IFN-β).

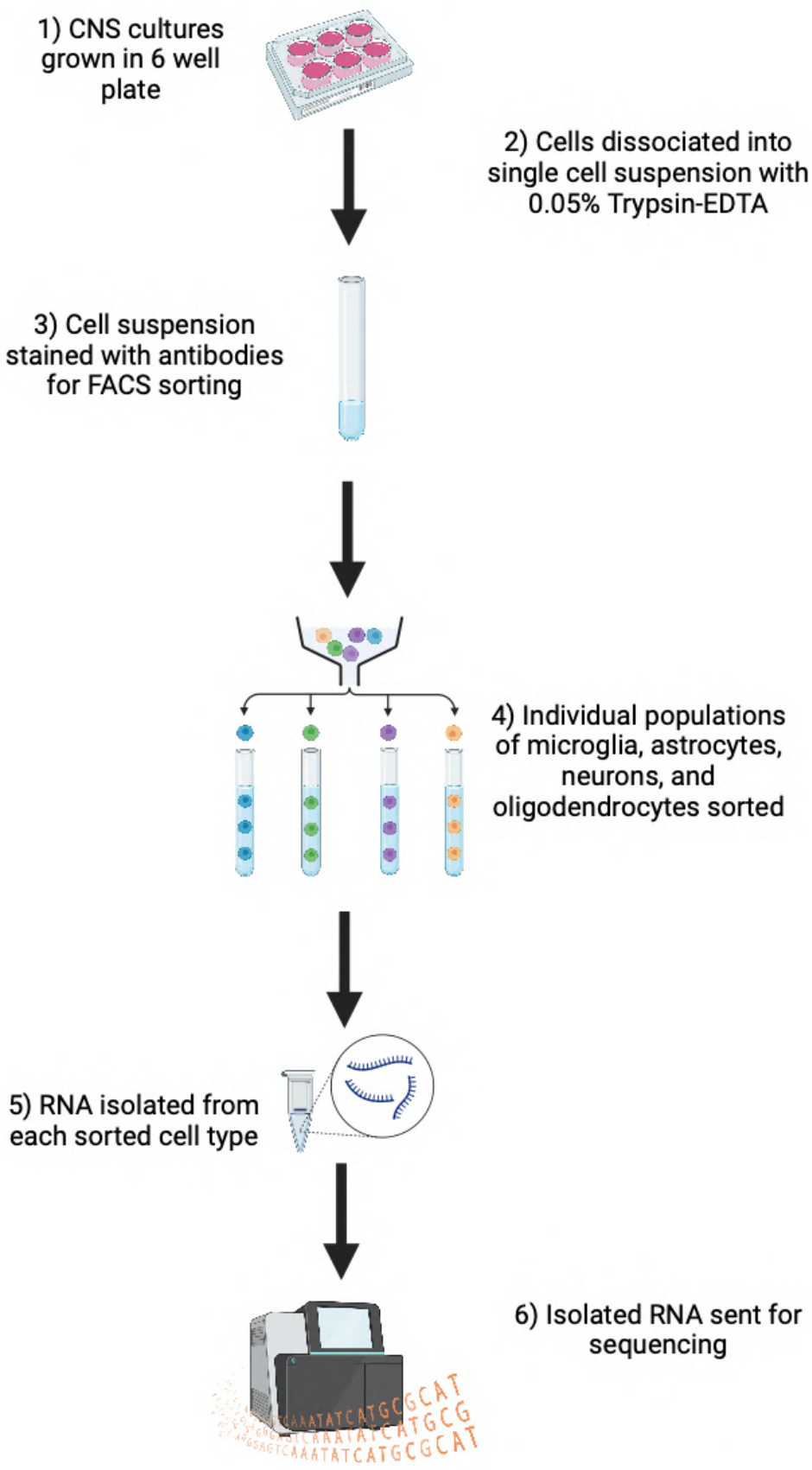


**Figure 4.6: Schematic of optimised fluorescence assisted cell sorting (FACS) of CNS cultures for RNAseq.**

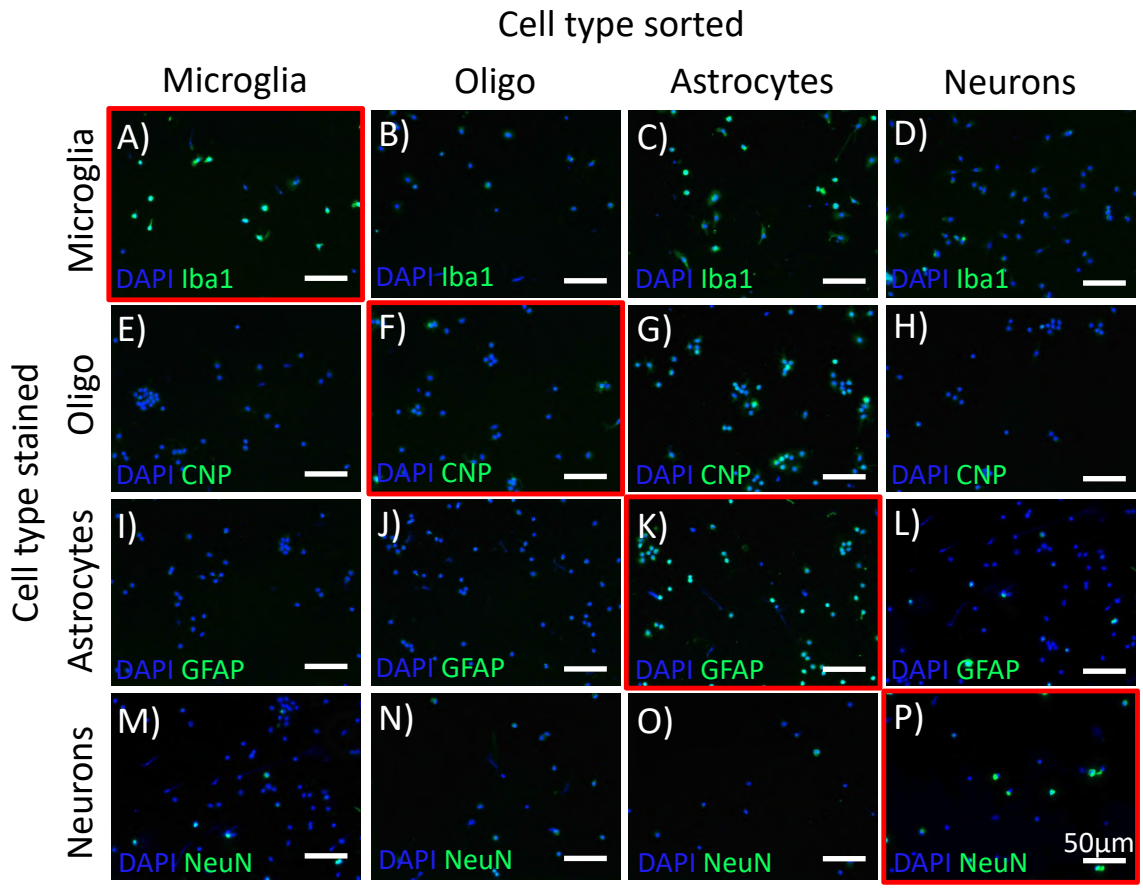


**Figure 4.7: Immunofluorescence images of sorted CNS culture cells.** Cells were plated for 4 hours post-sort before being fixed and stained with cell surface markers for CNS cells: Iba1 (A-D), CNP (E-H), GFAP (I-L), and NeuN (M-P). Red border shows cell type stained for its associated cell surface marker. n=1.

## 4.7 Summary and Discussion

In the work described in this chapter, I determined an optimal dose of IFN-β to induce a robust upregulation and expression of ISGs and developed and optimised a protocol for isolating individual cell-types from CNS cultures.

Initial investigation focussed on identifying an optimal dose of IFN-β to induce an upregulation in ISG transcription and translation. As I aimed to investigate the effect of IFN-β on the different cell types of the CNS, I focussed on ISGs that have previously been shown to be differentially expressed in the four major cell types of the CNS, the microglia, oligodendrocytes, neurons, and microglia. Previous work from our lab found that *Oasl1*, *Rsad2*, *Mx1*, and *Cxcl10* were upregulated ~200 fold following treatment with IgM antibody clone O4 (Hayden *et al.*, 2020), and therefore will likely be upregulated by IFN-β treatment alone. I found that *Rsad2* and *Mx1* had an $EC_{50}$ of ~25ng/mL, while *Cxcl10* and *Mx1* did not appear to reach a maximum induction dose under the tested concentrations of IFN-β. However, this could be due to there only being a biological n of 2 and therefore not reach statistical significance, which further testing could help elucidate.

IFN-β induces the ISGs mentioned here through Janus Kinase (JAK)-signal transducer and activator of transcription proteins (STATs) pathway, hereafter referred to JAK-STAT pathway. The ISG transcription is activated following an interferon response factor (IRF) binding to an interferon-stimulated response element (ISRE) sequence which activates the ISG. Different IRFs induce different ISGs, and here IRF9 (as part of the Interferon stimulated gene factor 3 (ISGF3)) induces *Oasl1* and *Mx1* (Ivashkiv and Donlin, 2014; Raftery and Stevenson, 2017), IRF1 induces *Rsad2* (Rivera-Serrano *et al.*, 2020), and IRF1/2 induces *Cxcl10* (Buttmann *et al.*, 2007). The exact mechanism of activation is not well understood; however, literature has linked *Oasl1* with inhibiting the activity of IRFs in viral infection (Lee *et al.*, 2013). Therefore, it is possible that *Mx1* and *Cxcl10* have not reached their maximum upregulation at 100ng/mL following IFN-β treatment due to another ISG such as OASL1 modulating their transcription. However, at 25ng/mL IFN-β induced ~50-100 fold upregulation in the four ISGs quantified.

There is often not a direct correlation between mRNA transcription and protein levels (Gygi *et al.*, 1999; Greenbaum *et al.*, 2003). As I was particularly interested in proteins expressed following IFN-β treatment, as possible targets for future therapeutics, I needed to

investigate the associated protein levels following IFN-β treatment. I focussed on CCL5 as it was highly expressed after treatment with rhIgM22/LPS **(Chapter 3)**. Indeed, the $EC_{50}$ for CCL5 in my culture system was ~50ng/mL of IFN-β, approximately two-fold higher than the $EC_{50}$ which induced robust ISG mRNA upregulation. Multiple factors play into the quantity of mRNA required to induce translation of protein, such as secondary mRNA structures (Nahvi, Barrick and Breaker, 2004), and protein turnover rates (Wu, Nie and Zhang, 2008). Therefore, I decided to continue with 50ng/mL IFN-β for further studies due to this concentration inducing an upregulation in both the mRNA and protein levels.

ISG upregulation peaked at 4 hours and decreased back to baseline by 24 hours when quantified by RT-qPCR. However, on the Luminex, the chemokine concentrations increased up to 48 hours post treatment. Literature does not adequately describe what could be happening here. CXCL10 expression is highly significantly increased ($p$<0.01**, 24hr, p<0.005***, 48hr), and can be upregulated through induction of additional pathways (T. Liu *et al.*, 2017). Another possible cause of the prolonged expression of CXCL10 could be the lack of the required receptor in the CNS for the chemokines to recycle the protein resulting in no active decrease in chemokine, however the receptor CXCR3 (the receptor for CXCL10) and CCR5 (a receptor for CCL5, also significantly upregulated) have both previously been described in the CNS (Sorce, Myburgh and Krause, 2011; Zhou *et al.*, 2019). Similarly, chemokine concentrations are known to decrease in a time dependent manner when stored at 37°C, with decreases of ~20% recorded in 24 hours (Handschin *et al.*, 2020). This likely implies that additional thus far not well described pathways are being upregulated and activated following IFN-β treatment to keep the chemokine concentrations high for at least 48 hours post treatment. These pathways are outside of the scope of this thesis and would require additional research to identify. At this time, I saw an increase in ISG concentrations from 4 to 48 hours post treatment. This likely means that the innate CNS cells are protected against viral infection from 4 hours until at least 48 hours post exposure to IFN-β. Therefore, studies of IFN-β as a therapeutic against viral infections should focus on this period to validate efficacy.

Uniquely, CCL4 expression remained at a consistent 1.5ng/mL across all timepoints measured. CCL4 induces inflammatory signalling, and is normally upregulated in response to CNS injury (Estevao *et al.*, 2021; Braun *et al.*, 2023). Therefore, this chemokine being

expressed at a similar level to CCL2 and CCL5 (significantly increased by 24 hours) at 4, 24, and 48 hours post treatment is a novel finding and deserves to be investigated further.

After validating and characterising the effect of IFN-β *in vitro*, I next wanted to investigate my hypothesis that IFN-β affects the innate cells-types of the CNS differently. Here, I describe a novel method of isolating individual cell-types from *in vitro* CNS cultures. The data suggests that an antibody panel of CD11b, CD45, O4, ACSA-2, and CD24 is sufficient to visualise the cell types in the CNS. Sorting the cells using FACS into 1mL 50% FCS / 50% PBS with a 130µm nozzle allowed high cell viability and yields of microglia, oligodendrocytes, neurons, and astrocytes to be obtained. Initially, there was contamination of the oligodendrocyte population by astrocytes and neurons (**Figure 4.6E**). However, in subsequent repeats increased distance between the O4+ and O4- gates was employed to increase the purity of the oligodendrocyte population. Overall, I found this to be a useful method to isolate individual cell types in the cultures to study the individual cell responses in isolation by RNAseq. Methods optimised in this chapter are useful to study the innate response of the CNS cultures, for instance to investigate therapeutic targets for viral infections.

# Chapter 5

## Cell-type specific responses to interferon beta

# 5.0 Cell type-specific responses to interferon beta

## 5.1 Introduction

In the previous chapter, I showed that cell sorting by FACS resulted in highly enriched populations of each of the major CNS cell types. Here, I investigated the mRNA expression profiles of each of the individual cell types following treatment with IFN-β in comparison to vehicle (PBS) treated controls using bulk RNAseq. My ultimate aim is to manipulate the intrinsic immune response of the CNS to protect against virus that has tropism towards oligodendrocytes. Therefore, I hypothesised that cell type-specific upregulation of anti-viral genes could be harnessed to identify relevant candidates.

The aims of this chapter were to:

1) Define the overall response of the CNS cell cultures to IFN-β by examining gene expression across the cell types as a whole.

2) Define the response of individual CNS cell types to IFN-β.

3) Determine if IFN-β induces expression of oligodendrocyte-specific ISGs.

To facilitate this, CNS cultures were grown in 6 well plates and treated with PBS (vehicle) or IFN-β for 24 hours before being dissociated and isolated into their individual cell-type populations as described previously (**Figure 4.6**) and the RNA isolated. The isolated RNA was sent for bulk RNA-seq of each individual cell type, and the transcriptional profile of the IFN-β treated cells were compared to the PBS (vehicle) treated cells. The results of which are described in this chapter.

## 5.2 Cell-type specific gene expression confirms that sorted cells are cell-type enriched.

CNS cell cultures are highly complex with multiple physical connections between the different cell types which could result in contamination of one cell type by another (Dahm, Kiebler and Macchi, 2007; Miyamoto *et al.*, 2016). Therefore, I first examined the RNAseq

data to determine whether I had obtained cell type-specific enrichment. To test for enrichment, I examined the expression of the cell type specific marker genes shown in **Table 5.1**.

Based on cell type specific gene expression, each cell type appears to be enriched in the relevant populations. **Figure 5.1** shows the normalised expression of the cell type-specific genes between the 4 different cell types.

The gene expression was normalised through dividing the number of reads of the gene in question by the total number of reads for each sample. Here I did not differentiate between PBS and IFN-β. The oligodendrocyte specific genes (*Cnp, p*<0.005 and *Mbp, p*<0.001, **Figure 5.1C,D**), the microglial genes (*Iba1* & *Tmem119, p*<0.001 **Figure 5.1A,B**), the astrocyte specific genes (*Gfap p*<0.001 and *Slc1a3*, *p*<0.05, **Figure 5.1G,H**), and the neuron specific genes (*Rbfox3, p*<0.001 and *Map2, p*<0.005, **Figure 5.1E,F**) were all significantly enriched in their respective cell types (**Figure 5.1**). The count of normalised reads is in general much lower in neurons (~500 counts for *Rbfox3*) compared to the other cell types (~5000 for *Gfap* and *Iba1*). *Map2* was found, in addition to neurons, to be expressed in oligodendrocytes and astrocytes. Nonetheless, as the other cell populations appeared to be appropriately enriched, further RNAseq analysis was performed comparing the expression profiles of the various cell types following IFN-β treatment.

### 5.2.1 The expression profiles of the individual cell types further implies separate populations of cells

Prior to generating a PCA plot to examine clustering over representation of highly expressed genes was corrected for by scaling gene expression values using the z-score transformation. When gene expression of the various cell types, treated with PBS or IFN-β, is viewed on a PCA plot, it appears that cell type dominates clustering more than treatment. Nonetheless, the PCA plot shows that in general, each of the biological replicates cluster according to cell type and to treatment, especially with respect to astrocytes and microglia. For example, PBS-treated astrocytes tend to cluster together and IFN-β -treated microglia tend to cluster together (**Figure 5.2A**).

**Table 5.1: Cell type specific genes and their associated proteins.**

| Cell Type | Gene | Protein Encoded | Reference |
|---|---|---|---|
| **Oligodendrocytes** | *Cnp1* | CNPase | (Gravel *et al.*, 1996; Yin *et al.*, 1997) |
| | *Mbp* | MBP | (Galiano *et al.*, 2006) |
| **Astrocytes** | *Gfap* | GFAP | (Yang and Wang, 2015) |
| | *Slc1a3* | EAAT1 / GLAST | (Batiuk *et al.*, 2020) |
| **Microglia** | *Tmem119* | TMEM119 | (Bennett *et al.*, 2016) |
| | *Iba1* | Iba1 | (Ito *et al.*, 1988; Imai *et al.*, 1996) |
| **Neurons** | *Rbfox3* | NeuN | (Lin *et al.*, 2016) |
| | *Map2* | Map2 | (Soltani *et al.*, 2005; DeGiosio *et al.*, 2022) |

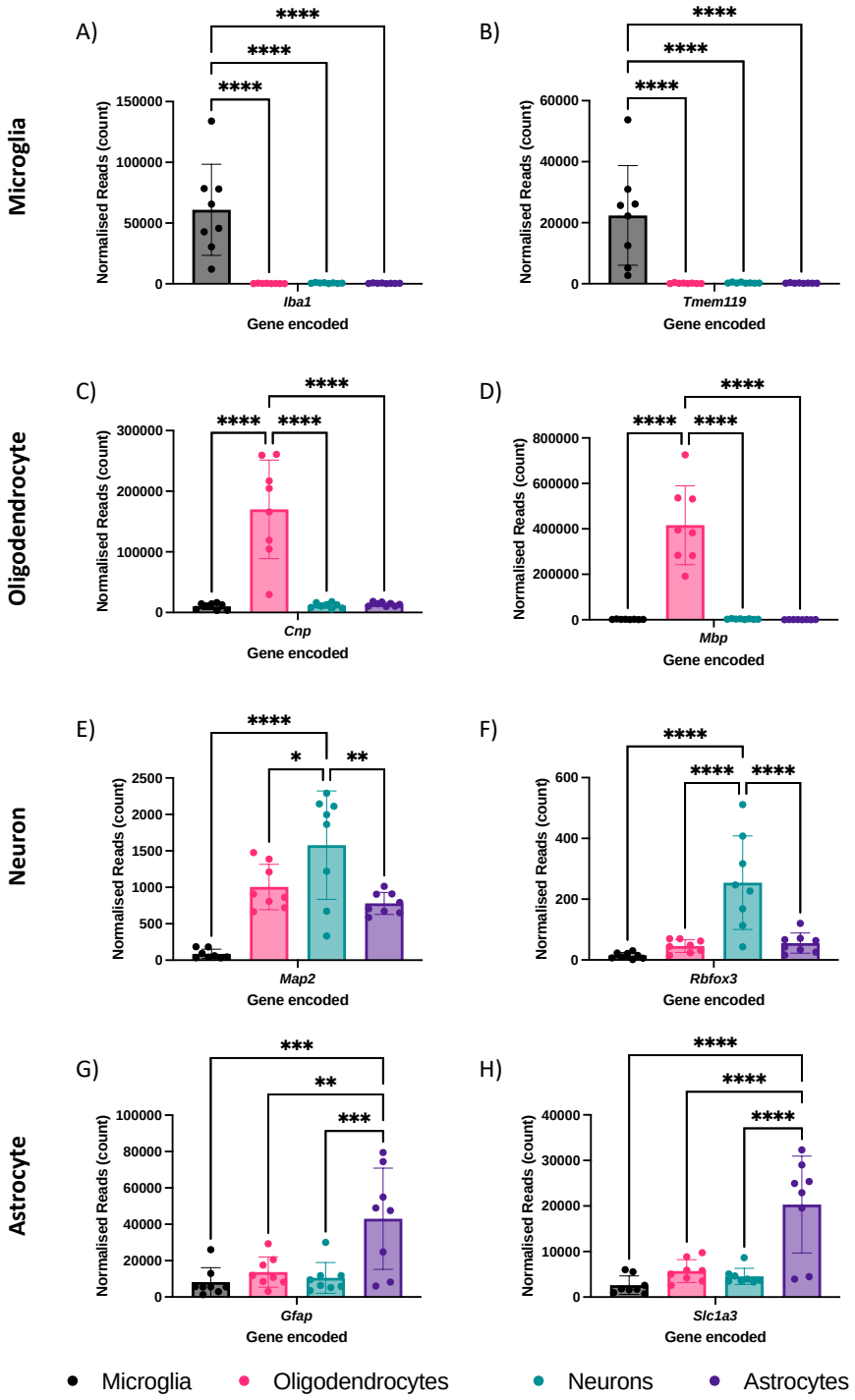


**Figure 5.1: Expression of cell type specific genes in FACS sorted cells confirms cell type-specific enrichment.** Graphs show gene expression normalised number of reads across sorted cell types. The expression of cell type specific genes for A,B) microglia, C,D) oligodendrocytes, E,F) neurons and G,H) astrocytes, across sorted cell populations are significantly enriched in the relevant cell type. *Map2* was also enriched in oligodendrocytes and astrocytes. Bars represent mean ± SD. Analysed by one-way ANOVA with Dunnett's multiple comparisons test, significance denoted as *$p$<0.05, **$p$<0.01, ***$p$<0.005, ****$p$<0.001. n=8.

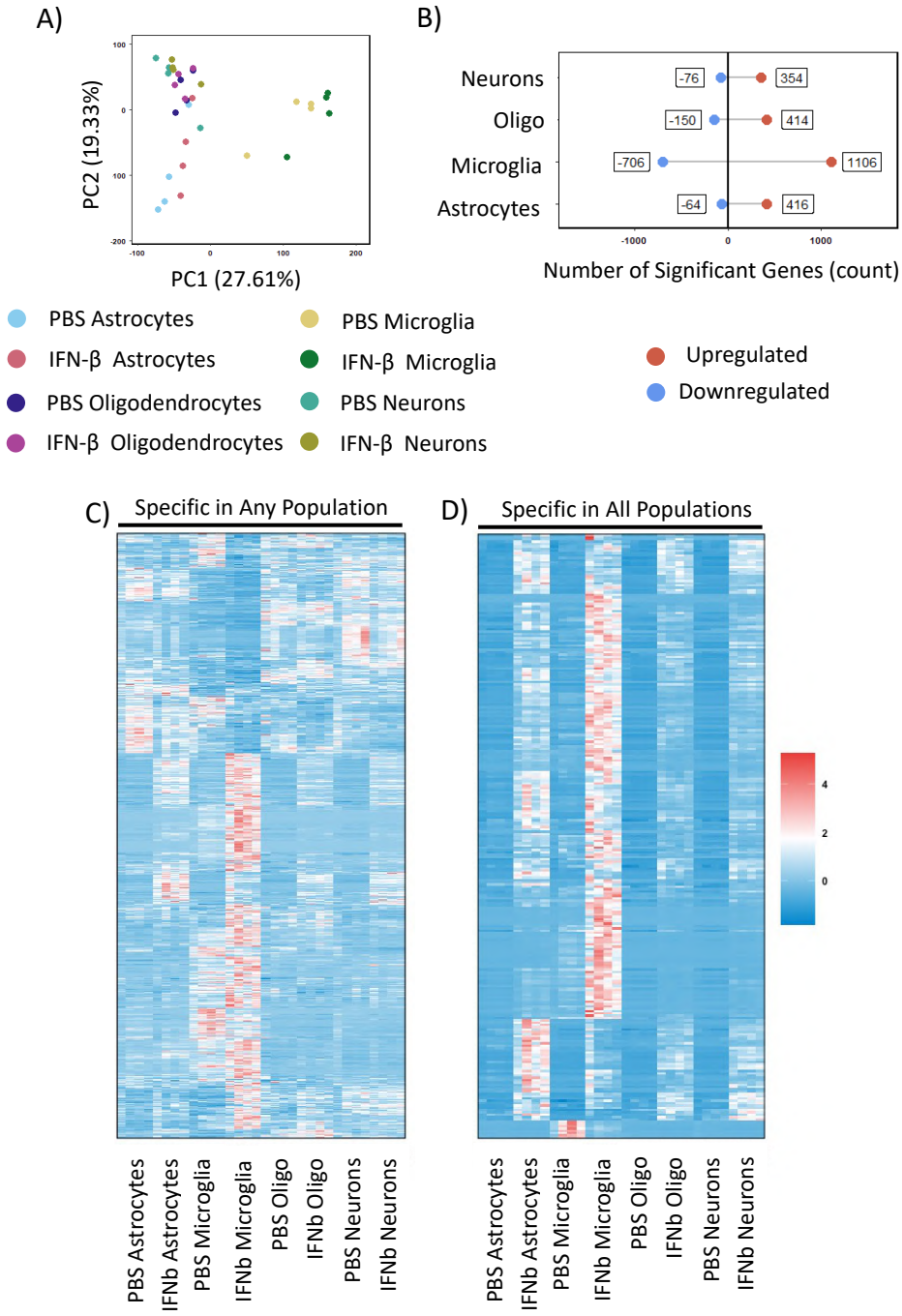


**Figure 5.2: PCA and differentially expressed genes in CNS cultures following IFN-β treatment.** Data generated from RNAseq of sorted cells. A) PCA scatter plot. Each individual sample represented by a single dot. Percentage total variation presented on X and Y axes for PC1 and PC2 respectively. B) Chart showing number of differentially expressed genes, with each dot generated from 4 independent replicates of each cell type following IFN-β treatment compared to PBS control, $p<0.001$. n=4. C-D) Heatmap of all differentially expressed genes for cell type specific populations (A) or all populations (B) compared to vehicle control. Data row standardised by scaling into z-scores to normalise expression. n=4 per condition.

As the cell-types cluster on the PCA, the expression profiles of each individual cell types seem similar and therefore appropriate conclusions can be drawn about the effect of IFN-β on each individual cell type. Since many genes were differentially upregulated in the presence of IFN-β (ranging from 354 in neurons to 1106 in microglia) across all the different cell types (**Figure 5.2B**), I was interested in identifying which pathways were involved.

## 5.3 Pathway analysis indicates CNS cultures become innately antiviral

Across all CNS culture cell types, the RNAseq data identified 2159 differentially expressed genes (**Appendix 8.1**), meaning they were significantly upregulated or downregulated in IFN-β treated cells compared to vehicle treated control cells (*p.adj*-value<0.0001, log2fold>2) (**Table 8.1**). As I aimed to identify proteins that are expressed by IFN-β treatment I focussed on specifically the upregulated genes for the remainder of the chapter.

### 5.3.1 Gene Ontology Pathway Analysis

Gene ontology (GO) analysis identifies functional terms that are over-represented in a dataset compared to their normal frequency in the genome (Ashburner *et al.*, 2000; Aleksander *et al.*, 2023). These terms can be grouped into their biological, molecular, and cellular processes. Initially, the DEGs for each cell type were pooled to investigate the effect of IFN-β as a treatment across the cell types, hereafter referred to as pooled-DEGs. Across all CNS cell types, 23 biological processes were enriched following IFN-β treatment (*p.adj*<0.0001, log2fold>2), all of which were related to interferon treatment or antiviral pathways (**Table 5.2**). The cellular component analysis indicated that this is related to downstream pathways of MHC antigen presentation (**Table 5.2**). Pattern associated molecular pattern (PAMP) receptors were upregulated, along with genes encoding MHC class I and II proteins (6.24 and 9.88 enrichment scores, respectively) suggesting IFN-β increases the ability to recognise invading pathogens and present the processed antigens to lymphocytes. Normalised read counts for the top 9 genes for each grouping identified in **Table 5.2**, identified due to having the greatest mean number of read counts across all 4 sorted cell types, are found in **Appendix 8.2**.

**Table 5.2: Gene ontology (GO) analysis of genes differentially upregulated in cells of CNS cultures by IFN-β**

| Pathways Upregulated for Significant Genes (*p*-Value<0.0001, log2fold>2) | | | | | | | | |
|---|---|---|---|---|---|---|---|---|
| **Term - Biological** | **GO Term ID** | **Count** | **Enrichment** | ***p*-value** | **M** | **O** | **N** | **A** |
| Response to interferon-beta | GO:0045089 | 98 | 4.03 | 1.93E-22 | Y | Y | Y | Y |
| | GO:0051607 | 85 | 4.09 | 1.96E-19 | Y | Y | Y | Y |
| | GO:0140546 | 85 | 4.07 | 2.43E-19 | Y | Y | Y | Y |
| | GO:0002218 | 62 | 4.71 | 6.35E-16 | Y | Y | Y | Y |
| | GO:1903900 | 51 | 4.16 | 7.13E-11 | Y | Y | Y | Y |
| | GO:0071346 | 39 | 4.39 | 2.70E-08 | Y | Y | Y | Y |
| | GO:0032648 | 27 | 4.56 | 3.04E-05 | Y | Y | Y | Y |
| Regulation of virus / pathogen | GO:0035456 | 44 | 7.33 | 4.46E-16 | Y | Y | Y | Y |
| | GO:0035458 | 38 | 7.45 | 1.02E-13 | Y | Y | Y | Y |
| | GO:0032479 | 43 | 4.02 | 2.32E-08 | Y | Y | Y | Y |
| | GO:0045071 | 26 | 5.65 | 1.59E-06 | Y | Y | Y | Y |
| | GO:0045069 | 32 | 4.47 | 1.63E-06 | Y | Y | Y | Y |
| | GO:0034340 | 22 | 6.69 | 3.48E-06 | Y | Y | Y | Y |
| Regulation of innate immune response | GO:0034341 | 52 | 4.62 | 1.23E-12 | Y | Y | Y | Y |
| | GO:0002221 | 37 | 4.2 | 2.71E-07 | Y | Y | Y | Y |
| | GO:0032481 | 30 | 4.45 | 6.66E-06 | Y | Y | Y | Y |
| | GO:0032728 | 23 | 5.38 | 3.70E-05 | Y | Y | Y | Y |
| **Term - Molecular** | **GO Term ID** | **Count** | **Enrichment** | ***p*-value** | **M** | **O** | **N** | **A** |
| PRR activity | GO:0038187 | 20 | 6.24 | 1.78E-05 | N | N | N | N |
| Nucleotidyl-transferase activity | GO:0016779 | 36 | 3.22 | 6.42E-05 | Y | Y | Y | Y |
| **Term - Cellular** | **GO Term ID** | **Count** | **Enrichment** | ***p*-value** | **M** | **O** | **N** | **A** |
| Regulation of MHC-I | GO:0042824 | 13 | 9.88 | 8.92E-05 | Y | Y | Y | Y |
| | GO:0042611 | 18 | 4.86 | 9.62E-04 | Y | Y | Y | Y |

**Table 5.2: Gene ontology (GO) analysis of genes differentially upregulated in cells of CNS cultures by IFN-β.** Table showing GO analysis of genes upregulated by IFN-β in any cell type sorted (*p.adj*-value <0.0001, fold enrichment >3) Terms grouped by similar representative term, with unique pathways enriched identified by ID. GO Term ID = unique pathway identifier. Count = number of genes associated with GO term. Enrichment = fold increase in number of genes significantly upregulated compared to the expected value. Pathways enriched in sorted microglial cells (M), oligodendrocytes (O), neuronal cells (N) or astrocytes (A). n=16 or 4 (for individual cell types).

Similarly, the GO pathways from the pooled-DEGs were compared to those for each individual cell type to determine if the pathway was upregulated also in a cell-type specific manner Across all individual cell types, the same GO term pathways were upregulated as in the pooled-DEGs apart from the PAMP receptor activity which was not upregulated in any single cell type. This implies that the IFN-β treatment, *per se*, or the products of IFN-β receptor activation, induces all individual cell types towards an antiviral state.

### 5.3.2 Reactome and KEGG Pathway Analysis

Like GO analysis, Reactome (Griss *et al.*, 2020; Gillespie *et al.*, 2022) and KEGG (Kanehisa and Goto, 2000a; Kanehisa, 2019; Kanehisa *et al.*, 2023) pathways show how different gene products interact and relate to each other, suggesting different pathways that could be enriched in the data. Here, pathways can include examples of human diseases (KEGG), and more specific pathway information (Reactome).

Across all CNS cell types, KEGG pathways identified multiple, distinct pathways enriched in human viral infectious disease such as Epstein-Barr virus (3.04 enrichment, **Table 5.3**), measles (2.89 enrichment, **Table 5.3**), and hepatitis C (2.36 enrichment, **Table 5.3**). Other pathways enriched included signalling pathways, and antigen processing and presentation (4.21 enrichment, **Table 5.3**). The pathways identified here are also found enriched in each of the individual 4 cell types. Reactome analysis identified antigen processing and presentation (4.2 enrichment, **Table 5.4**), which was enriched in all the individual cell types. Additional pathways were only enriched in the pooled-DEG analysis, and these included APC-mediated degradation of cell proteins (3.67 enrichment, **Table 5.4**), and regulation of cell cycle (3.2 enrichment, **Table 5.4**). The combined analysis with GO, KEGG, and Reactome suggest that each cell, while having a distinct response to IFN-β, acts as part of a concerted effort in the CNS to induce a profoundly antiviral effect. As previously, normalised read counts for the top 9 genes for each grouping identified in **Table 5.2**, identified due to having the greatest mean number of read counts across all 4 sorted cell types, are found in **Appendix 8.2**.

### 5.3.3 Functional annotation clustering

Each of the analyses mentioned thus far have identified many pathways upregulated in response to IFN-β. However, multiple pathways are related or overlapping. Therefore, functional annotation clustering was performed to collapse the results into clusters of similar pathways.

Using DAVID (the Database for Annotation, Visualisation, and Integrated Discovery), clusters were identified (**Figure 5.3)**. The pathways were clustered from the GO, KEGG, Reactome pathway analyses, but also additional information on protein domains and interactions from InterPro (Paysan-Lafosse *et al.*, 2023), PIR (Wu *et al.*, 2003), and SMART (Letunic, Khedkar and Bork, 2021). The clustering was performed on both the pooled-DEGs and also the cell-type specific DEGs.

Using slightly stricter exclusion criteria for ease of analysis, 18 clusters were identified ($p<0.0001$, log2fold>5) that were enriched following IFN-β treatment (**Figure 5.3**). For all cell types combined (**Figure 5.3A**), these were for innate immunity (27.56 enrichment, **Table 8.1**), response to virus (16.77 enrichment, **Table 8.2**), GTP-binding ( 8.74 enrichment, **Table 8.3**), virus related pathways

(7.15 enrichment, **Table 8.4**), defence response to protozoan (5.73 enrichment, **Table 8.5**), and activation of immune response (5.49 enrichment, **Table 8.6**). Some were found to be enriched in only certain cell types. In particular, negative regulation of viral genome (6.98 enrichment, **Table 8.11**) and response to type I interferon (5.94 enrichment, **Table 8.12**) were specific to microglia (**Figure 5.4C**); regulation of viral entry into the cell (5.47 enrichment, **Table 8.13**) and oligoadenylate synthetase (5.00 enrichment, **Table 8.14**) were specific to oligodendrocytes (**Figure 5.3D**; regulation of IFN-β production (7.10 enrichment, **Table 8.15**) and nucleotide binding (5.00 enrichment, **Table 8.16**) were specific to astrocytes (**Figure 5.4E**). These data point to each of the individual cell types of the CNS responding, in part, differently to IFN-β treatment.

When analysing these clusters I found substantial gene overlap, with some of the 670 distinct genes across all pathways (**Table 8.1**) being observed in multiple distinct clusters. Overall, the data show that IFN-β induced a profoundly antiviral response across the CNS cultures as a whole. This response also occurred in each individual cell type. There is also some preliminary data that each cell type responds differently to interferon beta treatment.

**Table 5.3: Kyoto encyclopaedia of genes and genomes (KEGG) analysis of genes differentially upregulated in cells of the CNS cultures following IFN-β treatment.**

| Pathways Upregulated for Significant Genes (*p*-Value<0.0001, log2fold>2) | | | | | | | | |
|---|---|---|---|---|---|---|---|---|
| **KEGG Term** | **KEGG ID** | **Count** | **Enrichment** | ***p*-Value** | **M** | **O** | **N** | **A** |
| Response to human pathogens | mmu05169 | 65 | 3.04955437 | 1.49E-16 | Y | Y | Y | Y |
| | mmu05164 | 48 | 3.00697722 | 4.79E-12 | Y | Y | Y | Y |
| | mmu05162 | 39 | 2.89498791 | 2.08E-09 | Y | Y | Y | Y |
| | mmu05167 | 50 | 2.41911765 | 6.08E-09 | Y | Y | Y | Y |
| | mmu05166 | 53 | 2.29758118 | 1.29E-08 | Y | Y | Y | Y |
| | mmu05416 | 27 | 3.32518717 | 4.62E-08 | Y | Y | Y | Y |
| | mmu05163 | 50 | 2.11672794 | 5.02E-07 | Y | Y | Y | Y |
| | mmu05203 | 36 | 2.36457754 | 1.96E-06 | Y | Y | Y | Y |
| | mmu05160 | 46 | 2.07721569 | 2.64E-06 | Y | Y | Y | Y |
| | mmu05170 | 36 | 2.16752941 | 1.51E-05 | N | N | N | N |
| | mmu05152 | 26 | 2.56162567 | 1.64E-05 | N | N | N | N |
| | mmu05145 | 45 | 2.12966864 | 1.73E-06 | Y | Y | Y | Y |
| | mmu05161 | 32 | 2.12763623 | 7.12E-05 | N | N | N | N |
| Antigen processing and presentation | mmu04612 | 35 | 4.21464052 | 1.53E-13 | Y | Y | Y | Y |
| Cell function and metabolism | mmu03050 | 22 | 5.07294118 | 1.75E-10 | N | N | N | N |
| | mmu04621 | 47 | 2.35819172 | 4.27E-08 | Y | Y | Y | Y |
| | mmu04145 | 40 | 2.38190045 | 3.88E-07 | Y | Y | Y | Y |
| | mmu04514 | 36 | 2.14371041 | 1.94E-05 | Y | Y | Y | Y |
| | mmu01232 | 21 | 2.70941176 | 5.62E-05 | N | N | N | N |
| Transplant rejection | mmu05330 | 23 | 3.95660131 | 1.72E-08 | Y | Y | Y | Y |
| | mmu05332 | 22 | 3.78457516 | 9.17E-08 | Y | Y | Y | Y |
| Autoimmune disease | mmu04940 | 22 | 3.40611765 | 6.85E-07 | Y | Y | Y | Y |
| | mmu05320 | 23 | 3.15526433 | 1.53E-06 | Y | Y | Y | Y |

**Table 5.3: Kyoto encyclopaedia of genes and genomes (KEGG) analysis of genes differentially upregulated in cells of the CNS cultures following IFN-β treatment.** Table showing GO analysis of genes upregulated by IFN-β in any cell type sorted (*p.adj*-value <0.0001, fold enrichment >3). Terms grouped by similar representative term, with unique pathways enriched identified by ID. KEGG ID = unique pathway identifier. Count = number of genes associated with KEGG term. Enrichment = fold increase in number of genes significantly upregulated compared to the expected value. Pathways enriched in sorted microglia (M), oligodendrocytes (O), neurons (N), or astrocytes (A) n=16 or (4 for individual cell types).

**Table 5.4: Reactome analysis of genes differentially upregulated in cells of the CNS cultures following IFN-β treatment**

| Reactome Term | Reactome ID | Count | Enrichment | *p*-Value | M | O | N | A |
|---|---|---|---|---|---|---|---|---|
| Antigen processing / presentation | R-MMU-1236975 | 41 | 4.20207347 | 3.23E-16 | Y | Y | Y | Y |
| | R-MMU-1236978 | 23 | 4.42587728 | 8.43E-10 | N | N | N | N |
| Response to oxidative stress | R-MMU-9755511 | 30 | 3.77161716 | 1.47E-10 | N | N | N | N |
| | R-MMU-9759194 | 22 | 3.84146192 | 4.58E-08 | N | N | N | N |
| | R-MMU-350562 | 22 | 4.06743027 | 1.38E-08 | N | N | N | N |
| Control of cell cycle | R-MMU-176814 | 30 | 3.67365308 | 3.09E-10 | N | N | N | N |
| | R-MMU-176409 | 29 | 3.59792427 | 1.13E-09 | N | N | N | N |
| | R-MMU-453276 | 30 | 3.2513941 | 8.32E-09 | N | N | N | N |
| | R-MMU-174143 | 30 | 3.2513941 | 8.32E-09 | N | N | N | N |
| | R-MMU-75815 | 22 | 4.06743027 | 1.38E-08 | N | N | N | N |
| | R-MMU-179419 | 27 | 3.44032647 | 1.42E-08 | N | N | N | N |
| | R-MMU-187577 | 24 | 3.77161716 | 1.45E-08 | N | N | N | N |
| | R-MMU-69202 | 26 | 3.50221594 | 1.84E-08 | N | N | N | N |
| | R-MMU-69656 | 26 | 3.40493216 | 3.54E-08 | N | N | N | N |
| | R-MMU-8854050 | 22 | 3.84146192 | 4.58E-08 | N | N | N | N |
| | R-MMU-174154 | 25 | 3.46655989 | 4.62E-08 | N | N | N | N |
| | R-MMU-174184 | 26 | 3.35828925 | 4.84E-08 | N | N | N | N |
| | R-MMU-69563 | 24 | 3.53589109 | 5.98E-08 | N | N | N | N |
| | R-MMU-69580 | 24 | 3.53589109 | 5.98E-08 | N | N | N | N |
| RNA degradation | R-MMU-450408 | 23 | 3.87264262 | 1.75E-08 | N | N | N | N |

**Table 5.4: Reactome analysis of genes differentially upregulated in cells of the CNS cultures following IFN-β treatment.** Table showing top 13 reactome analysis pathways of genes upregulated by IFN-β in any cell type sorted (*p.adj*-value <0.0001, fold enrichment >3). Terms grouped by similar representative term, with unique pathways enriched identified by ID. Reactome ID = unique pathway identifier. Count = number of genes associated with KEGG term. Enrichment = fold increase in number of genes significantly upregulated compared to the expected value. Pathway found enriched in sorted microglia (M), oligodendrocytes (O), neurons (N), or astrocytes (A) n=16, or 4 for individual cell types.

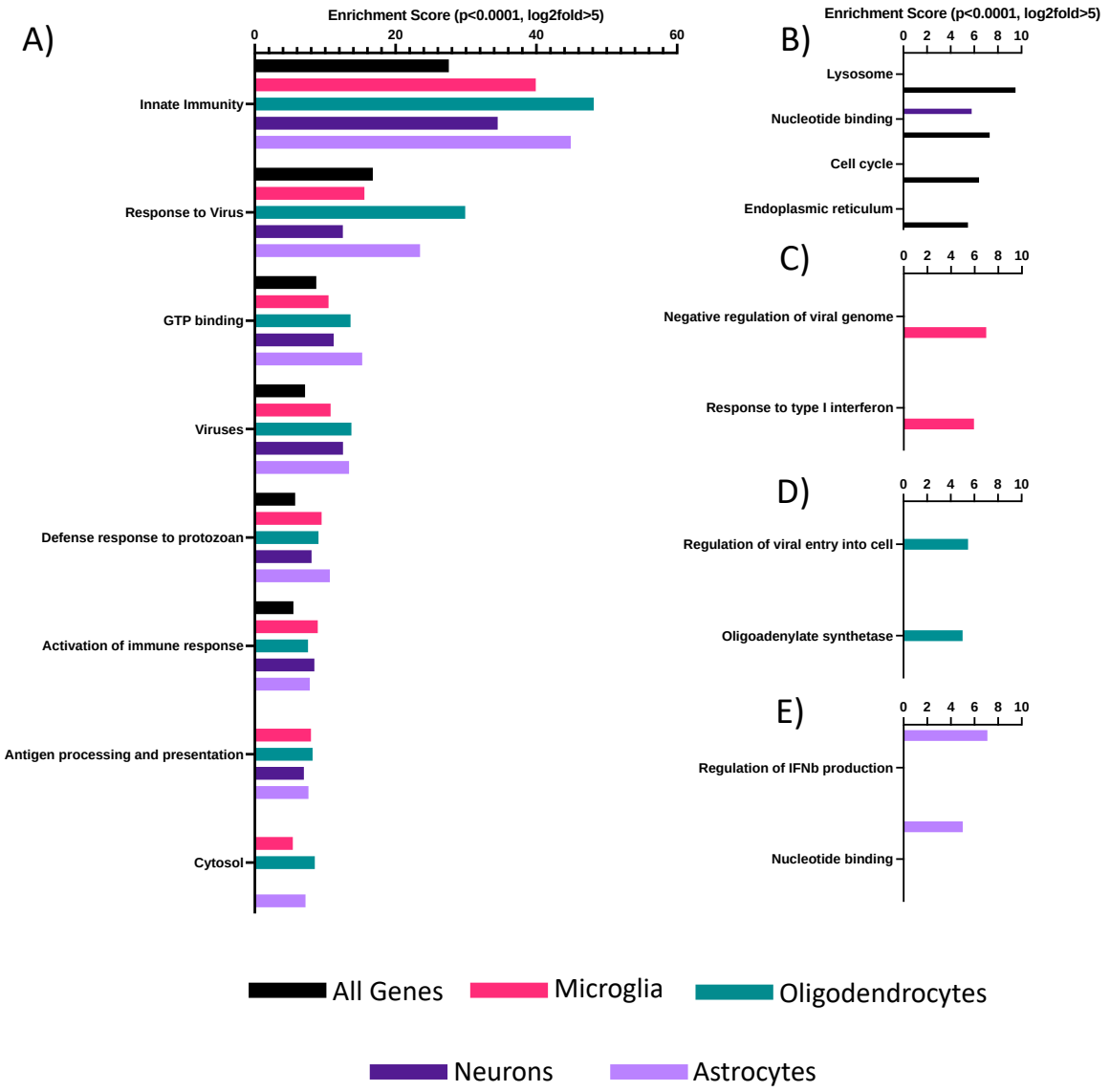


**Figure 5.3: Functional annotation clustering of genes differentially expressed by IFN-β.** Graph showing functional annotation clusters that were significantly increased following 24 hour treatment with IFN-β. A) Functional annotation clustering of at least 3 different cell types, found in all cell types combined (B), microglia (C), oligodendrocytes (D), or astrocytes (E). Data are presented as enrichment scores. Significantly upregulated genes are p<0.0001, log2fold>2. All clusters enriched with adjusted *p.adj*-Value <0.0001, and an enrichment score >5. n=16 or 4 for individual cell types.

## 5.4 Each individual cell type upregulates cell-specific genes following IFN-β treatment

Next, I asked if there are certain genes that are only significantly upregulated in specific cell types. Out of a total of 369 differentially expressed genes, a total of 11 genes were found to be upregulated specifically in oligodendrocytes (~3%), 7 in neurons (~2%), 15 in astrocytes (~4%), and 119 in microglia (~30%) (**Figure 5.4**). Of the 151 genes that were upregulated in all the 4 sorted cell types, these are primarily linked to response to virus, positive regulation of IFN-β pathway, and activation of innate immune response, when clustered by function.

Since I was primarily interested in investigating how to decrease the infectivity of the oligodendrocyte specific Human Polyomavirus 2, only the oligodendrocyte specific genes will be discussed for the remainder of the chapter.

## 5.5 Transcriptional profile of oligodendrocytes identified cell-type specific pathways and candidates

### 5.5.1: Pathway analysis of oligodendrocyte-specific differentially expressed genes

When investigating the differentially expressed genes in the oligodendrocytes specifically, 193 genes were upregulated following treatment with IFN-β (*p.adj*<0.0001, log2fold>2, **Appendix 8.3**). Pathway analysis identified multiple GO biological processes, which were primarily linked to protein ubiquitination, antigen binding, and immune mediated signalling pathways (**Table 5.5**). The antigen binding and immune mediated pathways were mirrored in the KEGG and Reactome pathway terms. Additionally, multiple KEGG terms identified are linked with human based viral diseases for multiple different viral strains and genome types implying the interferon response in the cells can induce an antiviral state against various viral infections. Again as previously, normalised read counts for the top 9 genes for each grouping identified in **Table 5.2**, identified due to having the greatest mean number of read counts across all 4 sorted cell types, are found in **Appendix 8.5**.

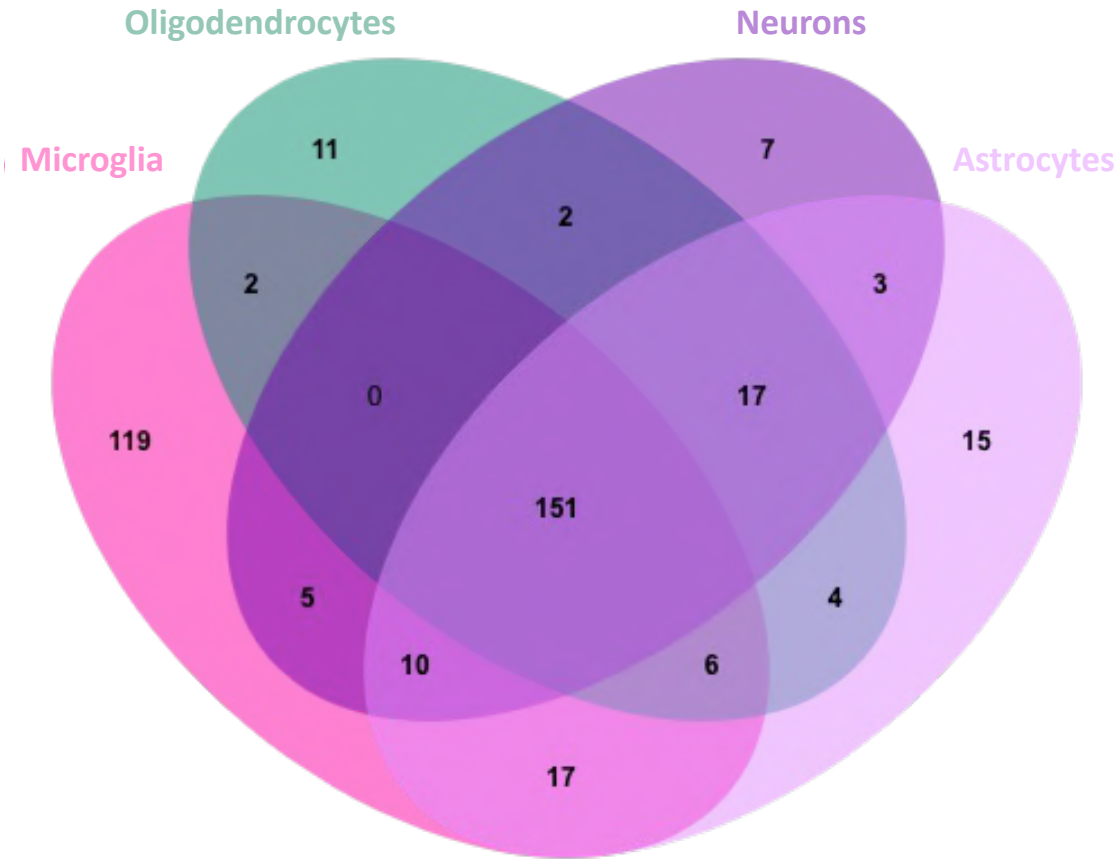


**Figure 5.4: Relationship between significantly differentially expressed genes following IFN-β treatment in the sorted CNS cultures.** Four set Venn diagram showing the genes significantly upregulated following IFN-β treatment in all 4 sorted cell types. Numbers indicate number of genes in each subset. n=4 for each treatment, condition, and cell type.

Functional annotation clustering identified 10 distinct clusters of genes. However, there was significant overlap of genes between some of these groups. When removing clusters that had more than 70% overlap in favour of the cluster that had more distinct DEGs, 4 clusters appeared that were distinct; these being innate immunity (**Table 8.18**), GTP binding / protein ubiquitination (**Table 8.19**), antigen presentation (**Table 8.20**), and cytosol-based processes (**Table 8.21**) (**Figure 5.5**). These clusters together contained 123 DEGs (63.7% of total oligodendrocyte specific genes). These clusters indicate that there is a broad immune response in oligodendrocytes following IFN-β treatment.

### 5.5.2 Oligodendrocyte specific DEGs as candidates for pharmacological manipulation.

Thus far I have confirmed the first two of my aims that IFN-β induces both the CNS cultures in total and oligodendrocytes specifically towards an antiviral state. I thirdly aimed to identify a gene target for pharmacological manipulation to decrease viral infectivity in specifically oligodendrocytes. To do this, I examined specifically genes that are only found differentially expressed in oligodendrocytes (**Figure 5.4**). When using the same strict exclusion criteria as previously (*p.adj*<0.0001, log2fold>2) 11 genes were identified (**Table 5.5**).

These genes are linked with protein ubiquitination (*Rnf225*, *Adamts6*, *Trim56*), immune mediated response (*Il10ra*, *Aoah*, *Trim12c*, *Gsdmd*, *Lck)*, and antigen presentation (*Erap1*), mirroring the findings from the GO term analysis. In addition, *Drd4*, which encodes dopamine receptor D4, had a high Log2 fold increase in expression (4.58). Normalised read counts of these genes can be found in **Figure 5.6**, with the read counts of the other 3 cell types analysed included in **Figure 8.3**. *Trim12c* (48.0±38.3 to 554.7±164.3); *Erap1* (80.9±43.1 to 397.0±103.3); and *Trim56* (49.5±35.3 to 248.4±30.7) had the greatest increases in normalised read counts when comparing PBS to IFN-β treated oligodendrocytes., while the other genes of interest all had less than 100 read counts following treatment with IFN-β.

Of the 11 candidates, 3 were identified for further investigation; *Drd4*, *Il10ra*, and *Erap1*. These were chosen due to their different immunological roles combined with the availability of relevant pharmacological agonists or inhibitors (**Table 5.7**).

**Table 5.5: Pathway analysis of IFN-β upregulated genes in sorted oligodendrocytes from CNS cultures.**

| GO Term | GO ID | Count | Enrichment | *p*-Value |
|---|---|---|---|---|
| Protein ubiquitination and processing | GO:0070534 | 9 | 20.34 | 1.80E-05 |
| | GO:0000209 | 14 | 7.68 | 8.00E-05 |
| | GO:0019787 | 18 | 5.31 | 4.67E-05 |
| | GO:0061659 | 16 | 6.04 | 5.55E-05 |
| | GO:0016755 | 18 | 5.13 | 7.79E-05 |
| Regulation of LPS Signalling | GO:0031664 | 5 | 31.11 | 8.97E-05 |
| Antigen binding | GO:0003823 | 15 | 6.99 | 2.50E-05 |

| KEGG Term | KEGG ID | Count | Enrichment | *p*-Value |
|---|---|---|---|---|
| Response to human pathogens | mmu05169 | 29 | 13.6057041 | 1.25E-24 |
| | mmu05168 | 33 | 7.7917724 | 9.47E-21 |
| | mmu05164 | 23 | 14.4084325 | 8.93E-20 |
| | mmu05160 | 19 | 12.4797148 | 4.80E-15 |
| | mmu05170 | 18 | 8.12823529 | 3.60E-11 |
| | mmu05162 | 15 | 11.1345689 | 4.13E-11 |
| | mmu05165 | 21 | 6.28703282 | 4.92E-11 |
| | mmu05167 | 17 | 8.225 | 1.29E-10 |
| | mmu05416 | 12 | 14.7786096 | 3.35E-10 |
| | mmu05171 | 17 | 7.39919679 | 6.22E-10 |
| | mmu05163 | 17 | 7.196875 | 9.35E-10 |
| | mmu05203 | 15 | 7.09889545 | 1.57E-08 |
| | mmu05166 | 15 | 6.50258824 | 4.77E-08 |
| Antigen processing and presentation | mmu04612 | 16 | 19.2669281 | 1.85E-15 |
| Cell function and metabolism | mmu04621 | 18 | 9.03137255 | 6.66E-12 |
| | mmu04145 | 14 | 8.33665158 | 8.38E-09 |
| | mmu04514 | 13 | 7.74117647 | 8.06E-08 |
| | mmu04218 | 11 | 6.47902813 | 6.08E-06 |
| | mmu04144 | 12 | 4.78131488 | 3.33E-05 |
| Transplant rejection | mmu05332 | 12 | 20.6431373 | 7.75E-12 |
| | mmu05330 | 12 | 20.6431373 | 7.75E-12 |
| Autoimmune disease | mmu04940 | 12 | 18.5788235 | 2.59E-11 |
| | mmu05320 | 12 | 16.4622487 | 1.01E-10 |
| Cell response to PAMPs | mmu04622 | 8 | 12.2114333 | 3.38E-06 |
| | mmu04623 | 8 | 11.5601569 | 4.90E-06 |

***Continues overleaf***

| Reactome Term | Reactome ID | Count | Enrichment | *p*-Value |
|---|---|---|---|---|
| General immune response | R-MMU-168256 | 41 | 3.46559172 | 4.31E-15 |
| | R-MMU-1280218 | 23 | 4.7240115 | 4.87E-10 |
| | R-MMU-2172127 | 9 | 19.1411911 | 1.52E-08 |
| | R-MMU-198933 | 9 | 12.3620192 | 4.88E-07 |
| | R-MMU-168249 | 22 | 3.11261142 | 1.97E-06 |
| Antigen processing and presentation | R-MMU-983170 | 12 | 38.593621 | 4.38E-15 |
| | R-MMU-1236974 | 11 | 42.661086 | 2.95E-14 |
| | R-MMU-1236975 | 14 | 20.0658863 | 8.81E-14 |
| | R-MMU-983169 | 20 | 7.68871944 | 2.85E-12 |
| | R-MMU-1236977 | 8 | 42.1956923 | 4.00E-10 |
| Interferon response | R-MMU-1169410 | 10 | 42.5359801 | 7.13E-13 |
| | R-MMU-913531 | 12 | 21.9769231 | 3.48E-12 |
| | R-MMU-1169408 | 9 | 43.9538462 | 1.22E-11 |
| | R-MMU-1280215 | 19 | 6.32668998 | 3.19E-10 |

**Table 5.5: Pathway analysis of IFN-β upregulated genes in sorted oligodendrocytes from CNS cultures.** Table of GO, KEGG, and Reactome pathway analysis of oligodendrocytes sorted from CNS cultures treated with IFN-β. Terms grouped by similar representative term, with unique pathways enriched identified by ID. ID = unique pathway ID. Count = number of upregulated genes in sorted oligodendrocytes found in pathway. Enrichment = fold increase compared to expected number of genes. Only significantly upregulated genes ($p<0.0001$, log2fold>2) compared to PBS control included in analysis. Only significantly enriched pathways included ($p<0.0001$, enrichment >5) n=4

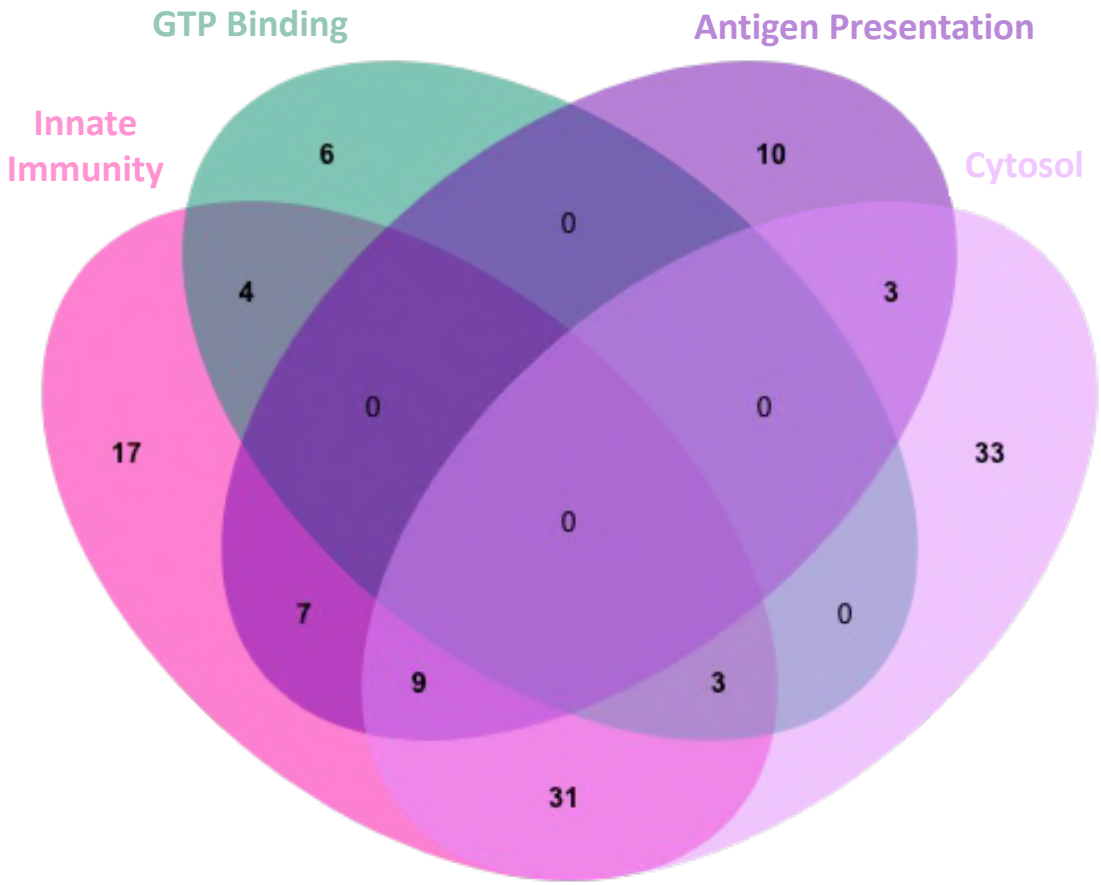


**Figure 5.5: Functional annotation clustering of upregulated genes in sorted oligodendrocytes from CNS cultures.** Four set Venn diagram showing the four groupings of pathways most enriched in sorted oligodendrocytes by IFN-β treatment from CNS cultures. Numbers indicate number of genes. n=4 for IFN-β treated & PBS control.

**Table 5.6: Genes specifically upregulated in oligodendrocytes.**

| Gene | Log2fold | *p*-value | Role | Ref |
|---|---|---|---|---|
| *Drd4* | 4.58 | 7.83E-05 | Dopamine receptor 4, inhibits postsynaptic potential, scavenger | (Ptáček *et al.*, no date; Bethesda (MD), 2004c) |
| *Rnf225* | 4.14 | 4.96E-07 | Enable ubiquitin protein ligase activity | (Bethesda (MD), 2004h) |
| *Il10ra* | 3.9 | 4.17E-05 | IL10 receptor subunit alpha, inhibits synthesis of proinflammatory cytokines | (Bethesda (MD), 2004f; Liff *et al.*, 2020; El Sayed *et al.*, 2022) |
| *Aoah* | 3.69 | 1.45E-05 | Lipase, breaks down LPS | (Munford *et al.*, 2003; Bethesda (MD), 2004b) |
| *Trim12C* | 3.51 | 4.09E-08 | Upregulates defence to invading pathogen. Located in P-body. | (Bethesda (MD), 2004i; Yang *et al.*, 2020) |
| *Gsdmd* | 3.31 | 3.29E-06 | Upregulates IL-1b, cellular response to stimulus. | (Bethesda (MD), 2004e; Shao *et al.*, 2022) |
| *Lck* | 3.06 | 7.80E-09 | Activate T cells | (Bethesda (MD), 2004g; Bommhardt, Schraven and Simeoni, 2019) |
| *Adamts6* | 2.79 | 1.52E-06 | Peptidase activity | (Bethesda (MD), 2004a; Mead, 2022) |
| *Trim56* | 2.33 | 6.71E-06 | RNA binding activity. Protein K63 linked ubiquitination. | (Bethesda (MD), 2004j; Fu *et al.*, 2023) |
| *Erap1* | 2.3 | 1.57E-08 | Trims HLA class I binding precursors for presentation on MHC class I molecules | (Bethesda (MD), 2004d; Reeves and James, 2018) |

**Table 5.6: Genes specifically upregulated in oligodendrocytes.** Table showing all genes upregulated specifically in oligodendrocytes in CNS cultures ($p<0.0001$, log2fold>2), and the associated role with reference. N=4 for both IFN-β and PBS treated.

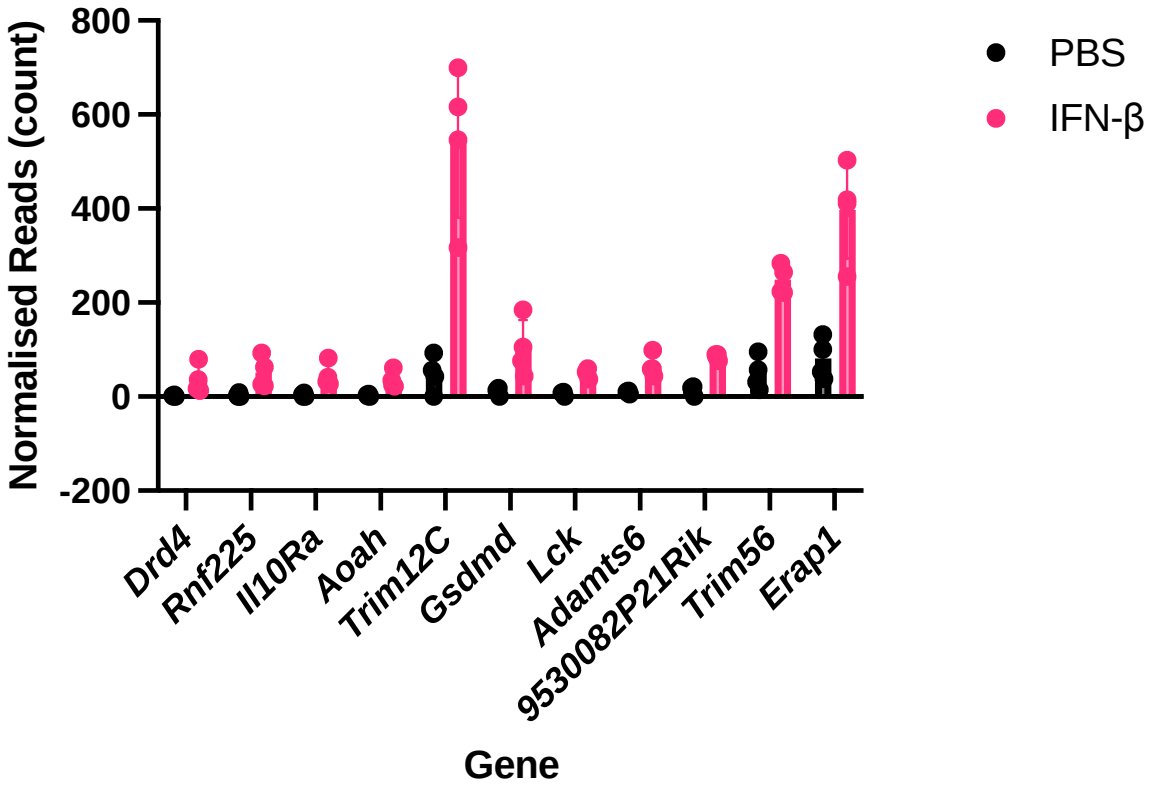


**Figure 5.6: Normalised read counts of oligodendrocyte specific DEGs.** Normalised gene expression of read counts across the different genes identified as being oligodendrocyte specific DEGs (p<0.0001, log2fold>2). n=4.

**Table 5.7: Oligodendrocyte specific gene candidates and associated drugs.**

| Gene | Drug | Inhibitor or Agonist | Hypothesised effect on virus |
|---|---|---|---|
| *Drd4* | Dopamine hydrochloride | Agonist | Decrease |
| *Il10ra* | IL10Ra blocker | Inhibitor | Increase |
| *Gsdmd* | LDC7559 | Inhibitor | Increase |
| *Erap1* | ERAP1-IN-1 | Inhibitor | Increase |

Table 5.7: Oligodendrocyte specific gene candidates and associated drugs. Table showing the oligodendrocyte specific genes (*p.adj*<0.0001, log2fold>2) chosen for further investigation along with associated agonists or inhibitors of the gene targets and their expected effect on viral infectivity.

## 5.7: Discussion

Treatment of CNS cell cultures with IFN-β induced a broad transcriptional signature indicating that the cultures as a whole, and specific cell types, acquire an antiviral phenotype. Furthermore, oligodendrocytes specifically upregulated unique genes compared to the other cell types. These data provide evidence that oligodendrocytes might be amenable to targeted pharmacological manipulation to decrease their susceptibility to human polyomavirus 2.

Due to the intertwined nature of CNS cells, in which physical connections occur between all cell types, it was important to demonstrate that I had achieved viable populations enriched in individual cell types. Oligodendrocyte processes have been found to contain RNA (Dahm, Kiebler and Macchi, 2007), and therefore any processes interacting with the cell body of neighbouring cells could alter the transcriptional profile. Ultimately, the cells were found to be significantly pure from the neighbouring populations (**Figure 5.1**).

However, *Map2* was found to be highly expressed in other populations of cells too (**Figure 5.1D**). Microtubule associated protein 2 has been found in both astrocytes and oligodendrocytes, particularly in reactive, inflamed astrocytes (Geisert *et al.*, 1990), and in oligodendrocytes in active myelination stages (Geisert *et al.*, 1990). The expression of *Map2* has been found to be lower in astrocytes than in neurons (Müller *et al.*, 1997), mirroring my data. Since the RNAseq data confirmed the flow cytometer (**Figure 4.6**) and microscopic data (**Figure 4.8**), I felt confident to undertake the RNAseq analysis on my cell populations.

The PCA analysis provided further assurance that the sorted cell types were enriched across the different replicates. According to the PCA plots, each of the cell types grouped into discrete clusters, with microglia being spatially separated from the remaining 3 cell types likely reflecting that microglia have a different ontogeny in comparison to neurons and microglia, which derive from the neuroepithelium (Liour and Yu, 2003; Ginhoux *et al.*, 2010). The expression profile of neurons and oligodendrocytes appeared to be similar as they clustered close together on the PCA plot, while astrocytes clustered separately. Astrocytes acquire a pro-inflammatory phenotype when treated with IFN-β, both in homeostatic and viral infection conditions expressing many pro-inflammatory molecules predicted to recruit lymphocytes to the CNS (Okada *et al.*, 2005; Clarke *et al.*, 2019; Ma *et*

*al.*, 2023). Meanwhile, neurons and oligodendrocytes have not classically been described as responsive to IFN-β (Heine *et al.*, 2006; Viengkhou and Hofer, 2023), and in fact neurons have quite a limited expression of chemokines and cytokines following type I IFN treatment (Wang and Campbell, 2005; Wang, Campbell and Zhang, 2008). These data explain why the oligodendrocytes and neurons grouped together on the PCA plot and also emphasise the novelty of my observations, in which I showed that both oligodendrocytes and neurons have distinct transcriptional profiles following IFN-β treatment as measured by PCA plot separation.

To decrease bias by focussing on specific genes that are relevant to the immune response, the data were investigated using pathway analysis, which provided a broad overview of responses to IFN-β. Functional annotation clustering, where numerous lists and pathway analysis methods are combined into one list of key pathways, was used to highlight specific pathways that are significant in an unbiased manner focussing on the full transcriptional profile instead of specific genes. The functional annotation clustering was formed, as mentioned, from the combined pathway analysis from gene ontology (GO), KEGG, Reactome, and protein-based analysis of InterPro, PIR, and Smart. These allowed the DEGs to be analysed using multiple distinct pathway databases to maximise the quantity and quality of the analysis, without bias. These pathway analysis databases were employed as they are considered “critical” to ensuring a wide and varied analysis of gene expression. GO correlates gene sets to biological processes (Ashburner *et al.*, 2000; Aleksander *et al.*, 2023), KEGG relates compounds, reactions, and full pathway maps (Kanehisa and Goto, 2000b; Kanehisa *et al.*, 2023), and Reactome is particularly useful for referencing disease models (Gillespie *et al.*, 2022). Combining analyses from all three enhances the accuracy and enriches the quality of data processing. As expected, the GO analysis identified *the response to IFN-β*, *type I interferon responses* in general, along with the *response to virus and host regulation of viral replication*, following treatment with IFN-β. This corresponds to the fact that IFN-β has been extensively linked previously with an antiviral response both in the body in general and in the CNS specifically (Katze, He and Gale, 2002). Similarly, both the KEGG and Reactome analyses identified the same, with KEGG identifying the enrichment of viral disease pathways while reactome identified cell-cycle inhibitors and antigen processing and presentation.

An important novel finding from my analysis is the concerted effort of the innate CNS cells to protect against viral infections. This is illustrated by the observation that some pathways were significantly upregulated when DEGs for all cell types were considered, but when analysed individually, these pathways lost significance. These included the *pattern recognition receptor (PRRs) activity* pathway from the gene ontology analysis (**Table 5.2**), and "proteosome" from KEGG pathway analysis. It is generally well known that microglia, acting as the tissue resident macrophages, and astrocytes, by modulating the immune response, contribute together to a pro-inflammatory environment during disease (Brambilla *et al.*, 2005, 2009; Yang *et al.*, 2010). My results demonstrate that both oligodendrocytes and neurons also mount an immune response, contributing to an antiviral phenotype in the CNS.

Functional annotation clustering demonstrated that IFN-β has a profound antiviral effect on CNS cell cultures, increasing the expression of genes related to *innate immunity*, *response to viruses*, and *antigen processing and presentation* among others (**Figure 5.3**). These are shared between all the different cells of the CNS, thus implying that IFN-β induces the whole CNS towards an antiviral state. However, cell specific pathways were enriched by IFN-β treatment, further confirming the analysis from the GO, Reactome and KEGG pathway analysis that each cell type has an individual role in protecting the CNS from infection. In the context of PML, only oligodendrocytes are infected and therefore for my analyses I focussed on the oligodendrocyte specific pathways – *regulation of viral entry to the cell* and *oligoadenylate synthetase*.

The key pathways enriched in the *regulation of viral entry to the cell* cluster are the *upregulation of the expression of RING-type proteins*, *PRR activity*, and *protein ubiquitination*. Key genes upregulated are the genes encoding RING (really interesting new gene) finger proteins *Rnf135*, *Rnf213*, *Rnf225*, and tripartite motif containing proteins including*, Trim14, Trim25* and *Trim56*. Protein ubiquitination has many varied roles in cells, and RNF proteins are known to modulate the activity of multiple PAMP pathways including cGAS-STING and JAK-STAT, the primary signalling pathway of IFN-β. RNFs enhance the expression of ISGs following IFN-β treatment, which have increased resistance to VSV infections (S. Liu *et al.*, 2018; Zuo *et al.*, 2020), with *Rnf213* activity directly linked with inhibiting herpesvirus by targeting the viral transcription factors for degradation (Tian *et al.*,

2023). TRIM proteins employ distinct mechanisms to protect the cell from viral infection, including targeting viral protein for degradation (*Trim14*) (Wang *et al.*, 2016), inhibiting viral RNA synthesis (*Trim25*) (Meyerson *et al.*, 2017), and inhibiting viral infection of cells (*Trim56*) (Wang *et al.*, 2011).

Additionally, oligoadenylate synthetase (OAS) related pathways and activity were enriched in solely oligodendrocytes. Key pathways enriched were the *negative regulation of type I interferon mediated signalling pathway*, *2'5' oligoadenylate synthetase activity*, and the *negative regulation of chemokine production* (particularly CXCL10 and CCL2). The ISG USP18, a potent inhibitor of the JAK-STAT signalling pathway (Meuwissen *et al.*, 2016; Arimoto *et al.*, 2017), is significantly upregulated in oligodendrocytes explaining the negative regulation of type-I IFN signalling. Additionally, OAS proteins degrade both host and viral RNA by binding and presenting it to intracellular RNase (Hovanessian and Justesen, 2007). Proteins encoded by genes in this cluster inhibit the activity of JAK-STAT, which in turn inhibits expression of OAS proteins, confounding the role of OAS proteins following IFN-β treatment.

These two unique clusters identified in oligodendrocytes implied innate oligodendrocyte-specific antiviral activity which warranted further investigation. Therefore, I performed pathway analysis on solely oligodendrocyte DEGs. This identified 193 DEGs were upregulated following treatment with IFN-β (*p.adj*<0.0001, log2fold>2). Pathway analysis identified multiple GO biological processes, which were primarily linked to *protein ubiquitination*, *antigen binding*, and *immune mediated signalling pathways* (**Table 5.5**). The *antigen binding* and *immune mediated pathways* are mirrored in the KEGG and Reactome pathway terms. Additionally, multiple KEGG terms identified are linked with human based viral diseases for multiple different viral strains and genome types implying the interferon response in oligodendrocytes can induce an antiviral state against many varied viral infections. Four unique clusters were identified of being particularly interesting, these being *innate immunity*, *GTP binding and GTPase activity*, *antigen processing and presentation*, and *cytosol-based compounds*.

The innate immunity cluster identified 71 unique genes which encode a broad range of interferon-induced proteins, for example, *Ifit2*, *Isg20*, *Rsad2*, *Mx1*, along with previously

discussed OAS proteins and *Trim14*, *Trim24*, *Trim56*. These large range of ISGs have all been previously described as having antiviral activity in this thesis, thereby concluding that oligodendrocytes are induced towards an antiviral state by IFN-β signalling.

GTPase binding and activity can modulate viral infectivity. GTPases play essential roles in cell proliferation, morphology, nuclear transport, and vesicle trafficking (Kahn, Der and Bokoch, 1992; Saverio and Retta, 2014). These proteins, for example those encoded by *Mx1*, can also inhibit viral replication by blocking the viral replication cycle (Haller *et al.*, 2015), implying a method of antiviral activity in oligodendrocytes.

However, the interesting finding was the expression of antigen processing and presentation. The key pathways enriched were MHC-I processing, CD8+ T cell binding, and numerous viral disease related pathways. The MHC-I genes of the *H2-q* and *H2-t* class are found upregulated in oligodendrocytes, along with MHC-II genes (such as *H2-aa*). MHC-I has only recently been described as having increased expression on oligodendrocytes, but their induction was caused by type-II IFN (Kirby *et al.*, 2019a; Harrington *et al.*, 2023). Therefore, this presents a novel finding that oligodendrocytes respond to type-I interferon to increase their expression of MHC-I. As MHC-I recruits cytotoxic T cells to sites of infection (Hewitt, 2003), my results indicate a possible suicide response following viral infection to protect the surrounding cells and CNS milieu from viral infection. As previously, further investigation on the expression of MCH-I on oligodendrocytes is necessary to validate these findings.

Oligodendrocytes ultimately upregulated 11 genes that were not found upregulated in other cell types of the CNS, as detailed in **Table 5.6**. These genes encoded multiple distinct proteins with varied roles. For example, *Trim56*, which has previously been discussed in this chapter decreases viral infectivity (Fu *et al.*, 2023).

Dopamine receptor d4, *Drd4*, was the highest expressed gene after IFN-β treatment. D4 has been linked with multiple neurological and psychiatric disorders (Ptáček *et al.*, 2011) and participates in promoting a pro-inflammatory phenotype in the CNS through modulating T cell activity (Jafari *et al.*, 2013). However, oligodendrocytes have thus far not been shown to express D4 (Broome *et al.*, 2020), and therefore further studies of the receptor are

necessary to clarify what role it may have on modulating viral infections for oligodendrocytes.

Interleukin 10 receptor, *Il10ra*, is the membrane bound protein for IL-10, an anti-inflammatory cytokine produced by glia in the CNS (Burmeister and Marriott, 2018). IL-10R has been found on rat oligodendrocytes previously, but not in humans (Molina-Holgado *et al.*, 2001; Hulshof *et al.*, 2002), and IL-10 has been linked with decreasing inflammation in glial cells in response to pathogenic microbes (Balasingam and Wee Yong, 1996; Rasley *et al.*, 2006). Decreasing IL-10R signalling could promote a pro-inflammatory phenotype in the innate CNS cells. However, blocking IL-10R has been linked with inducing a lymphoproliferative response in bacterial infected dogs (Santos *et al.*, 2021) which could result in enhanced clearance of virus from the CNS therefore implying a possible therapeutic role in JCV infections.

Acyloxyacyl hydrolase, *Aoah*, is a lipase that is classically known to act upon bacterial LPS to relase tetraacyl LPS which has been linked with decreasing the sensitivity of toll-like receptor (TLR) 4(Hall and Munford, 1983; Zou *et al.*, 2017). While AOAH has no active effect on viral infections it can clear oxidised phospholipids that arise as a product of viral infections to mediate the inflammatory response in the lungs (Imai *et al.*, 2008). In the CNS, deficiency of AOAH results in a pro-inflammatory phenotype with microglia becoming activated through a proposed dysregulation of lipid metabolism (Rahman-Enyart *et al.*, 2022). Pharmacological manipulation of AOAH this could result in increased inflammation and penetration of immune cells to the CNS resulting in possibly viral clearance.

Gasdermin D, *Gsdmd*, is a pore-forming protein that promotes a pro-inflammatory phenotype (Shi *et al.*, 2015). Blocking Gasdermin D decreased the neutrophil response *in vivo* following influenza infection which decreased mortality of infected mice (Speaks et al., 2023). Additionally, blocking Gasdermin D was linked with enhancing virus replication through decreasing viral mediated pyroptosis, an inflammatory form of programmed cell death, of coronavirus and rotavirus infected macrophages (Zhu *et al.*, 2017; Zheng *et al.*, 2020). Therefore, modulating this could elicit a protective effect, however as this decreases the adaptive immune response and increases intracellular viral replication this would likely need to form part of a co-therapy to elicit a neuroprotective effect.

Endoplasmic reticulum aminopeptidase 1 (ERAP1), *Erap1*, is a metalloprotease involved in antigen presentation. ERAP1 trims antigenic proteins to the appropriate length for loading onto MHC-I (Hammer, Kanaseki and Shastri, 2007; Mattorre *et al.*, 2022), and therefore have important roles in recruiting CD8+ T cells. Blocking ERAP1 blocks the production of processed antigens and decreases the proliferation of CD8+ T cells in HBV infection (Liu *et al.*, 2022). Therefore, modulating this response could result in an increase in viral infectivity to JCV and warrants further investigation.

Some of the proteins identified have not been characterised in either the CNS or in infection thus far, and therefore their roles are a mystery. RNF225, *Rnf225*, is a membrane bound RING protein that, as of yet, has not been characterised. However, through acting as an E3 ligase the function can be presumed to be like another RING protein such as those described previously (Wang *et al.*, 2011). TRIM12C, another ubiquitin ligase, was also identified. This protein stimulates type-I IFN pathways through binding to TRAF6, a part of the PRR signalling pathway, to enhance the activation of IFN signalling (Chang, Yoshimi and Ozato, 2015). Lymphocyte-specific tyrosine kinase (Lck) is important for activating T receptor cell signalling. Lck has been found in the CNS and is a potent biomarker for glioblastoma (Ge *et al.*, 2020), however its role in infection is not characterised. A disintegrin and metalloproteinase with thrombospondin motifs (ADAMTS) are extracellular peptidases with varied roles. ADAMTS6 was identified to be upregulated in oligodendrocytes, however the exact substrate has not been identified thus far (Kelwick *et al.*, 2015).

For further studies, *Drd4*, *Il10ra*, and *Erap1* were identified from the above list of candidates to investigate their antiviral effects both *in vitro* and *in vivo*. The proteins encoded by the genes have distinct and varied roles in immunity, ranging from inducing a pro-inflammatory phenotype (D4), inducing an anti-inflammatory phenotype (IL-10R), and modulating antigen presentation (ERAP1). At the same time, these proteins all have readily available pharmacological manipulators. To modulate D4, dopamine hydrochloride was chosen as a receptor agonist as this activates the receptor (Ishige *et al.*, 2001). IL-10R can be blocked by a monoclonal antibody, and therefore would result in a decrease in IL-10R mediated signalling (Silva and Appelberg, 2001). ERAP1 is blocked by the potent inhibitor ERAP1-IN-1 (Liu *et al.*, 2022). These drugs have been trialled *in vitro* and have been shown to induce an

effect, however they have not been characterised in the CNS and therefore characterisation and dose curves need to be generated before investigating any antiviral effect. While these candidates were selected due to their readily available pharmacological manipulators they did not have the largest quantity of normalised read counts, aside from *Erap1*. *Erap1*, *Trim12c*, and *Trim56* all had an increase of >200 reads. Therefore, while *Trim12c* and *Trim56* were not selected to investigate their antiviral activity in this thesis the modulation of these genes could have an undescribed antiviral activity that warrants further investigation.

The following chapter will focus on both the antiviral effects of IFN-β and the IFN-β derived oligodendrocyte specific candidates D4, IL-10R, and ERAP1. It is expected that one of these treatments will modulate the infectivity of a neurotropic virus, specifically SFV. The efficacy will be characterised both *in vitro* and *in vivo*, in particular as both IL-10R and ERAP1 are involved in the adaptive immune response and *in vitro* cultures may not capture the full effect.

# Chapter 6

## Interferon beta and oligodendrocyte-specific candidates modify viral replication *in vitro* and *in vivo*

# Chapter 6: IFN-β and oligodendrocyte-specific candidates modify virus replication *in vitro* and *in vivo*

## 6.1 Introduction

Having shown that IFN-β induces a strong ISG response in all major CNS cell types *in vitro*, including an oligodendrocyte-specific response, I aimed to examine the ability of these candidates to modify the infectivity of an neurotropic virus. Semliki-forest virus (SFV) has a similar tropism to human polyomavirus 2 (Fazakerley and Webb, 1987; Fazakerley *et al.*, 2006). Therefore, SFV was chosen to investigate the effects of oligodendrocyte-specific candidates on viral infectivity both *in vitro* and *in vivo*. The aims of this chapter were to:

1) Confirm that IFN-β can reduce SFV infectivity *in vitro.*
2) Investigate the effect of pharmacologically manipulating oligodendrocyte-specific candidates *in vitro.*
3) Confirm that IFN-β, when administered intranasally, can reduce infectivity of SFV *in vivo.*
4) Investigate the effect of pharmacologically manipulating an oligodendrocyte specific targets identified by RNAseq *in vivo.*

## 6.2 SFV infects specifically oligodendrocytes and neurons

Initially I aimed to confirm that SFV infects primarily oligodendrocytes in CNS cell cultures. For my *in vitro* infectivity assays I used SFV6-ZsGreen which encodes the green fluorescent protein, ZsGreen. ZsGreen is produced at the same time as the viral structural proteins but is not bound to a protein and can diffuse freely to fill the cell, therefore making the cell fluorescent when excited with blue light (Hawley, Hawley and Telford, 2017). CNS cultures were inoculated with SFV6 (MOI=$3x10^{-5}$) for 1 hour and fixed 24hpi for immunofluorescence microscopy. Cells with active viral replication (**Figure 6.1C-E,H,I**) could be easily distinguished from uninfected cells (**Figure 6.1A,B,F,G**). ZsGreen co-localised with both $CNP^+$ oligodendrocytes (**Figure 6.1C,D**) and $NeuN^+$ neurons (**Figure 6.1C,E**). When the cells were stained for $GFAP^+$ (mature astrocytes) and $Iba1^+$ (microglia) the ZsGreen signal was not observed to colocalise with either. (**Figure 6.1H,I**).

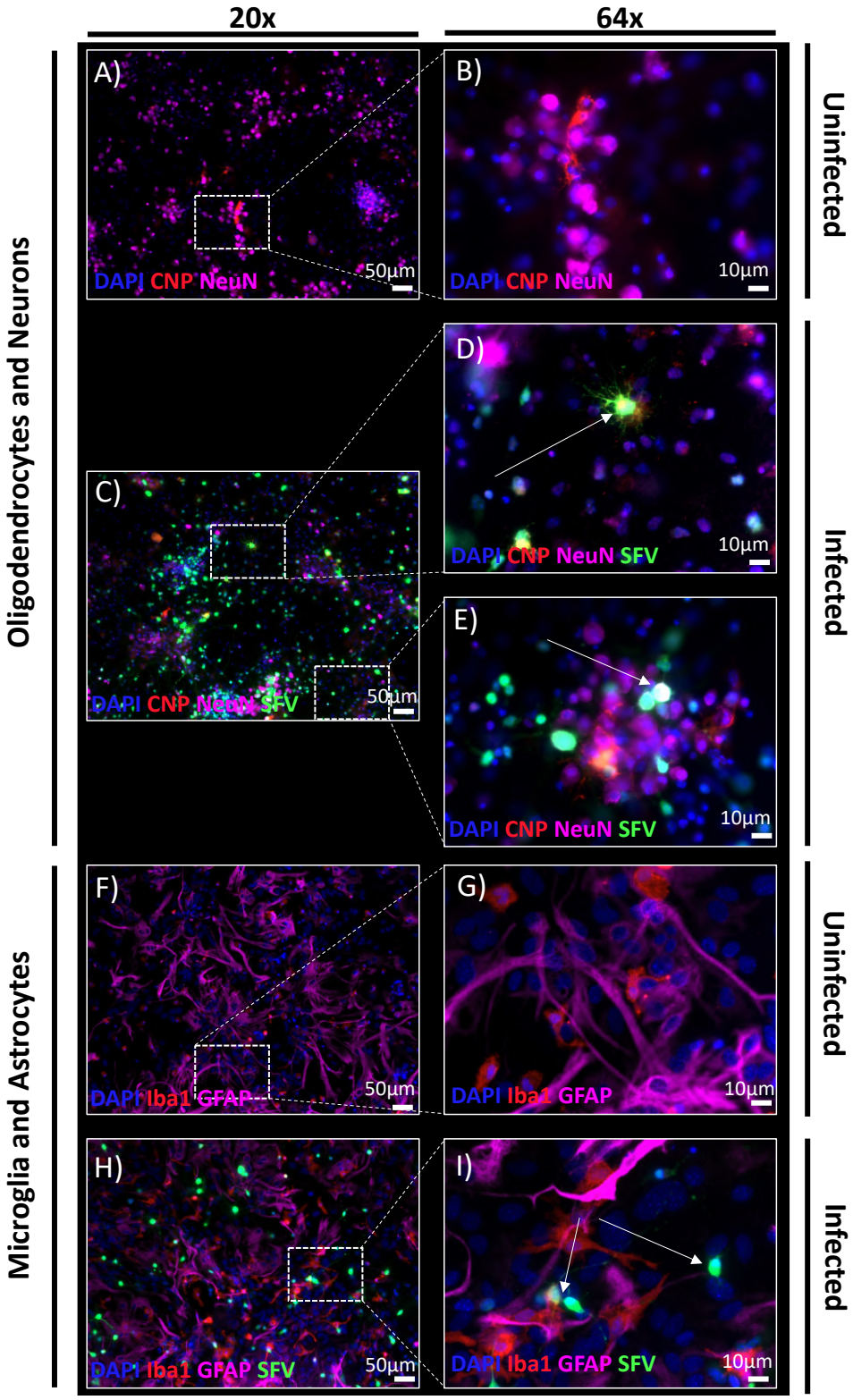


**Figure 6.1: SFV6 exhibits oligodendroglial and neuronal cell tropism.** Representative immunofluorescence images of CNS cell cultures uninfected (A,B,H,I) or SFV6-ZsGreen infected (A-C,H,I) stained with anti-CNP and anti-NeuN (A-E) or anti-Iba1 and anti-GFAP (F-I). In all cases, virus is seen in the green channel due to ZsGreen expression. Images taken 48hpi with MOI = $3x10^{-5}$.

I conclude that, in line with *in vivo* literature (Fragkoudis *et al.*, 2009), SFV6 preferentially infects oligodendrocytes and neurons in my CNS cell culture system.

## 6.3 IFN-β decreases SFV infectivity in CNS cell cultures

To determine whether IFN-β is protective against viral infection, CNS cultures were pre-treated with PBS (vehicle control), Poly(I:C) (positive control), or IFN-β for 4 hours, inoculated with SFV6 (MOI = $3x10^{-5}$) for 1 hour, then at either 24hpi or 48hpi supernatants stored for plaque assay, cells lysed for RT-qPCR, or cells fixed for immunofluorescence microscopy. Pre-treatment with IFN-β significantly reduced the quantity of virus in the cell culture supernatants at both 24hpi ($p$ <0.05, **Figure 6.2E**) and 48hpi ($p$ <0.01, **Figure 6.2F**) as determined by plaque assay. By qRT-PCR, there was a downward trend in the viral gene *E1*, that however did not reach significance, at 24hpi ($p$ =~0.2, **Figure 6.2C**). Viral *E1* mRNA levels were unchanged compared to control at 48hpi.

These data demonstrate an overall reduction in infection, but they do not indicate which cell types are protected. To examine cell-type specific infection I used flow cytometry. Following IFN-β pre-treatment, the proportions of ZsGreen+ oligodendrocytes and ZsGreen+ neurons were significantly decreased compared to vehicle treated controls (p < 0.05, Figure 6.2G) and ($p$<0.01, **Figure 6.2H**), respectively. The gating strategy for SFV6+ live, single cells is shown in **Figure 6.2A,B**. When visualised using immunofluorescence imaging, there appeared to be a decrease in the proportion of SFV+ oligodendrocytes and neurons at both 24hpi (**Figure 6.3B,D**) and 48hpi (**Figure 6.3F,H**).

The collective results show that pre-treatment with IFN-β reduced SFV6 replication in CNS cell cultures.

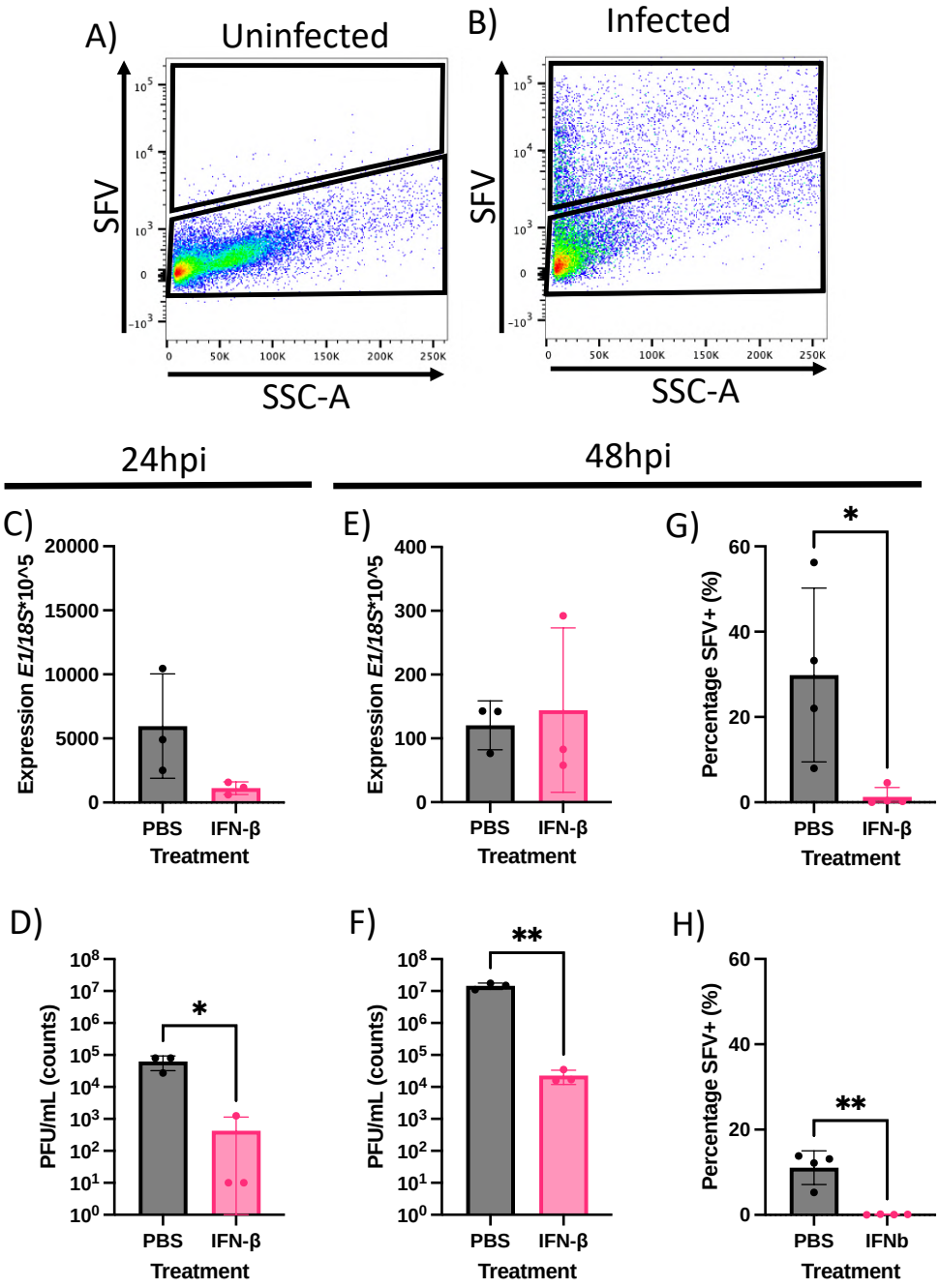


**Figure 6.2: Pre-treatment with IFN-β decreases SFV infection**. CNS cultures were pre-treated with IFN-β for 4hr, infected with SFV and analysed after 24 (C,E) or 48 hours (D,F-H), before being analysed by RT-qPCR for viral gene E1 (C,D), plaque assays on supernatant for production of new virus (E,F), or flow cytometry to measure ZsGreen production as measurement of viral proteins (A,B,G,H). Oligodendrocytes (G) and neurons (H) were examined for the presence of SFV-ZsGreen. Bars represent mean ± SEM. Analysis was by unpaired t-tests. Each symbol represents the mean value of an independent experiment. Significant differences denoted as $p<0.05$ *, $p<0.01$ **. n=3 (RT-qPCR, plaque assays), n=4 (flow cytometry).

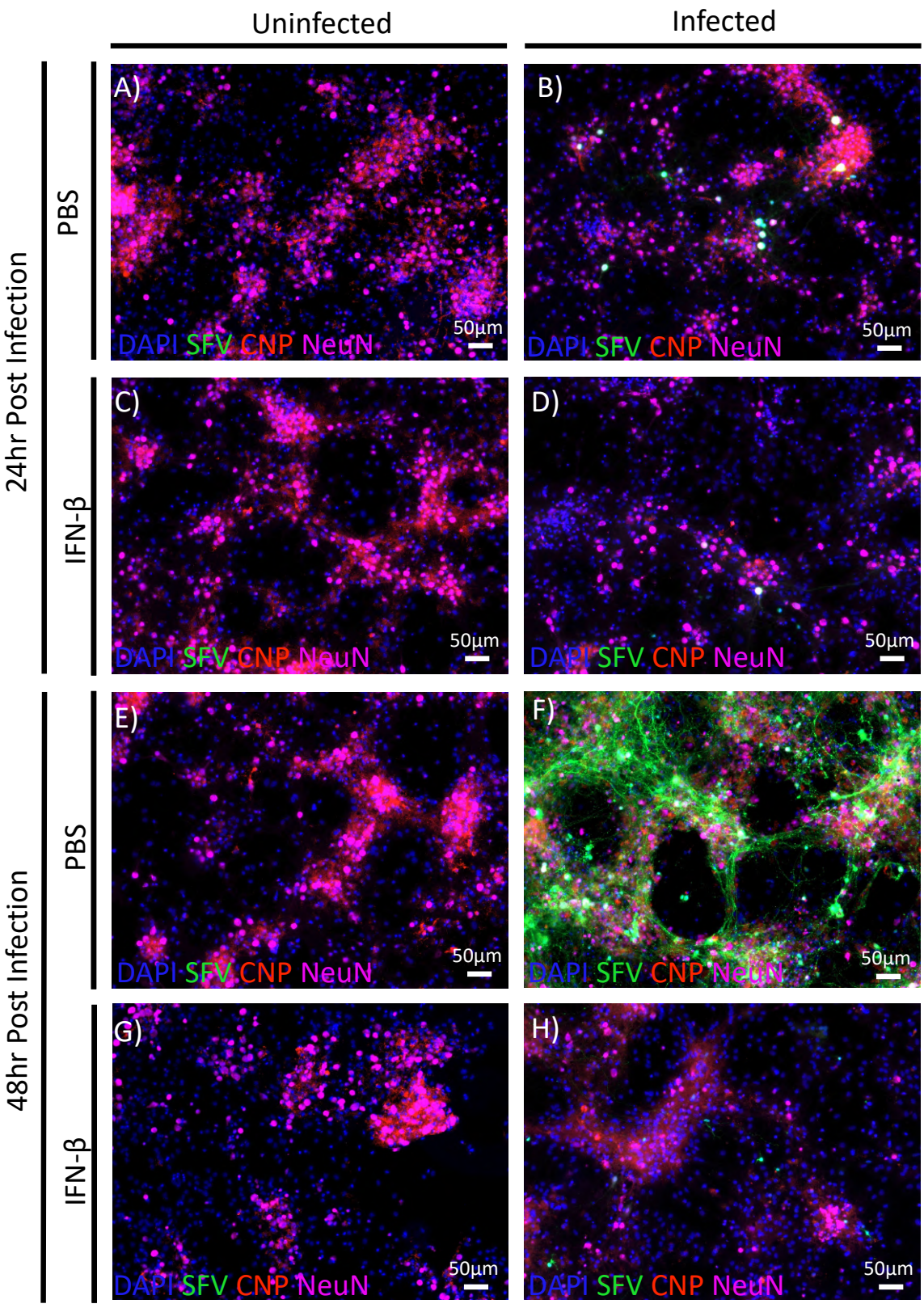


**Figure 6.3: Representative images showing effect of IFN-β on SFV infectivity**. Representative images of CNS cultures uninfected (A,C,E,G) or infected with SFV (B,D,F,H) at 24hpi (A-D) or 48hpi (E-H) that were pre-treated with IFN-β (C,D,G,H). Cells stained with anti-CNP and anti-NeuN. In all cases, virus is seen in the green channel due to ZsGreen expression.

## 6.4 IFN-β treatment post infection can convey similar antiviral effects as pre-treatment

Clinically, pre-treatment is not a relevant therapeutic approach to combat viral infection. Therefore, I asked whether treating CNS cultures with IFN-β at the point of inoculation compared to 4 hours pre-inoculation would result in similar antiviral effects, 24 and 48 hours post infection with SFV6 (MOI = $3x10^{-5}$), as quantified by both plaque assay of supernatants and immunofluorescence microscopy. Similar controls as **6.3** were employed (PBS and poly(I:C)). Between pre-treatment and coincident treatment, based on viral production as measured by plaque assay, I observed similar levels of protection independent of time of IFN-β treatment administration. (**Figure 6.4G,H**). Similar ameliorative effects were seen when visualising by immunofluorescence imaging (**Figure 6.4A-E**), as there was no visible difference in the proportion of ZsGreen+ cells at either 24hpi (**Figure 6.4B,C**) or 48hpi (**Figure 6.4E,F**) when comparing pre-treatment to coincidental treatment. Therefore, the collective results suggest that IFN-β treatment at the point of infection decreases SFV infectivity with the same efficacy as a 4-hour pre-treatment. Subsequent studies were conducted with coincident treatment and infection.

## 6.5 Oligodendrocyte-candidates identified by RNAseq tend to reduce viral infectivity in oligodendrocytes in CNS cell cultures

After confirming that SFV infectivity was decreased by IFN-β in cell culture, I aimed to characterise the effect of the oligodendrocyte specific targets identified in **5.5.2** on SFV infectivity. I tested this by treating the cultures with the pharmacological manipulators listed in **Table 5.7**. Appropriate concentrations of agents were obtained from previous studies performed: 20µg/mL dopamine hydrochloride (H. H. Li *et al.*, 2017), 1µg/mL IL-10R blocking antibody (Shouval *et al.*, 2014), and 25µg/mL ERAP1-IN-1 (Schott *et al.*, 2022). CNS cultures were inoculated with SFV6 (MOI=$3x10^{-5}$) for 1 hour, then treated with appropriate doses of IFN-β (as positive control), dopamine hydrochlorise, IL-10R blocking antibody, or ERAP1-IN-1. At 48hpi supernatants were stored for plaque assay, and the cells were lysed for RT-qPCR. PBS and 0.1% DMSO were employed as vehicle controls.

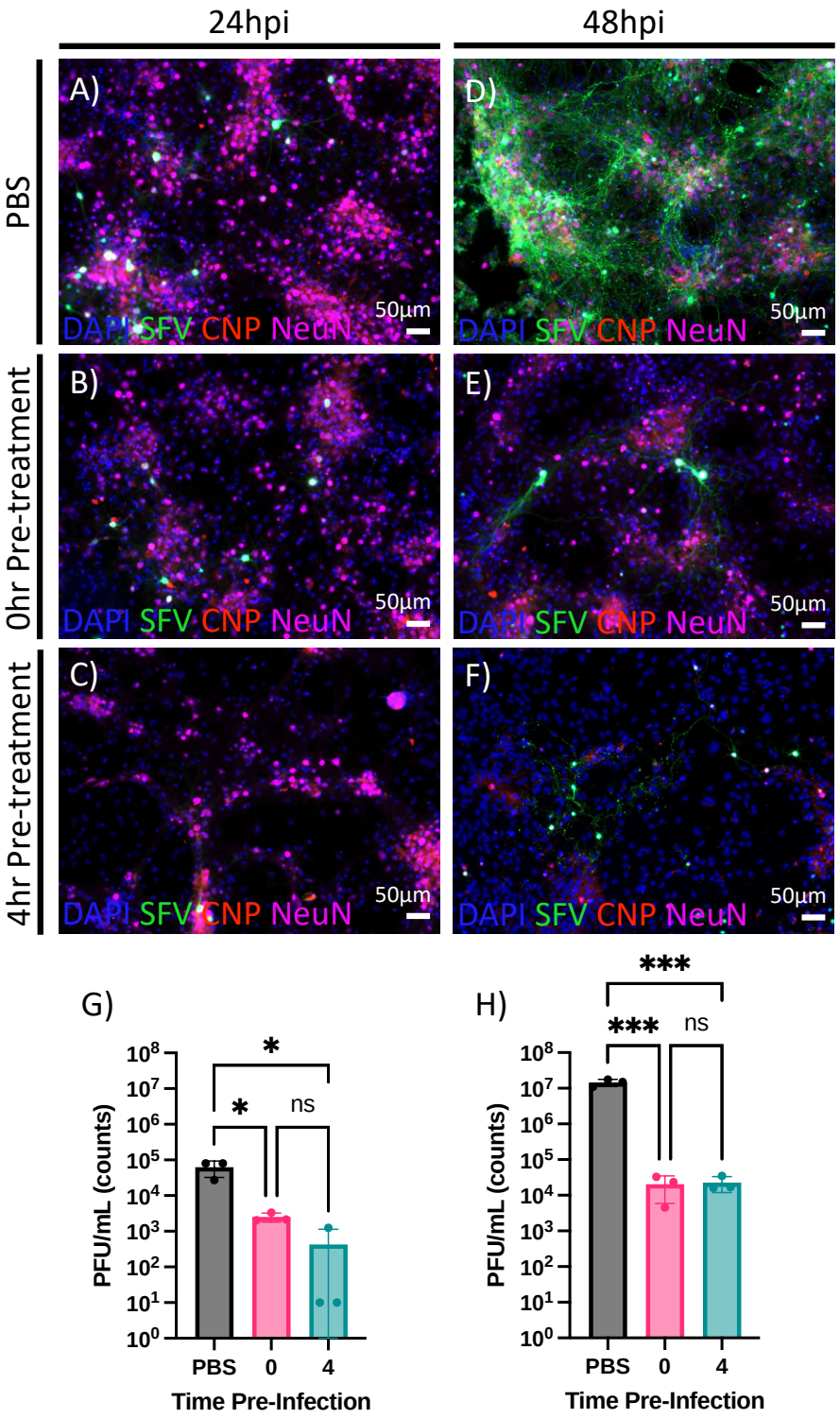


**Figure 6.4: Treatment with IFN-β at point of infection decreases SFV infectivity.** CNS cultures treated with IFN-β, infected with SFV and analysed after 24hpi (A-C,G) or 48hpi and (D-F,H) before being imaged by immunofluorescence microscopy (A-F) or analysed by plaque assays on supernatant for production of new virus (G-H). Cells stained with anti-CNP and anti-NeuN. In all cases, virus is seen in the green channel due to ZsGreen expression. Plaque assay data presented as mean ± SEM. Statistical analysis by one-way ANOVA with Tukey's multiple comparisons test. Significance denoted as $p<0.05$*, $p<0.005$***. (n=3)

Treatment of uninfected culture with dopamine caused a significant decrease in the percentage of CNP+ oligodendrocytes (**Figure 6.5A**) suggesting that dopamine hydrochloride is cytotoxic to oligodendrocytes. Since one of the two cell types (neurons and oligodendrocytes) infected by SFV are being killed by the dopamine, that explains the significant decrease in PFU/mL (**Figure 6.5C**) and the trend that there are less SFV+ oligodendrocytes in the cultures (**Figure 6.5B**). There is however no significant change in SFV infectivity between vehicle control and IL-10R blocking antibody (**Figure 6.5E-G**) or ERAP1-IN-1 (**Figure 6.5H-J**). However, these compounds could still influence viral infectivity that in cell cultures cannot be captured due to their lack of an adaptive immune system (Gamble *et al.*, 2023). There was a slight increase in the percentage of SFV+ oligodendrocytes treated with IL-10R blocking antibody (n.s.) compard to vehicle control, however further investigation of this effect *in vivo* is necessary to elucidate any effect this may have as IL-10 is not expressed in these cultures following IFN-β treatment (**Figure 4.4**).

## 6.6 Modulating SFV infectivity *in vivo*

As the CNS cell cultures do not fully capture the complexity of the CNS, in particular in relation to the lack of an adaptive immune system, I next tested the effect of IFN-β against SFV infectivity *in vivo*. SFV strain A7(74) has been used extensively to study both encephalitis and virus-induced demyelination *in vivo* (Fazakerley and Webb, 1987; Fazakerley *et al.*, 2006). Therefore, the model has relevance both to PML and viral encephalitis. Previous work by my lab demonstrated that intranasal (IN) administration of treatment and virus results in direct entry to the CNS through the olfactory bulb, without need for intraperitoneal (IP) or intracerebral injection. Treatments have an effect 24 hours post treatment, and viral dissemination is seen by 48 hours post infection.

Seven-week-old female C57BL/6J mice were anaesthetised with isoflurane and treated intranasally with 100µg/mL IFN-β in 10 µL dPBS 5mg/mL IL-10R blocking Antibody in 10µL dPBS or 10µL dPBS as a vehicle control, 6 mice per group. Endotoxin controlled for by purchasing low-endotoxin purified reagents. After 24 hours mice were infected with $1x10^5$ pfu SFV. Mice were treated 24hpi with a repeat dose of their initial treatment, before being culled at 48hpi. Mouse brain and pancreas were analysed by RT-qPCR for ISG *Cxcl10* and Viral *E1*, and viral titres from all tissues were obtained.

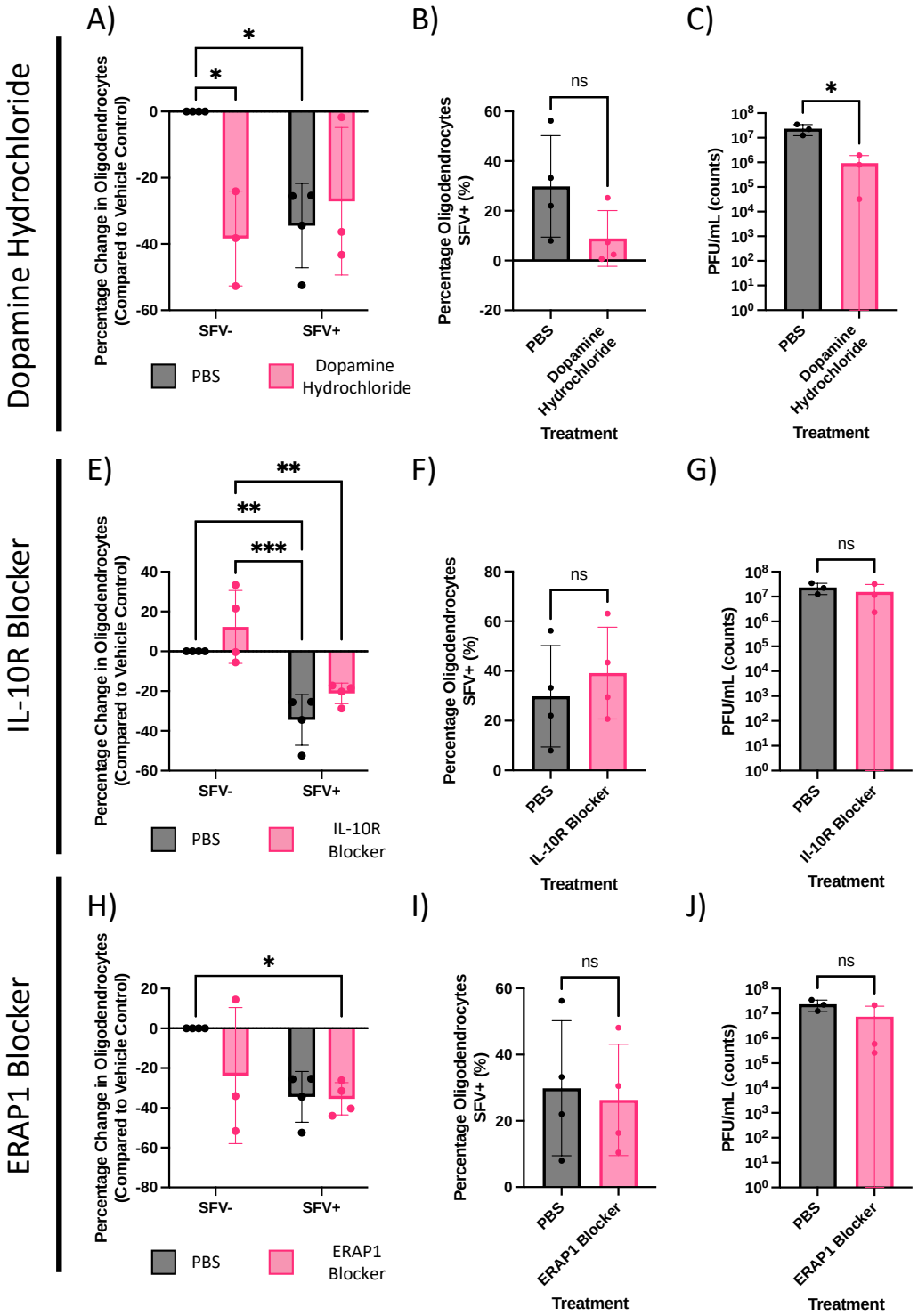


**Figure 6.5: Effect of manipulation of oligodendrocyte targets on SFV infectivity.** CNS cultures were treated with pharmacological manipulators dopamine hydrochloride (A-C), IL-10R blocking antibody (E-G), or the ERAP1 blocker ERAP1-IN-1 (H-J) 0hpi with SFV for 48 hours. Percentage change in oligodendrocytes (A,E,H), percentage oligodendrocytes SFV+ (B,F,I), and virus titre (C,G,J) plotted as mean ± SD. Percentage change analysed as 2 way ANOVA with Tukeys multiple comparison test. Remaining graphs analysed by unpaired *t*-test. Significance denoted as $p<0.05$ *, $p<0.01$ **, $p<0.005$ ***. N=4 for percentage change, n=3 for remaining.

### 6.6.1 IFN-β decreases viral infectivity *in vivo*

IFN-β decreased the quantity of actively replicating virus in the olfactory bulb and cortex, assessed by (**Figure 6.6B**), and resulted in a decreased viral titre in the olfactory bulb (**Figure 6.6C**). There was a trend towards a decrease in actively replicating virus in the cortex, assessed by plaque assay and viral RNA, however intra-group variability meant this did not reach significance. No significant decrease in the animals' weight was observed for the duration of the experiment (**Figure 6.6D**). *Cxcl10* mRNA levels were unaltered in the presence of IFN-β. The quantity of virus was highest in the olfactory bulb which is the site of infection, and trends towards 0 the more posterior through the CNS, as quantified by RT-qPCR (**Figure 6.6B**) and viral titre (**Figure 6.6C**) across all treatment regimens. These data suggests that IFN-β can induce a localised response *in vivo* to restrict SFV-A7(74) replication.

### 6.6.2 Blocking IL-10R decreases viral infectivity *in vivo*

As intranasal administration of IFN-β can induce an antiviral response against SFV-A7(74) *in vivo*, I next investigated the effect of an oligodendrocyte-specific candidate against viral infection. I chose to investigate the effect of blocking IL-10R because the IL-10R blocking Ab has already been trialled *in vivo* and deemed safe (Shouval *et al.*, 2014), and therefore required less optimising than the other candidates within the limited amount of remaining time.

Blocking IL-10R significantly decreased SFV in the olfactory bulb, when quantified by RT-qPCR (**Figure 6.6B**), however had no significant effect on viral titre as assessed by plaque assay (**Figure 6.6C**). No significant change in animals' weight was observed (**Figure 6.6D**). These data suggest that IL-10R influences viral replication in the CNS, however additional replicates and optimisation are required to determine if this conclusion is valid.

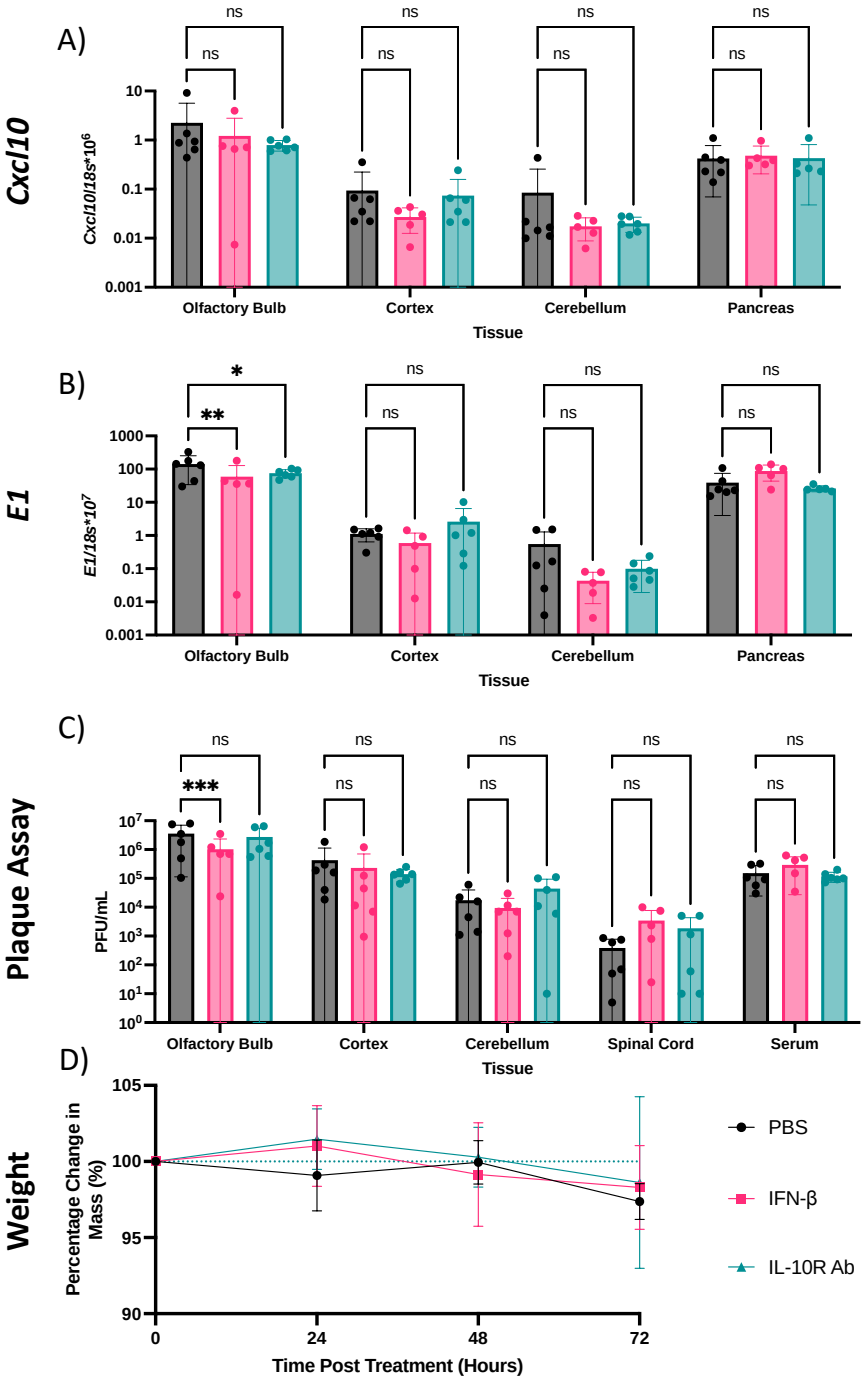


**Figure 6.6: IFN-β and IL-10R blocking Ab modulate viral infectivity *in vivo*.** RT-qPCR analysis (A-B) or viral titre (C) of 7 week old female C57Bl/6J mice treated intranasally with PBS, IFN-β, or IL-10R blocking Ab. RT-qPCR of (A) *Cxcl10* and (B) *E1* in olfactory bulb, cortex, or cerebellum, or pancreas, presented as mean ± SEM. Viral titre measured by plaque assay. Weight of mice for duration of experiment presented as % original weight ± SD. n=6. Significance determined by two-way ANOVA with Tukey's post *hoc* test.

## 6.8 Discussion

The data presented in this chapter demonstrate that IFN-β offers protection against a neurotropic virus *in vitro* and *in vivo* and identified a possible role for blocking IL-10R in neuroprotection against neurotropic virus. Specifically, I found that oligodendrocytes were protected by IFN-β in the context of viral infection, and therefore further investigation into downstream targets in the context of viral infection, not solely IFN-β treatment, could have wider implications for the treatment of PML and viral encephalitis.

Initially, I aimed to quantify the response of the CNS cultures to SFV infection. While SFV is of a different viral *genus* than JCV (*alphavirus* compared to *polyomavirus* respectively), SFV shares a similar tropism to JCV, and unlike JCV, is infectious in murine models. I chose SFV6 for the CNS cell culture studies as this virus is more neuroinvasive than other strains of SFV, such as SFV-A7(74) (Saul *et al.*, 2015). As SFV6 more rapidly replicates in the CNS than SFV-A7(74), it expedites experimentation. Similarly, as the tropism is more aggressive than SFV-A7(74), if any treatments decrease the infectivity of SFV6 they would decrease the infectivity of SFV-A7(74). However, the viral strain is novel to my CNS cell cultures and therefore needed to be characterised. I saw *in vitro* that SFV6 infects the CNS cell cultures and reaches peak infection within 48 hours after which time the cultures rapidly degenerate, implying less than 48 hours is a viable time to investigate the effect of immunomodulatory compounds, such as IFN-β, on viral infectivity.

I found that IFN-β was effective against SFV6 infection and the protection was not cell-type specific, as both neurons and oligodendrocytes were protected from viral infections. I also showed that IFN-β has a lasting therapeutic benefit even when administered immediately post-infection. Previous studies have shown that cells stop responding to IFN-β treatment within 2-4 hours when infected with alphaviruses (Marsh and Heleniust, 1989; Allsopp *et al.*, 1998), therefore I wondered how IFN-β can decrease infectivity up to 48 hours post infection. I infected my cultures with an MOI = 0.00003. This MOI equates to approximately 5 viral particles per treatment well the cultures are grown in. This is similar to what happens *in vivo* where SFV4 and SFV6 infection result in a “patchy” tropism where few viral particles cross the BBB across the brain, even from high infectious doses, and spread from the site of infection (Tamberg *et al.*, 2007; Bryden *et al.*, 2020). This phenomenon is particularly well described in HIV infections where transmitted fluids with high viral titres up to $1x10^6$ pfu/mL

only infect 1 or 2 cells to start the new infection in a new host (Keele *et al.*, 2008). Therefore, when treating my cultures, or an *in vivo* brain, I hypothesised IFN-β likely protects the uninfected cells, which make up the majority, from infection while the infected cells are likely destined to die.

As alphaviruses are released from a lysed cell within approximately 3-6 hours post infection (Strauss and Strauss, 1994), my results support this hypothesis. IFN-β treatment upregulates the expression of ISGs for up to 48 hours post infection (**Figure 4.4**G) inducing an antiviral state, over which time SFV6 had decreased infectivity in the CNS cell cultures. To further answer that question, however, the cultures would need to be infected with a higher infectious dose of SFV in addition to investigating the effect of post-infectious treatments. In the context of treatments for PML the virus is already in the CNS and undergoing active replication. My results imply that treatment post-infection could protect uninfected oligodendrocytes against JCV. Thus, prompt administration of an IFN-based therapy could be essential to prevent long-term neurological deficits associated with PML.

When investigating the effect of IFN-β *in vivo* I treated mice twice; 24 hours pre-infection and 24 hours post infection. As discussed, this could have protected cells from the initial wave of viral infection, and also protected uninfected cells from subsequent infection after the virus had lysed and disseminated within the CNS. Whether administration at both time points is required remains unanswered, but from a therapeutic point of view, treatment at the second time point only is the only viable route. It is relevant that for the *in vivo* experiments, I use avirulent SFV-A7(74) because this strain had been used previously in *in vivo* studies. It will be important in future preclinical studies to determine whether the treatment is effective against a more virulent strain, for example SFV6.

Following IFN-β treatment there were less actively replicating virus in the olfactory bulb and cortex, as quantified by RT-qPCR, and a lower viral titre in the olfactory bulb. The implication here is that the virus could initially infect cells in the olfactory bulb but enhanced infection with the release of viral particles was inhibited by IFN-β, supporting the previously discussed hypothesis. However, this anti-viral effect was lost towards the posterior of the CNS. These data suggest that IFN-β does not readily disseminate throughout the CNS, and instead acts primarily at the site of administration.

Chauhan and Chauhan showed that the IN route of administration has increased transport across the BBB compared to IP injection. This does not guarantee the compound will induce a neuroprotective effect more caudally, however, for example in the spinal cord (Chauhan and Chauhan, 2015). To investigate how readily IFN-β disseminates from the point of administration qPCR studies should be conducted on ISGs to identify how caudally IFN-β can induce its antiviral effect through the CNS, both in the context of viral challenge and homeostatic conditions. The results shown here add further credence to the possibility of using IFN-β derived therapeutics against JCV and additional encephalitic viruses. Nonetheless, my data also demonstrate a need to derive therapeutics that can reach all parts of the CNS as inducing protection at a single site is inadequate. An argument could be made for the induction of IFN-β itself in the CNS, for example using the viral mimetic poly(I:C) (Field *et al.*, 2010). Using extracellular vesicles containing poly(I:C) have been shown to cross the BBB and induce a potent upregulation of type-I IFNs more caudally in the CNS, for example in the hippocampus inside the cortex (Kulakauskienė *et al.*, 2021). However, IFN-β has been linked with side effects in the CNS, for example flu-like symptoms and mental deficiencies (Jakimovski *et al.*, 2018; Filipi and Jack, 2020). To avoid these side effects downstream pathways of IFN-β treatment, for example those identified in Chapter 5, may be more readily manipulated with pharmaceuticals that can cross the BBB easily while decreasing side effects of IFN-β treatment itself.

In Chapter 5 I identified *Drd4*, *IL-10Ra*, and *Erap1* were significantly upregulated in oligodendrocytes, and thus I investigated their effect in the context of homeostatic conditions and viral challenge *in vitro*. However, due to the observed cytotoxicity of dopamine, I ruled this target out early on. At neutral pH, dopamine quickly oxidises into toxic reactive compounds such as quinones, which have been implicated in the progression in Parkinson's disease (Zahid *et al.*, 2011). Dopamine eventually oxidises into neuromelanin which itself binds and clears reactive oxygen species (Monzani *et al.*, 2019). However, free floating neuromelanin can bind and activate microglia to produce and release pro-inflammatory compounds such as nitrous oxide (NO) and hydrogen peroxide ($H_2O_2$) (Zhang *et al.*, 2011); compounds that induce necrosis and apoptosis, respectively, in oligodendrocytes (Mitrovic *et al.*, 1995; Lee, Oh and Yune, 2011). The cytotoxic effects of

dopamine could be an *in vitro* artefact due to an overabundance of these cytotoxic compounds that anti-oxidants in the CNS cell cultures cannot clear.

Dopamine may have therapeutic benefit *in vivo*, as many immune cells express dopamine receptors (Channer *et al.*, 2023). In SARS-CoV-2 infections, dopamine was linked with decreased infectivity in the lung epithelium through upregulating the expression of ISGs and type-I IFNs (Limanaqi *et al.*, 2022). Dopamine could modulate the expression of type-I interferons in the CNS to decrease viral infectivity, however investigations into this would need to be performed to identify any therapeutic potential.

I found that blocking ERAP1 *in vitro* had no marked effect on viral infectivity. ERAP1 *in vivo* is involved with the processing and presentation of pathogen antigens to CD8+ T cells via MHC-I (Serwold *et al.*, 2002; Saveanu *et al.*, 2005). Therefore, in CNS cell cultures lacking CD8+ T cells, while antigens might be presented this will result in no effect. Oligodendrocytes express MHC-I following IFN-γ treatment and also in MS and by type 2 interferons (Falcão *et al.*, 2018; Kirby *et al.*, 2019b). In MS, oligodendrocytes at the edge of an active lesion present pro-inflammatory compounds to immune cells during inflammatory demyelination. Therefore, inhibiting this process could drive increased infectivity *in vivo* through decreasing the recruitment of effector CD8+ T cells to kill virus-infected cells. In the context of PML, recruitment of CD8+ T cells has been linked with a better disease prognosis, with more CD8 T cells being found in PML survivors than progressors (Gheuens *et al.*, 2011). Further investigation of ERAP1 is therefore warranted, particularly *in vivo* and in the context of a demyelinating disease such as EAE to identify any therapeutic value this may have.

The final identified target was *Il10ra*, the alpha subunit of the IL-10 receptor. Whilst not significant, there was a trend towards protection of oligodendrocytes by blocking IL-10R *in vitro* from virus mediated cell-death. Since I had previously discovered that IL-10 is not expressed in CNS cell cultures following IFN-β treatment, or at baseline (**Figure 4.4G**), this is unlikely to be as a direct result of blocking IL-10R. However, following viral infection, this is likely to change. Alphaviruses are linked with inducing the expression of IL-10 following infection (Kulcsar *et al.*, 2014), and IL-10 has been shown to promote the survival of oligodendrocytes in the context of injury by promoting the differentiation of OPCs to

mature oligodendrocytes (Dyck *et al.*, 2018; Smith *et al.*, 2020). I hypothesise that the IL-10R blocking Ab creates an anti-inflammatory environment *in vitro* by blocking the activity of IL-10 secreted from microglia, which induces the differentiation of OPCs to mature oligodendrocytes, thus explaining why there is simultaneously more oligodendrocytes infected and less oligodendroglia loss in the cultures. However, investigations into IL-10 concentrations post-infection or in the presence of IL-10 blocking Ab are necessary to confirm this.

IL-10 is known as a classically immunosuppressive cytokine *in vivo*. By blocking IL-10R, I saw a slight decrease in the quantity of *E1* in the olfactory bulb in mice infected with SFV. A previous study involving intranasal infection of an alphavirus showed that IL-10 is not induced in the brain until ~5 days post infection (Kulcsar *et al.*, 2014). Therefore, the results I have here could potentially be clearer at a later time point. Kulscar et al.'s study showed that IL-10 deficiencies resulted in more severe disease by increasing the Th1 cell count, and decreasing B cell responses (Kulcsar *et al.*, 2014). These data contrast with what I identified here, where I found that blocking IL-10R possibly decreased viral infectivity *in vivo*. However, as with the other oligodendrocyte specific targets identified, further investigation on the role of the adaptive immune system along with later timepoints are essential to identify any putative therapeutic role of blocking IL-10R on viral infectivity.

Ultimately, the data presented in this chapter show encouraging preliminary results regarding the efficacy of IFN-β and some oligodendrocyte-specific candidates identified by RNAseq to decrease viral infectivity and protect oligodendrocytes; the cell type that is primarily affected by JCV. While IFN-β only appears to have an antiviral effect at the site of administration, my results have exciting potential in respect to the development of future drugs. Therapies that can modulate downstream pathways, for example those identified in **Chapter 5**, may be easier to pharmacologically manipulate with drugs that can readily cross the BBB and to convey an antiviral effect to the whole CNS. My work with the RNAseq candidates has laid the groundwork to investigate these. Further experiments exploring the functional therapeutic value *in vivo* could prove beneficial for the development of drugs against JCV infection and viral encephalitis.

# Chapter 7

## Discussion

# 7.0 Discussion

The data presented in this thesis demonstrate that IFN-β induces an ISG response in all major cell types of the CNS. This combined response effectively limits viral replication of a neurotropic virus in oligodendrocytes and neurons. Additionally, this research provides information towards identifying oligodendrocyte specific candidates that may provide future therapeutic value in protecting the oligodendrocyte itself, or the CNS as a whole against infection by encephalitic viruses. Further confirmation of the antiviral effect of either IFN-β or IFN-β-derived therapies *in vivo* and in human tissue would be required to translate this research into clinical application. These results are particularly exciting as they imply that the innate antiviral activity of oligodendrocytes can be exploited therapeutically for people with MS who are on immunosuppressive medicines who are at risk or have developed PML disease pathology.

While many efficacious drugs have been approved for treatment of MS, several of these have been linked with developing PML. For example natalizumab, fingolimod, and dimethyl fumarate (Berger, 2017). These DMTs act primarily through suppressing the immune system; natalizumab blocks adhesion of leukocytes to the epithelial walls and therefore penetration into the CNS (Selewski *et al.*, 2010); fingolimod prevents lymphocyte egress from lymphoid tissues (Chun and Hartung, 2010); and dimethyl fumarate decreases lymphocyte counts in the patient (Mills *et al.*, 2018). Therefore, discovering that IFN-β induces innate antiviral activity in oligodendrocytes specifically, advocates that combined therapeutics with IFN-β and these DMTs could decrease MS disease pathology while limiting the risk of PML progression. This would allow patients safe access to higher efficacy drugs and improve overall quality of life and extend life expectancy.

While IFN-β induces a strong antiviral response in the CNS, the molecule is not effective for treating viral encephalitis in humans. The treatment can cause unintended side effects such as depression, flu-like symptoms, and inflammation at the site of injection (Filipi *et al.*, 2014). Furthermore, IFN-β also does not readily cross the BBB and is in fact linked with decreasing its permeability (Kraus *et al.*, 2008). Therefore, development of IFN-β derived therapeutics which can convey an antiviral effect in the CNS while being able to cross the BBB with minimal side effects is crucial. Investigation into the downstream effects of IFN-β,

as detailed in **Chapter 5**, not only provided further proof of the antiviral activity of IFN-β in the CNS, it identified candidates that could allow the development of novel therapies to protect specific cell types against viral infection. Previous studies have investigated the antiviral effect of IFN-β produced in the CNS, particularly by astrocytes (Kallfass *et al.*, 2012), against viral infection in the different cell types (Telikani *et al.*, 2022). However, focussed studies into the transcriptional profile following IFN-β treatment are centred on specific genes, for example the classical interferon-stimulated genes (Lang *et al.*, 2022). Therefore, my analysis provides novel information that could drive the development of therapies against viral infection in the individual cell types of the CNS. Increasing our understanding of IFN-β related therapies allows cell-type specific drugs to be developed which could induce an antiviral effect without the associated IFN-β side effects (Filipi *et al.*, 2014).

In the studies performed here, I only investigated the short-term effects of IFN-β, with a single dose being measured up to 96 hours of continuous application. I did not investigate the result of prolonged IFN-β treatment on the CNS cultures, for example treating for multiple weeks to months. MS is a life-long disease with no cure, so any therapies would need to be additionally investigated to ensure they remain effective in the long-term. Microglia and astrocytes have been shown to display immunological exhaustion and premature senescence in response to prolonged pro-inflammatory profiles (Bitto *et al.*, 2010; Angelova and Brown, 2019; Cohen and Torres, 2019; Izzy *et al.*, 2019). Therefore, prolonged treatment with IFN-β could result in a decrease in the innate antiviral effect in oligodendrocytes over time. There are no studies currently on the effect of long term IFN-β treatment as an antiviral. Studies in the context of MS treatment are contradictory but indicate that prolonged IFN-β treatment continues to effectively modify the immune response in the CNS (Chen, Wu and Watson, 2018). Whether IFN-β remains effective as an antiviral *in vivo* warrants further investigation *in vitro* to identify any possible side effects, such as the immunological exhaustion described, of this as a treatment to protect oligodendrocytes.

One aspect of the antiviral response that was not investigated fully was the contribution of ISGs to the adaptive immune system. Peripheral immune cells are found in the CNS in both MS and viral encephalitis and their presence is a dual-edged sword where they can convey both a protective and a damaging effect. The effect of IFN-β on peripheral immune cell

recruitment should be investigated *in vivo*. In MS, CD4+ and CD8+ T cells are considered a driving force behind disease progression (van Langelaar *et al.*, 2020), and therefore any positive antiviral effect of IFN-β must not be at the expense of exacerbated MS disease progression. This could be investigated *in vivo* using flow cytometry of digested murine CNS tissue with markers for T cells, B cells, and other associated myeloid cells following infiltration of these cells into the CNS. Similarly, this could be investigated *in vitro* with the CNS cultures using a split-chamber microfluidic device. Peripheral immune cells could be added to one compartment of the microfluidic device and CNS cells in the other. The compartment containing the CNS cultures would be treated with IFN-β and the migration of the immune cells monitored. An additional investigative step could be to work with individual cell types of the peripheral immune system, for example adding CD8+ T cells to the microfluidic chamber and characterising their response to IFN-β treatment in the context of the CNS cells. Investigations with iPSC derived human cells will improve translatability of results to human studies. However, a mixed-glial culture of human cells which contains microglia would need to be developed and optimised first. Such models could provide critical insight into the effect of IFN-β on recruitment of myeloid cells to the site of infection. This is essential for the oligodendrocyte-specific targets. IL-10 and ERAP1 are involved in the recruitment of the adaptive immune response, and therefore *in vitro* and *in vivo* investigation of the effect of blocking their activity on peripheral immune cells would increase the clarity and relevance of the research.

As detailed in **Chapter 5**, I identified multiple pathways that are enriched following IFN-β treatment in oligodendrocytes with varied immunological roles. While the discussion of Chapter 5 focussed on oligodendrocyte-specific candidates, I additionally identified multiple pathways enriched in the other major CNS cells that could be manipulated pharmacologically to convey a therapeutic benefit. Many additional experiments could be performed to deduce which of these targets convey an antiviral effect for additional CNS cell types.

Most of the targets identified did not have any pharmacological manipulators available. The only readily available drug not tested in **Chapter 6** was the Gasdermin D inhibitor LDC7559 (Cai *et al.*, 2023), which unfortunately did not arrive in time for adequate testing during this project. The other targets had siRNA available that would have knocked-down the

translation of the targets and therefore would allow studies of their antiviral effect. However, siRNA does not readily translate to *in vivo* studies (Fu *et al.*, 2021). Therefore, elucidating any antiviral effect in the *in vitro* cultures is essential before attempting to identify a mechanism *in vivo*.

A consistent thread throughout this thesis has been identifying therapeutics which can decrease viral infectivity in oligodendrocytes, as these are the cells infected by JCV and therefore relevant to PML disease pathology. However, IFN-β induces a profound antiviral effect against multiple viral strains (Wang and Campbell, 2005; Mantlo *et al.*, 2020; Zuo *et al.*, 2020). Therefore, the research identified here could be used for developing broad-spectrum antiviral therapies against other encephalitic viruses.

Viral encephalitis is a severe, life-threatening condition that particularly affects those with weak or underdeveloped immune systems, for example the elderly, infants, or immunocompromised people (Rozenberg, 2013). The incidence of viral encephalitis ranges between 7 and 15 cases per 100,000 people (Dubey *et al.*, 2018; Ferreira *et al.*, 2019; Lee *et al.*, 2023), however this number is expected to increase. Climate change will allow diseases that are currently sub-tropical to expand northward, particularly mosquito-borne viruses such as West-Nile Virus and Japanese Encephalitic Virus (Tolsá-García *et al.*, 2023). Onset of neurological symptoms is rapid and severe, therefore effective antiviral treatment is crucial to decrease neurological defects. However, antivirals only exist for herpes viruses and any treatments for other encephalitic viruses rely on supporting the body (Griffin, 1991; James, Kimberlin and Whitley, 2009). Additionally, there are significant challenges in diagnosing viral encephalitis due difficulties obtaining tissue samples and diagnostic tests being particularly upsetting for the patient, for example lumbar puncture to gain CSF samples. As the lack of effective drugs contributes significantly to high mortality, and the inherent difficulties in diagnosing viral encephalitis, there is an urgent and essential need to develop broad spectrum antiviral treatments that are effective within a short time-frame.

In this study, I used SFV, an ssRNA alphavirus as a model virus. Further investigation of this effect with genetically unrelated viruses such as influenza, an ssRNA orthomyxovirus, is necessary. Since SFV is an ssRNA virus, this is not fully comparable to JCV as this is a dsDNA virus and considerable differences in host response to DNA and RNA viruses has been

reported (Zhu *et al.*, 2014; Ghosh *et al.*, 2019). Therefore, further investigation of additional viral types would identify any broad-spectrum antiviral role of the response characterised here. JCV is a human obligate pathogen, as mentioned previously iPSC derived human tissue could be used to generate a culture of oligodendrocytes *in vitro*. When treated with IFN-β or an RNAseq identified candidate and infected with JCV these cultures would identify any antiviral potential the drugs may have. The recent COVID-19 pandemic further highlighted the essential nature of antivirals. The development of a broad-spectrum therapeutic is necessary, particularly since the increased prevalence of encephalitic viruses increases the likelihood of an encephalitic virus pandemic (Afrough, Dowall and Hewson, 2019).

This thesis has made progress towards understanding the exact role of IFN-β on the individual cell types of the CNS helping identify novel avenues for drug development to combat viral infection in the CNS. This would be particularly useful for developing drugs against JCV in the context of PML. This has laid the groundwork to explore this in greater detail in both murine and human *in vitro* and *in vivo* models, hopefully eventually resulting in decreased prevalence of PML and viral encephalitis.

# Chapter 8

## Appendices

# 8.0 Appendices

## 8.1 Differentially expressed genes in CNS cultures following IFN-β treatment

**Figure 8.1: QR Code to spreadsheet of genes differentially expressed in CNS cultures by IFN-β compared to PBS controls.** Table showing genes differentially regulated in IFN-β-treated CNS cultures compared to untreated controls. Fold change ≥ ±2, FDR adjusted *p* – value ≤ 0.0001.

Link:

https://bit.ly/3VfsgBX

8.2 Representative normalised reads of different Gene Ontology (GO), Kyoto Encyclopaedia of Genes and Genomes (KEGG), and Reactome pathway analysis groupings for pooled-DEGs.

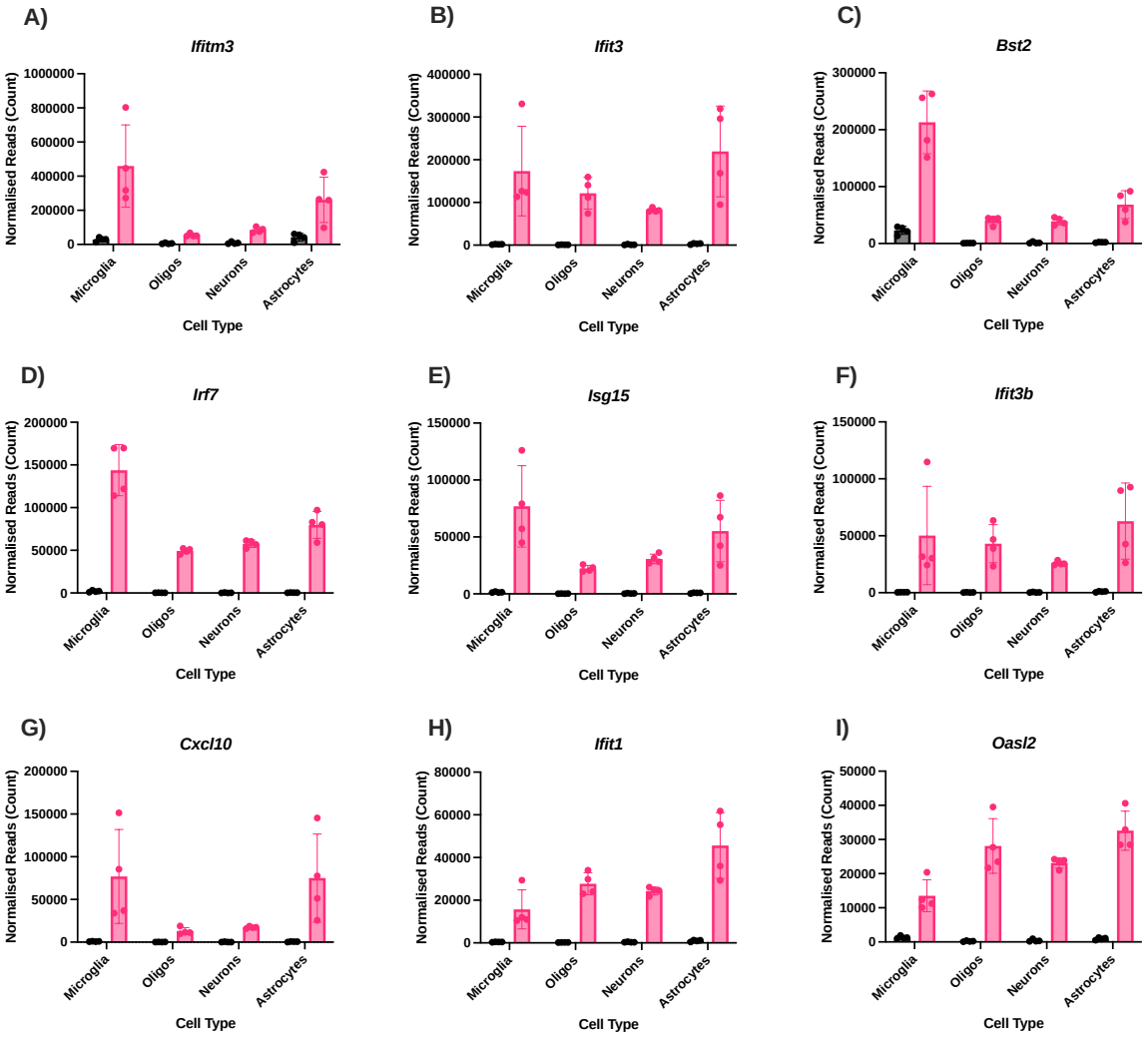


**Figure 8.2: Normalised read counts of top 9 expressed genes in *Response to interferon-beta* GO term.** Graphs show normalised number of reads across sorted cell types following treatment with PBS (vehicle) or IFN-β, with top 9 genes identified through having the greatest mean number of normalised read counts across all sorted cell types and treatment regimens. A) *Ifitm3*, B) *Ifit3*, C) *Bst2*, D) *Irf7*, E) *Isg15c*, F) *Ifitm3b*, G) *Cxcl10*, H) *Ifit1*, I) *Oasl2*. Bars represent mean ± SD. n=4.

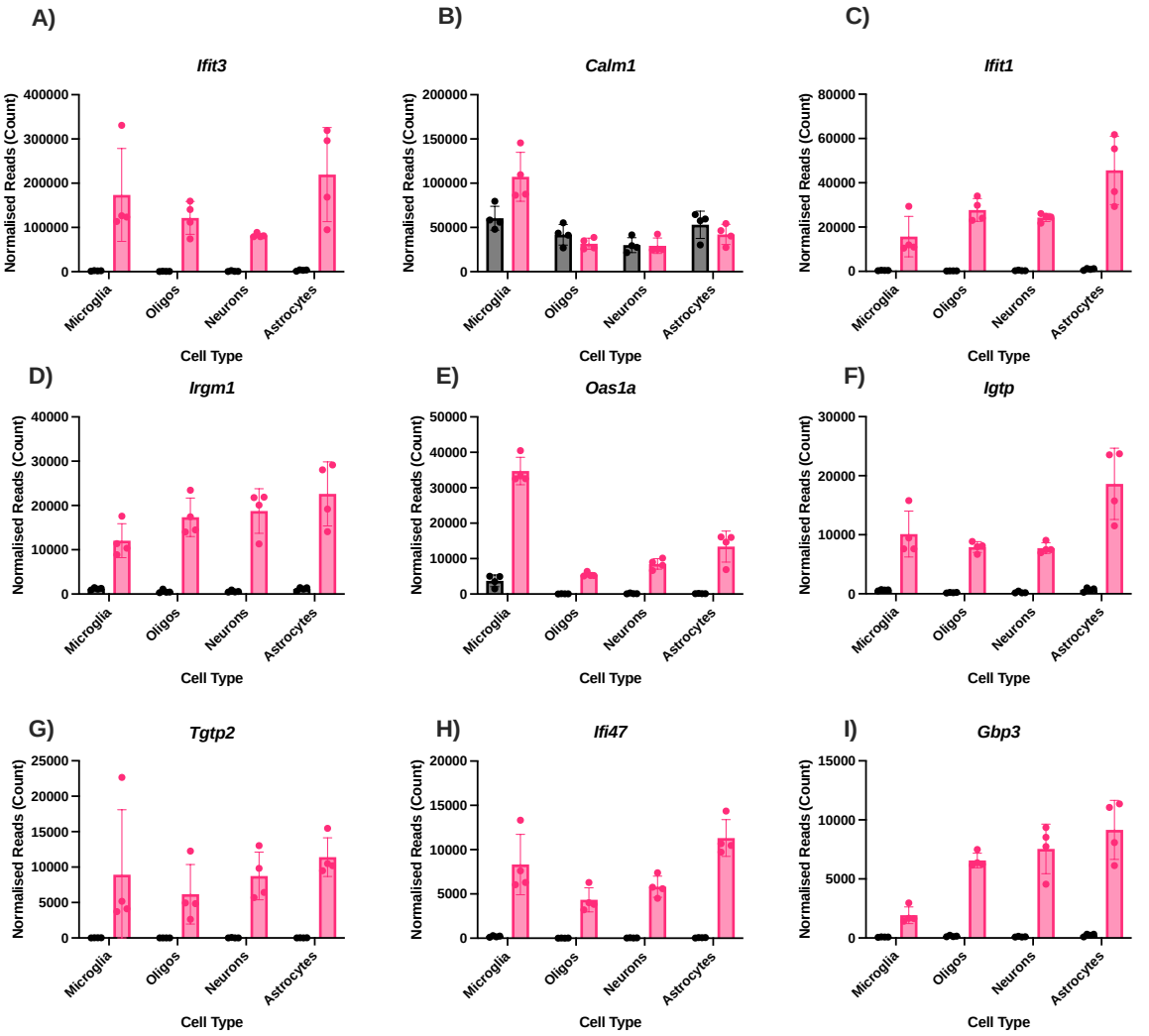


**Figure 8.3: Normalised read counts of top 9 expressed genes in *Regulation of virus / pathogen* GO term.** Graphs show normalised number of reads across sorted cell types following treatment with PBS (vehicle) or IFN-β, with top 9 genes identified through having the greatest mean number of normalised read counts across all sorted cell types and treatment regimens. A) *Ifit3*, B) *Calm1*, C) *Ifit1*, D) *Irgm1*, E) *Oas1a*, F) *Igtp*, G) *Tgtp2*, H) *Ifi47*, I) *Gbp3*. Bars represent mean ± SD. n=4.

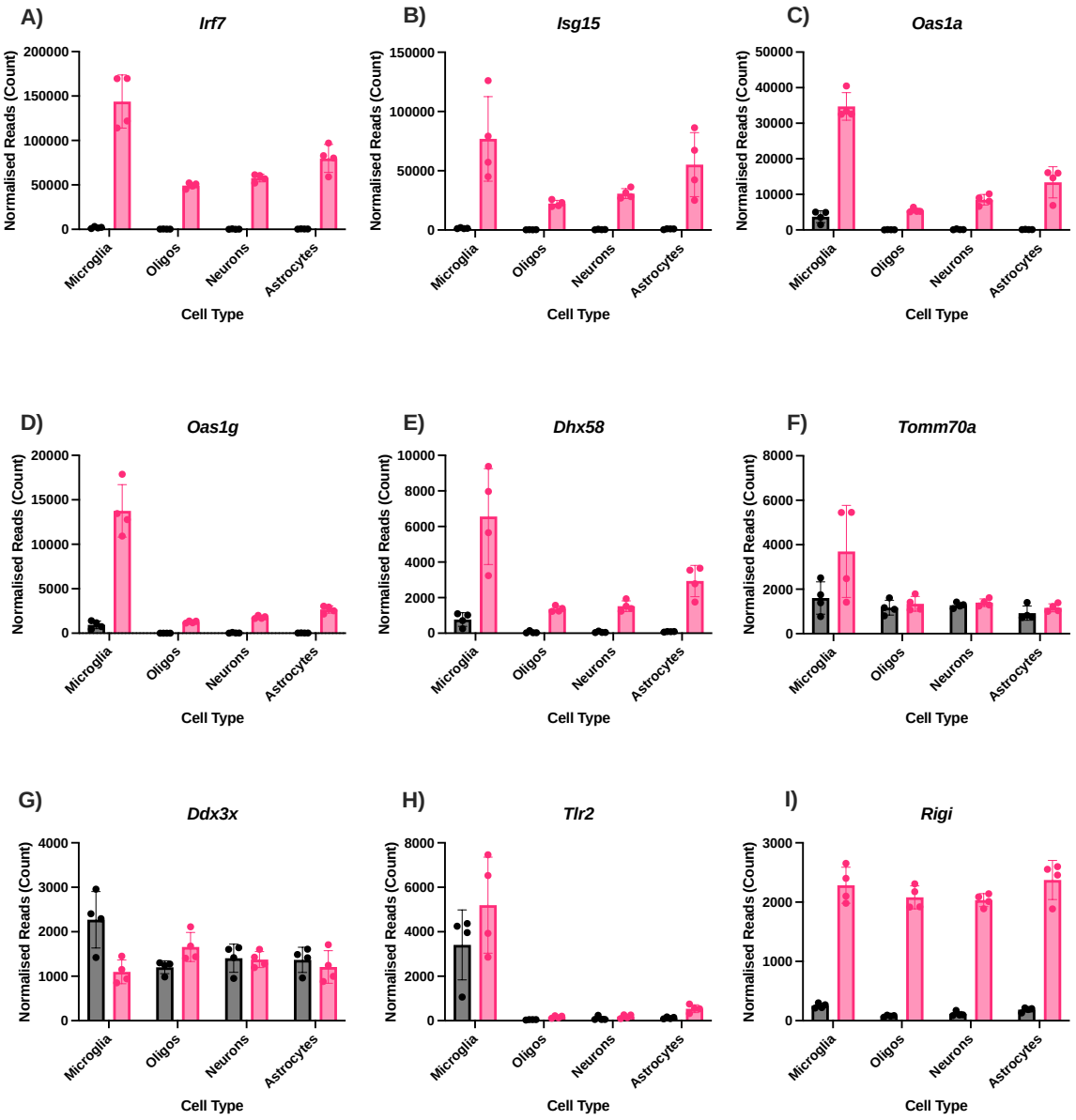


**Figure 8.4: Normalised read counts of top 9 expressed genes in *Regulation of innate immune response* GO term.** Graphs show normalised number of reads across sorted cell types following treatment with PBS (vehicle) or IFN-β, with top 9 genes identified through having the greatest mean number of normalised read counts across all sorted cell types and treatment regimens. A) *Irf7*, B) *Isg15*, C) *Oas1a*, D) *Oas1g*, E) *Dhx58*, F) *Tomm70a*, G) *Ddx3x*, H) *Tlr2*, I) *Rigi*. Bars represent mean ± SD. n=4.

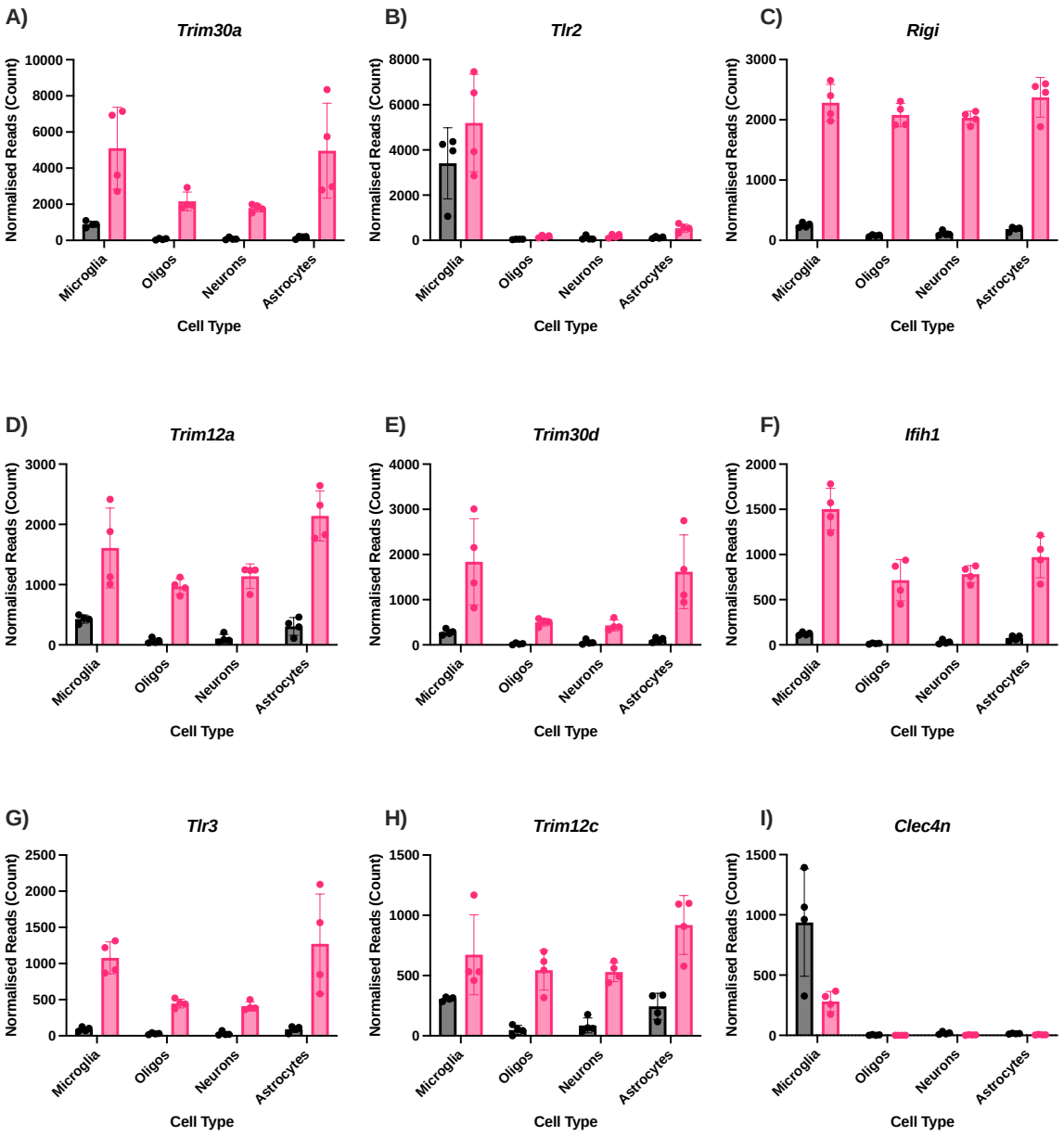


**Figure 8.5: Normalised read counts of top 9 expressed genes in *PRR activity* GO term.** Graphs show normalised number of reads across sorted cell types following treatment with PBS (vehicle) or IFN-β, with top 9 genes identified through having the greatest mean number of normalised read counts across all sorted cell types and treatment regimens. A) *Trim30a*, B) *Tlr2*, C) *Rigi*, D) *Trim12a*, E) *Trim30d*, F) *Ifih1*, G) *Tlr3*, H) *Trim12c*, I) *Clec4n*. Bars represent mean ± SD. n=4.

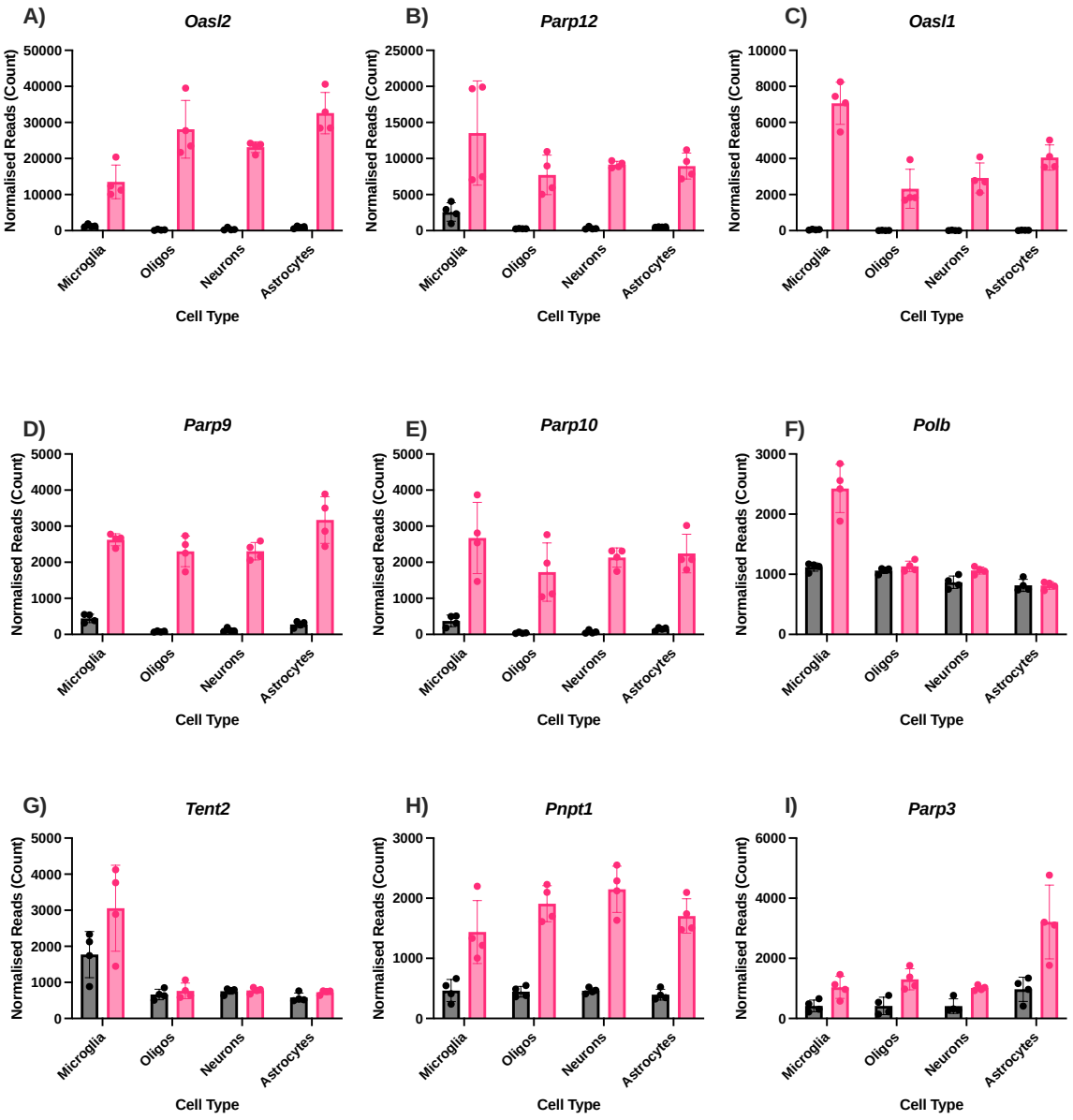


**Figure 8.6: Normalised read counts of top 9 expressed genes in *Nucleotidyltransferase activity* GO term.** Graphs show normalised number of reads across sorted cell types following treatment with PBS (vehicle) or IFN-β, with top 9 genes identified through having the greatest mean number of normalised read counts across all sorted cell types and treatment regimens. A) *Oasl2*, B) *Parp12*, C) *Oasl1*, D) *Parp9*, E) *Parp10*, F) *Polb*, G) *Tent2*, H) *Pnpt1*, I) *Parp3*. Bars represent mean ± SD. n=4.

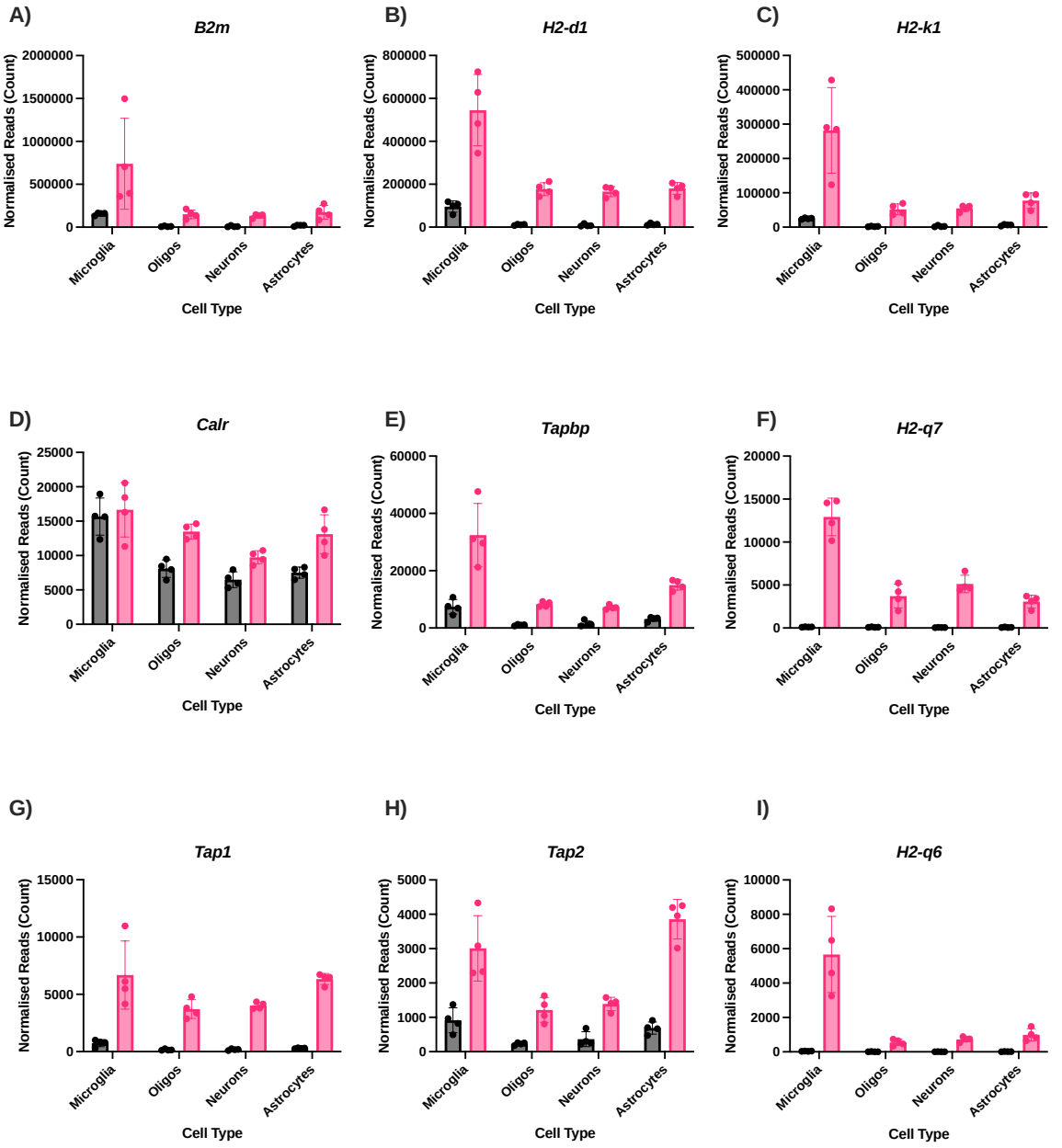


**Figure 8.7: Normalised read counts of top 9 expressed genes in *Regulation of MHC-I* GO term.** Graphs show normalised number of reads across sorted cell types following treatment with PBS (vehicle) or IFN-β, with top 9 genes identified through having the greatest mean number of normalised read counts across all sorted cell types and treatment regimens. A) *B2m*, B) *H2-d1*, C) *H2-k1*, D) *Calr*, E) *Tapbp*, F) *H2-q7*, G) *Tap1*, H) *Tap2*, I) *Ht-q6*. Bars represent mean ± SD. n=4.

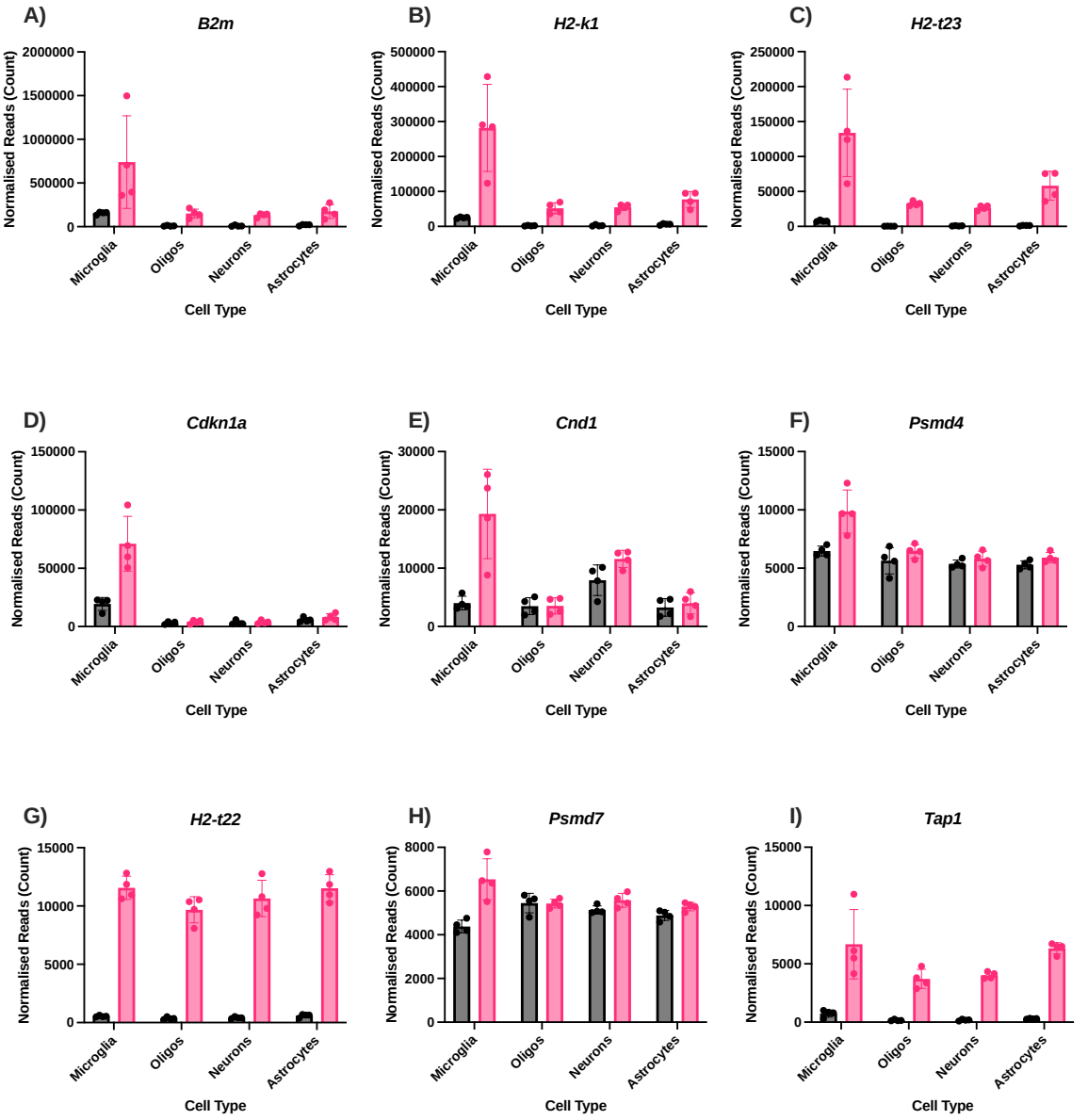


**Figure 8.8: Normalised read counts of top 9 expressed genes in *Response to human pathogens* KEGG term.** Graphs show normalised number of reads across sorted cell types following treatment with PBS (vehicle) or IFN-β, with top 9 genes identified through having the greatest mean number of normalised read counts across all sorted cell types and treatment regimens. A) *B2m*, B) *H2-k1*, C) *H2-t23*, D) *Cdkn1a*, E) *Cnd1*, F) *Psmd4*, G) *Ht-t22*, H) *Psmd7*, I) *Tap1*. Bars represent mean ± SD. n=4.

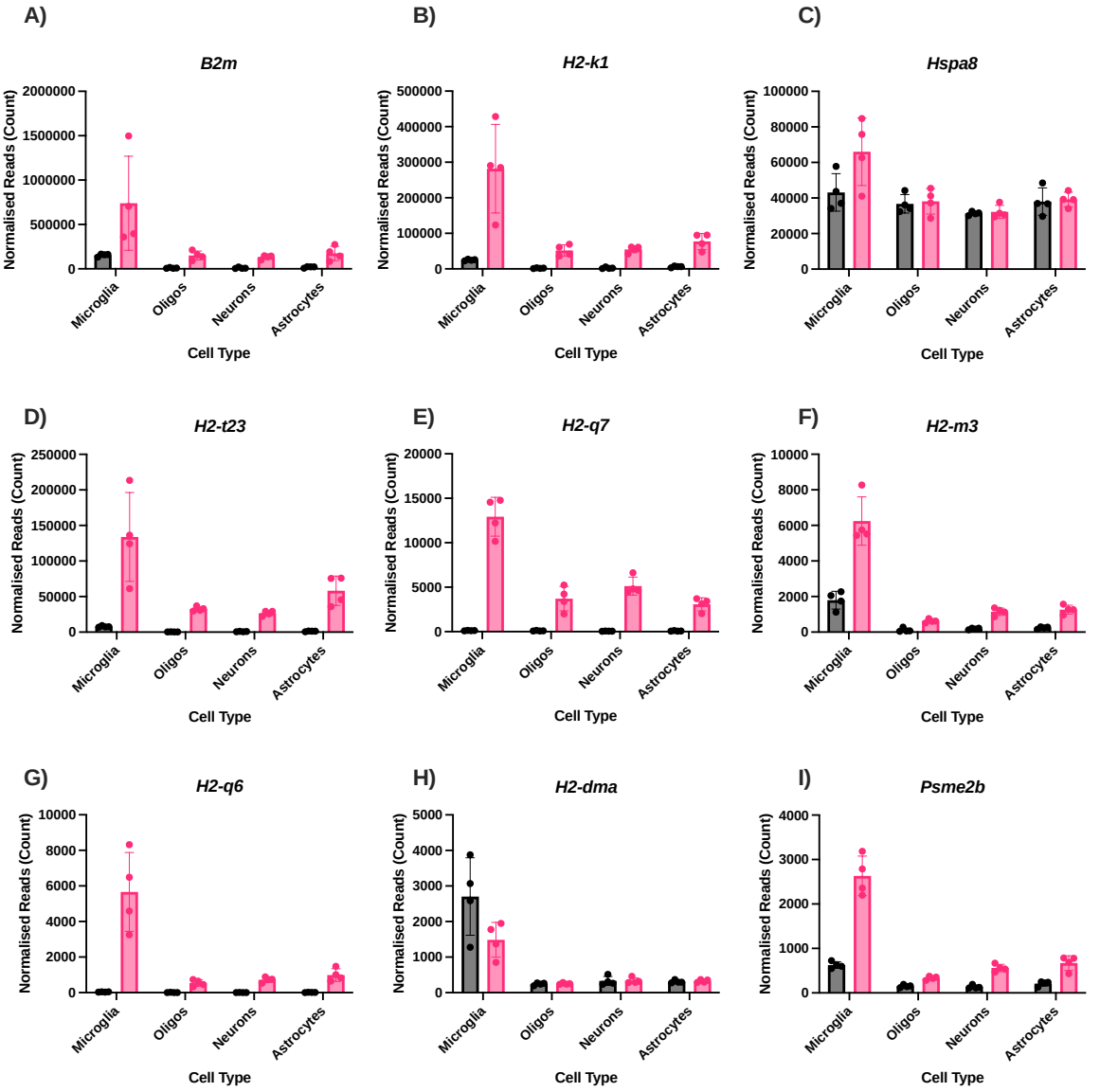


**Figure 8.9: Normalised read counts of top 9 expressed genes in *Antigen processing and presentation* KEGG term.** Graphs show normalised number of reads across sorted cell types following treatment with PBS (vehicle) or IFN-β, with top 9 genes identified through having the greatest mean number of normalised read counts across all sorted cell types and treatment regimens. A) *B2m*, B) *H2-k1*, C) *Hspa8*, D) *H2-t23*, E) *H2-q7*, F) *H2-m3*, G) *H2-q6*, H) *H2-dma*, I) *Psme2b*. Bars represent mean ± SD. n=4.

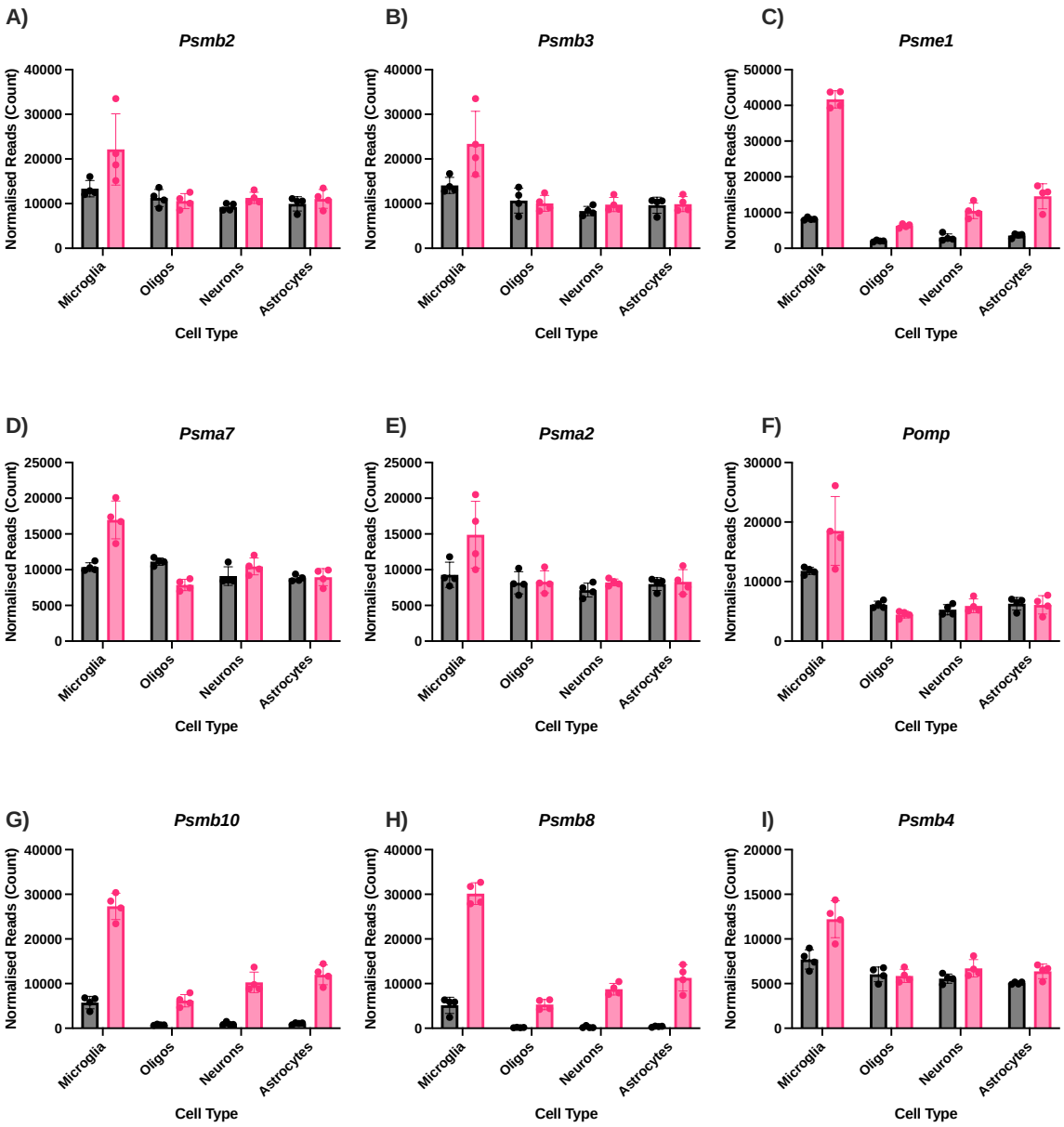


**Figure 8.10: Normalised read counts of top 9 expressed genes in *Cell function and metabolism* KEGG term.** Graphs show normalised number of reads across sorted cell types following treatment with PBS (vehicle) or IFN-β, with top 9 genes identified through having the greatest mean number of normalised read counts across all sorted cell types and treatment regimens. A) *PSmb2*, B) *Psmb3*, C) *Psme1*, D) *Psma7*, E) *Psma2*, F) *Pomp*, G) *Psmb10*, H) *Psmb8* I) *Psmb4*. Bars represent mean ± SD. n=4.

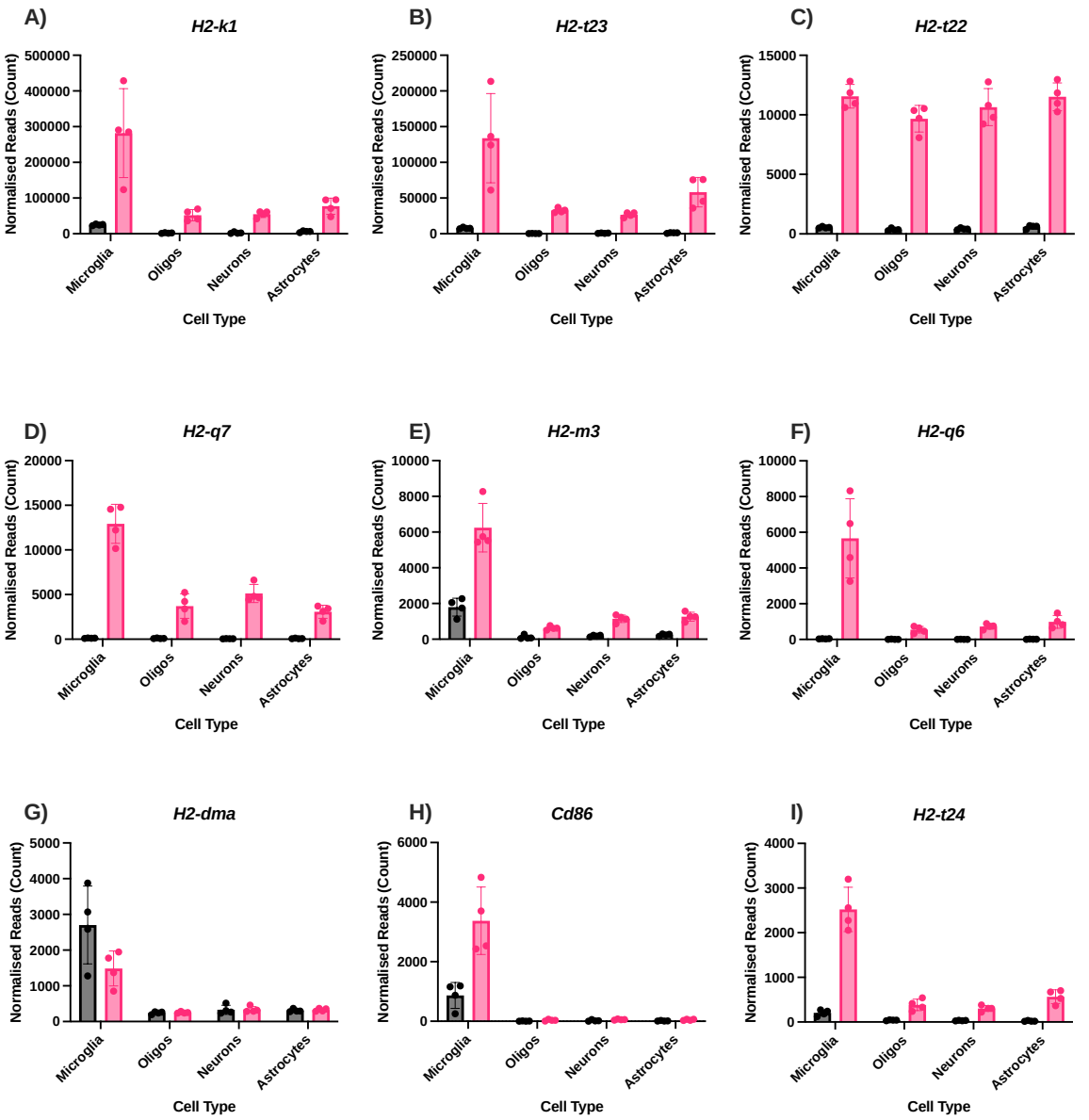


**Figure 8.11: Normalised read counts of top 9 expressed genes in *Transplant rejection* KEGG term.** Graphs show normalised number of reads across sorted cell types following treatment with PBS (vehicle) or IFN-β, with top 9 genes identified through having the greatest mean number of normalised read counts across all sorted cell types and treatment regimens. A) *H2-k1*, B) *H2-t23*, C) *H2-t22*, D) *H2-q7*, E) *H2-m3*, F) *H2-q6*, G) *H2-dma*, H) *Cd86*, I) *H2-t24*. Bars represent mean ± SD. n=4.

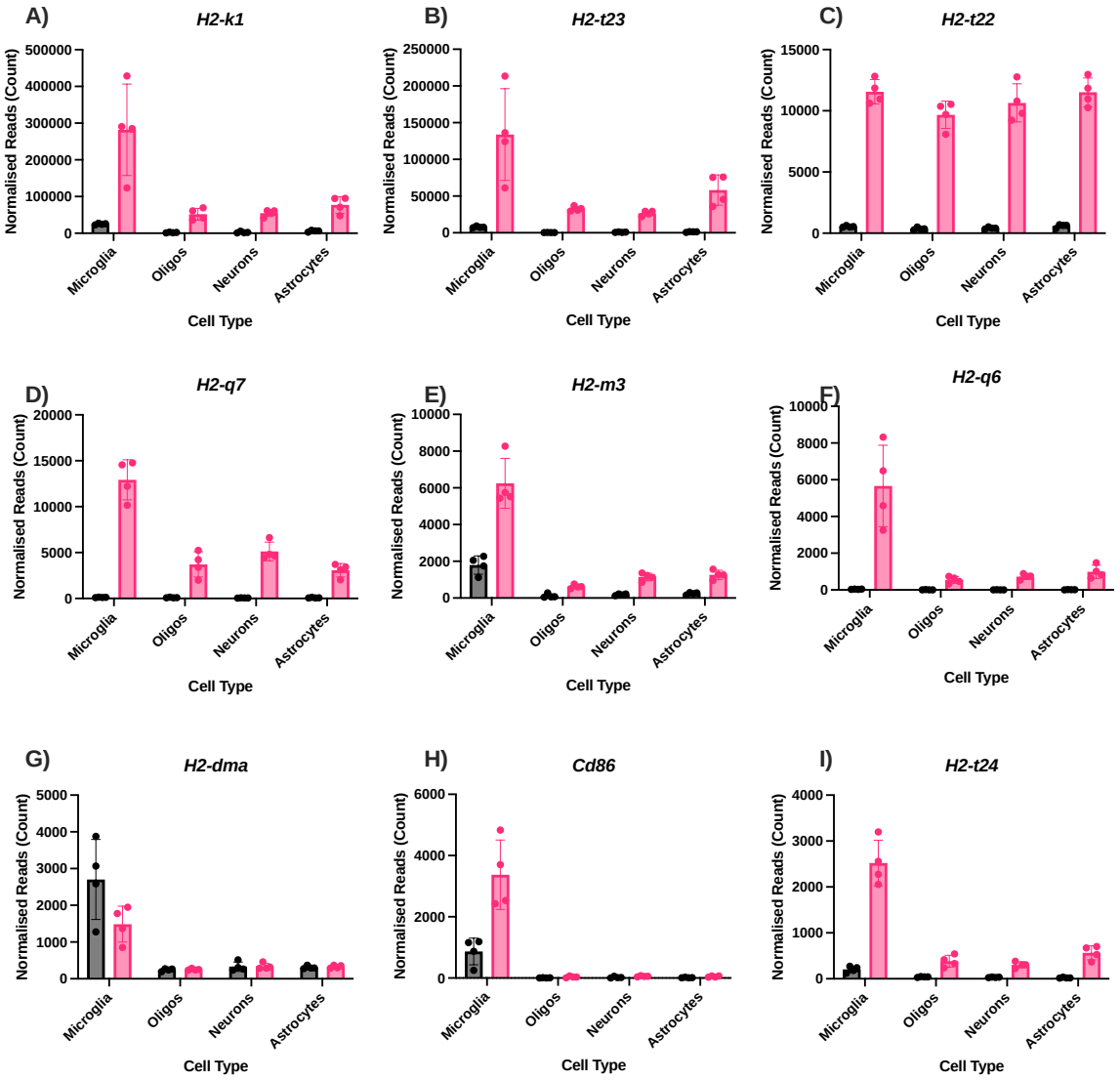


**Figure 8.12: Normalised read counts of top 9 expressed genes in *Autoimmune disease* KEGG term.** Graphs show normalised number of reads across sorted cell types following treatment with PBS (vehicle) or IFN-β, with top 9 genes identified through having the greatest mean number of normalised read counts across all sorted cell types and treatment regimens. A) *H2-k1*, B) *H2-t23*, C) *H2-t22*, D) *H2-q7*, E) *H2-m3*, F) *H2-q6*, G) *H2-dma*, H) *CD86*, I) *H2-t24*. Bars represent mean ± SD. n=4.

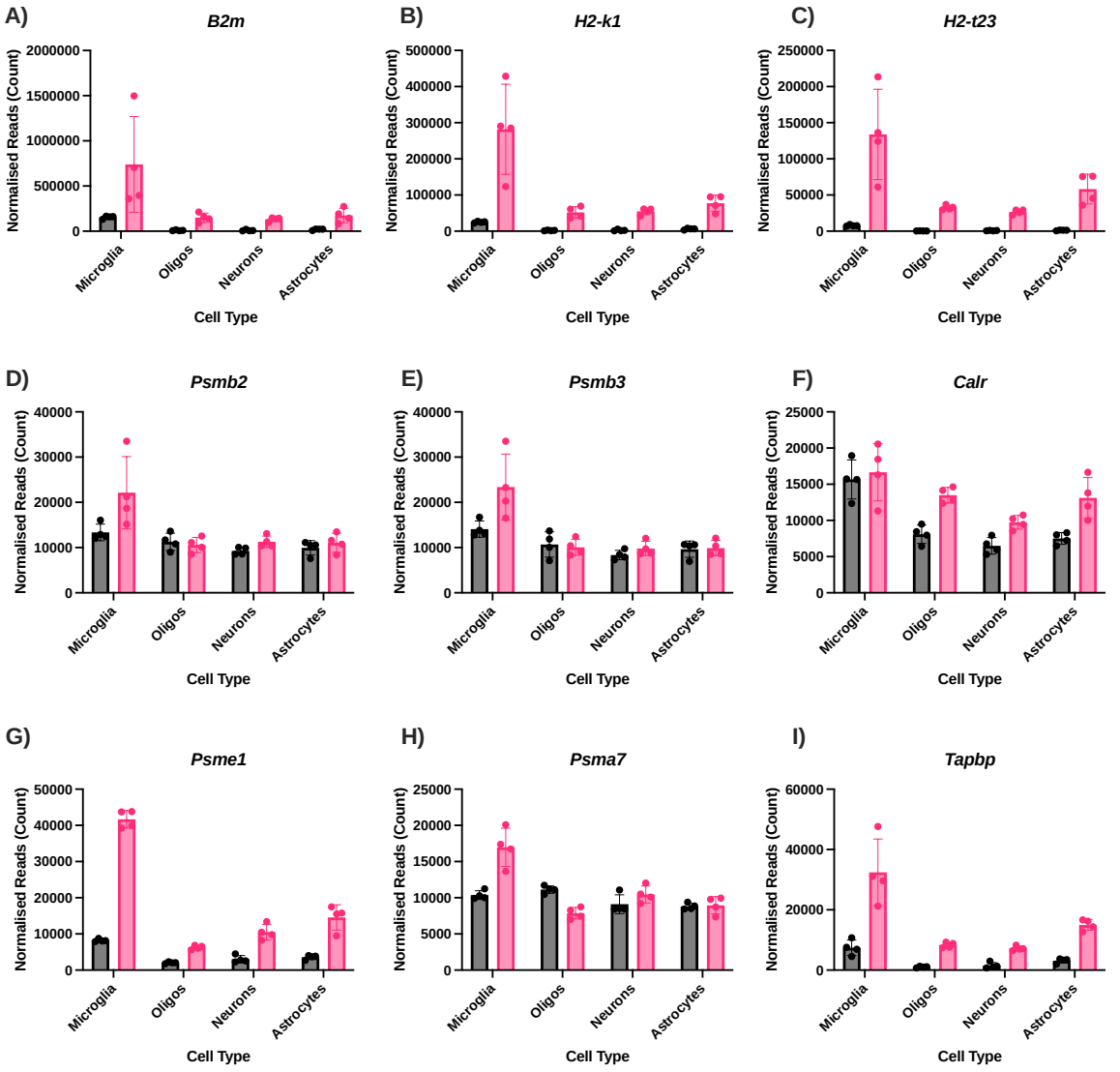


**Figure 8.13: Normalised read counts of top 9 expressed genes in *Antigen processing / presentation* Reactome term.** Graphs show normalised number of reads across sorted cell types following treatment with PBS (vehicle) or IFN-β, with top 9 genes identified through having the greatest mean number of normalised read counts across all sorted cell types and treatment regimens. A) *B2m*, B) *H2-k1*, C) *H2-t23*, D) *Psmb2*, E) *Psmb3*, F) *Calr*, G) *Psme1*, H) *Psme7*, I) *Tapbp*. Bars represent mean ± SD. n=4.

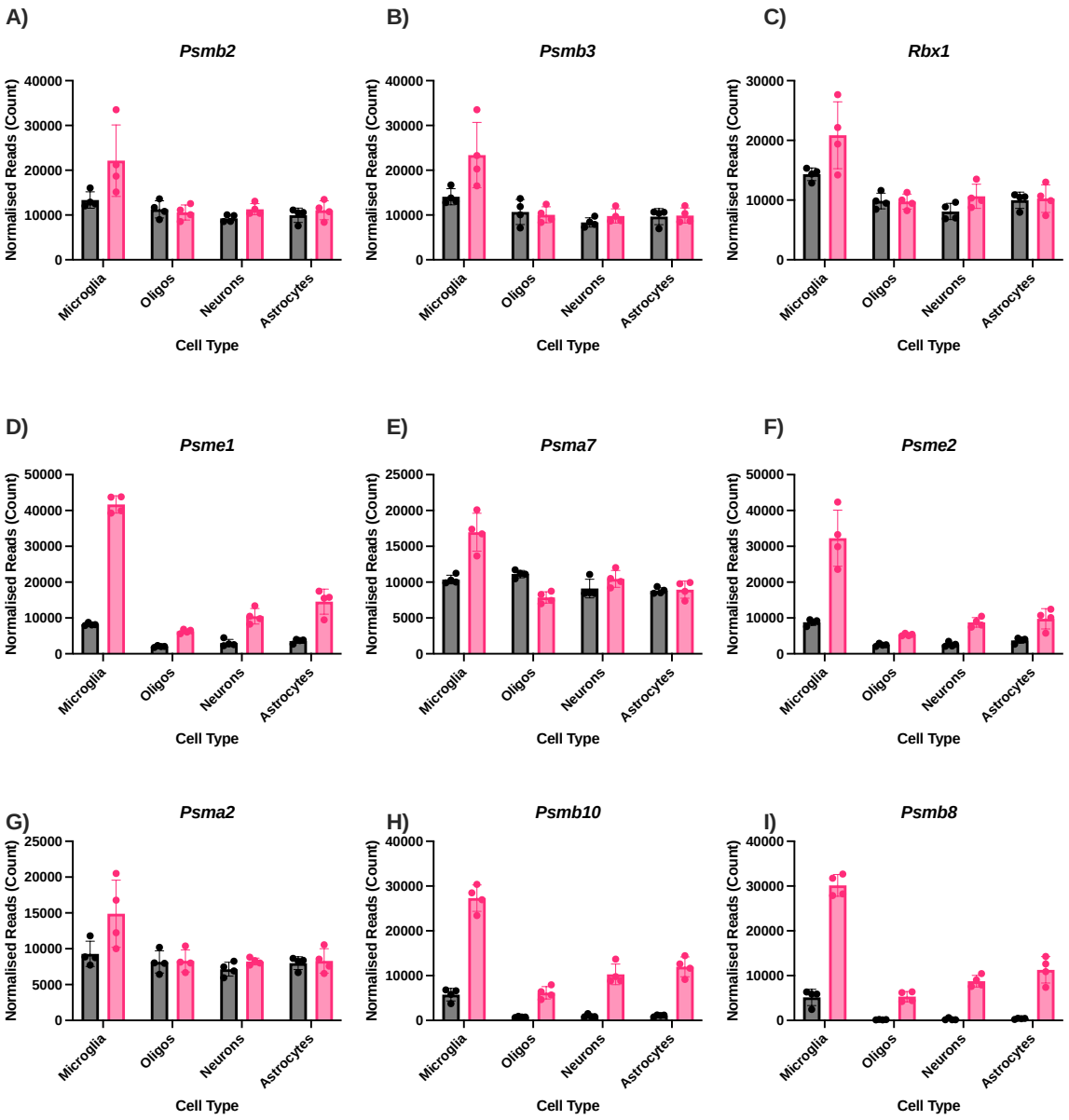


**Figure 8.14: Normalised read counts of top 9 expressed genes in *Response to oxidative stress* Reactome term.** Graphs show normalised number of reads across sorted cell types following treatment with PBS (vehicle) or IFN-β, with top 9 genes identified through having the greatest mean number of normalised read counts across all sorted cell types and treatment regimens. A) *Psmb2*, B) *Psmb3*, C) *Rbx1*, D) *Psme1*, E) *Psma7*, F) *Psme2*, G) *Psma2*, H) *Psmb10*, I) *Psmb8*. Bars represent mean ± SD. n=4.

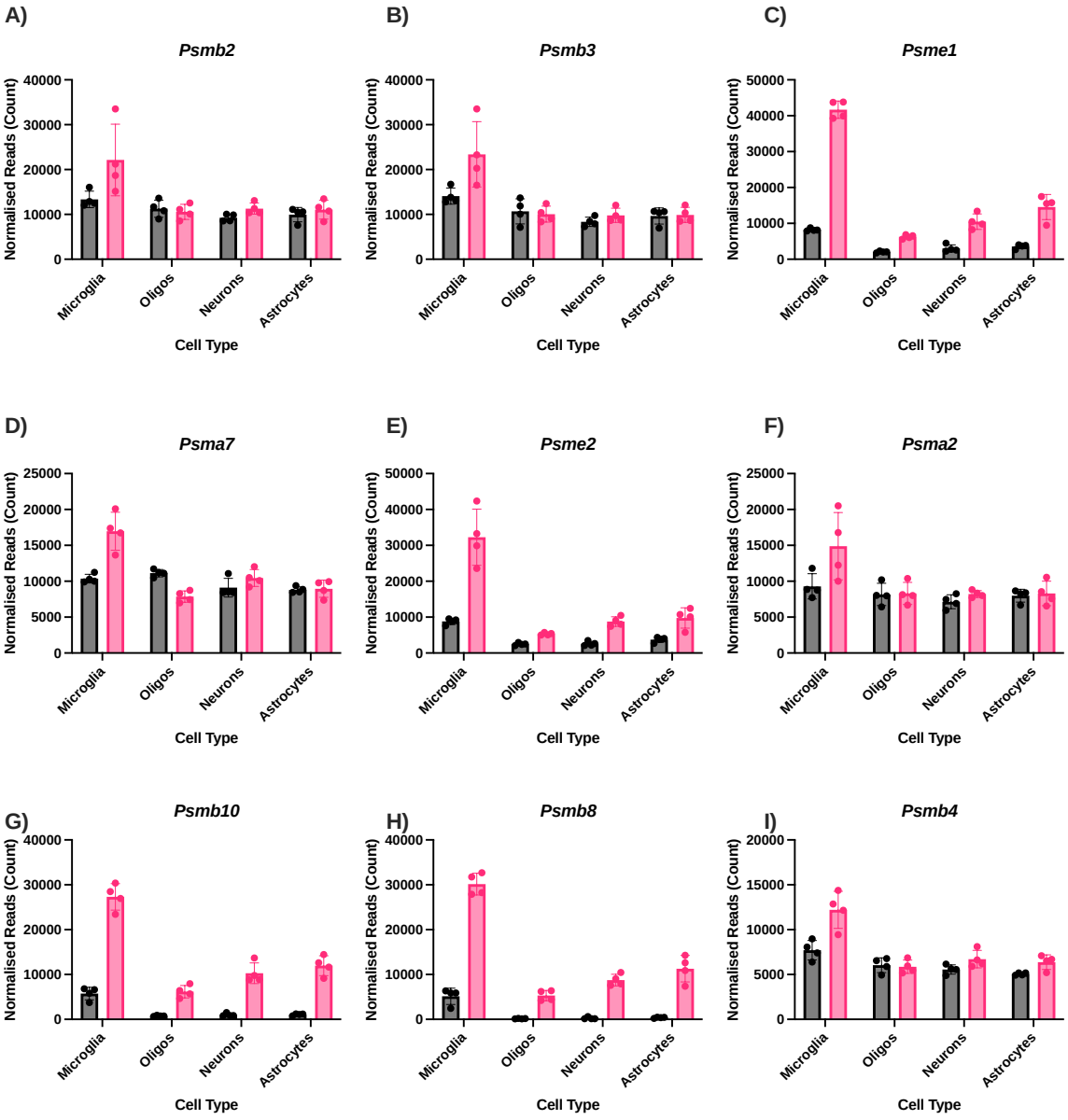


**Figure 8.15: Normalised read counts of top 9 expressed genes in *Control of cell cycle* Reactome term.** Graphs show normalised number of reads across sorted cell types following treatment with PBS (vehicle) or IFN-β, with top 9 genes identified through having the greatest mean number of normalised read counts across all sorted cell types and treatment regimens. A) *Psmb2*, B) *Psmb3*, C) *Psme1*, D) *Psma7*, E) *Psme2*, F) *Psma2*, G) *Psmb10*, H) *Psmb8*, I) *Psmb4*. Bars represent mean ± SD. N=4.

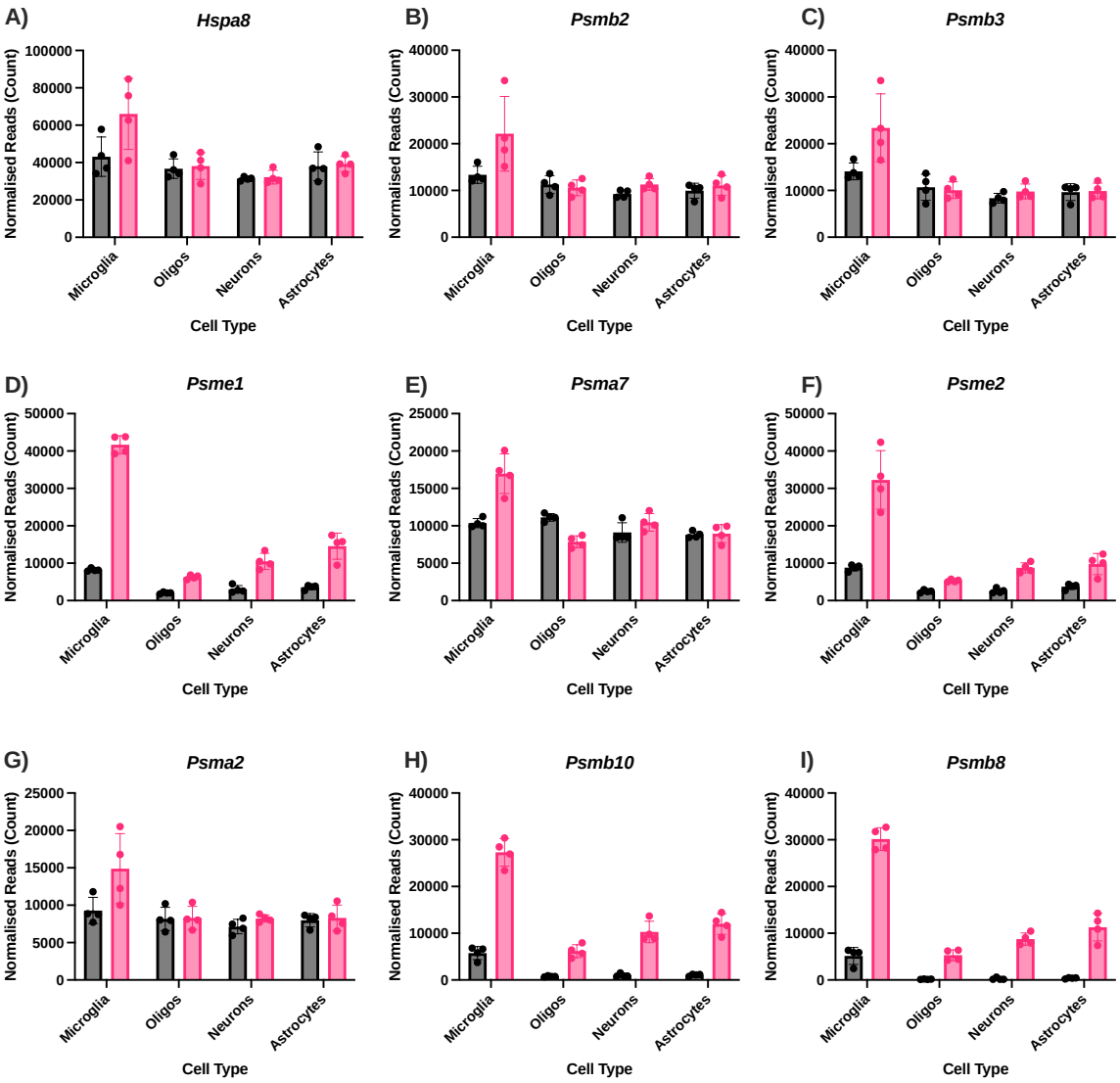


**Figure 8.16: Normalised read counts of top 9 expressed genes in *RNA degradation* Reactome term.** Graphs show normalised number of reads across sorted cell types following treatment with PBS (vehicle) or IFN-β, with top 9 genes identified through having the greatest mean number of normalised read counts across all sorted cell types and treatment regimens. A) *Hspa8*, B) *Psmb2*, C) *Psmb3*, D) *Psme1*, E) *Psma7*, F) *Psme2*, G) *Psma2*, H) *Psmb10*, I) *Psmb8*. Bars represent mean ± SD. n=4.

## 8.3 List of genes and annotation terms associated with each cluster identified in functional annotation cluster analysis

**Table 8.1 Functional annotation cluster analysis, cluster 1, innate immunity**

| **Annotation Cluster 1** | **Enrichment Score: 27.56** | | |
|---|---|---|---|
| **Database** | **Term** | **Count** | ***p.adj* Value** |
| GOTERM_BP_DIRECT | Immune system processes | 149 | 1.39E-39 |
| UP_KW_BIOLOGICAL_ PROCESS | Innate immunty | 112 | 1.63E-30 |
| UP_KW_BIOLOGICAL_ PROCESS | Immunity | 158 | 1.18E-27 |
| GOTERM_BP_DIRECT | Innate immune response | 126 | 2.10E-15 |

| **Gene Symbol** | **Gene Name** |
|---|---|
| *Acod1* | Aconitate Decarboxylase 1 |
| *Adar* | Adenosine Deaminase, RNA-Specific |
| *Apobec3* | Apolipoprotein B MRNA Editing Enzyme, Catalytic Polypeptide 3 |
| *Arid5a* | At Rich Interactive Domain 5A (Mrf1-Like) |
| *Axl* | Axl Receptor Tyrosine Kinase |
| *B2m* | Beta-2 Microglobulin |
| *Bst2* | Bone Marrow Stromal Cell Antigen 2 |
| *C1ra* | Complement Component 1, R Subcomponent A |
| *C2* | Complement Component 2 (Within H-2S) |
| *Cadm1* | Cell Adhesion Molecule 1 |
| *Casp4* | Caspase 4, Apoptosis-Related Cysteine Peptidase |
| *CD14* | CD14 Antigen |
| *CD180* | CD180 Antigen |
| *CD1d1* | CD1D1 Antigen |
| *CD274* | CD274 Antigen |
| *CD300e* | CD300E Molecule |
| *CD300lf* | CD300 Molecule Like Family Member F |
| *CD40* | CD40 Antigen |
| *CD5l* | CD5 Antigen-Like |
| *CD74* | CD74 Antigen (Invariant Polypeptide Of Major Histocompatibility Complex, Class Ii Antigen-Associated) |
| *CD86* | CD86 Antigen |
| *Cfb* | Complement Factor B |
| *Cfh* | Complement Component Factor H |
| *Clec4a2* | C-Type Lectin Domain Family 4, Member A2 |
| *Clec4e* | C-Type Lectin Domain Family 4, Member E |
| *Clec4n* | C-Type Lectin Domain Family 4, Member N |
| *Crcp* | Calcitonin Gene-Related Peptide-Receptor Component Protein |
| | ***Continued overleaf*** |

| | |
|---|---|
| *Csf1* | Colony Stimulating Factor 1 (Macrophage) |
| *Csk* | C-Src Tyrosine Kinase |
| *Cybc1* | Cytochrome B 245 Chaperone 1 |
| *Dbnl* | Drebrin-Like |
| *Dclre1c* | Dna Cross-Link Repair 1C |
| *Ddx3x* | Dead Box Helicase 3, X-Linked |
| *Dhx58* | Dexh (Asp-Glu-X-His) Box Polypeptide 58 |
| *Dtx3l* | Deltex 3-Like, E3 Ubiquitin Ligase |
| *Eif2ak2* | Eukaryotic Translation Initiation Factor 2-Alpha Kinase 2 |
| *Erap1* | Endoplasmic Reticulum Aminopeptidase 1 |
| *Fcgr1* | Fc Receptor, Igg, High Affinity I |
| *Fcgr4* | Fc Receptor, Igg, Low Affinity Iv |
| *G3bp2* | Gtpase Activating Protein (Sh3 Domain) Binding Protein 2 |
| *Gbp2* | Guanylate Binding Protein 2 |
| *Gbp5* | Guanylate Binding Protein 5 |
| *Gbp6* | Guanylate Binding Protein 6 |
| *Gbp7* | Guanylate Binding Protein 7 |
| *Gpr183* | G Protein-Coupled Receptor 183 |
| *Gsdmd* | Gasdermin D |
| *H2-aa* | Histocompatibility 2, Class Ii Antigen A, Alpha |
| *H2-ab1* | Histocompatibility 2, Class Ii Antigen A, Beta 1 |
| *H2-d1* | Histocompatibility 2, D Region Locus 1 |
| *H2-dma* | Histocompatibility 2, Class Ii, Locus Dma |
| *H2-eb1* | Histocompatibility 2, Class Ii Antigen E Beta |
| *H2-k1* | Histocompatibility 2, K1, K Region |
| *H2-q10* | Histocompatibility 2, Q Region Locus 10 |
| *H2-q7* | Histocompatibility 2, Q Region Locus 7 |
| *H2-t23* | Histocompatibility 2, T Region Locus 23 |
| *Hck* | Hemopoietic Cell Kinase |
| *Herc6* | Hect Domain And Rld 6 |
| *Hmgb3* | High Mobility Group Box 3 |
| *Icosl* | Icos Ligand |
| *Ifi204* | Interferon Activated Gene 204 |
| *Ifi35* | Interferon-Induced Protein 35 |
| *Ifih1* | Interferon Induced With Helicase C Domain 1 |
| *Ifit1* | Interferon-Induced Protein With Tetratricopeptide Repeats 1 |
| *Ifit2* | Interferon-Induced Protein With Tetratricopeptide Repeats 2 |
| *Ifit3* | Interferon-Induced Protein With Tetratricopeptide Repeats 3 |
| *Ifitm3* | Interferon Induced Transmembrane Protein 3 |
| *Iigp1* | Interferon Inducible Gtpase 1 |
| *Il1rl2* | Interleukin 1 Receptor-Like 2 |
| *Il2ra* | Interleukin 2 Receptor, Alpha Chain |

***Continued overleaf***

| | |
|---|---|
| *Ilrun* | Inflammation And Lipid Regulator With Uba-Like And Nbr1-Like Domains |
| *Irf1* | Interferon Regulatory Factor 1 |
| *Irf2* | Interferon Regulatory Factor 2 |
| *Irf7* | Interferon Regulatory Factor 7 |
| *Irf9* | Interferon Regulatory Factor 9 |
| *Irgm1* | Immunity-Related Gtpase Family M Member 1 |
| *Isg20* | Interferon-Stimulated Protein |
| *Jak2* | Janus Kinase 2 |
| *Klrk1* | Killer Cell Lectin-Like Receptor Subfamily K, Member 1 |
| *Lacc1* | Laccase Domain Containing 1 |
| *Lgals9* | Lectin, Galactose Binding, Soluble 9 |
| *Lst1* | Leukocyte Specific Transcript 1 |
| *Lyn* | Lyn Proto-Oncogene, Src Family Tyrosine Kinase |
| *Masp1* | Mannan-Binding Lectin Serine Peptidase 1 |
| *Mif* | Macrophage Migration Inhibitory Factor (Glycosylation-Inhibiting Factor) |
| *Morc3* | Microrchidia 3 |
| *Mpeg1* | Macrophage Expressed Gene 1 |
| *Myd88* | Myeloid Differentiation Primary Response Gene 88 |
| *Myo1G* | Myosin Ig |
| *N4bp1* | Nedd4 Binding Protein 1 |
| *Naip6* | Nlr Family, Apoptosis Inhibitory Protein 6 |
| *Nlrc5* | Nlr Family, Card Domain Containing 5 |
| *Nmi* | N-Myc (And Stat) Interactor |
| *Nod1* | Nucleotide-Binding Oligomerization Domain Containing 1 |
| *Nod2* | Nucleotide-Binding Oligomerization Domain Containing 2 |
| *Nono* | Non-Pou-Domain-Containing, Octamer Binding Protein |
| *Oas2* | 2'-5' Oligoadenylate Synthetase 2 |
| *Oas3* | 2'-5' Oligoadenylate Synthetase 3 |
| *Oasl1* | 2'-5' Oligoadenylate Synthetase-Like 1 |
| *Oasl2* | 2'-5' Oligoadenylate Synthetase-Like 2 |
| *Parp14* | Poly (Adp-Ribose) Polymerase Family, Member 14 |
| *Parp9* | Poly (Adp-Ribose) Polymerase Family, Member 9 |
| *Pirb* | Paired Ig-Like Receptor B |
| *Pld3* | Phospholipase D Family, Member 3 |
| *Pml* | Promyelocytic Leukemia |
| *Polr3b* | Polymerase (RNA) Iii (Dna Directed) Polypeptide B |
| *Polr3c* | Polymerase (RNA) Iii (Dna Directed) Polypeptide C |
| *Psmb10* | Proteasome (Prosome, Macropain) Subunit, Beta Type 10 |
| *Psmb8* | Proteasome (Prosome, Macropain) Subunit, Beta Type 8 (Large Multifunctional Peptidase 7) |
| *Psmb9* | Proteasome (Prosome, Macropain) Subunit, Beta Type 9 (Large Multifunctional Peptidase 2) |
| | ***Continued overleaf*** |

| | |
|---|---|
| *Rigi* | RNA Sensor Rig-I |
| *Rnf135* | Ring Finger Protein 135 |
| *Rnf19B* | Ring Finger Protein 19B |
| *Rnf213* | Ring Finger Protein 213 |
| *Rsad2* | Radical S-Adenosyl Methionine Domain Containing 2 |
| *Samhd1* | Sam Domain And Hd Domain, 1 |
| *Serinc5* | Serine Incorporator 5 |
| *Serpina3g* | Serine (Or Cysteine) Peptidase Inhibitor, Clade A, Member 3G |
| *Sirpb1a* | Signal-Regulatory Protein Beta 1A |
| *Sirpb1b* | Signal-Regulatory Protein Beta 1B |
| *Sirpb1c* | Signal-Regulatory Protein Beta 1C |
| *Slamf7* | Slam Family Member 7 |
| *Slc15a3* | Solute Carrier Family 15, Member 3 |
| *Slfn1* | Schlafen 1 |
| *Slfn2* | Schlafen 2 |
| *Slfn8* | Schlafen 8 |
| *Sp110* | Sp110 Nuclear Body Protein |
| *Spon2* | Spondin 2, Extracellular Matrix Protein |
| *Tap1* | Transporter 1, ATP-Binding Cassette, Sub-Family B (Mdr/Tap) |
| *Tap2* | Transporter 2, ATP-Binding Cassette, Sub-Family B (Mdr/Tap) |
| *Tapbpl* | Tap Binding Protein-Like |
| *Tasl* | Tlr Adaptor Interacting With Endolysosomal Slc15A4 |
| *Themis2* | Thymocyte Selection Associated Family Member 2 |
| *Ticam1* | Tir Domain Containing Adaptor Molecule 1 |
| *Tlr11* | Toll-Like Receptor 11 |
| *Tlr2* | Toll-Like Receptor 2 |
| *Tlr3* | Toll-Like Receptor 3 |
| *Tlr9* | Toll-Like Receptor 9 |
| *Tmem106a* | Transmembrane Protein 106A |
| *Traf3* | Tnf Receptor-Associated Factor 3 |
| *Trim14* | Tripartite Motif-Containing 14 |
| *Trim25* | Tripartite Motif-Containing 25 |
| *Trim26* | Tripartite Motif-Containing 26 |
| *Trim29* | Tripartite Motif-Containing 29 |
| *Trim56* | Tripartite Motif-Containing 56 |
| *Trpm4* | Transient Receptor Potential Cation Channel, Subfamily M, Member 4 |
| *Ythdf1* | Yth N6-Methyladenosine RNA Binding Protein 1 |
| *Zbp1* | Z-Dna Binding Protein 1 |
| *Zc3hav1* | Zinc Finger Ccch Type, Antiviral 1 |
| *Znfx1* | Zinc Finger, Nfx1-Type Containing 1 |

**Table 8.1: Functional annotation cluster analysis, cluster 1, innate immunity.** Table showing genes and annotation terms in cluster 1. “Database” indicates where the annotation term was derived, “Count” is the number of genes associated with the annotation term and *p.adj*-value is the Bonferroni adjusted *p*-value.

**Table 8.2 Functional annotation cluster analysis, cluster 2, response to virus**

| **Annotation Cluster 2** | **Enrichment Score: 16.77** | | |
|---|---|---|---|
| **Database** | **Term** | **Count** | ***p.adj* Value** |
| GOTERM_BP_DIRECT | Response to virus | 41 | 1.81E-18 |
| UP_KW_BIOLOGICAL_PROCESS | Antiviral defense | 42 | 1.88E-17 |
| GOTERM_BP_DIRECT | Negative regulation of viral genome | 28 | 1.44E-16 |

| **Gene Symbol** | **Gene Name** |
|---|---|
| *Adar* | Adenosine Deaminase, RNA-Specific |
| *Apobec3* | Apolipoprotein B MRNA Editing Enzyme, Catalytic Polypeptide 3 |
| *Crcp* | Calcitonin Gene-Related Peptide-Receptor Component Protein |
| *Ddit4* | Dna-Damage-Inducible Transcript 4 |
| *Dhx58* | Dexh (Asp-Glu-X-His) Box Polypeptide 58 |
| *Dtx3l* | Deltex 3-Like, E3 Ubiquitin Ligase |
| *Eif2ak2* | Eukaryotic Translation Initiation Factor 2-Alpha Kinase 2 |
| *Gbp7* | Guanylate Binding Protein 7 |
| *Ifih1* | Interferon Induced With Helicase C Domain 1 |
| *Ifitm3* | Interferon Induced Transmembrane Protein 3 |
| *Ifit1* | Interferon-Induced Protein With Tetratricopeptide Repeats 1 |
| *Ifit2* | Interferon-Induced Protein With Tetratricopeptide Repeats 2 |
| *Ifit3* | Interferon-Induced Protein With Tetratricopeptide Repeats 3 |
| *Irf1* | Interferon Regulatory Factor 1 |
| *Isg15* | Isg15 Ubiquitin-Like Modifier |
| *Isg20* | Interferon-Stimulated Protein |
| *Mx1* | Mx Dynamin-Like Gtpase 1 |
| *Mx2* | Mx Dynamin-Like Gtpase 2 |
| *Oas1a* | 2'-5' Oligoadenylate Synthetase 1A |
| *Oas1b* | 2'-5' Oligoadenylate Synthetase 1B |
| *Oas1g* | 2'-5' Oligoadenylate Synthetase 1G |
| *Oas2* | 2'-5' Oligoadenylate Synthetase 2 |
| *Oas3* | 2'-5' Oligoadenylate Synthetase 3 |
| *Oasl1* | 2'-5' Oligoadenylate Synthetase-Like 1 |
| *Oasl2* | 2'-5' Oligoadenylate Synthetase-Like 2 |
| *Parp9* | Poly (Adp-Ribose) Polymerase Family, Member 9 |
| *Pml* | Promyelocytic Leukemia |
| *Polr3b* | Polymerase (RNA) Iii (Dna Directed) Polypeptide B |
| *Polr3c* | Polymerase (RNA) Iii (Dna Directed) Polypeptide C |
| | ***Continued overleaf*** |

| | |
|---|---|
| *Rigi* | RNA Sensor Rig-I |
| *Rsad2* | Radical S-Adenosyl Methionine Domain Containing 2 |
| *Samhd1* | Sam Domain And Hd Domain, 1 |
| *Serinc5* | Serine Incorporator 5 |
| *Shfl* | Shiftless Antiviral Inhibitor Of Ribosomal Frameshifting |
| *Ticam1* | Tir Domain Containing Adaptor Molecule 1 |
| *Trim25* | Tripartite Motif-Containing 25 |
| *Trim34a* | Tripartite Motif-Containing 34A |
| *Trim34b* | Tripartite Motif-Containing 34B |
| *Trim56* | Tripartite Motif-Containing 56 |
| *Zbp1* | Z-Dna Binding Protein 1 |
| *Zc3hav1* | Zinc Finger Ccch Type, Antiviral 1 |
| *Znfx1* | Zinc Finger, Nfx1-Type Containing 1 |

**Table 8.2: Functional annotation cluster analysis, cluster 2, response to virus.** Table showing genes and annotation terms in cluster 2. “Database” indicates where the annotation term was derived, “Count” is the number of genes associated with the annotation term and *p.adj*-value is the Bonferroni adjusted *p*-value.

**Table 8.3 Functional annotation cluster analysis, cluster 3, lysosome**

| **Annotation Cluster 3** | **Enrichment Score: 9.48** | | |
|---|---|---|---|
| **Database** | **Term** | **Count** | ***p.adj* Value** |
| GOTERM_CC_DIRECT | Lysosomal membrane | 65 | 1.20E-13 |
| GOTERM_CC_DIRECT | Lysosome | 77 | 1.49E-08 |
| UP_KW_CELLULAR_ COMPONENT | Lysosome | 67 | 1.94E-08 |

| **Gene Symbol** | **Gene Name** |
|---|---|
| *Abhd6* | Abhydrolase Domain Containing 6 |
| *Ace* | Angiotensin I Converting Enzyme (Peptidyl-Dipeptidase A) 1 |
| *Acp2* | Acid Phosphatase 2, Lysosomal |
| *Arsb* | Arylsulfatase B |
| *ATP10b* | ATPase, Class V, Type 10B |
| *Bbc3* | Bcl2 Binding Component 3 |
| *Bloc1s2* | Biogenesis Of Lysosomal Organelles Complex-1, Subunit 2 |
| *Calr* | Calreticulin |
| *Cat* | Catalase |
| *CD164* | CD164 Antigen |
| *CD1d1* | CD1D1 Antigen |
| *CD74* | CD74 Antigen (Invariant Polypeptide Of Major Histocompatibility Complex, Class Ii Antigen-Associated) |
| *Clcn3* | Chloride Channel, Voltage-Sensitive 3 |
| *Clcn4* | Chloride Channel, Voltage-Sensitive 4 |
| *Creg1* | Cellular Repressor Of E1A-Stimulated Genes 1 |
| *Cst7* | Cystatin F (Leukocystatin) |
| *Ctsd* | Cathepsin D |
| *Ctsf* | Cathepsin F |
| *Dtx3l* | Deltex 3-Like, E3 Ubiquitin Ligase |
| *Flcn* | Folliculin |
| *Fyco1* | Fyve And Coiled-Coil Domain Containing 1 |
| *Galc* | Galactosylceramidase |
| *Ggh* | Gamma-Glutamyl Hydrolase |
| *Glb1* | Galactosidase, Beta 1 |
| *Gpc3* | Glypican 3 |
| *Grn* | Granulin |
| *H2-aa* | Histocompatibility 2, Class Ii Antigen A, Alpha |
| *H2-dma* | Histocompatibility 2, Class Ii, Locus Dma |
| *H2-ob* | Histocompatibility 2, O Region Beta Locus |
| *Hap1* | Huntingtin-Associated Protein 1 |
| *Hck* | Hemopoietic Cell Kinase |
| *Hexa* | Hexosaminidase A |
| | ***Continued overleaf*** |

| | |
|---|---|
| *Hgsnat* | Heparan-Alpha-Glucosaminide N-Acetyltransferase |
| *Hpse* | Heparanase |
| *Hspa8* | Heat Shock Protein 8 |
| *Ifitm3* | Interferon Induced Transmembrane Protein 3 |
| *Ifnar1* | Interferon (Alpha And Beta) Receptor 1 |
| *Irgm1* | Immunity-Related Gtpase Family M Member 1 |
| *Klc2* | Kinesin Light Chain 2 |
| *Lipa* | Lysosomal Acid Lipase A |
| *M6pr* | Mannose-6-Phosphate Receptor, Cation Dependent |
| *Mfsd12* | Major Facilitator Superfamily Domain Containing 12 |
| *Mmp13* | Matrix Metallopeptidase 13 |
| *Napsa* | Napsin A Aspartic Peptidase |
| *Npc2* | Npc Intracellular Cholesterol Transporter 2 |
| *Pcyox1* | Prenylcysteine Oxidase 1 |
| *Pgap6* | Post-Glycosylphosphatidylinositol Attachment To Proteins 6 |
| *Pip4p2* | Phosphatidylinositol-4,5-Bisphosphate 4-Phosphatase 2 |
| *Pld3* | Phospholipase D Family, Member 3 |
| *RNAse6* | Ribonuclease, RNAse A Family, 6 |
| *Rptor* | Regulatory Associated Protein Of Mtor, Complex 1 |
| *Rragd* | Ras-Related Gtp Binding D |
| *Scarb2* | Scavenger Receptor Class B, Member 2 |
| *Sidt2* | Sid1 Transmembrane Family, Member 2 |
| *Slc15a3* | Solute Carrier Family 15, Member 3 |
| *Slc17a5* | Solute Carrier Family 17 (Anion/Sugar Transporter), Member 5 |
| *Slc26a11* | Solute Carrier Family 26, Member 11 |
| *Slc29a3* | Solute Carrier Family 29 (Nucleoside Transporters), Member 3 |
| *Slc2a6* | Solute Carrier Family 2 (Facilitated Glucose Transporter), Member 6 |
| *Slc36a4* | Solute Carrier Family 36 (Proton/Amino Acid Symporter), Member 4 |
| *Slc39a14* | Solute Carrier Family 39 (Zinc Transporter), Member 14 |
| *Slc39a8* | Solute Carrier Family 39 (Metal Ion Transporter), Member 8 |
| *Slc49a4* | Solute Carrier Family 49 Member 4 |
| *Slc7a5* | Solute Carrier Family 7 (Cationic Amino Acid Transporter, Y+ System), Member 5 |
| *Snx14* | Sorting Nexin 14 |
| *Snx2* | Sorting Nexin 2 |
| *Sort1* | Sortilin 1 |
| *Sphk2* | Sphingosine Kinase 2 |
| *Sppl2a* | Signal Peptide Peptidase Like 2A |
| *Tasl* | Tlr Adaptor Interacting With Endolysosomal Slc15A4 |
| *Tcirg1* | T Cell, Immune Regulator 1, ATPase, H+ Transporting Lysosomal V0 Protein A3 |
| *Tlr9* | Toll-Like Receptor 9 |
| *Tmem106b* | Transmembrane Protein 106B |
| | ***Continued overleaf*** |

| | |
|---|---|
| *Tpcn1* | Two Pore Channel 1 |
| *Trim29* | Tripartite Motif-Containing 29 |
| *Trpm2* | Transient Receptor Potential Cation Channel, Subfamily M, Member 2 |
| *Vps13c* | Vacuolar Protein Sorting 13C |

**Table 8.3: Functional annotation cluster analysis, cluster 3, lysosome.** Table showing genes and annotation terms in cluster 3. “Database” indicates where the annotation term was derived, “Count” is the number of genes associated with the annotation term and *p.adj*-value is the Bonferroni adjusted *p*-value.

**Table 8.4 Functional annotation cluster analysis, cluster 4, Interferon inducible GTPase**

| **Annotation Cluster 4** | **Enrichment Score: 8.73** | | |
|---|---|---|---|
| **Database** | **Term** | **Count** | ***p.adj* Value** |
| UP_SEQ_FEATURE | DOMAIN:IRG-type G | 15 | 3.16E-12 |
| INTERPRO | IPR007743:Interferon-inducible GTPase | 13 | 1.22E-10 |
| GOTERM_BP_DIRECT | GO:0006952~defense response | 28 | 1.58E-05 |

| **Gene Symbol** | **Gene Name** |
|---|---|
| *9930111j21rik1* | RIKEN cDNA 9930111J21 Gene 1 |
| *9930111j21rik2* | RIKEN cDNA 9930111J21 Gene 2 |
| *Acod1* | Aconitate Decarboxylase 1 |
| *CD74* | CD74 Antigen (Invariant Polypeptide Of Major Histocompatibility Complex, Class Ii Antigen-Associated) |
| *Cxcl10* | Chemokine (C-X-C Motif) Ligand 10 |
| *Cxcl13* | Chemokine (C-X-C Motif) Ligand 13 |
| *Cxcl9* | Chemokine (C-X-C Motif) Ligand 9 |
| *F830016b08rik* | RIKEN cDNA F830016B08 Gene |
| *Gm12185* | Predicted Gene 12185 |
| *Gm4841* | Predicted Gene 4841 |
| *Gm5431* | Predicted Gene 5431 |
| *Ifi47* | Interferon Gamma Inducible Protein 47 |
| *Igtp* | Interferon Gamma Induced Gtpase |
| *Iigp1* | Interferon Inducible Gtpase 1 |
| *Irgm1* | Immunity-Related Gtpase Family M Member 1 |
| *Irgm2* | Immunity-Related Gtpase Family M Member 2 |
| *Nod1* | Nucleotide-Binding Oligomerization Domain Containing 1 |
| *Nod2* | Nucleotide-Binding Oligomerization Domain Containing 2 |
| *Pf4* | Platelet Factor 4 |
| *Stat1* | Signal Transducer And Activator Of Transcription 1 |
| *Stat2* | Signal Transducer And Activator Of Transcription 2 |
| *Stat5a* | Signal Transducer And Activator Of Transcription 5A |
| *Tap1* | Transporter 1, ATP-Binding Cassette, Sub-Family B (Mdr/Tap) |
| *Tapbp* | Tap Binding Protein |
| *Tgtp1* | T Cell Specific Gtpase 1 |
| *Tgtp2* | T Cell Specific Gtpase 1 |
| *Tlr2* | Toll-Like Receptor 2 |
| *Tlr3* | Toll-Like Receptor 3 |

**Table 8.4: Functional annotation cluster analysis, cluster 4, interferon inducible GTPase.** Table showing genes and annotation terms in cluster 4. “Database” indicates where the annotation term was derived, “Count” is the number of genes associated with the annotation term and *p.adj*-value is the Bonferroni adjusted *p*-value.

**Table 8.5 Functional annotation cluster analysis, cluster 5, nucleotide binding**

| **Annotation Cluster 5** | **Enrichment Score: 7.31** | | |
|---|---|---|---|
| **Database** | **Term** | **Count** | ***p.adj* Value** |
| INTERPRO | P-loop containing nucleoside triphosphate hydrolase | 139 | 3.04E-12 |
| GOTERM_MF_DIRECT | Nucleotide binding | 215 | 2.79E-09 |
| GOTERM_MF_DIRECT | ATP binding | 195 | 5.16E-09 |
| UP_KW_LIGAND | Nucleotide-binding | 230 | 2.39E-05 |

| **Gene Symbol** | **Gene Name** |
|---|---|
| *Abca14* | ATP-Binding Cassette, Sub-Family A (Abc1), Member 14 |
| *Abca17* | ATP-Binding Cassette, Sub-Family A (Abc1), Member 17 |
| *Abca6* | ATP-Binding Cassette, Sub-Family A (Abc1), Member 6 |
| *Abca9* | ATP-Binding Cassette, Sub-Family A (Abc1), Member 9 |
| *Abcb4* | ATP-Binding Cassette, Sub-Family B (Mdr/Tap), Member 4 |
| *Abcb8* | ATP-Binding Cassette, Sub-Family B (Mdr/Tap), Member 8 |
| *AbCD2* | ATP-Binding Cassette, Sub-Family D (Ald), Member 2 |
| *Abcf1* | ATP-Binding Cassette, Sub-Family F (Gcn20), Member 1 |
| *Abcg1* | ATP Binding Cassette Subfamily G Member 1 |
| *Acsl5* | Acyl-Coa Synthetase Long-Chain Family Member 5 |
| *Acss1* | Acyl-Coa Synthetase Short-Chain Family Member 1 |
| *Acss2* | Acyl-Coa Synthetase Short-Chain Family Member 2 |
| *Acta2* | Actin Alpha 2, Smooth Muscle, Aorta |
| *Actr2* | Arp2 Actin-Related Protein 2 |
| *Actr3* | Arp3 Actin-Related Protein 3 |
| *Acvrl1* | Activin A Receptor, Type Ii-Like 1 |
| *Adcy10* | Adenylate Cyclase 10 |
| *Adcy9* | Adenylate Cyclase 9 |
| *Adss* | Adenylosuccinate Synthetase, Non Muscle |
| *Ak4* | Adenylate Kinase 4 |
| *Ak5* | Adenylate Kinase 5 |
| *Akt3* | Thymoma Viral Proto-Oncogene 3 |
| *Aqr* | Aquarius |
| *Arf3* | Adp-Ribosylation Factor 3 |
| *Arf4* | Adp-Ribosylation Factor 4 |
| *Ascc3* | Activating Signal Cointegrator 1 Complex Subunit 3 |
| *Atl1* | Atlastin Gtpase 1 |
| *ATP10b* | ATPase, Class V, Type 10B |
| *ATP8a2* | ATPase, Aminophospholipid Transporter-Like, Class I, Type 8A, Member 2 |
| *Axl* | Axl Receptor Tyrosine Kinase |

***Continued overleaf***

| | |
|---|---|
| *Bmpr2* | Bone Morphogenetic Protein Receptor, Type Ii (Serine/Threonine Kinase) |
| *Bub1* | Bub1, Mitotic Checkpoint Serine/Threonine Kinase |
| *Cars* | Cysteinyl-TRNA Synthetase |
| *CDkl5* | Cyclin-Dependent Kinase-Like 5 |
| *Cit* | Citron |
| *Clcn3* | Chloride Channel, Voltage-Sensitive 3 |
| *Clcn4* | Chloride Channel, Voltage-Sensitive 4 |
| *Clp1* | Clp1, Cleavage And Polyadenylation Factor I Subunit |
| *Cmpk2* | Cytidine Monophosphate (Ump-Cmp) Kinase 2, Mitochondrial |
| *Cngb3* | Cyclic Nucleotide Gated Channel Beta 3 |
| *Coq8a* | Coenzyme Q8A |
| *Csk* | C-Src Tyrosine Kinase |
| *Ctps2* | Cytidine 5'-Triphosphate Synthase 2 |
| *Dck* | Deoxycytidine Kinase |
| *Ddx19b* | Dead Box Helicase 19B |
| *Ddx24* | Dead Box Helicase 24 |
| *Ddx28* | Dead Box Helicase 28 |
| *Ddx3x* | Dead Box Helicase 3, X-Linked |
| *Ddx4* | Dead Box Helicase 4 |
| *Ddx60* | Dexd/H Box Helicase 60 |
| *Dgke* | Diacylglycerol Kinase, Epsilon |
| *Dgkg* | Diacylglycerol Kinase, Gamma |
| *Dguok* | Deoxyguanosine Kinase |
| *Dhx32* | Deah (Asp-Glu-Ala-His) Box Polypeptide 32 |
| *Dhx58* | Dexh (Asp-Glu-X-His) Box Polypeptide 58 |
| *Dnah2* | Dynein, Axonemal, Heavy Chain 2 |
| *Dnah8* | Dynein, Axonemal, Heavy Chain 8 |
| *Dstyk* | Dual Serine/Threonine And Tyrosine Protein Kinase |
| *Dtymk* | Deoxythymidylate Kinase |
| *Dync1h1* | Dynein Cytoplasmic 1 Heavy Chain 1 |
| *Ehd1* | Eh-Domain Containing 1 |
| *Eif2ak2* | Eukaryotic Translation Initiation Factor 2-Alpha Kinase 2 |
| *Entpd5* | Ectonucleoside Triphosphate Diphosphohydrolase 5 |
| *Ep400* | E1A Binding Protein P400 |
| *Eral1* | Era (G-Protein)-Like 1 (E. Coli) |
| *Etnk1* | Ethanolamine Kinase 1 |
| *F13a1* | Coagulation Factor Xiii, A1 Subunit |
| *Fam20c* | Fam20C, Golgi Associated Secretory Pathway Kinase |
| *Fignl1* | Fidgetin-Like 1 |
| *Flad1* | Flavin Adenine Dinucleotide Synthetase 1 |
| *Flt4* | Fms-Like Tyrosine Kinase 4 |
| *Gbp2* | Guanylate Binding Protein 2 |
| | ***Continued overleaf*** |

| | |
|---|---|
| *Gbp3* | Guanylate Binding Protein 3 |
| *Gbp4* | Guanylate Binding Protein 3 |
| *Gbp5* | Guanylate Binding Protein 5 |
| *Gbp6* | Guanylate Binding Protein 6 |
| *Gbp7* | Guanylate Binding Protein 7 |
| *Gch1* | Gtp Cyclohydrolase 1 |
| *Gclc* | Glutamate-Cysteine Ligase, Catalytic Subunit |
| *Gm12250* | #N/A |
| *Gmppb* | Gdp-Mannose Pyrophosphorylase B |
| *Gspt2* | G1 To S Phase Transition 2 |
| *Gtpbp2* | Gtp Binding Protein 2 |
| *Gtpbp8* | Gtp-Binding Protein 8 (Putative) |
| *Guk1* | Guanylate Kinase 1 |
| *Gvin2* | Gtpase, Very Large Interferon Inducible, Family Member 2 |
| *Hck* | Hemopoietic Cell Kinase |
| *Helz2* | Helicase With Zinc Finger 2, Transcriptional Coactivator |
| *Hint3* | Histidine Triad Nucleotide Binding Protein 3 |
| *Hsp90ab1* | Heat Shock Protein 90 Alpha (Cytosolic), Class B Member 1 |
| *Hsp90b1* | Heat Shock Protein 90, Beta (Grp94), Member 1 |
| *Hspa1b* | Heat Shock Protein 1A |
| *Hspa1l* | Heat Shock Protein 1-Like |
| *Hspa8* | Heat Shock Protein 8 |
| *Hsph1* | Heat Shock 105Kda/110Kda Protein 1 |
| *Hyou1* | Hypoxia Up-Regulated 1 |
| *Idnk* | Idnk Gluconokinase Homolog (E. Coli) |
| *Ifih1* | Interferon Induced With Helicase C Domain 1 |
| *Igtp* | Interferon Gamma Induced Gtpase |
| *Iigp1* | Interferon Inducible Gtpase 1 |
| *Ikbke* | Inhibitor Of Kappab Kinase Epsilon |
| *Ino80* | Ino80 Complex Subunit |
| *Irgm1* | Immunity-Related Gtpase Family M Member 1 |
| *Irgm2* | Immunity-Related Gtpase Family M Member 2 |
| *Jak2* | Janus Kinase 2 |
| *Katna1* | Katanin P60 (ATPase-Containing) Subunit A1 |
| *Kdr* | Kinase Insert Domain Protein Receptor |
| *Kif14* | Kinesin Family Member 14 |
| *Kif18a* | Kinesin Family Member 18A |
| *Kif19a* | Kinesin Family Member 19A |
| *Kif22* | Kinesin Family Member 22 |
| *Kif23* | Kinesin Family Member 23 |
| *Kif3A* | Kinesin Family Member 3A |
| *Kifc2* | Kinesin Family Member C2 |
| *Lars2* | Leucyl-TRNA Synthetase, Mitochondrial |
| | ***Continued overleaf*** |

| | |
|---|---|
| *Lck* | Lymphocyte Protein Tyrosine Kinase |
| *Lyn* | Lyn Proto-Oncogene, Src Family Tyrosine Kinase |
| *Magi1* | Membrane Associated Guanylate Kinase, Ww And Pdz Domain Containing 1 |
| *Magi3* | Membrane Associated Guanylate Kinase, Ww And Pdz Domain Containing 3 |
| *Map2k1* | Mitogen-Activated Protein Kinase Kinase 1 |
| *Matk* | Megakaryocyte-Associated Tyrosine Kinase |
| *Mccc2* | Methylcrotonoyl-Coenzyme A Carboxylase 2 (Beta) |
| *Mki67* | Antigen Identified By Monoclonal Antibody Ki 67 |
| *Mlkl* | Mixed Lineage Kinase Domain-Like |
| *Mov10* | Mov10 Risc Complex RNA Helicase |
| *Msh5* | Muts Homolog 5 |
| *Mtpap* | Mitochondrial Poly(A) Polymerase |
| *Mx1* | #N/A |
| *Mx2* | Mx Dynamin-Like Gtpase 2 |
| *Myo10* | Myosin X |
| *Myo1g* | Myosin Ig |
| *Naip6* | Nlr Family, Apoptosis Inhibitory Protein 6 |
| *Nek2* | Nima (Never In Mitosis Gene A)-Related Expressed Kinase 2 |
| *Nek7* | Nima (Never In Mitosis Gene A)-Related Expressed Kinase 7 |
| *Nkiras2* | Nfkb Inhibitor Interacting Ras-Like Protein 2 |
| *Nlrc5* | Nlr Family, Card Domain Containing 5 |
| *Nme2* | Nme/Nm23 Nucleoside Diphosphate Kinase 2 |
| *Nmnat1* | Nicotinamide Nucleotide Adenylyltransferase 1 |
| *Nod1* | Nucleotide-Binding Oligomerization Domain Containing 1 |
| *Nod2* | Nucleotide-Binding Oligomerization Domain Containing 2 |
| *Npr1* | Natriuretic Peptide Receptor 1 |
| *Nt5c* | 5',3'-Nucleotidase, Cytosolic |
| *Nt5c3* | 5'-Nucleotidase, Cytosolic Iii |
| *Oas1a* | 2'-5' Oligoadenylate Synthetase 1A |
| *Oas2* | 2'-5' Oligoadenylate Synthetase 2 |
| *Oas3* | 2'-5' Oligoadenylate Synthetase 3 |
| *Oasl2* | 2'-5' Oligoadenylate Synthetase-Like 2 |
| *Orc4* | Origin Recognition Complex, Subunit 4 |
| *Pank1* | Pantothenate Kinase 1 |
| *Pank3* | Pantothenate Kinase 3 |
| *Pbk* | Pdz Binding Kinase |
| *Pccb* | Propionyl Coenzyme A Carboxylase, Beta Polypeptide |
| *Pdk1* | Pyruvate Dehydrogenase Kinase, Isoenzyme 1 |
| *Pdk3* | Pyruvate Dehydrogenase Kinase, Isoenzyme 3 |
| *Pif1* | Pif1 5'-To-3' Dna Helicase |
| *Pink1* | Pten Induced Putative Kinase 1 |
| | ***Continued overleaf*** |

| | |
|---|---|
| *Plk1* | Polo Like Kinase 1 |
| *Pnck* | Pregnancy Upregulated Non-Ubiquitously Expressed Cam Kinase |
| *Pomk* | Protein-O-Mannose Kinase |
| *Prkag1* | Protein Kinase, Amp-Activated, Gamma 1 Non-Catalytic Subunit |
| *Prkag2* | Protein Kinase, Amp-Activated, Gamma 2 Non-Catalytic Subunit |
| *Prkag3* | Protein Kinase, Amp-Activated, Gamma 3 Non-Catalytic Subunit |
| *Prkar2b* | Protein Kinase, Camp Dependent Regulatory, Type Ii Beta |
| *Prkx* | Protein Kinase, X-Linked |
| *Psmc4* | Proteasome (Prosome, Macropain) 26S Subunit, ATPase, 4 |
| *Psmc5* | Protease (Prosome, Macropain) 26S Subunit, ATPase 5 |
| *Pstk* | Phosphoseryl-TRNA Kinase |
| *Rab19* | Rab19, Member Ras Oncogene Family |
| *Rab21* | Rab21, Member Ras Oncogene Family |
| *Rab26* | Rab26, Member Ras Oncogene Family |
| *Rab34* | Rab34, Member Ras Oncogene Family |
| *Rab4a* | Rab4A, Member Ras Oncogene Family |
| *Rab5c* | Rab5C, Member Ras Oncogene Family |
| *Rab6b* | Rab6B, Member Ras Oncogene Family |
| *Rac3* | Rac Family Small Gtpase 3 |
| *Rad51* | Rad51 Recombinase |
| *Rad51b* | Rad51 Paralog B |
| *Rad51d* | Rad51 Paralog D |
| *Rad54b* | Rad54 Homolog B (S. Cerevisiae) |
| *Rap2c* | Rap2C, Member Of Ras Oncogene Family |
| *Rasd1* | Ras, Dexamethasone-Induced 1 |
| *Rhobtb2* | Rho-Related Btb Domain Containing 2 |
| *Rhobtb3* | Rho-Related Btb Domain Containing 3 |
| *Rhoc* | Ras Homolog Family Member C |
| *Rigi* | RNA Sensor Rig-I |
| *Rnf213* | Ring Finger Protein 213 |
| *Rragd* | Ras-Related Gtp Binding D |
| *Rrm1* | Ribonucleotide Reductase M1 |
| *Rtkn* | Rhotekin |
| *Samhd1* | Sam Domain And Hd Domain, 1 |
| *Slfn5* | Schlafen 5 |
| *Slfn8* | Schlafen 8 |
| *Slfn9* | Schlafen 9 |
| *Smc1b* | Structural Maintenance Of Chromosomes 1B |
| *Smc3* | Structural Maintenance Of Chromosomes 3 |
| *Smc6* | Structural Maintenance Of Chromosomes 6 |
| *Sphk1* | Sphingosine Kinase 1 |
| *Sphk2* | Sphingosine Kinase 2 |
| *Stk19* | Serine/Threonine Kinase 19 |
| | ***Continued overleaf*** |

| | |
|---|---|
| *Stk32c* | Serine/Threonine Kinase 32C |
| *Stk38l* | Serine/Threonine Kinase 38 Like |
| *Taok2* | Tao Kinase 2 |
| *Taok3* | Tao Kinase 3 |
| *Tap1* | Transporter 1, ATP-Binding Cassette, Sub-Family B (Mdr/Tap) |
| *Tap2* | Transporter 2, ATP-Binding Cassette, Sub-Family B (Mdr/Tap) |
| *Tent2* | Terminal Nucleotidyltransferase 2 |
| *Tent4a* | Terminal Nucleotidyltransferase 4A |
| *Tep1* | Telomerase Associated Protein 1 |
| *Tesk2* | Testis-Specific Kinase 2 |
| *Tex14* | Testis Expressed Gene 14 |
| *Tgm2* | Transglutaminase 2, C Polypeptide |
| *Tgtp1* | T Cell Specific Gtpase 1 |
| *Tgtp2* | T Cell Specific Gtpase 1 |
| *Tk1* | Thymidine Kinase 1 |
| *Tlk2* | Tousled-Like Kinase 2 (Arabidopsis) |
| *Top2A* | Topoisomerase (Dna) Ii Alpha |
| *Tor3a* | Torsin Family 3, Member A |
| *Trit1* | TRNA Isopentenyltransferase 1 |
| *Trpm4* | Transient Receptor Potential Cation Channel, Subfamily M, Member 4 |
| *Trpm7* | Transient Receptor Potential Cation Channel, Subfamily M, Member 7 |
| *Ttk* | Ttk Protein Kinase |
| *Txnrd3* | Thioredoxin Reductase 3 |
| *Tyk2* | Tyrosine Kinase 2 |
| *Ube2c* | Ubiquitin-Conjugating Enzyme E2C |
| *Ube2l6* | Ubiquitin-Conjugating Enzyme E2L 6 |
| *Ube2t* | Ubiquitin-Conjugating Enzyme E2T |
| *Ube2w* | Ubiquitin-Conjugating Enzyme E2W (Putative) |
| *Ulk2* | Unc-51 Like Kinase 2 |
| *Uprt* | Uracil Phosphoribosyltransferase |
| *Vrk2* | Vaccinia Related Kinase 2 |

**Table 8.5: Functional annotation cluster analysis, cluster 5, nucleotide binding.** Table showing genes and annotation terms in cluster 5. “Database” indicates where the annotation term was derived, “Count” is the number of genes associated with the annotation term and *p.adj*-value is the Bonferroni adjusted *p*-value.

**Table 8.6 Functional annotation cluster analysis, cluster 6, viruses**

| **Annotation Cluster 6** | **Enrichment Score: 7.15** | | |
|---|---|---|---|
| **Database** | **Term** | **Count** | ***p.adj* Value** |
| KEGG_PATHWAY | Influenza A | 48 | 4.79E-12 |
| KEGG_PATHWAY | Measles | 39 | 2.08E-09 |
| KEGG_PATHWAY | Hepatitis C | 36 | 1.96E-06 |

| **Gene Symbol** | **Gene Name** |
|---|---|
| *Adar* | Adenosine Deaminase, RNA-Specific |
| *Akt3* | Thymoma Viral Proto-Oncogene 3 |
| *Bak1* | Bcl2-Antagonist/Killer 1 |
| *Bax* | Bcl2-Associated X Protein |
| *Casp1* | Caspase 1 |
| *Ccl12* | Chemokine (C-C Motif) Ligand 12 |
| *Ccl2* | Chemokine (C-C Motif) Ligand 2 |
| *Ccl5* | Chemokine (C-C Motif) Ligand 5 |
| *Cxcl10* | Chemokine (C-X-C Motif) Ligand 10 |
| *Cycs* | Cytochrome C, Somatic |
| *Eif2ak2* | Eukaryotic Translation Initiation Factor 2-Alpha Kinase 2 |
| *Eif2s1* | Eukaryotic Translation Initiation Factor 2, Subunit 1 Alpha |
| *Ep300* | E1A Binding Protein P300 |
| *H2-aa* | Histocompatibility 2, Class Ii Antigen A, Alpha |
| *H2-ab1* | Histocompatibility 2, Class Ii Antigen A, Beta 1 |
| *H2-dma* | Histocompatibility 2, Class Ii, Locus Dma |
| *H2-eb1* | Histocompatibility 2, Class Ii Antigen E Beta |
| *H2-ob* | Histocompatibility 2, O Region Beta Locus |
| *Ifih1* | Interferon Induced With Helicase C Domain 1 |
| *Ifnar1* | Interferon (Alpha And Beta) Receptor 1 |
| *Ifngr1* | Interferon Gamma Receptor 1 |
| *Ikbke* | Inhibitor Of Kappab Kinase Epsilon |
| *Il18* | Interleukin 18 |
| *Irf7* | Interferon Regulatory Factor 7 |
| *Irf9* | Interferon Regulatory Factor 9 |
| *Jak2* | Janus Kinase 2 |
| *Kpna2* | Karyopherin (Importin) Alpha 2 |
| *Map2k1* | Mitogen-Activated Protein Kinase Kinase 1 |
| *Mx1* | Mx Dynamin-Like Gtpase 2 |
| *Mx2* | Mx Dynamin-Like Gtpase 2 |
| *Myd88* | Myeloid Differentiation Primary Response Gene 88 |
| *Nfkbib* | Nuclear Factor Of Kappa Light Polypeptide Gene Enhancer In B Cells Inhibitor, Beta |
| | ***Continued overleaf*** |

| | |
|---|---|
| *Oas1a* | 2'-5' Oligoadenylate Synthetase 1A |
| *Oas1b* | 2'-5' Oligoadenylate Synthetase 1B |
| *Oas1g* | 2'-5' Oligoadenylate Synthetase 1G |
| *Oas2* | 2'-5' Oligoadenylate Synthetase 2 |
| *Oas3* | 2'-5' Oligoadenylate Synthetase 3 |
| *Pml* | Promyelocytic Leukemia |
| *Rigi* | RNA Sensor Rig-I |
| *Rsad2* | Radical S-Adenosyl Methionine Domain Containing 2 |
| *Stat1* | Signal Transducer And Activator Of Transcription 1 |
| *Stat2* | Signal Transducer And Activator Of Transcription 2 |
| *Ticam1* | Tir Domain Containing Adaptor Molecule 1 |
| *Tlr3* | Toll-Like Receptor 3 |
| *Tnfsf10* | Tumor Necrosis Factor (Ligand) Superfamily, Member 10 |
| *Traf3* | Tnf Receptor-Associated Factor 3 |
| *Trim25* | Tripartite Motif-Containing 25 |
| *Tyk2* | Tyrosine Kinase 2 |

**Table 8.6: Functional annotation cluster analysis, cluster 6, viruses.** Table showing genes and annotation terms in cluster 6. “Database” indicates where the annotation term was derived, “Count” is the number of genes associated with the annotation term and *p.adj*-value is the Bonferroni adjusted *p*-value.

**Table 8.7 Functional annotation cluster analysis, cluster 7, cell cycle**

| **Annotation Cluster 7** | **Enrichment Score: 6.41** | | |
|---|---|---|---|
| **Database** | **Term** | **Count** | ***p.adj* Value** |
| GOTERM_BP_DIRECT | Cell division | 69 | 7.52E-09 |
| UP_KW_BIOLOGICAL_PROCESS | Mitosis | 55 | 9.89E-08 |
| UP_KW_BIOLOGICAL_PROCESS | Cell division | 67 | 6.44E-07 |
| GOTERM_BP_DIRECT | Cell cycle | 91 | 9.82E-07 |
| UP_KW_BIOLOGICAL_PROCESS | Cell cycle | 92 | 2.09E-05 |

| **Gene Symbol** | **Gene Name** |
|---|---|
| *Anapc5* | Anaphase-Promoting Complex Subunit 5 |
| *Ankle2* | Ankyrin Repeat And Lem Domain Containing 2 |
| *Apex2* | Apurinic/Apyrimidinic Endonuclease 2 |
| *Appl2* | Adaptor Protein, Phosphotyrosine Interaction, Ph Domain And Leucine Zipper Containing 2 |
| *Bin3* | Bridging Integrator 3 |
| *Birc5* | Baculoviral Iap Repeat-Containing 5 |
| *Birc6* | Baculoviral Iap Repeat-Containing 6 |
| *Brcc3* | Brca1/Brca2-Containing Complex, Subunit 3 |
| *Bub1* | Bub1, Mitotic Checkpoint Serine/Threonine Kinase |
| *Ccna2* | Cyclin A2 |
| *Ccnb1* | Cyclin B1 |
| *Ccnb2* | Cyclin B2 |
| *Ccnd1* | Cyclin D1 |
| *Ccne2* | Cyclin E2 |
| *Ccng1* | Cyclin G1 |
| *Ccng2* | Cyclin G2 |
| *Ccnh* | Cyclin H |
| *CD2ap* | CD2-Associated Protein |
| *CDc20* | Cell Division Cycle 20 |
| *CDca2* | Cell Division Cycle Associated 2 |
| *CDca3* | Cell Division Cycle Associated 3 |
| *CDkn1a* | Cyclin-Dependent Kinase Inhibitor 1A (P21) |
| *CDkn2c* | Cyclin Dependent Kinase Inhibitor 2C |
| *CDkn3* | Cyclin-Dependent Kinase Inhibitor 3 |
| *Cenpt* | Centromere Protein T |
| *Chmp1b2* | Charged Multivesicular Body Protein 1B2 |
| *Cit* | Citron |
| *Ckap2* | Cytoskeleton Associated Protein 2 |
| | ***Continued overleaf*** |

| | |
|---|---|
| *Cks2* | CDc28 Protein Kinase Regulatory Subunit 2 |
| *Clspn* | Claspin |
| *Cntrl* | Centriolin |
| *Dctn3* | Dynactin 3 |
| *Dmtf1* | Cyclin D Binding Myb Like Transcription Factor 1 |
| *Dscc1* | Dna Replication And Sister Chromatid Cohesion 1 |
| *Dsn1* | Dsn1 Homolog, Mis12 Kinetochore Complex Component |
| *Dync1h1* | Dynein Cytoplasmic 1 Heavy Chain 1 |
| *E2F7* | E2F Transcription Factor 7 |
| *Eml3* | Echinoderm Microtubule Associated Protein Like 3 |
| *Ensa* | Endosulfine Alpha |
| *Ep300* | E1A Binding Protein P300 |
| *Fam83d* | Family With Sequence Similarity 83, Member D |
| *Gmnn* | Geminin |
| *Gspt2* | G1 To S Phase Transition 2 |
| *Haus1* | Haus Augmin-Like Complex, Subunit 1 |
| *Ino80* | Ino80 Complex Subunit |
| *Ist1* | Increased Sodium Tolerance 1 Homolog (Yeast) |
| *Jtb* | Jumping Translocation Breakpoint |
| *Katna1* | Katanin P60 (ATPase-Containing) Subunit A1 |
| *Kif23* | Kinesin Family Member 23 |
| *Klhl18* | Kelch-Like 18 |
| *Klhl9* | Kelch-Like 9 |
| *Knl1* | Kinetochore Scaffold 1 |
| *Mad2l1* | Mad2 Mitotic Arrest Deficient-Like 1 |
| *Mad2l2* | Mad2 Mitotic Arrest Deficient-Like 2 |
| *Marveld1* | Marvel (Membrane-Associating) Domain Containing 1 |
| *Misp* | Mitotic Spindle Positioning |
| *Mitd1* | Mit, Microtubule Interacting And Transport, Domain Containing 1 |
| *Mki67* | Antigen Identified By Monoclonal Antibody Ki 67 |
| *Ncapg* | Non-Smc Condensin I Complex, Subunit G |
| *Ncapg2* | Non-Smc Condensin Ii Complex, Subunit G2 |
| *Nde1* | Nude Neurodevelopment Protein 1 |
| *Nek2* | Nima (Never In Mitosis Gene A)-Related Expressed Kinase 2 |
| *Nuf2* | Nuf2, Ndc80 Kinetochore Complex Component |
| *Nusap1* | Nucleolar And Spindle Associated Protein 1 |
| *Pimreg* | Picalm Interacting Mitotic Regulator |
| *Plk1* | Polo Like Kinase 1 |
| *Pmp22* | Peripheral Myelin Protein 22 |
| *Prc1* | Protein Regulator Of Cytokinesis 1 |
| *Psrc1* | Proline/Serine-Rich Coiled-Coil 1 |
| *Pttg1* | Pituitary Tumor-Transforming Gene 1 |
| *Racgap1* | Rac Gtpase-Activating Protein 1 |
| | ***Continued overleaf*** |

| | |
|---|---|
| *Rassf1* | Ras Association (Ralgds/Af-6) Domain Family Member 1 |
| *Rbbp8* | Retinoblastoma Binding Protein 8, Endonuclease |
| *Sass6* | Sas-6 Centriolar Assembly Protein |
| *Setdb2* | Set Domain, Bifurcated 2 |
| *Sgsm3* | Small G Protein Signaling Modulator 3 |
| *Ska1* | Spindle And Kinetochore Associated Complex Subunit 1 |
| *Ska3* | Spindle And Kinetochore Associated Complex Subunit 3 |
| *Smc1b* | Structural Maintenance Of Chromosomes 1B |
| *Smc3* | Structural Maintenance Of Chromosomes 3 |
| *Specc1l* | Sperm Antigen With Calponin Homology And Coiled-Coil Domains 1-Like |
| *Syce1* | Synaptonemal Complex Central Element Protein 1 |
| *Tbrg1* | Transforming Growth Factor Beta Regulated Gene 1 |
| *Tex14* | Testis Expressed Gene 14 |
| *Timeless* | Timeless Circadian Clock 1 |
| *Tipin* | Timeless Interacting Protein |
| *Tlk2* | Tousled-Like Kinase 2 (Arabidopsis) |
| *Tnks* | Tankyrase, Trf1-Interacting Ankyrin-Related Adp-Ribose Polymerase |
| *Tpx2* | Tpx2, Microtubule-Associated |
| *Trim21* | Tripartite Motif-Containing 21 |
| *Ube2c* | Ubiquitin-Conjugating Enzyme E2C |
| *Wdr6* | Wd Repeat Domain 6 |

**Table 8.7: Functional annotation cluster analysis, cluster 7, cell cycle.** Table showing genes and annotation terms in cluster 7. “Database” indicates where the annotation term was derived, “Count” is the number of genes associated with the annotation term and *p.adj*-value is the Bonferroni adjusted *p*-value.

**Table 8.8 Functional annotation cluster analysis, cluster 8, defence response to protozoan**

| **Annotation Cluster 8** | **Enrichment Score: 5.73** | | |
|---|---|---|---|
| **Database** | **Term** | **Count** | ***p.adj* Value** |
| GOTERM_BP_DIRECT | Defense response to protozoan | 20 | 4.57E-10 |
| UP_SEQ_FEATURE | GB1/RHD3-type G | 11 | 5.17E-08 |
| INTERPRO | Guanylate-binding protein, N-terminal | 11 | 6.93E-08 |
| INTERPRO | Guanylate-binding protein, C-terminal | 10 | 2.30E-07 |
| GOTERM_CC_DIRECT | Symbiont-containing vacuole membrane | 8 | 7.99E-07 |

| **Gene Symbol** | **Gene Name** |
|---|---|
| *Batf2* | Basic Leucine Zipper Transcription Factor, Atf-Like 2 |
| *CD40* | CD40 Antigen |
| *Enpp1* | Ectonucleotide Pyrophosphatase/Phosphodiesterase 1 |
| *Gbp10* | Guanylate-Binding Protein 10 |
| *Gbp11* | Guanylate Binding Protein 11 |
| *Gbp2* | Guanylate Binding Protein 2 |
| *Gbp3* | Guanylate Binding Protein 3 |
| *Gbp4* | Guanylate Binding Protein 3 |
| *Gbp6* | Guanylate Binding Protein 6 |
| *Gbp7* | Guanylate Binding Protein 7 |
| *Gbp8* | Guanylate-Binding Protein 8 |
| *Gbp9* | Guanylate-Binding Protein 9 |
| *Gm12250* | #N/A |
| *Igtp* | Interferon Gamma Induced Gtpase |
| *Iigp1* | Interferon Inducible Gtpase 1 |
| *Irgm2* | Immunity-Related Gtpase Family M Member 2 |
| *Myd88* | Myeloid Differentiation Primary Response Gene 88 |
| *Pf4* | Platelet Factor 4 |
| *Tgtp1* | T Cell Specific Gtpase 1 |
| *Tgtp2* | T Cell Specific Gtpase 1 |

**Table 8.8: Functional annotation cluster analysis, cluster 8, response to protozoan.** Table showing genes and annotation terms in cluster 8. “Database” indicates where the annotation term was derived, “Count” is the number of genes associated with the annotation term and *p.adj*-value is the Bonferroni adjusted *p*-value.

**Table 8.9 Functional annotation cluster analysis, cluster 9, activation of immune response**

| **Annotation Cluster 9** | **Enrichment Score: 5.49** | | |
|---|---|---|---|
| **Database** | **Term** | **Count** | ***p.adj* Value** |
| GOTERM_BP_DIRECT | Activation of innate immune response | 27 | 1.86E-15 |
| INTERPRO | HIN-200/IF120x | 9 | 2.70E-07 |
| UP_SEQ_FEATURE | HIN-200 | 8 | 6.30E-07 |
| UP_SEQ_FEATURE | Pyrin | 11 | 3.48E-05 |

| **Gene Symbol** | **Gene Name** |
|---|---|
| *Gbp2* | Guanylate Binding Protein 2 |
| *Gbp3* | Guanylate Binding Protein 3 |
| *Gbp5* | Guanylate Binding Protein 5 |
| *Gbp7* | Guanylate Binding Protein 7 |
| *Ifi203* | Interferon Activated Gene 203 |
| *Ifi204* | Interferon Activated Gene 204 |
| *Ifi205* | Interferon Activated Gene 205 |
| *Ifi206* | Interferon Activated Gene 206 |
| *Ifi207* | Interferon Activated Gene 207 |
| *Ifi208* | Interferon Activated Gene 208 |
| *Ifi209* | Interferon Activated Gene 209 |
| *Ifi211* | Interferon Activated Gene 211 |
| *Ifi213* | Interferon Activated Gene 213 |
| *Ifi214* | Interferon Activated Gene 214 |
| *Mndal* | Myeloid Nuclear Differentiation Antigen Like |
| *Nono* | Non-Pou-Domain-Containing, Octamer Binding Protein |
| *Tlr9* | Toll-Like Receptor 9 |
| *Tomm70a* | Translocase Of Outer Mitochondrial Membrane 70A |
| *Trim12a* | Tripartite Motif-Containing 12A |
| *Trim12c* | Tripartite Motif-Containing 12C |
| *Trim30a* | Tripartite Motif-Containing 30A |
| *Trim30b* | Tripartite Motif-Containing 30B |
| *Trim30c* | Tripartite Motif-Containing 30C |
| *Trim30d* | Tripartite Motif-Containing 30D |
| *Trim5* | Tripartite Motif-Containing 5 |
| *Zbp1* | Z-Dna Binding Protein 1 |
| *Znfx1* | Zinc Finger, Nfx1-Type Containing 1 |

**Table 8.9: Functional annotation cluster analysis, cluster 9, activation of immune response.** Table showing genes and annotation terms in cluster 8. “Database” indicates where the annotation term was derived, “Count” is the number of genes associated with the annotation term and *p.adj*-value is the Bonferroni adjusted *p*-value.

**Table 8.10 Functional annotation cluster analysis, cluster 10, endoplasmic reticulum**

| **Annotation Cluster 10** | **Enrichment Score: 5.47** | | |
|---|---|---|---|
| **Database** | **Term** | **Count** | ***p.adj* Value** |
| GOTERM_CC_DIRECT | Endoplasmic reticulum | 206 | 7.52E-09 |
| UP_KW_CELLULAR_ COMPONENT | Endoplasmic reticulum | 151 | 3.17E-05 |
| GOTERM_CC_DIRECT | Endoplasmic reticulum membrane | 115 | 1.56E-04 |

| **Gene Symbol** | **Gene Name** |
|---|---|
| *1600014C10rik* | RIKEN cDNA 1600014C10 Gene |
| *Abca17* | ATP-Binding Cassette, Sub-Family A (Abc1), Member 17 |
| *Abcg1* | ATP Binding Cassette Subfamily G Member 1 |
| *Acer3* | Alkaline Ceramidase 3 |
| *Aco1* | Aconitase 1 |
| *Acsl5* | Acyl-Coa Synthetase Long-Chain Family Member 5 |
| *Ahsa1* | Aha1, Activator Of Heat Shock Protein ATPase 1 |
| *Alg12* | Asparagine-Linked Glycosylation 12 (Alpha-1,6-Mannosyltransferase) |
| *Alg3* | Asparagine-Linked Glycosylation 3 (Alpha-1,3-Mannosyltransferase) |
| *Alg6* | Asparagine-Linked Glycosylation 6 (Alpha-1,3,-Glucosyltransferase) |
| *Ankle2* | Ankyrin Repeat And Lem Domain Containing 2 |
| *Arv1* | Arv1 Homolog, Fatty Acid Homeostasis Modulator |
| *Atl1* | Atlastin Gtpase 1 |
| *ATP10b* | ATPase, Class V, Type 10B |
| *Bak1* | Bcl2-Antagonist/Killer 1 |
| *Bax* | Bcl2-Associated X Protein |
| *Bbc3* | Bcl2 Binding Component 3 |
| *Bcap29* | B Cell Receptor Associated Protein 29 |
| *Bnip3l* | Bcl2/Adenovirus E1B Interacting Protein 3-Like |
| *Calr* | Calreticulin |
| *Casp4* | Caspase 4, Apoptosis-Related Cysteine Peptidase |
| *Cat* | Catalase |
| *CCDc134* | Coiled-Coil Domain Containing 134 |
| *CCDc47* | Coiled-Coil Domain Containing 47 |
| *CD1d1* | CD1D1 Antigen |
| *CD36* | CD36 Molecule |
| *CD74* | CD74 Antigen (Invariant Polypeptide Of Major Histocompatibility Complex, Class Ii Antigen-Associated) |
| *Cers5* | Ceramide Synthase 5 |
| *Cers6* | Ceramide Synthase 6 |
| *Ch25h* | Cholesterol 25-Hydroxylase |
| *Ckap4* | Cytoskeleton-Associated Protein 4 |
| | ***Continued overleaf*** |

| | |
|---|---|
| *Clcn4* | Chloride Channel, Voltage-Sensitive 4 |
| *Clec2d* | C-Type Lectin Domain Family 2, Member D |
| *Copg2* | Coatomer Protein Complex, Subunit Gamma 2 |
| *Creb3l2* | Camp Responsive Element Binding Protein 3-Like 2 |
| *Creg2* | Cellular Repressor Of E1A-Stimulated Genes 2 |
| *Cst7* | Cystatin F (Leukocystatin) |
| *Ctsf* | Cathepsin F |
| *Cybc1* | Cytochrome B 245 Chaperone 1 |
| *Dhh* | Desert Hedgehog |
| *Dnaja1* | Dnaj Heat Shock Protein Family (Hsp40) Member A1 |
| *Dnajb14* | Dnaj Heat Shock Protein Family (Hsp40) Member B14 |
| *Dnase1l3* | Deoxyribonuclease 1-Like 3 |
| *Dpagt1* | Dolichyl-Phosphate N-Acetylglucosaminephosphotransferase 1 |
| *Entpd5* | Ectonucleoside Triphosphate Diphosphohydrolase 5 |
| *Erap1* | Endoplasmic Reticulum Aminopeptidase 1 |
| *Extl3* | Exostosin-Like Glycosyltransferase 3 |
| *Fam20C* | Fam20C, Golgi Associated Secretory Pathway Kinase |
| *Fbxw7* | F-Box And Wd-40 Domain Protein 7 |
| *Fktn* | Fukutin |
| *Gabarapl1* | Gamma-Aminobutyric Acid (Gaba) A Receptor-Associated Protein-Like 1 |
| *Ganab* | Alpha Glucosidase 2 Alpha Neutral Subunit |
| *Gdpd1* | Glycerophosphodiester Phosphodiesterase Domain Containing 1 |
| *Ggcx* | Gamma-Glutamyl Carboxylase |
| *Gh* | Growth Hormone |
| *Grina* | Glutamate Receptor, Ionotropic, N-Methyl D-Aspartate-Associated Protein 1 (Glutamate Binding) |
| *Grip1* | Glutamate Receptor Interacting Protein 1 |
| *Grn* | Granulin |
| *H2-d1* | Histocompatibility 2, D Region Locus 1 |
| *H2-k1* | Histocompatibility 2, K1, K Region |
| *H2-m3* | Histocompatibility 2, M Region Locus 3 |
| *H2-q1* | Histocompatibility 2, Q Region Locus 1 |
| *H2-q10* | Histocompatibility 2, Q Region Locus 10 |
| *H2-q4* | Histocompatibility 2, Q Region Locus 4 |
| *H2-q6* | Histocompatibility 2, Q Region Locus 6 |
| *H2-q7* | Histocompatibility 2, Q Region Locus 7 |
| *H2-t10* | #N/A |
| *H2-t22* | Histocompatibility 2, T Region Locus 22 |
| *H2-t23* | Histocompatibility 2, T Region Locus 23 |
| *HaCD1* | 3-Hydroxyacyl-Coa Dehydratase 1 |
| *Hadhb* | Hydroxyacyl-Coa Dehydrogenase Trifunctional Multienzyme Complex Subunit Beta |
| *Hap1* | Huntingtin-Associated Protein 1 |
| | ***Continued overleaf*** |

| | |
|---|---|
| *Hax1* | Hcls1 Associated X-1 |
| *Hmox1* | Heme Oxygenase 1 |
| *Hmox2* | Heme Oxygenase 2 |
| *Hsp90b1* | Heat Shock Protein 90, Beta (Grp94), Member 1 |
| *Hyou1* | Hypoxia Up-Regulated 1 |
| *Ifi47* | Interferon Gamma Inducible Protein 47 |
| *Ifit2* | Interferon-Induced Protein With Tetratricopeptide Repeats 2 |
| *Ifitm3* | Interferon Induced Transmembrane Protein 3 |
| *Ifngr1* | Interferon Gamma Receptor 1 |
| *Igtp* | Interferon Gamma Induced Gtpase |
| *Iigp1* | Interferon Inducible Gtpase 1 |
| *Il2rg* | Interleukin 2 Receptor, Gamma Chain |
| *Inpp5k* | Inositol Polyphosphate 5-Phosphatase K |
| *Irgm1* | Immunity-Related Gtpase Family M Member 1 |
| *Itpr1* | Inositol 1,4,5-Trisphosphate Receptor 1 |
| *Kcnma1* | Potassium Large Conductance Calcium-Activated Channel, Subfamily M, Alpha Member 1 |
| *Kdr* | Kinase Insert Domain Protein Receptor |
| *Keap1* | Kelch-Like Ech-Associated Protein 1 |
| *Kifap3* | Kinesin-Associated Protein 3 |
| *Lacc1* | Laccase Domain Containing 1 |
| *Lpin1* | Lipin 1 |
| *Lrp6* | Low Density Lipoprotein Receptor-Related Protein 6 |
| *Lrrc8b* | Leucine Rich Repeat Containing 8 Family, Member B |
| *Mamdc2* | Mam Domain Containing 2 |
| *Man1c1* | Mannosidase, Alpha, Class 1C, Member 1 |
| *Map2k1* | Mitogen-Activated Protein Kinase Kinase 1 |
| *Marchf5* | Membrane Associated Ring-Ch-Type Finger 5 |
| *Mblac2* | Metallo-Beta-Lactamase Domain Containing 2 |
| *Mctp1* | Multiple C2 Domains, Transmembrane 1 |
| *Mesd* | Mesoderm Development Lrp Chaperone |
| *Mgst3* | Microsomal Glutathione S-Transferase 3 |
| *Mmgt1* | Membrane Magnesium Transporter 1 |
| *Mospd1* | Motile Sperm Domain Containing 1 |
| *Ms4a4b* | Membrane-Spanning 4-Domains, Subfamily A, Member 4B |
| *Ms4a4c* | Membrane-Spanning 4-Domains, Subfamily A, Member 4C |
| *Ms4a4d* | Membrane-Spanning 4-Domains, Subfamily A, Member 4D |
| *Nat8l* | N-Acetyltransferase 8-Like |
| *Nfe2l1* | Nuclear Factor, Erythroid Derived 2,-Like 1 |
| *Notch4* | Notch 4 |
| *Npc2* | Npc Intracellular Cholesterol Transporter 2 |
| *Nt5c3* | 5'-Nucleotidase, Cytosolic Iii |
| *Oas1a* | 2'-5' Oligoadenylate Synthetase 1A |
| | ***Continued overleaf*** |

| | |
|---|---|
| *Osbpl6* | Oxysterol Binding Protein-Like 6 |
| *P3h1* | Prolyl 3-Hydroxylase 1 |
| *P3h2* | Prolyl 3-Hydroxylase 2 |
| *P3h3* | Prolyl 3-Hydroxylase 3 |
| *P4ha1* | Procollagen-Proline, 2-Oxoglutarate 4-Dioxygenase (Proline 4-Hydroxylase), Alpha 1 Polypeptide |
| *Parp16* | Poly (Adp-Ribose) Polymerase Family, Member 16 |
| *Pcsk6* | Proprotein Convertase Subtilisin/Kexin Type 6 |
| *Pcsk7* | Proprotein Convertase Subtilisin/Kexin Type 7 |
| *Pex16* | Peroxisomal Biogenesis Factor 16 |
| *Pgap2* | Post-Gpi Attachment To Proteins 2 |
| *Pgrmc1* | Progesterone Receptor Membrane Component 1 |
| *Piezo1* | Piezo-Type Mechanosensitive Ion Channel Component 1 |
| *Pigf* | Phosphatidylinositol Glycan Anchor Biosynthesis, Class F |
| *Pigu* | Phosphatidylinositol Glycan Anchor Biosynthesis, Class U |
| *Pink1* | Pten Induced Putative Kinase 1 |
| *Pja2* | Praja Ring Finger Ubiquitin Ligase 2 |
| *Pkd1* | Polycystin 1, Transient Receptor Potential Channel Interacting |
| *Pkd2* | Polycystin 2, Transient Receptor Potential Cation Channel |
| *Pld3* | Phospholipase D Family, Member 3 |
| *Plekhf2* | Pleckstrin Homology Domain Containing, Family F (With Fyve Domain) Member 2 |
| *Plod3* | Procollagen-Lysine, 2-Oxoglutarate 5-Dioxygenase 3 |
| *Pmel* | Premelanosome Protein |
| *Pml* | Promyelocytic Leukemia |
| *Poglut2* | Protein O-Glucosyltransferase 2 |
| *Pomk* | Protein-O-Mannose Kinase |
| *Pomp* | Proteasome Maturation Protein |
| *Ppib* | Peptidylprolyl Isomerase B |
| *Ppp1r15b* | Protein Phosphatase 1, Regulatory Subunit 15B |
| *Psen2* | Presenilin 2 |
| *Psmf1* | Proteasome (Prosome, Macropain) Inhibitor Subunit 1 |
| *Ptgfrn* | Prostaglandin F2 Receptor Negative Regulator |
| *Ptgis* | Prostaglandin I2 (Prostacyclin) Synthase |
| *Rab21* | Rab21, Member Ras Oncogene Family |
| *Rcn2* | Reticulocalbin 2 |
| *Rhbdf1* | Rhomboid 5 Homolog 1 |
| *Rnf139* | Ring Finger Protein 139 |
| *Rnf170* | Ring Finger Protein 170 |
| *Rnf19b* | Ring Finger Protein 19B |
| *Rpn1* | Ribophorin I |
| *Rps24* | Ribosomal Protein S24 |
| *Rrbp1* | Ribosome Binding Protein 1 |
| | ***Continued overleaf*** |

| | |
|---|---|
| *Rsad2* | Radical S-Adenosyl Methionine Domain Containing 2 |
| *Sdf2l1* | Stromal Cell-Derived Factor 2-Like 1 |
| *Sec63* | Sec63-Like (S. Cerevisiae) |
| *Selenot* | Selenoprotein T |
| *Sez6l2* | Seizure Related 6 Homolog Like 2 |
| *Sgpl1* | Sphingosine Phosphate Lyase 1 |
| *Shisa5* | Shisa Family Member 5 |
| *Sirt6* | Sirtuin 6 |
| *Slc26a11* | Solute Carrier Family 26, Member 11 |
| *Smo* | Smoothened, Frizzled Class Receptor |
| *Smpd5* | Sphingomyelin Phosphodiesterase 5 |
| *Snx10* | Sorting Nexin 10 |
| *Sort1* | Sortilin 1 |
| *Spcs3* | Signal Peptidase Complex Subunit 3 Homolog (S. Cerevisiae) |
| *Sphk2* | Sphingosine Kinase 2 |
| *Sptssa* | Serine Palmitoyltransferase, Small Subunit A |
| *Srpx* | Sushi-Repeat-Containing Protein |
| *St6gal1* | Beta Galactoside Alpha 2,6 Sialyltransferase 1 |
| *Stbd1* | Starch Binding Domain 1 |
| *Stt3b* | Stt3, Subunit Of The Oligosaccharyltransferase Complex, Homolog B (S. Cerevisiae) |
| *Stx16* | Syntaxin 16 |
| *Sumf2* | Sulfatase Modifying Factor 2 |
| *Svip* | Small Vcp/P97-Interacting Protein |
| *Tap1* | Transporter 1, ATP-Binding Cassette, Sub-Family B (Mdr/Tap) |
| *Tap2* | Transporter 2, ATP-Binding Cassette, Sub-Family B (Mdr/Tap) |
| *Tapbp* | Tap Binding Protein |
| *Tapbpl* | Tap Binding Protein-Like |
| *Tbxas1* | Thromboxane A Synthase 1, Platelet |
| *Tgm2* | Transglutaminase 2, C Polypeptide |
| *Tlr3* | Toll-Like Receptor 3 |
| *Tlr9* | Toll-Like Receptor 9 |
| *Tmbim6* | Transmembrane Bax Inhibitor Motif Containing 6 |
| *Tmcc3* | Transmembrane And Coiled Coil Domains 3 |
| *Tmem106c* | Transmembrane Protein 106C |
| *Tmem117* | Transmembrane Protein 117 |
| *Tmem50b* | Transmembrane Protein 50B |
| *Tmem64* | Transmembrane Protein 64 |
| *Tor1aip2* | Torsin A Interacting Protein 2 |
| *Tor3a* | Torsin Family 3, Member A |
| *Tram1* | Translocating Chain-Associating Membrane Protein 1 |
| *Trappc5* | Trafficking Protein Particle Complex 5 |

***Continued overleaf***

| | |
|---|---|
| *Trpm4* | Transient Receptor Potential Cation Channel, Subfamily M, Member 4 |
| *Tspo* | Translocator Protein |
| *Txnrd3* | Thioredoxin Reductase 3 |
| *Usp25* | Ubiquitin Specific Peptidase 25 |
| *Vcpip1* | Valosin Containing Protein (P97)/P47 Complex Interacting Protein 1 |
| *Vkorc1* | Vitamin K Epoxide Reductase Complex, Subunit 1 |
| *Vps13c* | Vacuolar Protein Sorting 13C |
| *Vrk2* | Vaccinia Related Kinase 2 |
| *Yipf6* | Yip1 Domain Family, Member 6 |
| *Zdhhc20* | Zinc Finger, Dhhc Domain Containing 20 |

**Table 8.10: Functional annotation cluster analysis, cluster 10, endoplasmic reticulum.** Table showing genes and annotation terms in cluster 10. “Database” indicates where the annotation term was derived, “Count” is the number of genes associated with the annotation term and *p.adj*-value is the Bonferroni adjusted *p*-value.

**Table 8.11 Functional annotation cluster analysis, microglia specific, cluster 1, negative regulation of viral genome**

| **Microglia Annotation Cluster 1** | **Enrichment Score: 6.98** | | |
|---|---|---|---|
| **Database** | **Term** | **Count** | ***p.adj* Value** |
| GOTERM_BP_DIRECT | Negative regulation of viral genome replication | 21 | 1.58E-25 |
| GOTERM_BP_DIRECT | Negative regulation of type I interferon-mediated signaling pathway | 11 | 2.96E-13 |
| GOTERM_BP_DIRECT | Positive regulation of interferon-beta production | 13 | 1.57E-12 |
| GOTERM_MF_DIRECT | Double-stranded RNA binding | 15 | 3.99E-12 |
| GOTERM_BP_DIRECT | Type I interferon signaling pathway | 11 | 4.79E-12 |
| INTERPRO | 2'-5'-oligoadenylate synthetase 1, domain 2/C-terminal | 8 | 2.61E-11 |
| INTERPRO | 2'-5'-oligoadenylate synthase | 8 | 2.61E-11 |
| GOTERM_BP_DIRECT | Regulation of ribonuclease activity | 8 | 6.32E-11 |
| INTERPRO | 2-5-oligoadenylate synthetase, conserved site | 7 | 8.06E-11 |
| GOTERM_BP_DIRECT | Cellular response to interferon-alpha | 9 | 1.96E-10 |
| GOTERM_MF_DIRECT | 2'-5'-oligoadenylate synthetase activity | 7 | 3.76E-10 |
| INTERPRO | 2-5-oligoadenylate synthetase, N-terminal | 7 | 5.92E-10 |
| GOTERM_BP_DIRECT | Toll-like receptor 3 signaling pathway | 7 | 5.35E-08 |
| UP_SEQ_FEATURE | 2'-5'-oligoadenylate synthetase 1 | 6 | 5.52E-08 |
| INTERPRO | Nucleotidyl transferase domain | 6 | 1.83E-07 |
| UP_KW_MOLECULAR_FUNCTION | Nucleotidyltransferase | 10 | 2.19E-06 |
| GOTERM_BP_DIRECT | Negative regulation of IP-10 production | 5 | 6.89E-06 |
| GOTERM_BP_DIRECT | Negative regulation of chemokine (C-X-C motif) ligand 2 production | 5 | 6.89E-06 |
| GOTERM_BP_DIRECT | Toll-like receptor 4 signaling pathway | 6 | 1.75E-05 |
| GOTERM_BP_DIRECT | Interleukin-27-mediated signaling pathway | 4 | 1.81E-05 |

| **Gene Symbol** | **Gene Name** |
|---|---|
| *Bst2* | Bone Marrow Stromal Cell Antigen 2 |
| *Ccl5* | Chemokine (C-C Motif) Ligand 5 |
| *Ifi204* | Interferon Activated Gene 204 |
| | ***Continued overleaf*** |

| | |
|---|---|
| *Ifi206* | Interferon Activated Gene 206 |
| *Ifih1* | Interferon Induced With Helicase C Domain 1 |
| *Ifitm3* | Interferon Induced Transmembrane Protein 3 |
| *Ifitm6* | Interferon Induced Transmembrane Protein 6 |
| *Isg15* | Isg15 Ubiquitin-Like Modifier |
| *Isg20* | Interferon-Stimulated Protein |
| *Mx2* | Mx Dynamin-Like Gtpase 2 |
| *Oas1a* | 2'-5' Oligoadenylate Synthetase 1A |
| *Oas1b* | 2'-5' Oligoadenylate Synthetase 1B |
| *Oas1c* | 2'-5' Oligoadenylate Synthetase 1C |
| *Oas1g* | 2'-5' Oligoadenylate Synthetase 1G |
| *Oas2* | 2'-5' Oligoadenylate Synthetase 2 |
| *Oas3* | 2'-5' Oligoadenylate Synthetase 3 |
| *Oasl1* | 2'-5' Oligoadenylate Synthetase-Like 1 |
| *Oasl2* | 2'-5' Oligoadenylate Synthetase-Like 2 |
| *Parp10* | Poly (Adp-Ribose) Polymerase Family, Member 10 |
| *Rsad2* | Radical S-Adenosyl Methionine Domain Containing 2 |
| *Znfx1* | Zinc Finger, Nfx1-Type Containing 1 |

**Table 8.11: Functional annotation cluster analysis for sorted microglia, cluster 1, negative regulation of viral genome.** Table showing genes and annotation terms in cluster 1 for sorted microglia. “Database” indicates where the annotation term was derived, “Count” is the number of genes associated with the annotation term and *p.adj*-value is the Bonferroni adjusted *p*-value.

**Table 8.12 Functional annotation cluster analysis, microglia specific, cluster 2, response to type I interferon**

| **Microglia Annotation Cluster 2** | **Enrichment Score: 5.94** | | |
|---|---|---|---|
| **Database** | **Term** | **Count** | ***p.adj* Value** |
| GOTERM_BP_DIRECT | Response to interferon-gamma | 9 | 4.99E-09 |
| GOTERM_BP_DIRECT | Response to interferon-alpha | 5 | 1.47E-05 |
| GOTERM_BP_DIRECT | Response to interferon-beta | 5 | 2.03E-05 |

| **Gene Symbol** | **Gene Name** |
|---|---|
| *Bst2* | Bone Marrow Stromal Cell Antigen 2 |
| *Ccl5* | Chemokine (C-C Motif) Ligand 5 |
| *CD40* | CD40 Antigen |
| *Ifitm3* | Interferon Induced Transmembrane Protein 3 |
| *Ifitm6* | Interferon Induced Transmembrane Protein 6 |
| *Sp100* | Nuclear Antigen Sp100 |
| *Stat1* | Signal Transducer And Activator Of Transcription 1 |
| *Tgtp1* | T Cell Specific Gtpase 1 |
| *Trim21* | Tripartite Motif-Containing 21 |

**Table 8.12: Functional annotation cluster analysis for sorted microglia, cluster 2, response to interferon.** Table showing genes and annotation terms in cluster 2 for sorted microglia. “Database” indicates where the annotation term was derived, “Count” is the number of genes associated with the annotation term and *p.adj*-value is the Bonferroni adjusted *p*-value.

**Table 8.13 Functional annotation cluster analysis, oligodendrocyte specific, cluster 1, regulation of viral entry into cell**

| **Oligodendrocyte Annotation Cluster 1** | **Enrichment Score: 5.46** | | |
|---|---|---|---|
| **Database** | **Term** | **Count** | ***p.adj* Value** |
| GOTERM_BP_DIRECT | Regulation of viral entry into host cell | 9 | 6.92E-12 |
| GOTERM_BP_DIRECT | Negative regulation by host of viral release from host cell | 9 | 1.03E-11 |
| GOTERM_BP_DIRECT | Negative regulation of viral entry into host cell | 9 | 3.06E-10 |
| INTERPRO | Zinc finger, RING-type, conserved site | 14 | 6.28E-10 |
| UP_SEQ_FEATURE | B box-type | 10 | 7.94E-10 |
| INTERPRO | Zinc finger, B-box | 10 | 3.82E-09 |
| SMART | BBOX | 10 | 3.92E-09 |
| GOTERM_BP_DIRECT | Positive regulation of autophagy | 11 | 4.66E-09 |
| GOTERM_MF_DIRECT | Pattern recognition receptor activity | 8 | 6.00E-09 |
| INTERPRO | Butyrophylin-like | 9 | 1.59E-08 |
| INTERPRO | Zinc finger, RING/FYVE/PHD-type | 19 | 3.32E-08 |
| GOTERM_BP_DIRECT | Protein K63-linked ubiquitination | 9 | 4.15E-08 |
| GOTERM_BP_DIRECT | Positive regulation of I-kappaB kinase/NF-kappaB signaling | 12 | 6.80E-08 |
| UP_SEQ_FEATURE | RING-type | 13 | 9.00E-08 |
| INTERPRO | SPla/RYanodine receptor SPRY | 9 | 1.60E-07 |
| SMART | RING | 14 | 2.24E-07 |
| UP_SEQ_FEATURE | B30.2/SPRY | 9 | 2.48E-07 |
| GOTERM_CC_DIRECT | Omegasome | 5 | 2.72E-07 |
| INTERPRO | B30.2/SPRY domain | 9 | 3.19E-07 |
| SMART | SPRY | 9 | 4.02E-07 |
| GOTERM_MF_DIRECT | Ubiquitin-protein transferase activity | 14 | 4.65E-07 |
| INTERPRO | Zinc finger, RING-type | 14 | 6.11E-07 |
| GOTERM_BP_DIRECT | Positive regulation of NF-kappaB transcription factor activity | 11 | 8.81E-07 |
| GOTERM_BP_DIRECT | Positive regulation of sequence-specific DNA binding transcription factor activity | 10 | 1.08E-06 |
| GOTERM_BP_DIRECT | Regulation of lipopolysaccharide-mediated signaling pathway | 5 | 1.96E-06 |
| UP_SEQ_FEATURE | RING-type | 11 | 2.22E-06 |
| GOTERM_MF_DIRECT | Ubiquitin protein ligase activity | 15 | 2.35E-06 |
| GOTERM_BP_DIRECT | Regulation of protein localization | 9 | 4.44E-06 |
| GOTERM_BP_DIRECT | Protein polyubiquitination | 10 | 2.76E-05 |

***Continued overleaf***

| | | | |
|---|---|---|---|
| INTERPRO | Concanavalin A-like lectin/glucanase, subgroup | 10 | 5.15E-05 |
| GOTERM_BP_DIRECT | Protein ubiquitination | 14 | 6.66E-05 |
| GOTERM_MF_DIRECT | Protein binding, bridging | 8 | 9.55E-05 |

| **Gene Symbol** | **Gene Name** |
|---|---|
| *Adamts6* | A Disintegrin-Like And Metallopeptidase (Reprolysin Type) With Thrombospondin Type 1 Motif, 6 |
| *Adar* | Adenosine Deaminase, RNA-Specific |
| *Aoah* | Acyloxyacyl Hydrolase |
| *Dhx58* | Dexh (Asp-Glu-X-His) Box Polypeptide 58 |
| *Drd4* | Dopamine Receptor D4 |
| *Dtx3l* | Deltex 3-Like, E3 Ubiquitin Ligase |
| *Erap1* | Endoplasmic Reticulum Aminopeptidase 1 |
| *Helz2* | Helicase With Zinc Finger 2, Transcriptional Coactivator |
| *Ifih1* | Interferon Induced With Helicase C Domain 1 |
| *Isg20* | Interferon-Stimulated Protein |
| *Oas1a* | 2'-5' Oligoadenylate Synthetase 1A |
| *Oas2* | 2'-5' Oligoadenylate Synthetase 2 |
| *Oas3* | 2'-5' Oligoadenylate Synthetase 3 |
| *Oasl2* | 2'-5' Oligoadenylate Synthetase-Like 2 |
| *Parp12* | Poly (Adp-Ribose) Polymerase Family, Member 12 |
| *Phf11a* | Phd Finger Protein 11A |
| *Phf11b* | Phd Finger Protein 11B |
| *Phf11d* | Phd Finger Protein 11D |
| *Pml* | Promyelocytic Leukemia |
| *Rigi* | RNA Sensor Rig-I |
| *Rnf135* | Ring Finger Protein 135 |
| *Rnf213* | Ring Finger Protein 213 |
| *Rnf225* | Ring Finger Protein 225 |
| *Rsad2* | Radical S-Adenosyl Methionine Domain Containing 2 |
| *Rtp4* | Receptor Transporter Protein 4 |
| *Slfn8* | Schlafen 8 |
| *Slfn9* | Schlafen 9 |
| *Sp100* | Nuclear Antigen Sp100 |
| *Tap1* | Transporter 1, ATP-Binding Cassette, Sub-Family B (Mdr/Tap) |
| *Tap2* | Transporter 2, ATP-Binding Cassette, Sub-Family B (Mdr/Tap) |
| *Tnfsf10* | Tumor Necrosis Factor (Ligand) Superfamily, Member 10 |
| *Trim12a* | Tripartite Motif-Containing 12A |
| *Trim12c* | Tripartite Motif-Containing 12C |
| *Trim14* | Tripartite Motif-Containing 14 |
| *Trim21* | Tripartite Motif-Containing 21 |
| | ***Continued overleaf*** |

| | |
|---|---|
| *Trim25* | Tripartite Motif-Containing 25 |
| *Trim30a* | Tripartite Motif-Containing 30A |
| *Trim30c* | Tripartite Motif-Containing 30C |
| *Trim30d* | Tripartite Motif-Containing 30D |
| *Trim34a* | Tripartite Motif-Containing 34A |
| *Trim56* | Tripartite Motif-Containing 56 |
| *Xaf1* | Xiap Associated Factor 1 |
| *Zc3Hav1* | Zinc Finger Ccch Type, Antiviral 1 |
| *Znfx1* | Zinc Finger, Nfx1-Type Containing 1 |

**Table 8.13: Functional annotation cluster analysis for sorted oligodendrocytes, cluster 1, regulation of viral entry to the cell.** Table showing genes and annotation terms in cluster 1 for sorted oligodendrocytes. “Database” indicates where the annotation term was derived, “Count” is the number of genes associated with the annotation term and *p.adj*-value is the Bonferroni adjusted *p*-value.

**Table 8.14 Functional annotation cluster analysis, olygodendrocyte specific, cluster 2, oligoadenylate synthetase**

| **Oligodendrocyte Annotation Cluster 2** | **Enrichment Score: 5.00** | | |
|---|---|---|---|
| **Database** | **Term** | **Count** | ***p.adj* Value** |
| INTERPRO | 2-5-oligoadenylate synthetase, conserved site | 7 | 6.35E-12 |
| GOTERM_BP_DIRECT | Negative regulation of type I interferon-mediated signaling pathway | 9 | 2.16E-11 |
| INTERPRO | 2'-5'-oligoadenylate synthetase 1, domain 2/C-terminal | 7 | 2.04E-10 |
| INTERPRO | 2'-5'-oligoadenylate synthase | 7 | 2.04E-10 |
| GOTERM_BP_DIRECT | Regulation of ribonuclease activity | 7 | 4.23E-10 |
| GOTERM_MF_DIRECT | 2'-5'-oligoadenylate synthetase activity | 6 | 5.96E-09 |
| INTERPRO | 2-5-oligoadenylate synthetase, N-terminal | 6 | 7.27E-09 |
| GOTERM_BP_DIRECT | Toll-like receptor 3 signaling pathway | 6 | 2.59E-07 |
| UP_SEQ_FEATURE | 2'-5'-oligoadenylate synthetase 1 | 5 | 6.80E-07 |
| INTERPRO | Nucleotidyl transferase domain | 5 | 1.81E-06 |
| GOTERM_BP_DIRECT | Interleukin-27-mediated signaling pathway | 4 | 5.16E-06 |
| GOTERM_BP_DIRECT | Toll-like receptor 4 signaling pathway | 5 | 6.31E-05 |
| GOTERM_BP_DIRECT | Negative regulation of IP-10 production | 4 | 8.22E-05 |
| GOTERM_BP_DIRECT | Negative regulation of chemokine (C-X-C motif) ligand 2 production | 4 | 8.22E-05 |

| **Gene Symbol** | **Gene Name** |
|---|---|
| *Adar* | Adenosine Deaminase, RNA-Specific |
| *Ifih1* | Interferon Induced With Helicase C Domain 1 |
| *Isg15* | Isg15 Ubiquitin-Like Modifier |
| *Lgals9* | Lectin, Galactose Binding, Soluble 9 |
| *Nlrc5* | Nlr Family, Card Domain Containing 5 |
| *Nmi* | N-Myc (And Stat) Interactor |
| *Oas1a* | 2'-5' Oligoadenylate Synthetase 1A |
| *Oas1b* | 2'-5' Oligoadenylate Synthetase 1B |
| *Oas1g* | 2'-5' Oligoadenylate Synthetase 1G |
| *Oas2* | 2'-5' Oligoadenylate Synthetase 2 |
| *Oas2* | 2'-5' Oligoadenylate Synthetase 2 |
| *Oas3* | 2'-5' Oligoadenylate Synthetase 3 |
| *Oasl1* | 2'-5' Oligoadenylate Synthetase-Like 1 |
| *Oasl2* | 2'-5' Oligoadenylate Synthetase-Like 2 |
| | ***Continued overleaf*** |

| | |
|---|---|
| *Scimp* | Slp Adaptor And Csk Interacting Membrane Protein |
| *Slfn8* | Schlafen 8 |
| *Slfn9* | Schlafen 9 |
| *Stat1* | Signal Transducer And Activator Of Transcription 1 |
| *Stat2* | Signal Transducer And Activator Of Transcription 2 |
| *Tap2* | Transporter 2, ATP-Binding Cassette, Sub-Family B (Mdr/Tap) |
| *Tlr3* | Toll-Like Receptor 3 |
| *Usp18* | Ubiquitin Specific Peptidase 18 |

**Table 8.14: Functional annotation cluster analysis for sorted oligodendrocytes, cluster 2, oligoadenylate synthetase.** Table showing genes and annotation terms in cluster 2 for sorted oligodendrocytes. “Database” indicates where the annotation term was derived, “Count” is the number of genes associated with the annotation term and *p.adj*-value is the Bonferroni adjusted *p*-value.

**Table 8.15 Functional annotation cluster analysis, astrocyte specific, cluster 1, regulation of IFN-β production**

| **Astrocyte Annotation Cluster 1** | **Enrichment Score: 7.08** | | |
|---|---|---|---|
| **Database** | **Term** | **Count** | ***p.adj* Value** |
| GOTERM_BP_DIRECT | Positive regulation of interferon-beta production | 14 | 1.39E-15 |
| GOTERM_MF_DIRECT | Double-stranded RNA binding | 16 | 3.83E-15 |
| GOTERM_BP_DIRECT | Negative regulation of type I interferon-mediated signaling pathway | 11 | 1.66E-14 |
| INTERPRO | 2'-5'-oligoadenylate synthetase 1, domain 2/C-terminal | 8 | 3.40E-12 |
| INTERPRO | 2'-5'-oligoadenylate synthase | 8 | 3.40E-12 |
| GOTERM_BP_DIRECT | Regulation of ribonuclease activity | 8 | 8.41E-12 |
| GOTERM_BP_DIRECT | Type I interferon signaling pathway | 10 | 1.29E-11 |
| INTERPRO | 2-5-oligoadenylate synthetase, conserved site | 7 | 1.40E-11 |
| GOTERM_BP_DIRECT | Cellular response to interferon-alpha | 9 | 1.99E-11 |
| GOTERM_MF_DIRECT | 2'-5'-oligoadenylate synthetase activity | 7 | 7.05E-11 |
| INTERPRO | 2-5-oligoadenylate synthetase, N-terminal | 7 | 1.04E-10 |
| GOTERM_BP_DIRECT | Toll-like receptor 3 signaling pathway | 7 | 9.72E-09 |
| UP_SEQ_FEATURE | 2'-5'-oligoadenylate synthetase 1 | 6 | 1.22E-08 |
| INTERPRO | Nucleotidyl transferase domain | 6 | 4.34E-08 |
| GOTERM_BP_DIRECT | Negative regulation of IP-10 production | 5 | 2.21E-06 |
| GOTERM_BP_DIRECT | Negative regulation of chemokine (C-X-C motif) ligand 2 production | 5 | 2.21E-06 |
| GOTERM_BP_DIRECT | Toll-like receptor 4 signaling pathway | 6 | 4.37E-06 |
| GOTERM_BP_DIRECT | Interleukin-27-mediated signaling pathway | 4 | 7.66E-06 |
| GOTERM_BP_DIRECT | Positive regulation of monocyte chemotactic protein-1 production | 5 | 3.73E-05 |
| UP_SEQ_FEATURE | Polymerase nucleotidyl transferase | 4 | 5.43E-05 |

| **Gene Symbol** | **Gene Name** |
|---|---|
| *Adar* | Adenosine Deaminase, RNA-Specific |
| *Ddx60* | Dexd/H Box Helicase 60 |
| *Dhx58* | Dexh (Asp-Glu-X-His) Box Polypeptide 58 |
| *Eif2ak2* | Eukaryotic Translation Initiation Factor 2-Alpha Kinase 2 |
| *Ifi204* | Interferon Activated Gene 204 |
| *Ifih1* | Interferon Induced With Helicase C Domain 1 |
| *Ifit1* | Interferon-Induced Protein With Tetratricopeptide Repeats 1 |
| *Ifit2* | Interferon-Induced Protein With Tetratricopeptide Repeats 2 |
| | ***Continued overleaf*** |

| | |
|---|---|
| *Ifit3* | Interferon-Induced Protein With Tetratricopeptide Repeats 3 |
| *Ifit3b* | Interferon-Induced Protein With Tetratricopeptide Repeats 3B |
| *Ifitm3* | Interferon Induced Transmembrane Protein 3 |
| *Irf7* | Interferon Regulatory Factor 7 |
| *Isg15* | Isg15 Ubiquitin-Like Modifier |
| *Lgals9* | Lectin, Galactose Binding, Soluble 9 |
| *Nlrc5* | Nlr Family, Card Domain Containing 5 |
| *Nmi* | N-Myc (And Stat) Interactor |
| *Oas1a* | 2'-5' Oligoadenylate Synthetase 1A |
| *Oas1b* | 2'-5' Oligoadenylate Synthetase 1B |
| *Oas1G* | 2'-5' Oligoadenylate Synthetase 1G |
| *Oas1h* | 2'-5' Oligoadenylate Synthetase 1H |
| *Oas2* | 2'-5' Oligoadenylate Synthetase 2 |
| *Oas3* | 2'-5' Oligoadenylate Synthetase 3 |
| *Oasl1* | 2'-5' Oligoadenylate Synthetase-Like 1 |
| *Oasl2* | 2'-5' Oligoadenylate Synthetase-Like 2 |
| *Rigi* | RNA Sensor Rig-I |
| *Rnf135* | Ring Finger Protein 135 |
| *Samhd1* | Sam Domain And Hd Domain, 1 |
| *Scimp* | Slp Adaptor And Csk Interacting Membrane Protein |
| *Slfn8* | Schlafen 8 |
| *Slfn9* | Schlafen 9 |
| *Stat1* | Signal Transducer And Activator Of Transcription 1 |
| *Stat2* | Signal Transducer And Activator Of Transcription 2 |
| *Tap1* | Transporter 1, ATP-Binding Cassette, Sub-Family B (Mdr/Tap) |
| *Tap2* | Transporter 2, ATP-Binding Cassette, Sub-Family B (Mdr/Tap) |
| *Tlr3* | Toll-Like Receptor 3 |
| *Usp18* | Ubiquitin Specific Peptidase 18 |
| *Zbp1* | Z-Dna Binding Protein 1 |
| *Zc3hav1* | Zinc Finger Ccch Type, Antiviral 1 |

**Table 8.15: Functional annotation cluster analysis for sorted astrocytes, cluster 1, regulation of IFN-β production.** Table showing genes and annotation terms in cluster 1 for sorted astrocytes. “Database” indicates where the annotation term was derived, “Count” is the number of genes associated with the annotation term and *p.adj*-value is the Bonferroni adjusted *p*-value.

**Table 8.16 Functional annotation cluster analysis, astrocyte specific, cluster 2, nucleotide binding**

| **Astrocyte Annotation Cluster 2** | **Enrichment Score: 5.00** | | |
|---|---|---|---|
| **Database** | **Term** | **Count** | ***p.adj* Value** |
| UP_KW_LIGAND | Nucleotide-binding | 40 | 6.61E-06 |
| UP_KW_LIGAND | GTP-binding | 16 | 6.71E-06 |
| UP_KW_MOLECULAR_FUNCTION | Hydrolase | 32 | 2.20E-05 |

| **Gene Symbol** | **Gene Name** |
|---|---|
| *Ascc3* | Activating Signal Cointegrator 1 Complex Subunit 3 |
| *Cmpk2* | Cytidine Monophosphate (Ump-Cmp) Kinase 2, Mitochondrial |
| *Cngb3* | Cyclic Nucleotide Gated Channel Beta 3 |
| *Ddx60* | Dexd/H Box Helicase 60 |
| *Dhx58* | Dexh (Asp-Glu-X-His) Box Polypeptide 58 |
| *Eif2ak2* | Eukaryotic Translation Initiation Factor 2-Alpha Kinase 2 |
| *Gbp2* | Guanylate Binding Protein 2 |
| *Gbp3* | Guanylate Binding Protein 3 |
| *Gbp4* | Guanylate Binding Protein 3 |
| *Gbp5* | Guanylate Binding Protein 5 |
| *Gbp6* | Guanylate Binding Protein 6 |
| *Gbp7* | Guanylate Binding Protein 7 |
| *Gm12250* | #N/A |
| *Helz2* | Helicase With Zinc Finger 2, Transcriptional Coactivator |
| *Ifih1* | Interferon Induced With Helicase C Domain 1 |
| *Igtp* | Interferon Gamma Induced Gtpase |
| *Iigp1* | Interferon Inducible Gtpase 1 |
| *Irgm1* | Immunity-Related Gtpase Family M Member 1 |
| *Irgm2* | Immunity-Related Gtpase Family M Member 2 |
| *Mlkl* | Mixed Lineage Kinase Domain-Like |
| *Mov10* | Mov10 Risc Complex RNA Helicase |
| *Mx1* | Mx Dynamin-Like Gtpase 1 |
| *Mx2* | Mx Dynamin-Like Gtpase 2 |
| *Nlrc5* | Nlr Family, Card Domain Containing 5 |
| *Oas1a* | 2'-5' Oligoadenylate Synthetase 1A |
| *Oas2* | 2'-5' Oligoadenylate Synthetase 2 |
| *Oas3* | 2'-5' Oligoadenylate Synthetase 3 |
| *Oasl2* | 2'-5' Oligoadenylate Synthetase-Like 2 |
| *Rigi* | RNA Sensor Rig-I |
| *Rnf213* | Ring Finger Protein 213 |
| *Samhd1* | Sam Domain And Hd Domain, 1 |
| *Slfn5* | Schlafen 5 |

***Continued overleaf***

| | |
|---|---|
| *Slfn8* | Schlafen 8 |
| *Slfn9* | Schlafen 9 |
| *Tap1* | Transporter 1, ATP-Binding Cassette, Sub-Family B (Mdr/Tap) |
| *Tap2* | Transporter 2, ATP-Binding Cassette, Sub-Family B (Mdr/Tap) |
| *Tgtp1* | T Cell Specific Gtpase 1 |
| *Tgtp2* | T Cell Specific Gtpase 1 |
| *Tor3a* | Torsin Family 3, Member A |
| *Ube2l6* | Ubiquitin-Conjugating Enzyme E2L 6 |

**Table 8.16: Functional annotation cluster analysis for sorted astrocytes, cluster 2, nucleotide binding.** Table showing genes and annotation terms in cluster 2 for sorted astrocytes. “Database” indicates where the annotation term was derived, “Count” is the number of genes associated with the annotation term and *p.adj*-value is the Bonferroni adjusted *p*-value.

**Table 8.17 Functional annotation cluster analysis, microglia, astrocyte, oligodendrocyte specific, cluster 1, cytosol**

| **Microglia, Astrocyte, Oligodendrocyte** | |
|---|---|
| **Annotation Cluster 1** | **Enrichment Score: 5.41** |

| **Database** | **Term** | **Count** | ***p.adj* Value** |
|---|---|---|---|
| GOTERM_CC_DIRECT | Cytosol | 101 | 1.09E-10 |
| GOTERM_CC_DIRECT | Cytoplasm | 121 | 5.06E-04 |
| UP_KW_CELLULAR_COMPONENT | Cytoplasm | 88 | 0.00105707 |

| **Gene Symbol** | **Gene Name** |
|---|---|
| *1600014c10rik* | RIKEN cDNA 1600014C10 Gene |
| *Adar* | Adenosine Deaminase, RNA-Specific |
| *Aftph* | Aftiphilin |
| *Bcl2a1a* | B Cell Leukemia/Lymphoma 2 Related Protein A1A |
| *Bst2* | Bone Marrow Stromal Cell Antigen 2 |
| *Cabp4* | Calcium Binding Protein 4 |
| *Ccl2* | Chemokine (C-C Motif) Ligand 2 |
| *Ccl5* | Chemokine (C-C Motif) Ligand 5 |
| *Ccnd1* | Cyclin D1 |
| *Ccnj* | Cyclin J |
| *CD40* | CD40 Antigen |
| *Cmpk2* | Cytidine Monophosphate (Ump-Cmp) Kinase 2, Mitochondrial |
| *Daxx* | Fas Death Domain-Associated Protein |
| *Dck* | Deoxycytidine Kinase |
| *Ddx4* | Dead Box Helicase 4 |
| *Ddx60* | Dexd/H Box Helicase 60 |
| *Dhx58* | Dexh (Asp-Glu-X-His) Box Polypeptide 58 |
| *Dtx3L* | Deltex 3-Like, E3 Ubiquitin Ligase |
| *Fabp3* | Fatty Acid Binding Protein 3, Muscle And Heart |
| *Flt4* | Fms-Like Tyrosine Kinase 4 |
| *Fpr2* | Formyl Peptide Receptor 2 |
| *Gbp2* | Guanylate Binding Protein 2 |
| *Gbp3* | Guanylate Binding Protein 3 |
| *Gbp5* | Guanylate Binding Protein 5 |
| *Hap1* | Huntingtin-Associated Protein 1 |
| *Helz2* | Helicase With Zinc Finger 2, Transcriptional Coactivator |
| *Herc6* | Hect Domain And Rld 6 |
| *Hsh2d* | Hematopoietic Sh2 Domain Containing |
| *Ifi203* | Interferon Activated Gene 203 |
| *Ifi203-ps* | Interferon Activated Gene 203, ps |
| *Ifi204* | Interferon Activated Gene 204 |
| | ***Continued overleaf*** |

| | |
|---|---|
| *Ifi205* | Interferon Activated Gene 205 |
| *Ifi206* | Interferon Activated Gene 206 |
| *Ifi208* | Interferon Activated Gene 208 |
| *Ifi209* | Interferon Activated Gene 209 |
| *Ifi211* | Interferon Activated Gene 211 |
| *Ifi213* | Interferon Activated Gene 213 |
| *Ifi214* | Interferon Activated Gene 214 |
| *Ifi35* | Interferon-Induced Protein 35 |
| *Ifi44* | Interferon-Induced Protein 44 |
| *Ifih1* | Interferon Induced With Helicase C Domain 1 |
| *Ifit1* | Interferon-Induced Protein With Tetratricopeptide Repeats 1 |
| *Ifit1Bl1* | Interferon Induced Protein With Tetratricpeptide Repeats 1B Like 1 |
| *Ifit1Bl2* | Interferon Induced Protein With Tetratricopeptide Repeats 1B Like 2 |
| *Ifit2* | Interferon-Induced Protein With Tetratricopeptide Repeats 2 |
| *Ifit3* | Interferon-Induced Protein With Tetratricopeptide Repeats 3 |
| *Ifit3b* | Interferon-Induced Protein With Tetratricopeptide Repeats 3B |
| *Ifitm3* | Interferon Induced Transmembrane Protein 3 |
| *Iigp1* | Interferon Inducible Gtpase 1 |
| *Il15* | Interleukin 15 |
| *Il1Rn* | Interleukin 1 Receptor Antagonist |
| *Irf1* | Interferon Regulatory Factor 1 |
| *Irf7* | Interferon Regulatory Factor 7 |
| *Isg15* | Isg15 Ubiquitin-Like Modifier |
| *Isg20* | Interferon-Stimulated Protein |
| *Itpr1* | Inositol 1,4,5-Trisphosphate Receptor 1 |
| *Lgals9* | Lectin, Galactose Binding, Soluble 9 |
| *Lst1* | Leukocyte Specific Transcript 1 |
| *Misp* | Mitotic Spindle Positioning |
| *Mlkl* | Mixed Lineage Kinase Domain-Like |
| *Mndal* | Myeloid Nuclear Differentiation Antigen Like |
| *Mov10* | Mov10 Risc Complex RNA Helicase |
| *Mx1* | Mx Dynamin-Like Gtpase 1 |
| *Mx2* | Mx Dynamin-Like Gtpase 2 |
| *Naa25* | N(Alpha)-Acetyltransferase 25, Natb Auxiliary Subunit |
| *Nlrc5* | Nlr Family, Card Domain Containing 5 |
| *Nme2* | Nme/Nm23 Nucleoside Diphosphate Kinase 2 |
| *Nmi* | N-Myc (And Stat) Interactor |
| *Nmral1* | Nmra-Like Family Domain Containing 1 |
| *Nod1* | Nucleotide-Binding Oligomerization Domain Containing 1 |
| *Npsr1* | Neuropeptide S Receptor 1 |
| *Oas1a* | 2'-5' Oligoadenylate Synthetase 1A |
| *Oas1b* | 2'-5' Oligoadenylate Synthetase 1B |
| *Oas1c* | 2'-5' Oligoadenylate Synthetase 1C |
| | ***Continued overleaf*** |

| | |
|---|---|
| *Oas1g* | 2'-5' Oligoadenylate Synthetase 1G |
| *Oas2* | 2'-5' Oligoadenylate Synthetase 2 |
| *Oas3* | 2'-5' Oligoadenylate Synthetase 3 |
| *Oasl1* | 2'-5' Oligoadenylate Synthetase-Like 1 |
| *Ogfr* | Opioid Growth Factor Receptor |
| *Parp10* | Poly (Adp-Ribose) Polymerase Family, Member 10 |
| *Parp14* | Poly (Adp-Ribose) Polymerase Family, Member 14 |
| *Parp9* | Poly (Adp-Ribose) Polymerase Family, Member 9 |
| *Pml* | Promyelocytic Leukemia |
| *Prkag3* | Protein Kinase, Amp-Activated, Gamma 3 Non-Catalytic Subunit |
| *Psmb10* | Proteasome (Prosome, Macropain) Subunit, Beta Type 10 |
| *Psmb8* | Proteasome (Prosome, Macropain) Subunit, Beta Type 8 (Large Multifunctional Peptidase 7) |
| *Psmb9* | Proteasome (Prosome, Macropain) Subunit, Beta Type 9 (Large Multifunctional Peptidase 2) |
| *Psme1* | Proteasome (Prosome, Macropain) Activator Subunit 1 (Pa28 Alpha) |
| *Psrc1* | Proline/Serine-Rich Coiled-Coil 1 |
| *Pttg1* | Pituitary Tumor-Transforming Gene 1 |
| *Rigi* | RNA Sensor Rig-I |
| *Rnf213* | Ring Finger Protein 213 |
| *Rtp4* | Receptor Transporter Protein 4 |
| *Samd9L* | Sterile Alpha Motif Domain Containing 9-Like |
| *Sass6* | Sas-6 Centriolar Assembly Protein |
| *Selenow* | Selenoprotein W |
| *Serpina3g* | Serine (Or Cysteine) Peptidase Inhibitor, Clade A, Member 3G |
| *Slc25a22* | Solute Carrier Family 25 (Mitochondrial Carrier, Glutamate), Member 22 |
| *Slfn1* | Schlafen 1 |
| *Slfn2* | Schlafen 2 |
| *Slfn8* | Schlafen 8 |
| *Slfn9* | Schlafen 9 |
| *Sp100* | Nuclear Antigen Sp100 |
| *Stat1* | Signal Transducer And Activator Of Transcription 1 |
| *Stat2* | Signal Transducer And Activator Of Transcription 2 |
| *Tent4a* | Terminal Nucleotidyltransferase 4A |
| *Tgm2* | Transglutaminase 2, C Polypeptide |
| *Tlr3* | Toll-Like Receptor 3 |
| *Tor3A* | Torsin Family 3, Member A |
| *Trim21* | Tripartite Motif-Containing 21 |
| *Trim25* | Tripartite Motif-Containing 25 |
| *Trim30a* | Tripartite Motif-Containing 30A |
| *Trim30b* | Tripartite Motif-Containing 30B |
| *Trim30c* | Tripartite Motif-Containing 30C |
| *Trim30d* | Tripartite Motif-Containing 30D |
| | ***Continued overleaf*** |

| | |
|---|---|
| *Trim34a* | Tripartite Motif-Containing 34A |
| *Uba7* | Ubiquitin-Like Modifier Activating Enzyme 7 |
| *Xaf1* | Xiap Associated Factor 1 |
| *Zbp1* | Z-Dna Binding Protein 1 |
| *Znfx1* | Zinc Finger, Nfx1-Type Containing 1 |
| *Zup1* | Zinc Finger Containing Ubiquitin Peptidase 1 |

**Table 8.17: Functional annotation cluster analysis for sorted microglia, oligodendrocytes, and astrocytes, cluster 1, cytosol.** Table showing genes and annotation terms in cluster 1 for sorted microglia, oligodendrocytes, and astrocytes. “Database” indicates where the annotation term was derived, “Count” is the number of genes associated with the annotation term and *p.adj*-value is the Bonferroni adjusted *p*-value.

## 8.4 List of genes differentially expressed by IFN-β in oligodendrocytes

**Figure 8.17: QR Code to spreadsheet of genes differentially expressed in oligodendrocytes sorted from CNS cultures by IFN-β compared to PBS controls.** Table showing genes differentially regulated in IFN-β -treated CNS cultures compared to untreated controls. Fold change ≥ ±2, FDR adjusted *p* – value ≤ 0.0001.

Link:
https://bit.ly/4a4xDbk

8.5 Representative normalised reads of different Gene Ontology (GO), Kyoto Encyclopaedia of Genes and Genomes (KEGG), and Reactome pathway analysis groupings for oligodendrocyte specific DEGs.

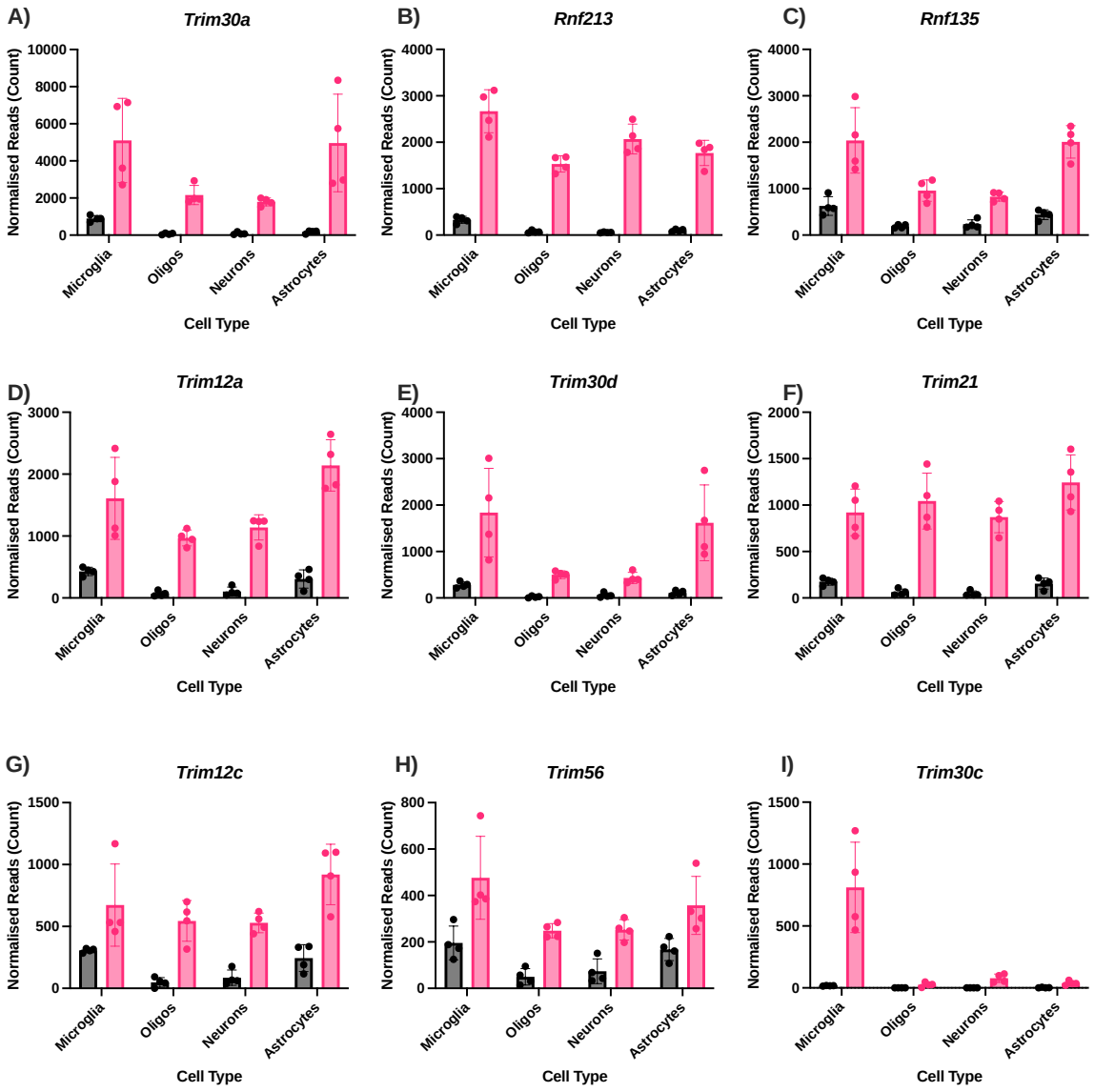


**Figure 8.18: Normalised read counts of top 9 expressed genes in *Protein ubiquitination and processing* oligodendrocyte specific GO term.** Graphs show normalised number of reads across sorted cell types following treatment with PBS (vehicle) or IFN-β in pathways found to be enriched in specifically sorted oligodendrocytes, with top 9 genes identified through having the greatest mean number of normalised read counts across all sorted cell types and treatment regimens. A) *Trim30a*, B) *Rnf213*, C) *Rnf135*, D) *Trim12a*, E) *Trim30d*, F) *Trim21*, G) *Trim12c*, H) *Trim56*, I) *Trim30c*. Bars represent mean ± SD. n=4.

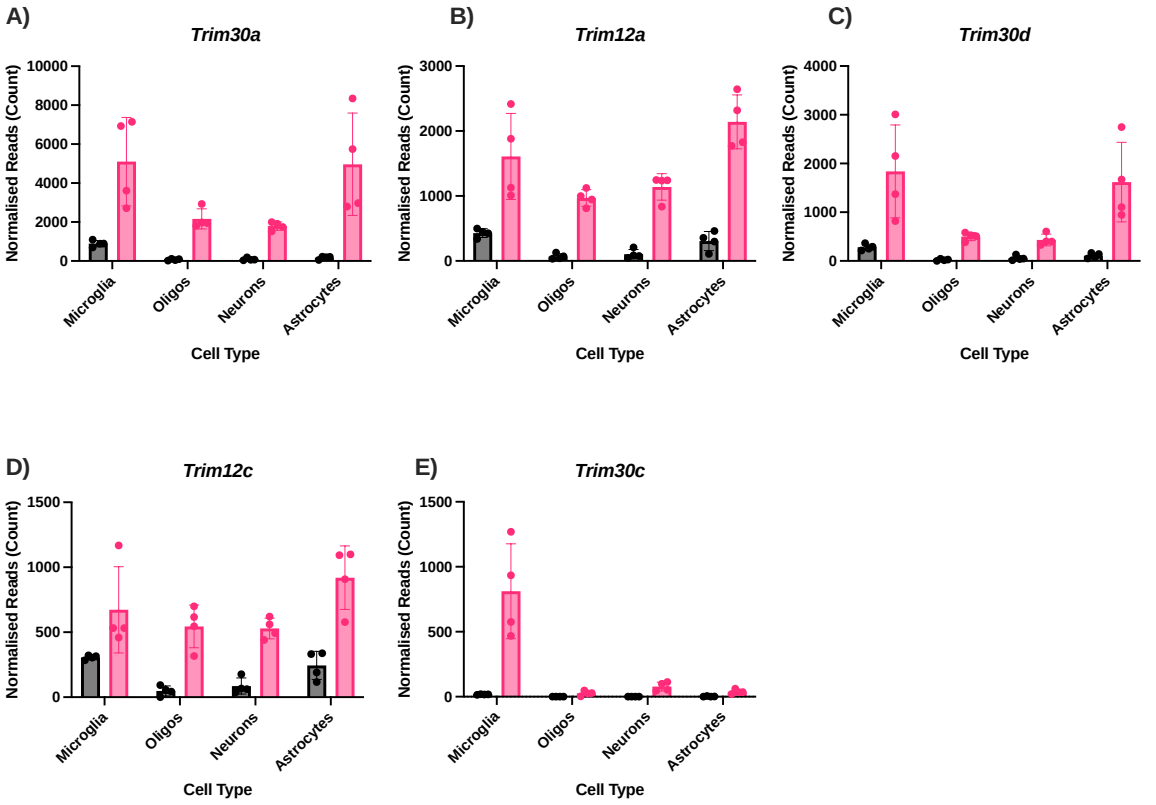


**Figure 8.19: Normalised read counts of all expressed genes in *Regulation of LPS signalling* oligodendrocyte specific GO term**. Graphs show normalised number of reads across sorted cell types following treatment with PBS (vehicle) or IFN-β in pathways found to be enriched in specifically sorted oligodendrocytes. A) *Trim30a*, B) *Trim12a*, C) *Trim30d*, D) *Trim12c*, E) *Trim30c*. Bars represent mean ± SD. n=4.

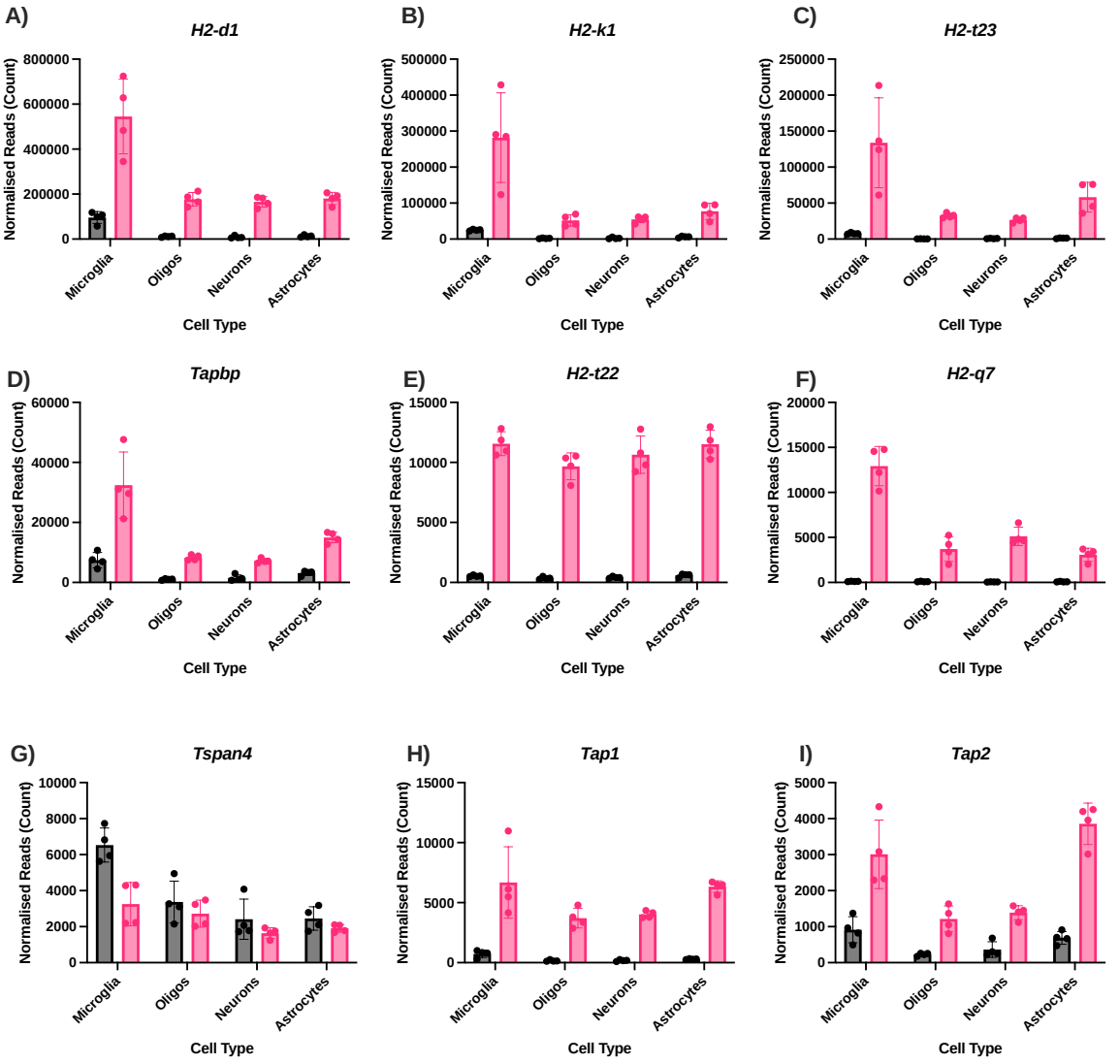


**Figure 8.20: Normalised read counts of top 9 expressed genes in *Antigen binding* oligodendrocyte specific GO term.** Graphs show normalised number of reads across sorted cell types following treatment with PBS (vehicle) or IFN-β in pathways found to be enriched in specifically sorted oligodendrocytes, with top 9 genes identified through having the greatest mean number of normalised read counts across all sorted cell types and treatment regimens. A) *H2-d1*, B) *H2-k1*, C) *H2-t23*, D) *Tapbp*, E) *H2-t22*, F) *H2-q7*, G) *Tspan4*, H) *Tap1*, I) *Tap2*. Bars represent mean ± SD. N=4.

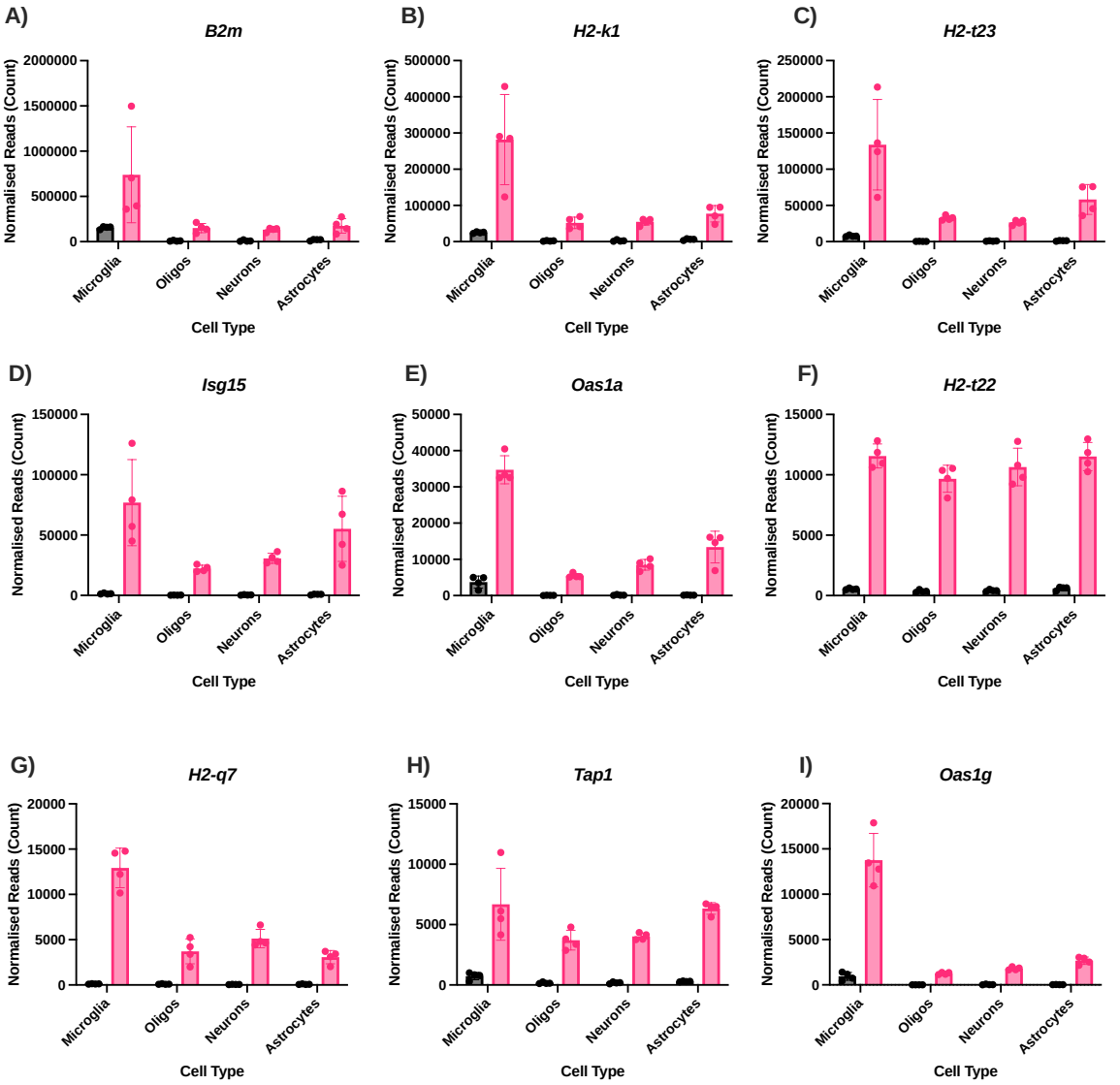


**Figure 8.21 Normalised read counts of top 9 expressed genes in *Response to human pathogens* oligodendrocyte specific KEGG term**. Graphs show normalised number of reads across sorted cell types following treatment with PBS (vehicle) or IFN-β in pathways found to be enriched in specifically sorted oligodendrocytes, with top 9 genes identified through having the greatest mean number of normalised read counts across all sorted cell types and treatment regimens. A) *B2m*, B) *H2-k1*, C) *H2-t23*, D) *Isg15*, E) *Oas1a*, F) *H2-t22*, G) *H2-q7*, H) *Tap1*, I) *Oas1g*. Bars represent mean ± SD. N=4.

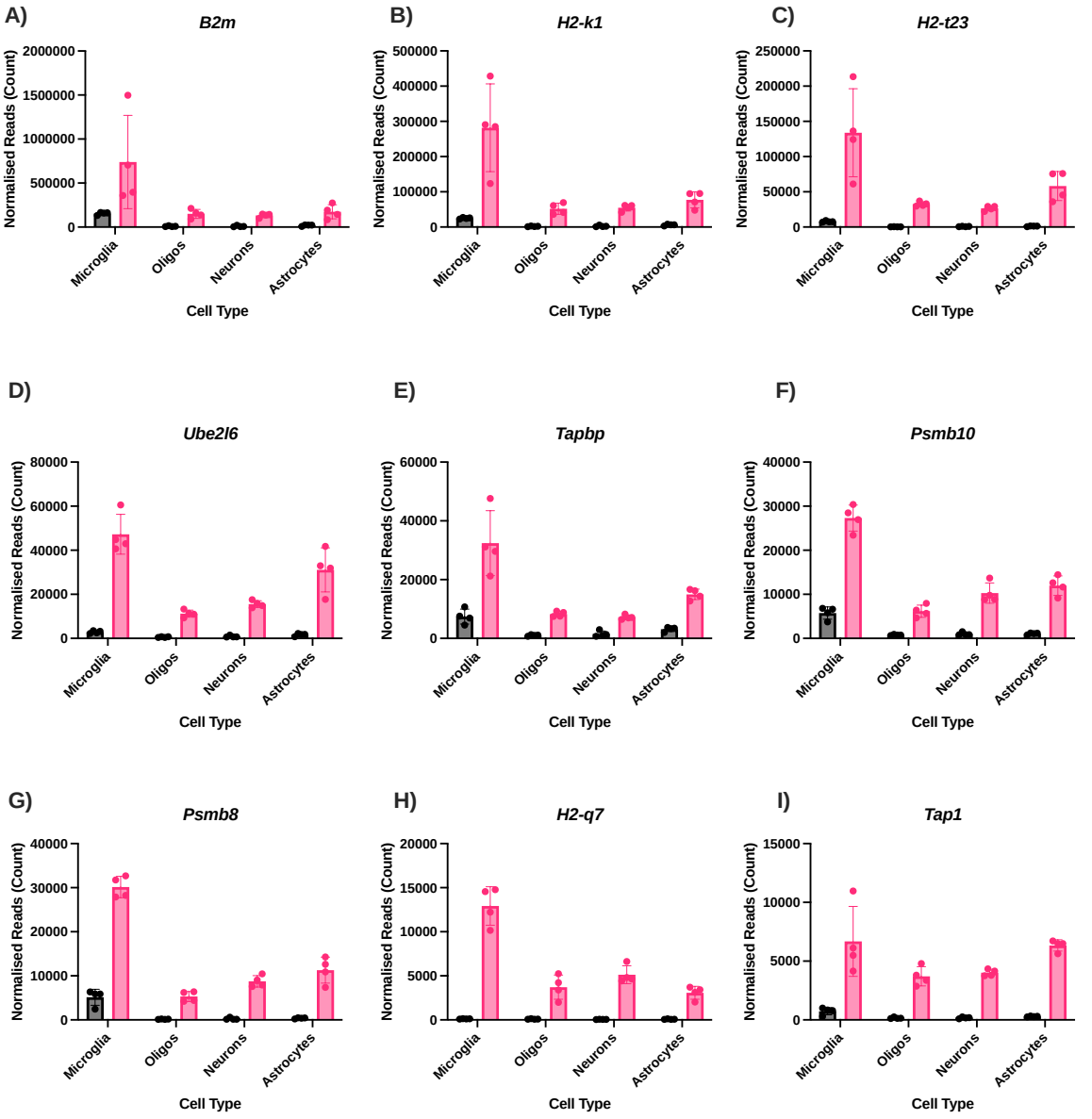


**Figure 8.22: Normalised read counts of top 9 expressed genes in *Antigen processing / presentation* oligodendrocyte specific KEGG term**. Graphs show normalised number of reads across sorted cell types following treatment with PBS (vehicle) or IFN-β in pathways found to be enriched in specifically sorted oligodendrocytes, with top 9 genes identified through having the greatest mean number of normalised read counts across all sorted cell types and treatment regimens. A) *B2m*, B) *i*H2-k1 C) *H2-t23*, D) *Ube2l6*, E) *Tapbp*, F) *Psmb10*, G) *Psmb8*, H) *H2-q7*, I) *Tap1*. Bars represent mean ± SD. n=4.

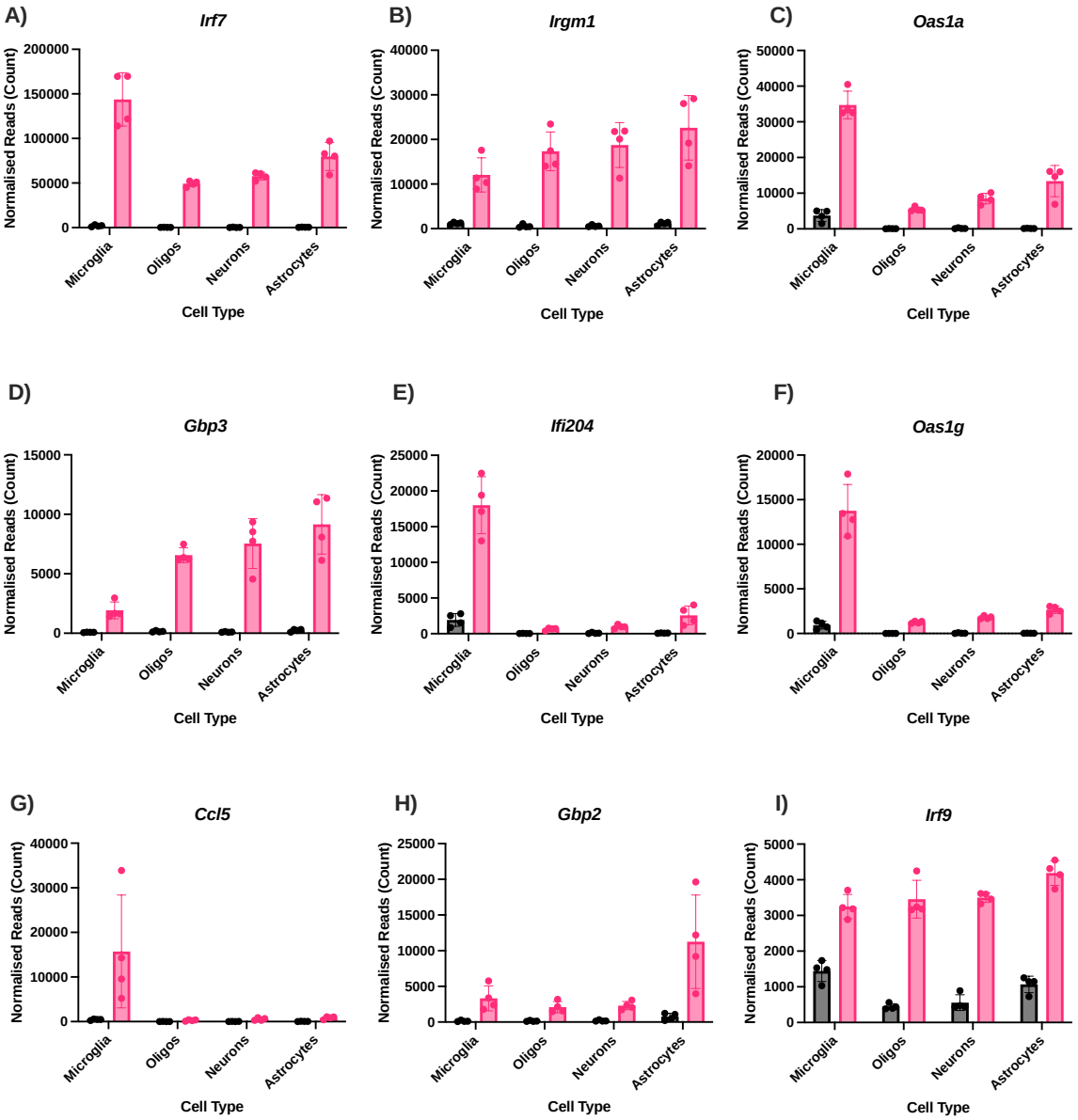


**Figure 8.23: Normalised read counts of top 9 expressed genes in *cell function and metabolism* oligodendrocyte specific KEGG term.** Graphs show normalised number of reads across sorted cell types following treatment with PBS (vehicle) or IFN-β in pathways found to be enriched in specifically sorted oligodendrocytes, with top 9 genes identified through having the greatest mean number of normalised read counts across all sorted cell types and treatment regimens. A) *Irf7*, B) *Irgm1*, C) *Oas1a*, D) *Gbp3*, E) *Ifi204*, F) *Oas1g*, G) *Ccl5*, H) *Gbp2*, I) *Irf9*. Bars represent mean ± SD. n=4.

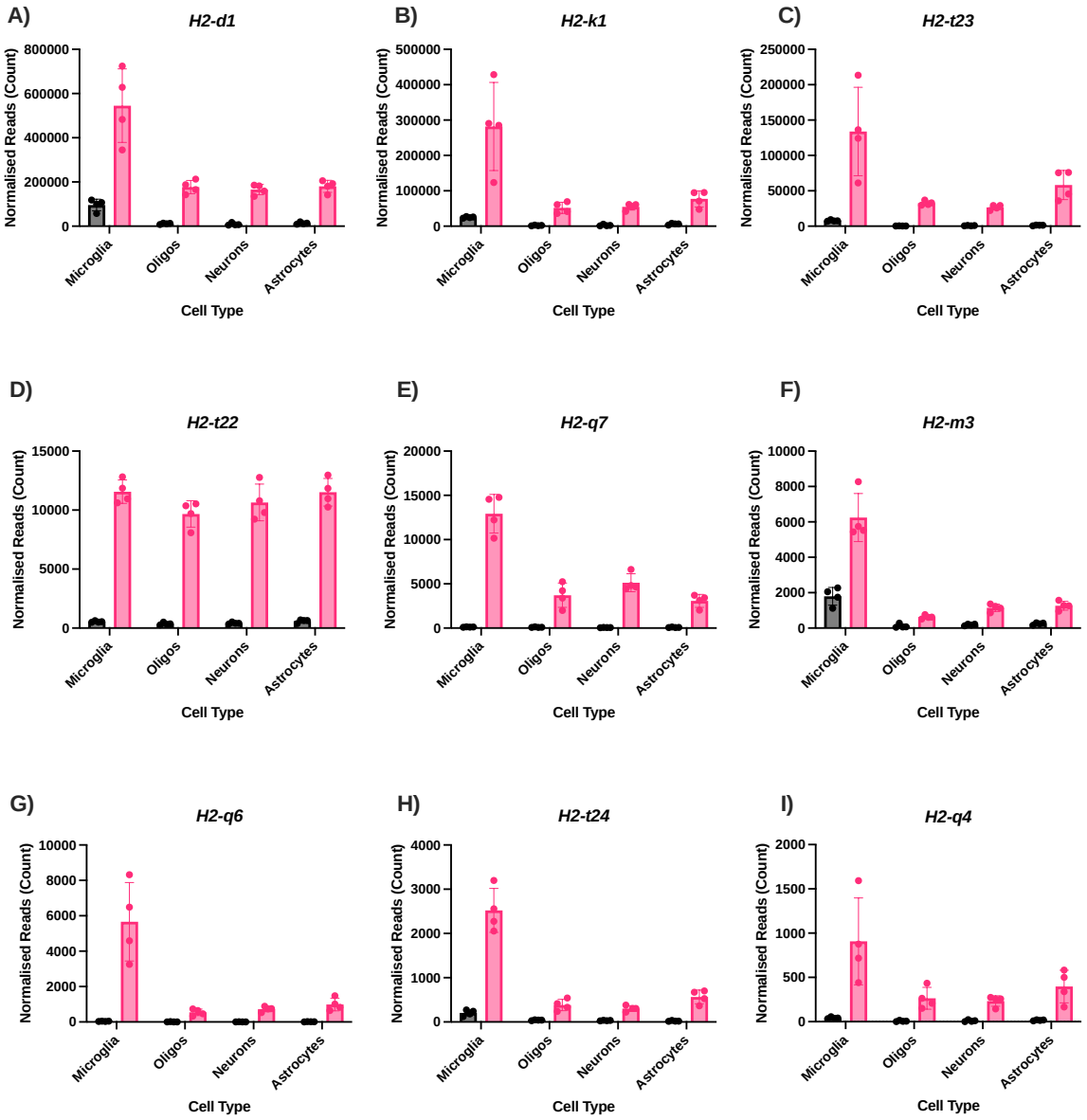


**Figure 8.24: Normalised read counts of top 9 expressed genes in *Transplant rejection* oligodendrocyte specific KEGG term.** Graphs show normalised number of reads across sorted cell types following treatment with PBS (vehicle) or IFN-β in pathways found to be enriched in specifically sorted oligodendrocytes, with top 9 genes identified through having the greatest mean number of normalised read counts across all sorted cell types and treatment regimens. A) *H2-d1*, B) *H2-k1*, C) *H2-t23*, D) *H2-t22*, E) *H2-q7*, F) *H2-m3*, G) *H2-q6*, H) *H2-t24*, I) *H2-q4*. Bars represent mean ± SD. n=4.

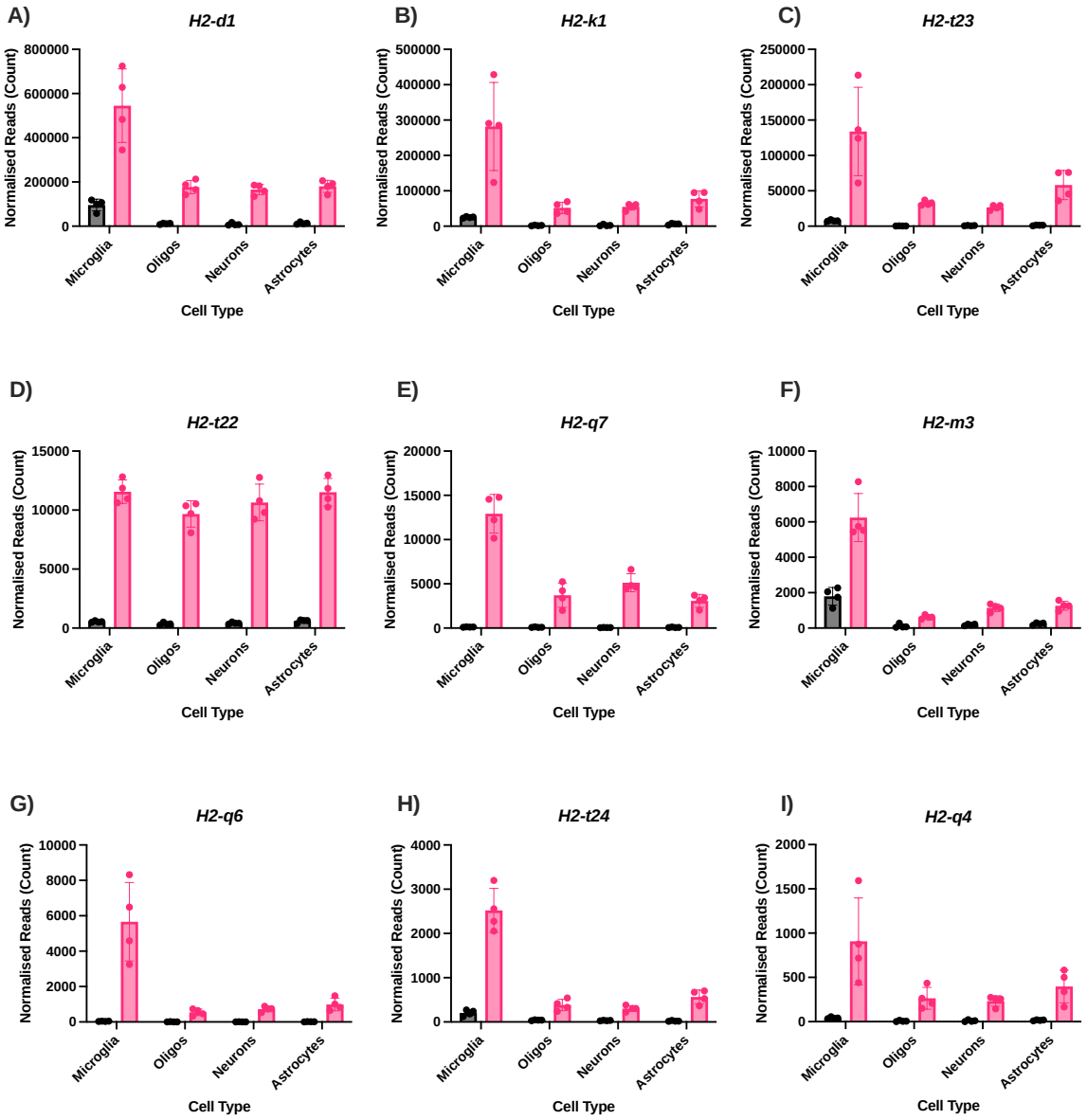


**Figure 8.25: Normalised read counts of top 9 expressed genes in *Autoimmune disease* oligodendrocyte specific KEGG term.** Graphs show normalised number of reads across sorted cell types following treatment with PBS (vehicle) or IFN-β in pathways found to be enriched in specifically sorted oligodendrocytes, with top 9 genes identified through having the greatest mean number of normalised read counts across all sorted cell types and treatment regimens. A) *H2-d1*, B) *H2-k1*, C) *H2-t23*, D) *H2-t22*, E) *H2-q7*, F) *H2-m3*, G) *H2-q6*, H) *H2-t24*, I) *H2-q4*. Bars represent mean ± SD. n=4.

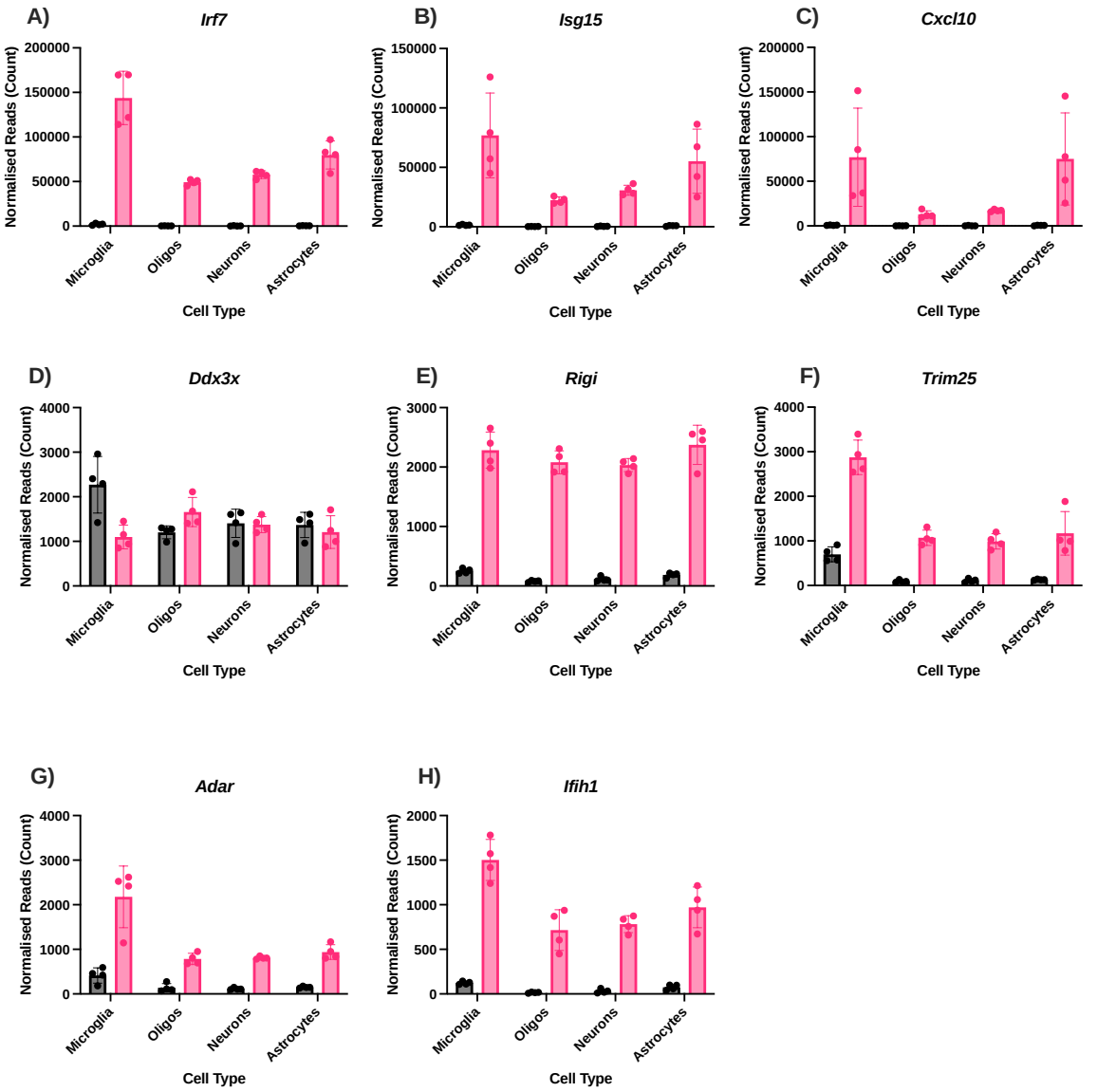


**Figure 8.26: Normalised read counts all expressed genes in *Cell response to PAMPs* oligodendrocyte specific KEGG term.** Graphs show normalised number of reads across sorted cell types following treatment with PBS (vehicle) or IFN-β in pathways found to be enriched in specifically sorted oligodendrocytes. A) *Irf7*, B) *Isg15*, C) *Cxcl10*, D) *Ddx3x*, E) *Rigi*, F) *Trim25*, G) *Adar*, H) *Ifih*. Bars represent mean ± SD. n=4.

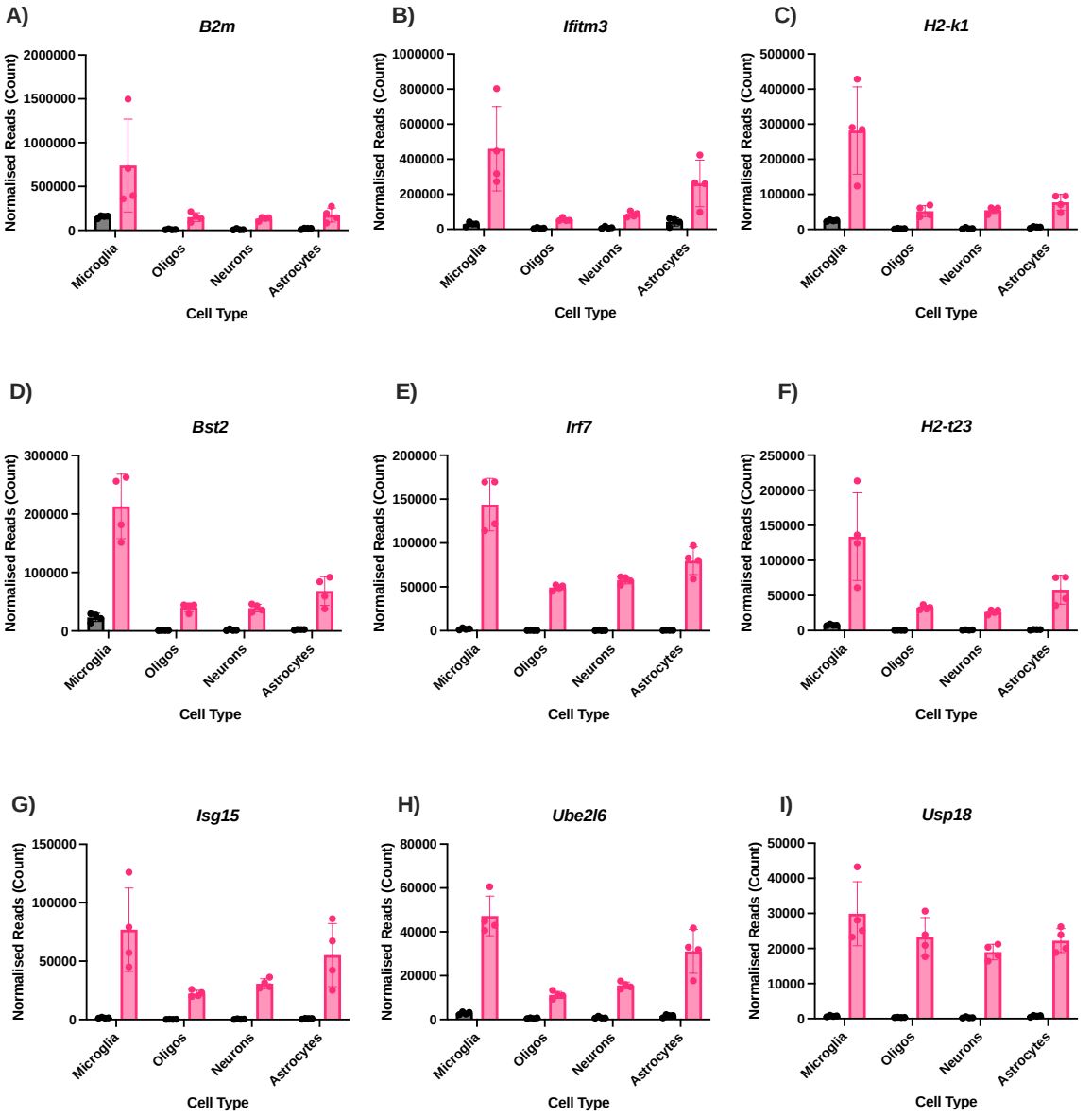


**Figure 8.27: Normalised read counts of top 9 expressed genes in *General immune response* oligodendrocyte specific Reactome term.** Graphs show normalised number of reads across sorted cell types following treatment with PBS (vehicle) or IFN-β in pathways found to be enriched in specifically sorted oligodendrocytes, with top 9 genes identified through having the greatest mean number of normalised read counts across all sorted cell types and treatment regimens. A) *B2m*, B) *Ifitm3*, C) *H2-k1*, D) *Bst2*, E) *Irf7*, F) *H2-t23*, G) *Isg15*, H) *Ube2l6*, I) *Usp18*. Bars represent mean ± SD. n=4.

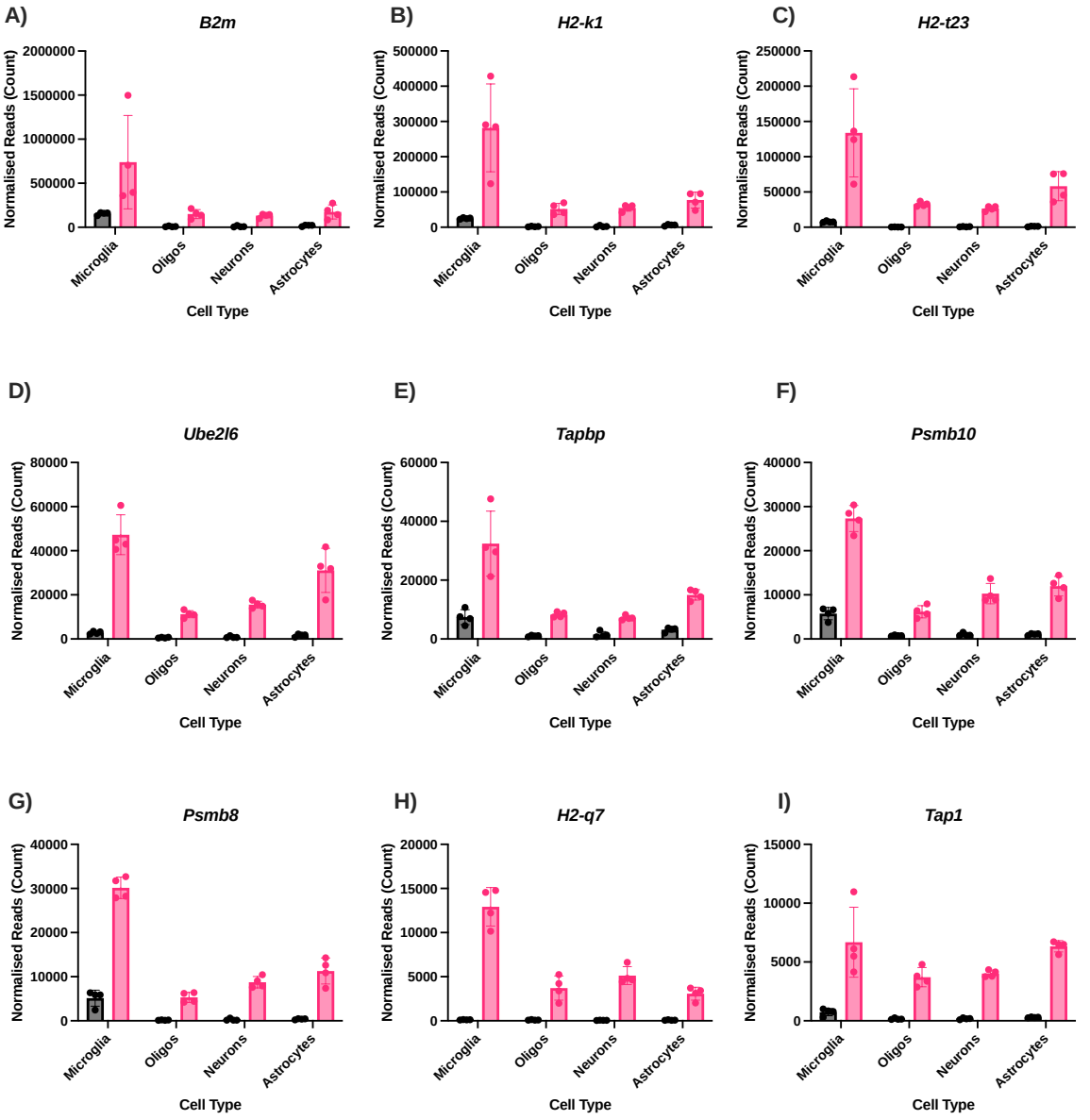


**Figure 8.28: Normalised read counts of top 9 expressed genes in *Antigen processing / presentation* oligodendrocyte specific Reactome term.** Graphs show normalised number of reads across sorted cell types following treatment with PBS (vehicle) or IFN-β in pathways found to be enriched in specifically sorted oligodendrocytes, with top 9 genes identified through having the greatest mean number of normalised read counts across all sorted cell types and treatment regimens. A) *B2m*, B) *H2-k1*, C) *H2-t23,* D) *Ube2l6*, E) *Tapbp*, F) *Psmb10*, G) *Psmb8*, H) *H2-q7*, I) *Tap1*. Bars represent mean ± SD. n=4.

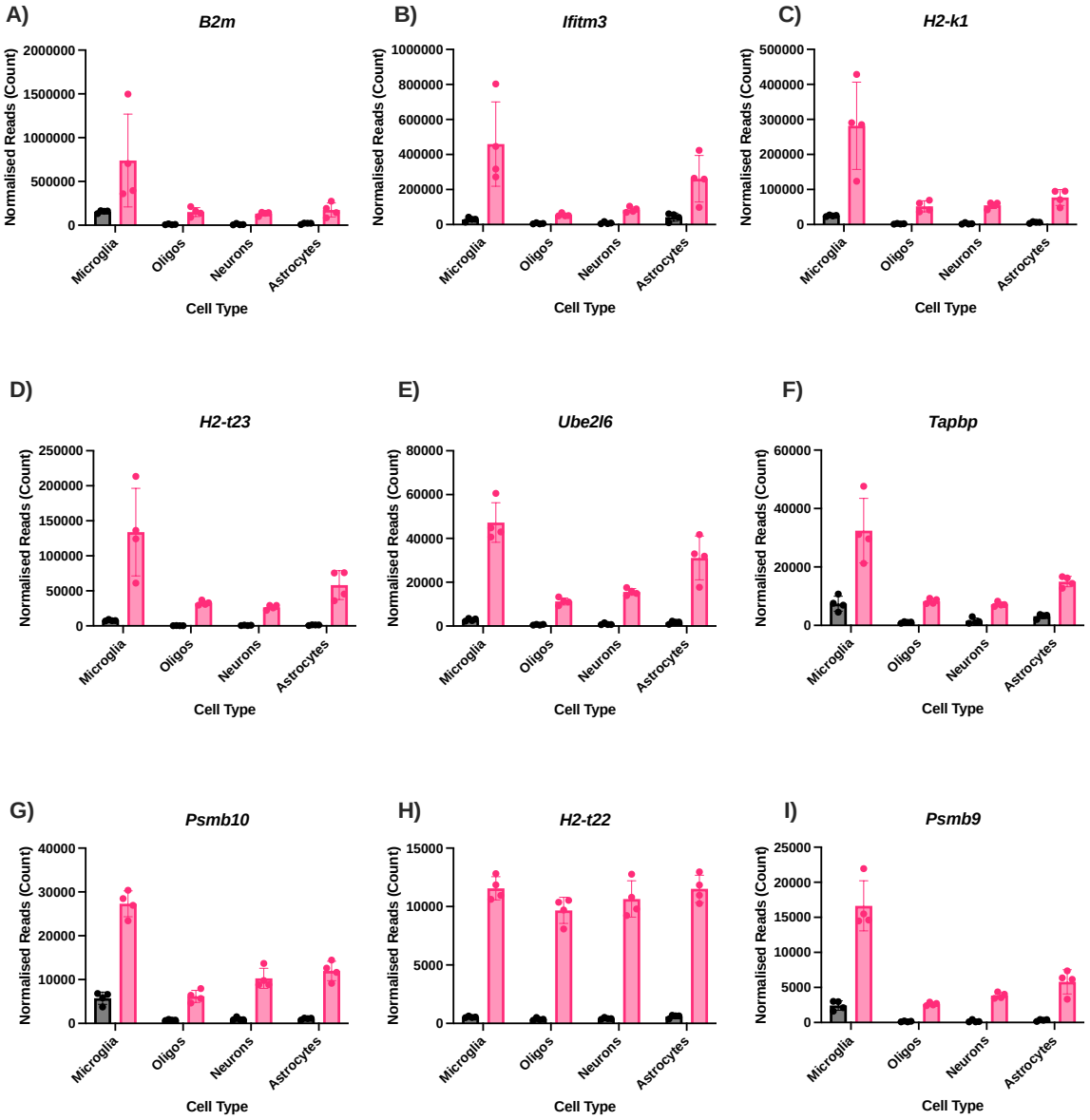


**Figure 8.29: Normalised read counts of top 9 expressed genes in *Interferon response* oligodendrocyte specific Reactome term.** Graphs show normalised number of reads across sorted cell types following treatment with PBS (vehicle) or IFN-β in pathways found to be enriched in specifically sorted oligodendrocytes, with top 9 genes identified through having the greatest mean number of normalised read counts across all sorted cell types and treatment regimens. A) *B2m*, B) *Ifitm3*, C) *H2-k1*, D) *H2-t23*, E) *Ube2l6*, F) *Tapbp*, G) *Psmb10*, H) *H2-t22*, I) *Psmb9*. Bars represent mean ± SD. n=4.

## 8.5 List of genes and annotation terms associated with each cluster identified in functional annotation cluster analysis of oligodendrocytes

**Table 8.18 Functional annotation clustering analysis, cluster 1, innate immunity**

| **Annotation Cluster 1** | **Enrichment Score: 48.15** | | |
|---|---|---|---|
| **Database** | **Term** | **Count** | ***p.adj* Value** |
| UP_KW_BIOLOGICAL_PROCESS | Immunity | 71 | 1.71E-54 |
| GOTERM_BP_DIRECT | Immune system process | 61 | 1.78E-51 |
| UP_KW_BIOLOGICAL_PROCESS | Innate immunity | 55 | 7.28E-49 |
| GOTERM_BP_DIRECT | Innate immune response | 58 | 1.05E-40 |

| **Gene Symbol** | **Gene Name** |
|---|---|
| *Acod1* | Aconitate Decarboxylase 1 |
| *Adar* | Adenosine Deaminase, RNA-Specific |
| *B2m* | Beta-2 Microglobulin |
| *Bst2* | Bone Marrow Stromal Cell Antigen 2 |
| *CD274* | CD274 Antigen |
| *Dhx58* | Dexh (Asp-Glu-X-His) Box Polypeptide 58 |
| *Dtx3l* | Deltex 3-Like, E3 Ubiquitin Ligase |
| *Eif2ak2* | Eukaryotic Translation Initiation Factor 2-Alpha Kinase 2 |
| *Erap1* | Endoplasmic Reticulum Aminopeptidase 1 |
| *Gbp2* | Guanylate Binding Protein 2 |
| *Gbp3* | Guanylate Binding Protein 3 |
| *Gbp4* | Guanylate Binding Protein 3 |
| *Gbp5* | Guanylate Binding Protein 5 |
| *Gbp6* | Guanylate Binding Protein 6 |
| *Gbp7* | Guanylate Binding Protein 7 |
| *Gm12250* | #N/A |
| *Gsdmd* | Gasdermin D |
| *H2-aa* | Histocompatibility 2, Class Ii Antigen A, Alpha |
| *H2-d1* | Histocompatibility 2, D Region Locus 1 |
| *H2-k1* | Histocompatibility 2, K1, K Region |
| *H2-q7* | Histocompatibility 2, Q Region Locus 7 |
| *H2-t23* | Histocompatibility 2, T Region Locus 23 |
| *Herc6* | Hect Domain And Rld 6 |
| *Ifi204* | Interferon Activated Gene 204 |
| *Ifi35* | Interferon-Induced Protein 35 |
| *Ifih1* | Interferon Induced With Helicase C Domain 1 |

***Continued overleaf***

| | |
|---|---|
| *Ifit1* | Interferon-Induced Protein With Tetratricopeptide Repeats 1 |
| *Ifit2* | Interferon-Induced Protein With Tetratricopeptide Repeats 2 |
| *Ifit3* | Interferon-Induced Protein With Tetratricopeptide Repeats 3 |
| *Ifitm3* | Interferon Induced Transmembrane Protein 3 |
| *Igtp* | Interferon Gamma Induced Gtpase |
| *Iigp1* | Interferon Inducible Gtpase 1 |
| *Irf7* | Interferon Regulatory Factor 7 |
| *Irgm1* | Immunity-Related Gtpase Family M Member 1 |
| *Irgm2* | Immunity-Related Gtpase Family M Member 2 |
| *Isg20* | Interferon-Stimulated Protein |
| *Lgals9* | Lectin, Galactose Binding, Soluble 9 |
| *Mx1* | Mx Dynamin-Like Gtpase 1 |
| *Mx2* | Mx Dynamin-Like Gtpase 2 |
| *Nlrc5* | Nlr Family, Card Domain Containing 5 |
| *Nmi* | N-Myc (And Stat) Interactor |
| *Oas1a* | 2'-5' Oligoadenylate Synthetase 1A |
| *Oas1b* | 2'-5' Oligoadenylate Synthetase 1B |
| *Oas1g* | 2'-5' Oligoadenylate Synthetase 1G |
| *Oas2* | 2'-5' Oligoadenylate Synthetase 2 |
| *Oas3* | 2'-5' Oligoadenylate Synthetase 3 |
| *Oasl1* | 2'-5' Oligoadenylate Synthetase-Like 1 |
| *Oasl2* | 2'-5' Oligoadenylate Synthetase-Like 2 |
| *Parp14* | Poly (Adp-Ribose) Polymerase Family, Member 14 |
| *Parp9* | Poly (Adp-Ribose) Polymerase Family, Member 9 |
| *Pml* | Promyelocytic Leukemia |
| *Psmb8* | Proteasome (Prosome, Macropain) Subunit, Beta Type 8 (Large Multifunctional Peptidase 7) |
| *Psmb9* | Proteasome (Prosome, Macropain) Subunit, Beta Type 9 (Large Multifunctional Peptidase 2) |
| *Rigi* | RNA Sensor Rig-I |
| *Rnf135* | Ring Finger Protein 135 |
| *Rnf213* | Ring Finger Protein 213 |
| *Rsad2* | Radical S-Adenosyl Methionine Domain Containing 2 |
| *Slfn2* | Schlafen 2 |
| *Slfn8* | Schlafen 8 |
| *Sp110* | Sp110 Nuclear Body Protein |
| *Tap1* | Transporter 1, ATP-Binding Cassette, Sub-Family B (Mdr/Tap) |
| *Tap2* | Transporter 2, ATP-Binding Cassette, Sub-Family B (Mdr/Tap) |
| *Tgtp1* | T Cell Specific Gtpase 1 |
| *Tgtp2* | T Cell Specific Gtpase 1 |
| *Tlr3* | Toll-Like Receptor 3 |
| *Trim14* | Tripartite Motif-Containing 14 |
| *Trim25* | Tripartite Motif-Containing 25 |
| | ***Continued overleaf*** |

| | |
|---|---|
| *Trim56* | Tripartite Motif-Containing 56 |
| *Zbp1* | Z-Dna Binding Protein 1 |
| *ZchHav1* | Unknown |
| *Znfx1* | Zinc Finger, Nfx1-Type Containing 1 |

**Table 8.18: Functional annotation cluster analysis for sorted oligodendrocytes, cluster 1, innate immunity.** Table showing genes and annotation terms in cluster 1 for sorted oligodendrocytes. “Database” indicates where the annotation term was derived, “Count” is the number of genes associated with the annotation term and *p.adj*-value is the Bonferroni adjusted *p*-value.

**Table 8.19 Functional annotation clustering analysis, cluster 2, GTP binding / protein ubiquitination**

| **Annotation Cluster 2** | **Enrichment Score: 13.59** | | |
|---|---|---|---|
| **Database** | **Term** | **Count** | ***p.adj* Value** |
| UP_SEQ_FEATURE | IRG-type G | 13 | 1.36E-21 |
| INTERPRO | Interferon-inducible GTPase | 11 | 5.82E-18 |
| GOTERM_BP_DIRECT | Defense response | 19 | 4.49E-17 |
| GOTERM_MF_DIRECT | GTPase activity | 22 | 1.20E-12 |
| GOTERM_MF_DIRECT | GTP binding | 23 | 4.40E-12 |
| GOTERM_CC_DIRECT | Endoplasmic reticulum membrane | 21 | 1.35E-04 |

| **Gene Symbol** | **Gene Name** |
|---|---|
| *9930111j21rik2* | RIKEN cDNA 9930111J21 Gene 2 |
| *Bc023105* | #N/A |
| *F830016b08rik* | RIKEN cDNA F830016B08 Gene |
| *Gbp10* | Guanylate-Binding Protein 10 |
| *Gbp2* | Guanylate Binding Protein 2 |
| *Gbp3* | Guanylate Binding Protein 3 |
| *Gbp4* | Guanylate Binding Protein 3 |
| *Gbp5* | Guanylate Binding Protein 5 |
| *Gbp6* | Guanylate Binding Protein 6 |
| *Gbp7* | Guanylate Binding Protein 7 |
| *Gbp8* | Guanylate-Binding Protein 8 |
| *Gbp9* | Guanylate-Binding Protein 9 |
| *Gm12185* | Predicted Gene 12185 |
| *Gm4841* | Predicted Gene 4841 |
| *Ifi47* | Interferon Gamma Inducible Protein 47 |
| *Igtp* | Interferon Gamma Induced Gtpase |
| *Iigp1* | Interferon Inducible Gtpase 1 |
| *Irgm1* | Immunity-Related Gtpase Family M Member 1 |
| *Mx1* | Mx Dynamin-Like Gtpase 1 |
| *Mx2* | Mx Dynamin-Like Gtpase 2 |
| *Rigi* | RNA Sensor Rig-I |
| *Tgtp1* | T Cell Specific Gtpase 1 |
| *Tgtp2* | T Cell Specific Gtpase 1 |

**Table 8.19: Functional annotation cluster analysis for sorted oligodendrocytes, cluster 2, GTP binding.** Table showing genes and annotation terms in cluster 2 for sorted oligodendrocytes. “Database” indicates where the annotation term was derived, “Count” is the number of genes associated with the annotation term and *p.adj*-value is the Bonferroni adjusted *p*-value.

**Table 8.20 Functional annotation clustering analysis, cluster 3, antigen presentation**

| **Annotation Cluster 3** | **Enrichment Score: 8.19** | | |
|---|---|---|---|
| **Database** | **Term** | **Count** | ***p.adj* Value** |
| KEGG_PATHWAY | Epstein-Barr virus infection | 29 | 1.25E-24 |
| KEGG_PATHWAY | Herpes simplex virus 1 infection | 33 | 9.47E-21 |
| GOTERM_BP_DIRECT | Positive regulation of T cell mediated cytotoxicity | 14 | 1.83E-15 |
| KEGG_PATHWAY | Antigen processing and presentation | 16 | 1.85E-15 |
| GOTERM_BP_DIRECT | Positive regulation of tumor necrosis factor production | 18 | 2.28E-15 |
| GOTERM_MF_DIRECT | TAP2 binding | 11 | 1.51E-14 |
| GOTERM_MF_DIRECT | Peptide antigen binding | 15 | 1.99E-14 |
| UP_SEQ_FEATURE | MHC class I-like antigen recognition-like | 10 | 2.04E-14 |
| GOTERM_MF_DIRECT | TAP1 binding | 11 | 2.32E-14 |
| GOTERM_CC_DIRECT | MHC class I protein complex | 11 | 3.21E-14 |
| INTERPRO | MHC class I, alpha chain, alpha1/alpha2 | 12 | 5.97E-14 |
| GOTERM_BP_DIRECT | Antigen processing and presentation of endogenous peptide antigen via MHC class Ib | 12 | 7.36E-14 |
| GOTERM_BP_DIRECT | Defense response to Gram-positive bacterium | 19 | 1.17E-13 |
| INTERPRO | MHC class I-like antigen recognition | 12 | 1.28E-13 |
| GOTERM_MF_DIRECT | MHC class I protein binding | 12 | 2.21E-13 |
| GOTERM_BP_DIRECT | Protection from natural killer cell mediated cytotoxicity | 11 | 2.67E-13 |
| GOTERM_BP_DIRECT | Antigen processing and presentation of exogenous peptide antigen via MHC class Ib | 10 | 4.99E-13 |
| INTERPRO | MHC classes I/II-like antigen recognition protein | 13 | 5.11E-13 |
| INTERPRO | Immunoglobulin C1-set | 15 | 5.18E-13 |
| INTERPRO | Immunoglobulin/major histocompatibility complex, conserved site | 14 | 9.35E-13 |
| GOTERM_CC_DIRECT | MHC class Ib protein complex | 10 | 9.63E-13 |
| GOTERM_CC_DIRECT | MHC class I peptide loading complex | 9 | 1.01E-12 |
| GOTERM_MF_DIRECT | T cell receptor binding | 11 | 1.04E-12 |
| GOTERM_BP_DIRECT | Antigen processing and presentation of endogenous peptide antigen via MHC class I via ER pathway, TAP-independent | 11 | 1.81E-12 |
| GOTERM_MF_DIRECT | Beta-2-microglobulin binding | 10 | 4.18E-12 |
| | ***Continued overleaf*** | | |

| | | | |
|---|---|---|---|
| KEGG_PATHWAY | Allograft rejection | 12 | 7.75E-12 |
| KEGG_PATHWAY | Graft-versus-host disease | 12 | 7.75E-12 |
| GOTERM_MF_DIRECT | Natural killer cell lectin-like receptor binding | 11 | 7.94E-12 |
| GOTERM_BP_DIRECT | Positive regulation of antibody-dependent cellular cytotoxicity | 9 | 2.16E-11 |
| GOTERM_BP_DIRECT | Regulation of natural killer cell mediated immunity | 9 | 2.16E-11 |
| GOTERM_BP_DIRECT | Positive regulation of CD8-positive, alpha-beta T cell activation | 9 | 2.16E-11 |
| KEGG_PATHWAY | Type I diabetes mellitus | 12 | 2.59E-11 |
| GOTERM_BP_DIRECT | Natural killer cell tolerance induction | 9 | 3.05E-11 |
| GOTERM_BP_DIRECT | Positive regulation of TRAIL production | 9 | 3.05E-11 |
| SMART | IGc1 | 14 | 3.54E-11 |
| KEGG_PATHWAY | Human immunodeficiency virus 1 infection | 18 | 3.60E-11 |
| GOTERM_BP_DIRECT | Positive regulation of natural killer cell mediated immunity | 9 | 4.24E-11 |
| GOTERM_BP_DIRECT | Immune response | 24 | 4.45E-11 |
| KEGG_PATHWAY | Human papillomavirus infection | 21 | 4.92E-11 |
| GOTERM_MF_DIRECT | CD8 receptor binding | 9 | 5.65E-11 |
| GOTERM_BP_DIRECT | Positive regulation of CD8-positive, alpha-beta T cell proliferation | 9 | 5.81E-11 |
| KEGG_PATHWAY | Autoimmune thyroid disease | 12 | 1.01E-10 |
| KEGG_PATHWAY | Kaposi sarcoma-associated herpesvirus infection | 17 | 1.29E-10 |
| GOTERM_BP_DIRECT | Positive regulation of natural killer cell cytokine production | 9 | 1.40E-10 |
| GOTERM_BP_DIRECT | CD8-positive, alpha-beta T cell activation | 9 | 1.40E-10 |
| GOTERM_BP_DIRECT | Negative regulation of natural killer cell mediated cytotoxicity | 9 | 3.06E-10 |
| KEGG_PATHWAY | Viral myocarditis | 12 | 3.35E-10 |
| GOTERM_BP_DIRECT | Positive regulation of natural killer cell proliferation | 9 | 6.23E-10 |
| KEGG_PATHWAY | Human cytomegalovirus infection | 17 | 9.35E-10 |
| GOTERM_BP_DIRECT | Positive regulation of interleukin-13 production | 9 | 1.19E-09 |
| GOTERM_BP_DIRECT | Positive regulation of natural killer cell mediated cytotoxicity | 10 | 1.25E-09 |
| GOTERM_CC_DIRECT | Cis-Golgi network membrane | 8 | 5.34E-09 |
| UP_SEQ_FEATURE | Ig-like C1-type | 8 | 7.81E-09 |
| KEGG_PATHWAY | Phagosome | 14 | 8.38E-09 |
| GOTERM_BP_DIRECT | Positive regulation of interleukin-4 production | 9 | 8.70E-09 |
| | ***Continued overleaf*** | | |
| | | 15 | 1.57E-08 |

| | | | |
|---|---|---|---|
| KEGG_PATHWAY | Viral carcinogenesis | | |
| GOTERM_BP_DIRECT | Positive regulation of immunoglobulin production | 9 | 1.60E-08 |
| xz | Human T-cell leukemia virus 1 infection | 15 | 4.77E-08 |
| KEGG_PATHWAY | Cell adhesion molecules | 13 | 8.06E-08 |
| UP_SEQ_FEATURE | Alpha-1 | 6 | 1.45E-07 |
| UP_SEQ_FEATURE | Alpha-2 | 6 | 1.45E-07 |
| GOTERM_BP_DIRECT | Adaptive immune response | 15 | 1.86E-07 |
| GOTERM_CC_DIRECT | Early endosome membrane | 12 | 2.76E-07 |
| GOTERM_CC_DIRECT | Phagocytic vesicle membrane | 8 | 4.00E-07 |
| GOTERM_BP_DIRECT | Antibacterial humoral response | 10 | 8.85E-07 |
| GOTERM_MF_DIRECT | 14-3-3 protein binding | 8 | 9.13E-07 |
| UP_KW_CELLULAR_ COMPONENT | MHC I | 5 | 1.30E-06 |
| GOTERM_MF_DIRECT | TAP binding | 5 | 1.79E-06 |
| GOTERM_BP_DIRECT | Antigen processing and presentation of peptide antigen via MHC class I | 5 | 1.96E-06 |
| UP_SEQ_FEATURE | Alpha-3 | 5 | 2.27E-06 |
| GOTERM_CC_DIRECT | Lysosomal membrane | 13 | 3.54E-06 |
| KEGG_PATHWAY | Cellular senescence | 11 | 6.08E-06 |
| UP_SEQ_FEATURE | Connecting peptide | 6 | 9.00E-06 |
| GOTERM_BP_DIRECT | T cell mediated cytotoxicity | 5 | 2.23E-05 |
| KEGG_PATHWAY | Endocytosis | 12 | 3.33E-05 |
| GOTERM_CC_DIRECT | Golgi medial cisteRNA | 5 | 5.19E-05 |
| GOTERM_CC_DIRECT | ExteRNAl side of plasma membrane | 18 | 8.77E-05 |

| **Gene Symbol** | **Gene Name** |
|---|---|
| *B2m* | Beta-2 Microglobulin |
| *Bst2* | Bone Marrow Stromal Cell Antigen 2 |
| *Ccl5* | Chemokine (C-C Motif) Ligand 5 |
| *Eif2ak2* | Eukaryotic Translation Initiation Factor 2-Alpha Kinase 2 |
| *H2-aa* | Histocompatibility 2, Class Ii Antigen A, Alpha |
| *H2-d1* | Histocompatibility 2, D Region Locus 1 |
| *H2-k1* | Histocompatibility 2, K1, K Region |
| *H2-m3* | Histocompatibility 2, M Region Locus 3 |
| *H2-q4* | Histocompatibility 2, Q Region Locus 4 |
| *H2-q6* | Histocompatibility 2, Q Region Locus 6 |
| *H2-q7* | Histocompatibility 2, Q Region Locus 7 |
| *H2-t-ps* | Histocompatibility 2, T Region Locus, Pseudogene |
| *H2-t10* | #N/A |
| *H2-t22* | Histocompatibility 2, T Region Locus 22 |
| *H2-t23* | Histocompatibility 2, T Region Locus 23 |
| *H2-t24* | Histocompatibility 2, T Region Locus 24 |
| | ***Continued overleaf*** |

| | |
|---|---|
| *Ifih1* | Interferon Induced With Helicase C Domain 1 |
| *Irf7* | Interferon Regulatory Factor 7 |
| *Irf9* | Interferon Regulatory Factor 9 |
| *Oas1a* | 2'-5' Oligoadenylate Synthetase 1A |
| *Oas1b* | 2'-5' Oligoadenylate Synthetase 1B |
| *Oas1g* | 2'-5' Oligoadenylate Synthetase 1G |
| *Oas2* | 2'-5' Oligoadenylate Synthetase 2 |
| *Oas3* | 2'-5' Oligoadenylate Synthetase 3 |
| *Pml* | Promyelocytic Leukemia |
| *Rigi* | RNA Sensor Rig-I |
| *Sp100* | Nuclear Antigen Sp100 |
| *Stat1* | Signal Transducer And Activator Of Transcription 1 |
| *Stat2* | Signal Transducer And Activator Of Transcription 2 |
| *Tap1* | Transporter 1, ATP-Binding Cassette, Sub-Family B (Mdr/Tap) |
| *Tap2* | Transporter 2, ATP-Binding Cassette, Sub-Family B (Mdr/Tap) |
| *Tapbp* | Tap Binding Protein |
| *Tlr3* | Toll-Like Receptor 3 |

**Table 8.20: Functional annotation cluster analysis for sorted oligodendrocytes, cluster 3, antigen presentation.** Table showing genes and annotation terms in cluster 3 for sorted oligodendrocytes. “Database” indicates where the annotation term was derived, “Count” is the number of genes associated with the annotation term and *p.adj*-value is the Bonferroni adjusted *p*-value.

**Table 8.21 Functional annotation clustering analysis, cluster 4, cytosol based processes**

| **Annotation Cluster 4** | **Enrichment Score: 8.51** | | |
|---|---|---|---|
| **Database** | **Term** | **Count** | ***p.adj* Value** |
| GOTERM_CC_DIRECT | Cytosol | 79 | 1.61E-13 |
| UP_KW_CELLULAR_COMPONENT | Cytoplasm | 72 | 3.44E-07 |
| GOTERM_CC_DIRECT | Cytoplasm | 93 | 4.96E-07 |

| **Gene Symbol** | **Gene Name** |
|---|---|
| *Adar* | Adenosine Deaminase, RNA-Specific |
| *Bst2* | Bone Marrow Stromal Cell Antigen 2 |
| *Ccl5* | Chemokine (C-C Motif) Ligand 5 |
| *Cmpk2* | Cytidine Monophosphate (Ump-Cmp) Kinase 2, Mitochondrial |
| *Ddx60* | Dexd/H Box Helicase 60 |
| *Dhx58* | Dexh (Asp-Glu-X-His) Box Polypeptide 58 |
| *Drd4* | Dopamine Receptor D4 |
| *Dtx3l* | Deltex 3-Like, E3 Ubiquitin Ligase |
| *Eif2ak2* | Eukaryotic Translation Initiation Factor 2-Alpha Kinase 2 |
| *Erap1* | Endoplasmic Reticulum Aminopeptidase 1 |
| *Gbp2* | Guanylate Binding Protein 2 |
| *Gbp3* | Guanylate Binding Protein 3 |
| *Gbp5* | Guanylate Binding Protein 5 |
| *Gsdmd* | Gasdermin D |
| *Helz2* | Helicase With Zinc Finger 2, Transcriptional Coactivator |
| *Herc6* | Hect Domain And Rld 6 |
| *Ifi203* | Interferon Activated Gene 203 |
| *Ifi204* | Interferon Activated Gene 204 |
| *Ifi206* | Interferon Activated Gene 206 |
| *Ifi208* | Interferon Activated Gene 208 |
| *Ifi209* | Interferon Activated Gene 209 |
| *Ifi211* | Interferon Activated Gene 211 |
| *Ifi213* | Interferon Activated Gene 213 |
| *Ifi35* | Interferon-Induced Protein 35 |
| *Ifi44* | Interferon-Induced Protein 44 |
| *Ifih1* | Interferon Induced With Helicase C Domain 1 |
| *Ifit1* | Interferon-Induced Protein With Tetratricopeptide Repeats 1 |
| *Ifit1bl1* | Interferon Induced Protein With Tetratricopeptide Repeats 1BL1 |
| *Ifit1bl2* | Interferon Induced Protein With Tetratricopeptide Repeats 1BL2 |
| *Ifit2* | Interferon-Induced Protein With Tetratricopeptide Repeats 2 |
| *Ifit3* | Interferon-Induced Protein With Tetratricopeptide Repeats 3 |
| *Ifit3b* | Interferon-Induced Protein With Tetratricopeptide Repeats 3B |
| *Ifitm3* | Interferon Induced Transmembrane Protein 3 |
| | ***Continued overleaf*** |

| | |
|---|---|
| *Iigp1* | Interferon Inducible Gtpase 1 |
| *Il10ra* | Interleukin 10 Receptor, Alpha |
| *Irf7* | Interferon Regulatory Factor 7 |
| *Isg15* | Isg15 Ubiquitin-Like Modifier |
| *Isg20* | Interferon-Stimulated Protein |
| *Lck* | Lymphocyte Protein Tyrosine Kinase |
| *Lgals9* | Lectin, Galactose Binding, Soluble 9 |
| *Mlkl* | Mixed Lineage Kinase Domain-Like |
| *Mndal* | Myeloid Nuclear Differentiation Antigen Like |
| *Mov10* | Mov10 Risc Complex RNA Helicase |
| *Mx1* | #N/A |
| *Mx2* | Mx Dynamin-Like Gtpase 2 |
| *Nlrc5* | Nlr Family, Card Domain Containing 5 |
| *Nmi* | N-Myc (And Stat) Interactor |
| *Oas1a* | 2'-5' Oligoadenylate Synthetase 1A |
| *Oas1b* | 2'-5' Oligoadenylate Synthetase 1B |
| *Oas1g* | 2'-5' Oligoadenylate Synthetase 1G |
| *Oas2* | 2'-5' Oligoadenylate Synthetase 2 |
| *Oas3* | 2'-5' Oligoadenylate Synthetase 3 |
| *Oasl1* | 2'-5' Oligoadenylate Synthetase-Like 1 |
| *Ogfr* | Opioid Growth Factor Receptor |
| *Parp10* | Poly (Adp-Ribose) Polymerase Family, Member 10 |
| *Parp14* | Poly (Adp-Ribose) Polymerase Family, Member 14 |
| *Parp9* | Poly (Adp-Ribose) Polymerase Family, Member 9 |
| *Piwil4* | Piwi-Like RNA-Mediated Gene Silencing 4 |
| *Pml* | Promyelocytic Leukemia |
| *Pnpt1* | Polyribonucleotide Nucleotidyltransferase 1 |
| *Psmb10* | Proteasome (Prosome, Macropain) Subunit, Beta Type 10 |
| *Psmb8* | Proteasome (Prosome, Macropain) Subunit, Beta Type 8 (Large ifunctional Peptidase 7) |
| *Psmb9* | Proteasome (Prosome, Macropain) Subunit, Beta Type 9 (Large ifunctional Peptidase 2) |
| *Rigi* | RNA Sensor Rig-I |
| *Rnf135* | Ring Finger Protein 135 |
| *Rnf213* | Ring Finger Protein 213 |
| *Rtp4* | Receptor Transporter Protein 4 |
| *Samd9l* | Sterile Alpha Motif Domain Containing 9-Like |
| *Slfn2* | Schlafen 2 |
| *Slfn8* | Schlafen 8 |
| *Slfn9* | Schlafen 9 |
| *Sp100* | Nuclear Antigen Sp100 |
| *Stat1* | Signal Transducer And Activator Of Transcription 1 |
| *Stat2* | Signal Transducer And Activator Of Transcription 2 |

***Continued overleaf***

| | |
|---|---|
| *Tent5a* | Terminal Nucleotidyltransferase 5A |
| *Tlr3* | Toll-Like Receptor 3 |
| *Tnfaip8l3* | Tumor Necrosis Factor, Alpha-Induced Protein 8-Like 3 |
| *Tor3A* | Torsin Family 3, Member A |
| *Trim12a* | Tripartite Motif-Containing 12A |
| *Trim12c* | Tripartite Motif-Containing 12C |
| *Trim14* | Tripartite Motif-Containing 14 |
| *Trim21* | Tripartite Motif-Containing 21 |
| *Trim25* | Tripartite Motif-Containing 25 |
| *Trim30a* | Tripartite Motif-Containing 30A |
| *Trim30c* | Tripartite Motif-Containing 30C |
| *Trim30d* | Tripartite Motif-Containing 30D |
| *Trim34a* | Tripartite Motif-Containing 34A |
| *Trim56* | Tripartite Motif-Containing 56 |
| *Uba7* | Ubiquitin-Like Modifier Activating Enzyme 7 |
| *Xaf1* | Xiap Associated Factor 1 |
| *Zbp1* | Z-Dna Binding Protein 1 |
| *Zc3Hav1* | Zinc Finger Ccch Type, Antiviral 1 |
| *Znfx1* | Zinc Finger, Nfx1-Type Containing 1 |

**Table 8.21: Functional annotation cluster analysis for sorted oligodendrocytes, cluster 4, cytosol.** Table showing genes and annotation terms in cluster 4 for sorted oligodendrocytes. “Database” indicates where the annotation term was derived, “Count” is the number of genes associated with the annotation term and *p.adj*-value is the Bonferroni adjusted *p*-value.

## 8.6 Normalised reads of oligodendrocyte specific genes across all cell types

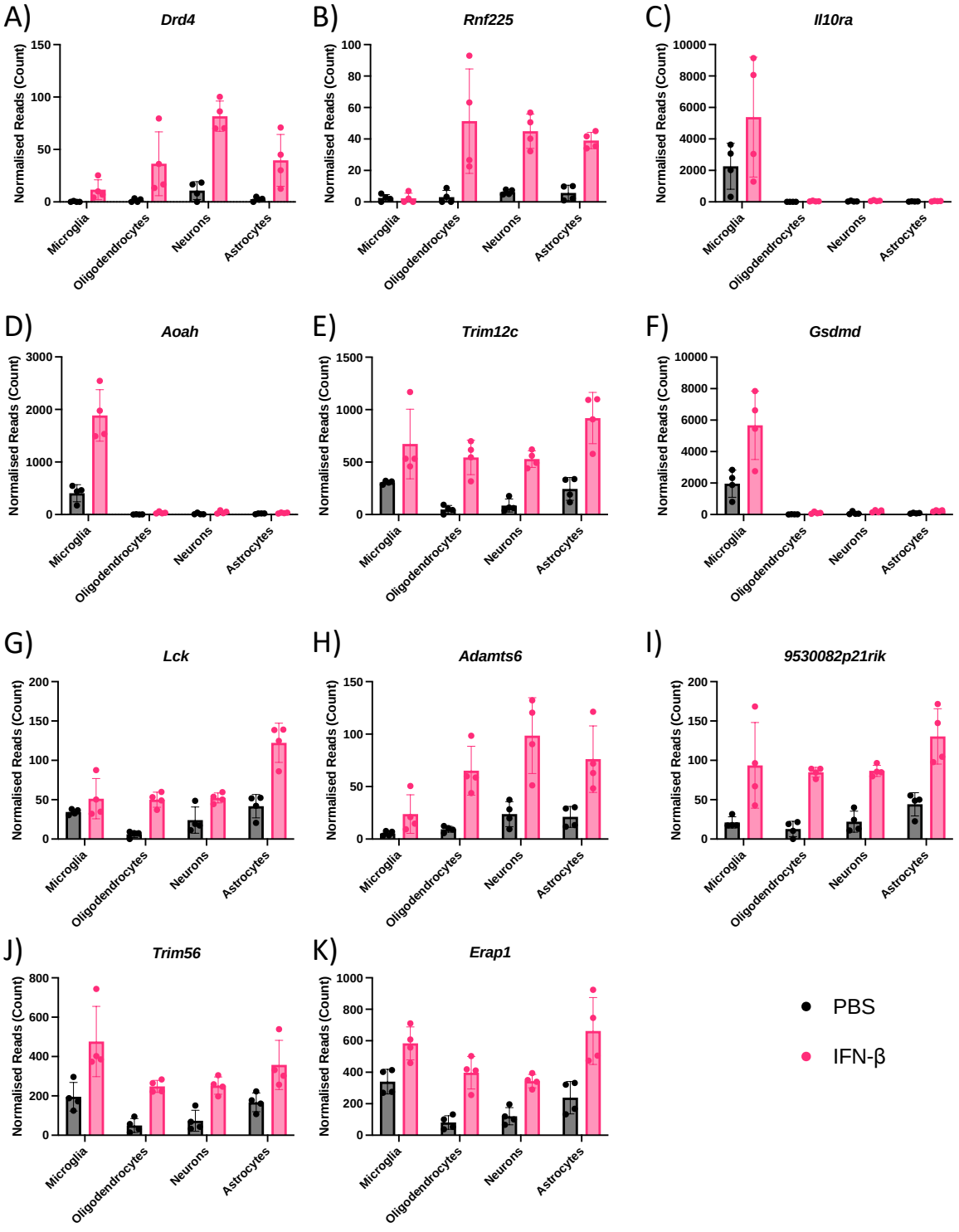


**Figure 8.30: Expression of oligodendrocyte-specific genes in all sorted cells types.** Graphs show gene expression normalised number of reads across sorted cell types. A) *Drd4*, B) *Rnf225*, C) *Il10ra*, D) *Aoah*, E) *Trim12c*, F) *Gsdmd*, G) *Lck*, H) *Adamts6*, I)*9530082p21rik*, J) *Trim56*, K) *Erap1*. Bars represent mean ± SD. n=4.

## 8.7 Gamble et al. 2023

**TITLE:** Establishing mixed neuronal and glial cell cultures from embryonic mouse brains to study infection and innate immunity.

**AUTHORS AND AFFILIATIONS:**
Alistair Gamble[1], a.gamble.1@research.gla.ac.uk
Maria Suessmilch[1], m.suessmilch.1@research.gla.ac.uk
Anniek Bonestroo[1], a.bonestroo.1@student.rug.nl
Andres Merits[2], andres.merits@ut.ee
Gerard J Graham[1], Gerard.graham@glasgow.ac.uk
Jonathan Cavanagh[1], Jonathan.Cavanagh@glasgow.ac.uk
Julia M Edgar[1], Julia.Edgar@glasgow.ac.uk
Marieke Pingen[1], Marieke.pingen@glasgow.ac.uk
[1] University of Glasgow, School of Infection and Immunity.
[2] University of Tartu, Faculty of Science and Technology, Institute of Technology
Correspondence to Marieke Pingen.

**SUMMARY:**
This protocol presents a novel way of generating central nervous system cell cultures from embryonic day 17 mouse brains for neuro(immuno)logy research. This model can be analyzed using various experimental techniques, including RT-qPCR, microscopy, ELISA, and flow cytometry.

**ABSTRACT:**
Models of the central nervous system (CNS) must recapitulate the complex network of interconnected cells found *in vivo.* The CNS consists primarily of neurons, astrocytes, oligodendrocytes, and microglia. Due to increasing efforts to replace and reduce animal use, a variety of *in vitro* cell culture systems have been developed by others to explore innate cell properties which will allow the development of therapeutics for CNS infections and pathologies. Whilst certain research questions can be addressed by human based cell culture systems such as (induced) pluripotent stem cells, working with human cells has its own limitations with regards to availability, costs and ethics.

Here we describe a novel protocol for isolating and culturing cells from embryonic mouse brains. The resulting mixed neural cell cultures mimic several of the cell populations and interactions that are found in the brain *in vivo*. Compared to current equivalent methods this protocol more closely mimics the characteristics of the brain and also garners more cells, therefore allowing for more experimental conditions to be investigated from one pregnant mouse. Further, the protocol is relatively easy and highly reproducible. These cultures have been optimized for use at various scales, including 96-well based high throughput screens, 24-well microscopy analysis and 6-well cultures for flow cytometry and qRT-PCR analysis. This novel culture method is a powerful tool to investigate infection

and immunity within the context of some of the complexity of the CNS with the convenience of *in vitro* methods.

**INTRODUCTION:**

Improving our understanding of the central nervous system (CNS) is critical to improve therapeutic options for many neuroinflammatory and neurodegenerative diseases. The CNS, a complex network of interconnected cells within the brain, spinal cord, and optic nerve, is primarily made up of neurons, oligodendrocytes, astrocytes, and their own innate immune cells, the microglia[1]. An *in vitro* approach can often drastically reduce the numbers of mice required to do meaningful research; however, the complex nature of the CNS makes it impossible to recapitulate the *in vivo* situation using cell lines. Mixed neural cell cultures provide an extremely valuable research tool to investigate neuro(immuno)logy questions in a relevant model, in line with the Replacement, Reduction and Refinement (3Rs) principles[2,3].

Thomson et al (2008) described a cell culture method using prenatal spinal cord cells that differentiate into all the aforementioned main CNS cell types[4]. This system has also got synapse formation, myelinated axons, and nodes of Ranvier. The main limitation of this culturing method is that, being spinal cord, it does not usefully model the brain and the cell yields from embryonic day 13 (E13) spinal cords are constricting, thus limiting the number of experimental conditions that can be investigated. Therefore, we aimed to develop a new cell culture system that recapitulates the characteristics of the brain with increased cell yield to reduce the requirement for animals.

Using Thomson et al (2008) as a starting point we have developed a cell culture model derived purely from the prenatal mouse brains. These cultures have all the same cell populations, interconnectivity, and treatment options as the spinal cord cultures except there is less myelination by comparison. However, having a CNS *in vitro* model with approximately three times higher cell yield is more efficient, requiring fewer mice and less time processing embryos. We optimized this novel culture system for multiple downstream applications and scales, including glass coverslips for microscopy analysis and various sizes of plastic well plates, including 96 well for high-throughput research.

**PROTOCOL:**

Schematic Diagram

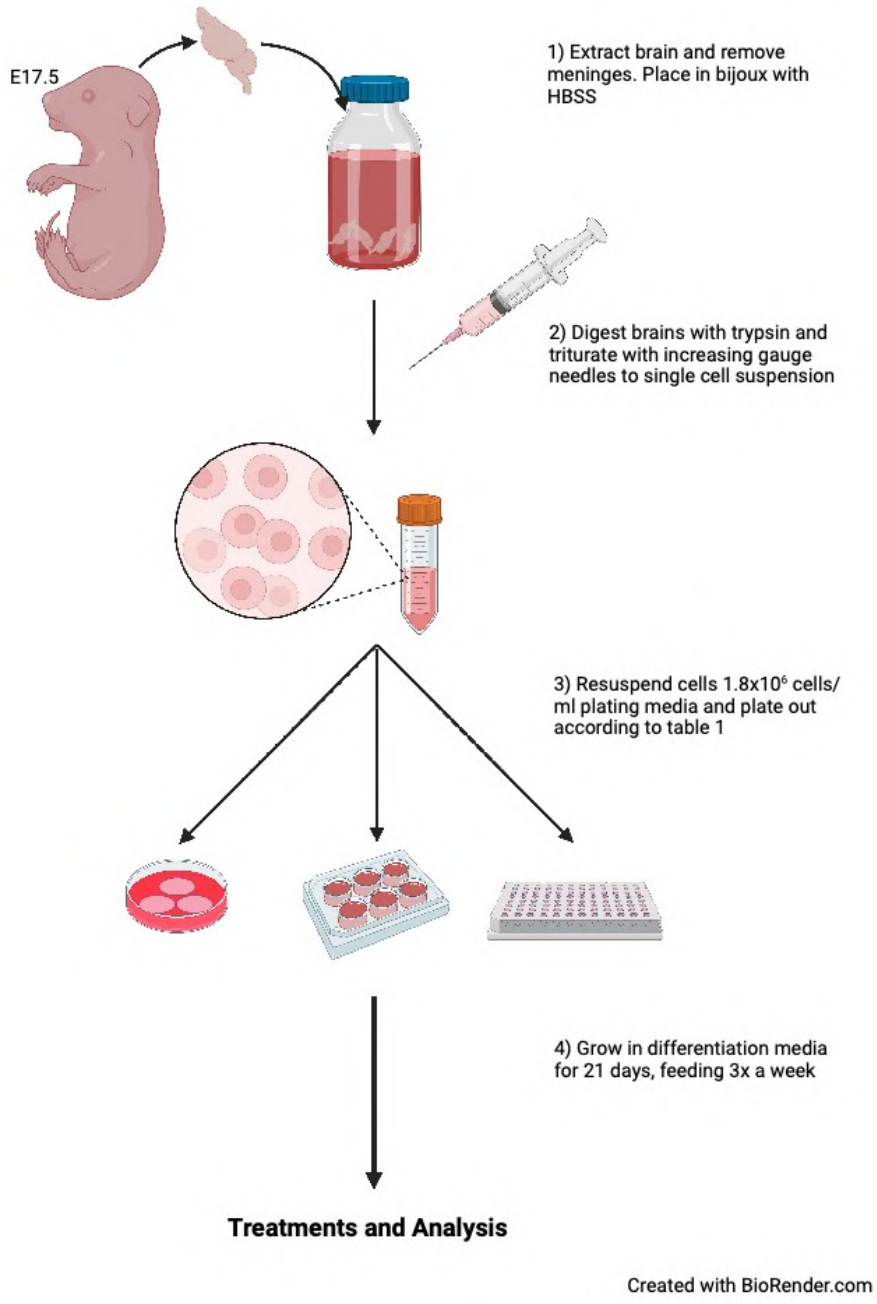


**Figure 1: Schematic overview of described method to generate mixed neuronal and glial cultures.**

Protocol:

All animal experiments should be performed compliant with local law and guidelines for animal use. Animals were housed in specific-pathogen free conditions in accordance with the UK Animals Scientific Procedures Act 1986, under the auspices of a UK Home Office Project License and were approved by the local Ethical Review Committee at the University of Glasgow. For this study, inhouse bred adult C57BL/6J mice were used. The use of young females (8-12 weeks) is recommended due to the higher success rate of pregnancy; males can be reused for multiple rounds of breeding. Figure 1 represents a schematic overview of the described method to generate mixed neuronal and glial cultures.

**1) Prepare the required tissue culture consumables**

**Table 1: Required volumes for preparation of coated tissue culture plastics.**

| Required format | BA-PLL/well | Water for wash | Volume cells in Plating Media (PM) to plate out | Topping up Media | Remove/add when feeding cultures (3x/week) |
|---|---|---|---|---|---|
| 6 well format ($9.6cm^2$) | 1000 µL | 1000 µL | 1000 µL | -400 µL +600 µL DM+ | -500 µL Media +600 µL DM+/- |
| 96 well format ($0.32\ cm^2$) | 100µL | 100 µL | 50 µL | +60 µL DM+ | -50 µL Media +60 µL DM+/- |
| Coverslip in dish format | 20 mL per 200 coverslips | 20 mL | 100 µL per coverslip | +600 µL DM+ +300 µL PM | -500 µL Media +600 µL DM+/- |

1.1) Prepare the plates and/or dishes containing microscopy coverslips inside a Class 2 Safety cabinet. Sterilize all reagents or autoclave to ensure sterility during the culture period.

1.2) Add the appropriate volume BA-PLL (13.2 µg/mL poly-L-lysinehydrobromide (PLL) in boric acid buffer (BA) (50mM boric acid, 12.5mM sodium tetraborate, pH 8.5)) to each well (1000 uL/well in 6-well plate, 100ul in 96-well format, volumes summarized in Table 1). For microscopy coverslips, add 20 mL BA-PLL to a 9 cm diameter tissue culture dish containing 200 sterile coverslips, swirl to distribute evenly.

1.3) Incubate at 37°C for 1-2 hours.

1.4) Remove the BA-PLL solution from each well or dish containing microscopy coverslips, and wash by adding 20 mL sterile water, swirling the coverslips, then removing the water. Repeat this wash step three times. For a dish containing coverslips, leave sterile water in tissue culture dish on the final wash for ease of removing the coverslips.

1.5) Remove as much liquid as possible with a sterile pipette and allow to dry for at least 2 hours or up to overnight.

1.6) Coated plates can be stored at 4°C for up to 2 months.

NOTE: The boric acid with poly-l-lysine (BA-PLL) solution can be reused up to 3x, adding new PLL each time. Store BA-PLL at 4°C. Dishes are treated with BA-PLL as the PLL allows the cells to stick down and grow. Without this treatment the cells will lift after approximately one week of culture and no longer be able to differentiate.

**2) <u>Dissection of E17 embryonal brains</u>**

2.1) Cohouse one or multiple female mice with a male mouse. Check females daily for a mucus plug indicating mating has taken place. Any “plugged” female mice should be separated from the male to ensure correct start date of gestation. Mice can be weighed to confirm pregnancy or monitored visually.

2.2) Cull the pregnant mouse at E17 using appropriate methods in compliance with local animal welfare guidance and laws, for example rising carbon dioxide concentration, lethal overdose of anesthetic or dislocation of the neck.
NOTE: The chosen method must not disrupt the embryos. For this study, exposure to a rising concentration of carbon dioxide gas followed by confirmation of death by severing the femoral artery was used to cull the pregnant dams.

2.3) Place the culled, pregnant mouse on its back on a dissection board; while pinning it down is not required it might make it easier for unexperienced researchers. Pinch the midline of the abdomen using forceps. Using sharp scissors, cut open the abdomen through the skin and the peritoneum over the midline from genitalia to ribcage, being careful not to puncture the uterus.

I. The mouse uterus consists of two horns, each typically containing 1-5 embryos. Remove the uterus containing the embryos from the mother and immediately place on ice.

2.4) Cut through the yolk sack on the side of the placentas, being careful to not damage the embryos and remove the embryos from their yolk sack.

2.5) Immediately decapitate the embryos, adding the heads into a dish with Hanks' Balanced Salt Solutions (HBSS) without calcium ($Ca^{2+}$) and magnesium ($Mg^{2+}$) (HBSS-/-) on ice.
NOTE: If genotyping is required, one can remove the tail at this stage for genetic analysis. When multiple genotypes are expected, the heads of each embryo should be kept separately for culturing.

2.6) Using angled forceps, position the head on its side facing left.

2.7) Pierce the eye with one edge of the forceps, holding the chin firmly with the other edge.

2.8) Starting at the nape, gently tear the skin of the scalp along the midline towards the tip of the snout.

2.9) Entering through the spinal cord, noticeable as a white oval, use the angled forceps to crack open the skull along the midline exposing the brain.

2.10) Gently peel the skull away on the side facing upwards, exposing the brain.

2.11) Lift the brain out of the skull, disposing of the skull once the brain is completely removed.

2.12) Remove the meninges using the forceps, which are noticeable as a thin membrane with dense blood vessels.

2.13) Place the brains into a bijou containing 2 mL HBSS-/- on ice.

2.14) Repeat steps 2.6) to 2.13) with the remaining brains, adding up to 4 brains per bijou.

2.15) Add 250 µL 10x trypsin to the bijou and triturate the brains by shaking the bijou. Incubate for 15 minutes at 37 °C.
NOTE: All steps from this point forward should be performed in a sterile tissue culture hood.

2.16) Thaw 2 mL of Soybean Trypsin (SD) Inhibitor (Leibovitz L-15, 0.52 mg/mL trypsin inhibitor from soybean, 40 µg/mL DNase I, 3mg/mL BSA fraction V) per bijou containing up to 4 brains from -20° C by placing it at 37 °C.

2.17) Add 2 ml SD inhibitor to each bijou containing brains (per bijou containing up to four brains), shaking the bijou again to disperse it evenly.

NOTE: SD inhibitor decreases the activity of the trypsin to prevent unnecessary digestion of the samples to preserve cell viability.

2.18) Without centrifugation, remove 2 mL of the supernatant from each bijou transferring it into a 15 mL falcon tube, being careful not to transfer cell clumps.

2.19) Triturate the remaining cells in the bijou with a 19 G needle attached to a 5 mL syringe by aspirating the suspension twice. This will create a thick mucus-like mixture.

I. Repeat twice more using a 21 G needle. If there are clumps remaining, triturate once more with the 21 G needle.

2.20) Transfer the cells from the bijou to the same 15 mL centrifuge tube (from 2.18) using a 23 G needle.

2.21) Centrifuge at 200 x *g* at room temperature (RT) for 5 minutes.

2.22) Remove all the supernatant using a 5 ml stripette and transfer it to another 15 mL falcon being careful to not disturb the loose pellet at the bottom which contains the required cells.

2.23) Centrifuge the supernatant again at 200 x *g* at RT for 5 minutes.
NOTE: This step is not essential, but if you require many cells or had few embryos one could perform this step to recover as many cells as possible from the supernatant.

2.24) Using 10 mL of plating media (PM) (49% Dulbecco's Modified Eagle Medium (DMEM), 1% Penicillin/Streptomycin (Pen/Strep), 25% horse serum, 25% HBSS with $Ca^{2+}$ and $Mg^{2+}$ (HBSS+/+)), combine and resuspend the two pellets together to create a whole cell suspension.

2.25) Count cells using trypan blue and either a hemocytometer or digital cell counter and dilute the cell suspension with PM to a concentration of $1.8x10^6$ cells/mL.

**3) <u>Plating the cells:</u>**

3.1) Add the required volume of cell suspension to the required format as detailed in Table 1:

- 1000 µL per well in 6-well format
- 50 µL per well in 96-well format
- 100 µL per coverslip.

3.2) Incubate for 2-4 hours at 37 °C with 5-7% $CO_2$. Check cells have adhered using an inverted microscope.

3.3) Top cells up by removing the media and topping up with new differentiation media (DM+: DM- including 10µg/ml insulin. DM-: DMEM, 1% Pen/Strep, 50 nM hydrocortisone, 10 ng/mL biotin, 2.5 mL 100x N1 media supplement). Volumes as detailed in Table 1. Press down any floating coverslips using a sterile pipette tip.

**4) Maintaining the cultures:**

NOTE: These cultures require feeding thrice weekly to support optimal growth and differentiation. Cultures will reach the optimum health and maturity for experiments on days in vitro (DIV) 21. Cells can be kept in culture for up to 28 days, after which the cultures quickly degenerate.

4.1) Three times per week until DIV12, replace part of the supernatant with fresh DM+ by removing 500 µL per well in 6-well format, 50 µL per well in 96-well format or 500 µL per dish containing 3 coverslips, and adding 600 µL per well in 6-well format, 60 µL per well in 96-well format or 500 µL per coverslip dish (Table 1).

4.2) Three times per week from DIV13 onwards, replace part of the supernatant with fresh DM- by removing 500 µL per well in 6-well format, 50 µL per well in 96-well format or 500 µL per dish containing 3 coverslips, and adding 600 µL per well in 6-well format, 60 µL per
well in 96-well format or 500 µL per coverslip dish (Table 1).

**REPRESENTATIVE RESULTS:**

**Microscopy:** Cultures grown on glass coverslips are ideal to analyze by microscopy. To visualize the development of the cultures, coverslips were fixed in 4% PFA at multiple timepoints from DIV0 (once cells were attached) until DIV28. The cultures were stained for immunofluorescence imaging as previously described[5] using three different staining combinations: NG2 (immature oligodendrocytes) and Nestin (neuronal stem/progenitor cells) as developmental markers, SMI31 (axons), MBP (myelin) and NeuN (neuron cell body) as neuronal markers or CNP (oligodendrocytes), GFAP (astrocytes), and Iba1 (microglia) as glial markers (Figure 2).

The various cell types were quantified using CellProfiler pipelines (based on https://github.com/muecs/cp/tree/v1.1). Each individual data point was generated from an average of 10 images taken from 3 coverslips per timepoint. For quantifying quantity of astrocytes percentage field of view was used instead of number of cells. This was due to difficulties differentiating between the individual cells as they frequently overlap. (Figure 2M-N). The cultures reach peak maturity and cell density at DIV21, after which the cultures start to degrade (Figure 2N).

Importantly, these cultures can easily be treated with drugs such as potential therapeutics or used to trace *in vitro* infections. In this example, cultures on coverslips were transferred to a 24 well plate and infected with the highly neurotropic virus Semliki Forest virus (SFV) (strain SFV6)[6] which expresses zsGreen in infected cells. To ensure low level infection, we used a Multiplicity of Infection (MOI, or number of added virus particles per cell) of 0.05 as titrated on BHK cells. After 0-72 hours post infection (hpi), cultures were fixed in 4% PFA and stained for analysis by immunofluorescent imaging. Figure 3 illustrates that in line with *in vivo* infection, SFV mainly infects oligodendrocytes and neurons[6].

**Reverse Transcription (RT)-quantitive (q)PCR:** In addition to microscopy, our CNS cultures can be used for analysis by molecular methods such as RT-qPCR of mRNA responses to treatment. To further investigate the innate antiviral response, 6 well plate cultures were treated with a range of doses of the potent antiviral cytokine interferon beta (IFN-β) for 24 hours. Cultures were lysed with guanidium-thiocyanate/phenol and the RNA isolated, converted to cDNA and analyzed by qPCR as previously described[7]. Using this method differential expression of many genes can be measured. Here, upregulation of *Ccl5* was quantified against the housekeeping gene *18s*. CCL5 is a chemotactic cytokine (chemokine) involved in the inflammatory response. Indeed, here, IFN-β treatment results in an upregulation of *Ccl5* mRNA in the cultures (Figure 4A).

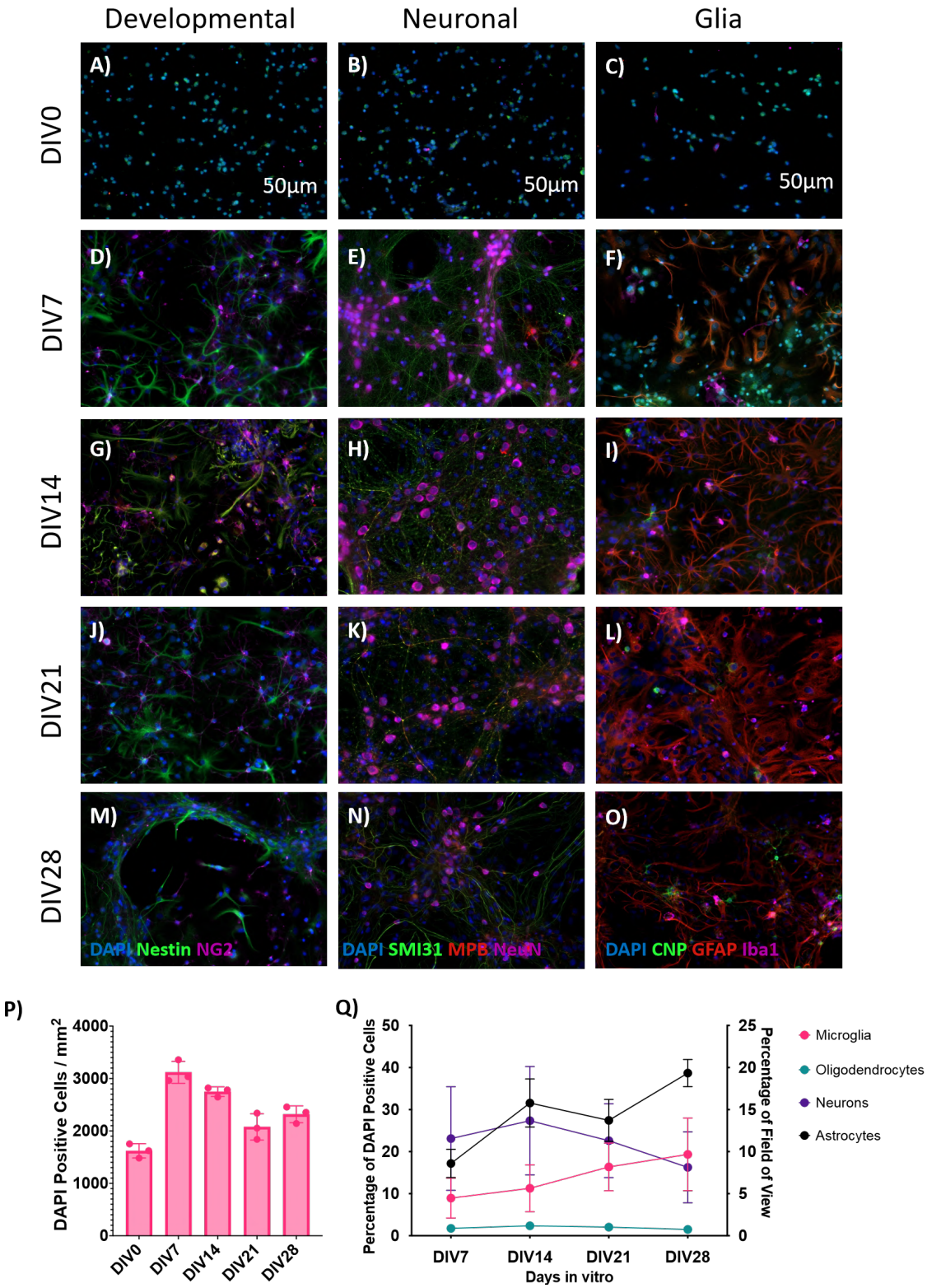


**Figure 2: E17 CNS cultures stained for immunofluorescence imaging cell markers over time.** Cells were fixed with 4% PFA before being permeabilized and stained to visualize different populations. Representative images of A,D,G,J,M) developmental markers NG2 and Nestin; B, E,H,K,N) neuronal markers SMI31 (axons), MBP (myelin) and NeuN (neuron cell body); and C,F,I,L,O) glial markers CNP (oligodendrocytes), GFAP (astrocytes), and Iba1 (microglia). P) Counts of DAPI per $mm^2$, n=3, each n from technical triplicates of 10 images per triplicate. Q) Cell counts as percentage of DAPI positive cells (microglia,

oligodendrocytes and neurons) and percentage of field of view (astrocytes), n=3, each n from technical triplicates of 10 images per triplicate. Error bars are ±SEM.

**ELISA**: The 96-well format of cultures is an excellent tool for high throughput screenings of treatments. To investigate that the upregulation of *Ccl5* mRNA results in expression of CCL5 protein we measured CCL5 in the supernatant of the cultures by ELISA. In this example, 96 well cultures were treated in duplicate with 27 incremental doses of IFN-β to generate a dose response curve (Figure 4B). In line with the increasing mRNA expression (Figure 4A), there is an increase in CCL5 released in the supernatant. As expected, Figure 4C demonstrates a clear correlation between mRNA and protein expression.

**Flow cytometry**: Flow cytometry is a powerful tool to investigate expression of many intra- and extracellular markers simultaneously. However, analyzing complex highly interactive cultures by flow cytometry can be challenging due to cell damage and death when taking cells from culture to single cell suspension for processing and analysis. Comparing a variety of protocols using 0.050.5% Trypsin-EDTA, 1-10x trypsin without EDTA and gentle dissociation reagent, we found that treating the 6 well plate cultures with 0.05% Trypsin/EDTA for 10 minutes at 37 °C with gentle agitation we were able to lift the cells with gentle trituration to create a single cell suspension. Especially for flow cytometric analysis of CNS cells, it is critical to be gentle during cell preparation, minimize wash steps and take great care to keep cells on 4 °C or ice at all times.

To assess viability and cell types in this single cell suspension, cells were stained with a viability dye, and fluorescently labelled antibodies against CD45, CD11b, O4, ACSA-2, and CD24 to allow visualization of each individual cell population in the cultures (Figure 5).

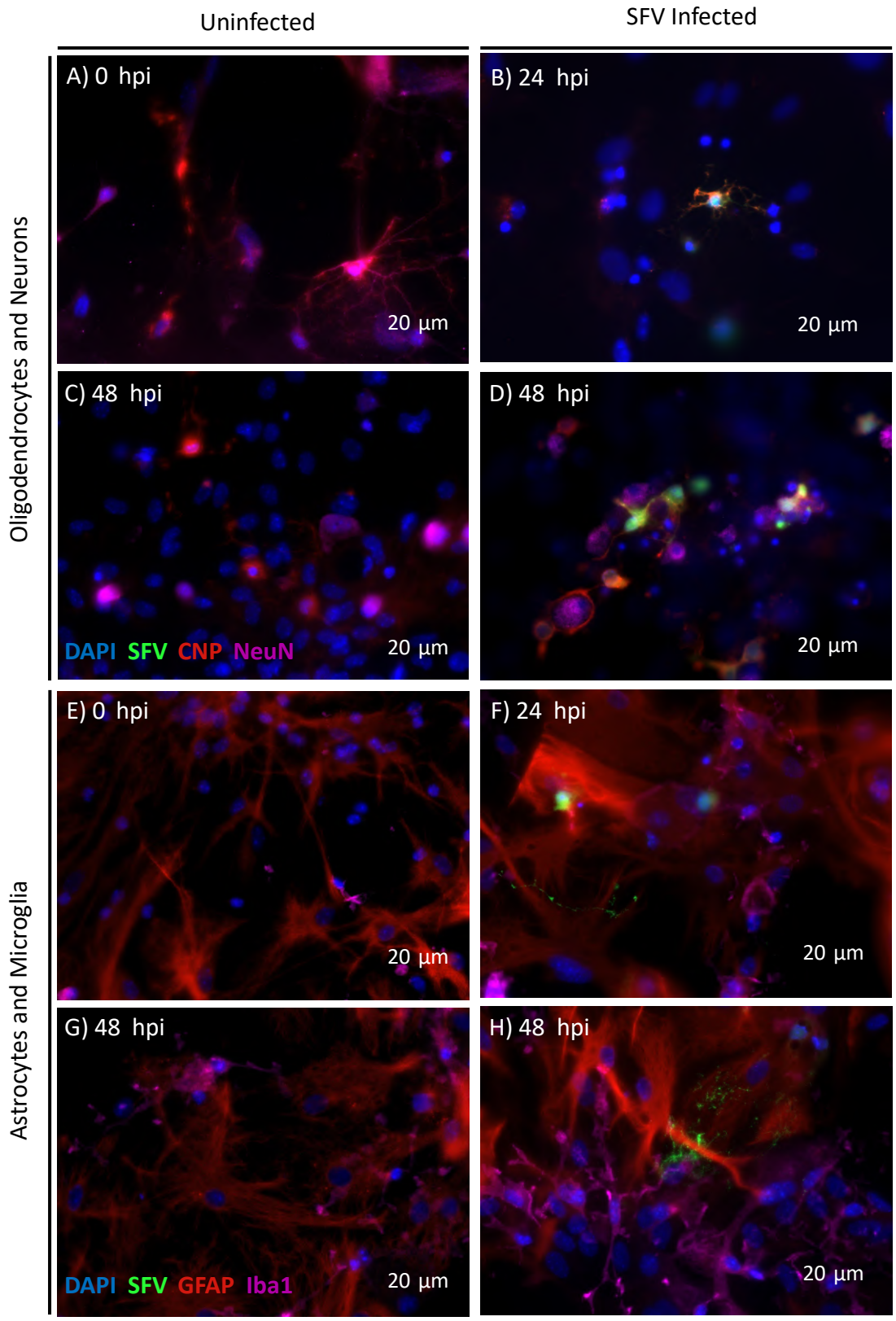


**Figure 3: Semliki Forest virus (SFV) infection of E17 CNS cultures over time.** Representative images of uninfected control cultures (A, D); and cultures infected with 0.03 MOI SFV (B-C, E-F). Cells were infected for 0-48 hours and stained with CNP (oligodendrocyte marker) and NeuN (neuron marker) or GFAP (astrocytes) and Iba1 (microglia). White arrows indicate an infected cell. This strain of SFV expresses the green fluorescent protein zsGreen to enable tracing of viral infection.

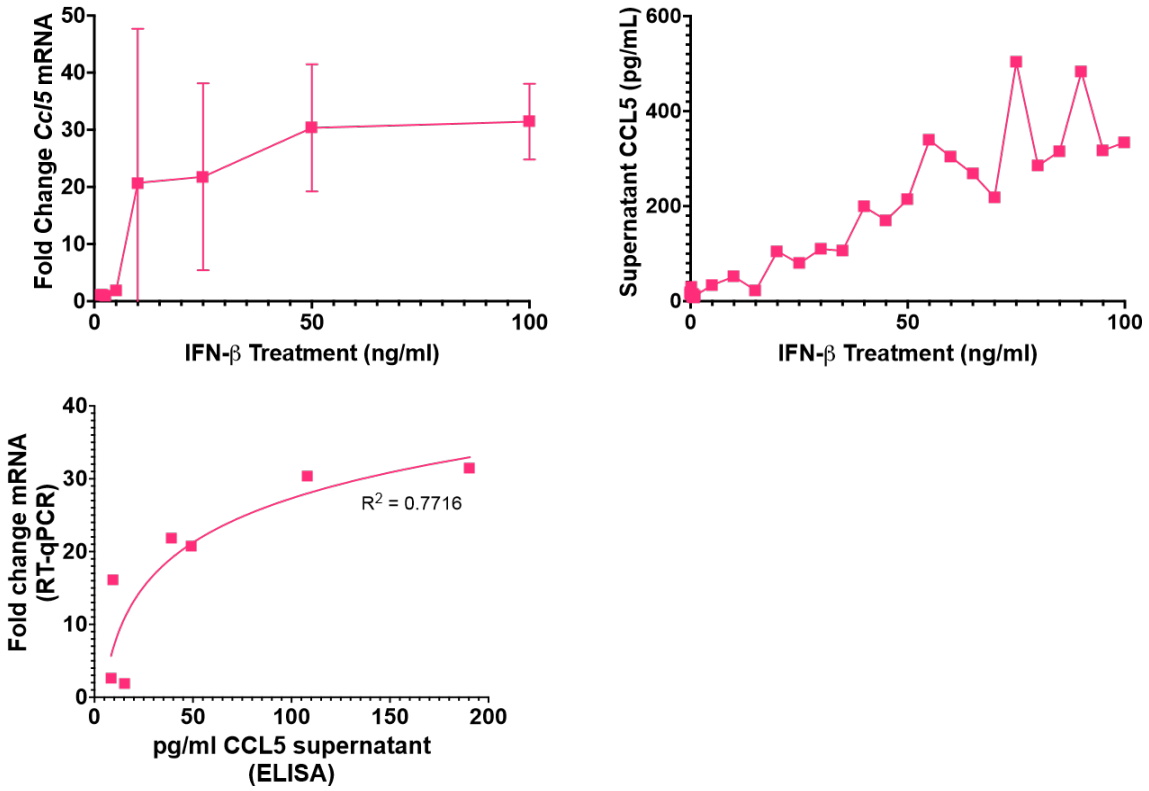


**Figure 4: CCL5 mRNA and protein expression of E17 CNS cultures following IFN-β treatment.** Cells were treated in the 6 well plate format (mRNA) or the 96 well plate format (protein) for 24 hours with a range of doses of IFN-β. A) Expression of Ccl5 mRNA after treatment with 0-100 ng/mL IFN-β, biological n=2, each taken from technical triplicates. B) CCL5 concentration in supernatant following 0-100 ng/mL IFNβ treatment, biological n=1, taken from technical triplicates. C) cellular mRNA Ccl5 upregulation vs CCL5 protein concentration in supernatant with log trendline. Error bars are ±SEM.

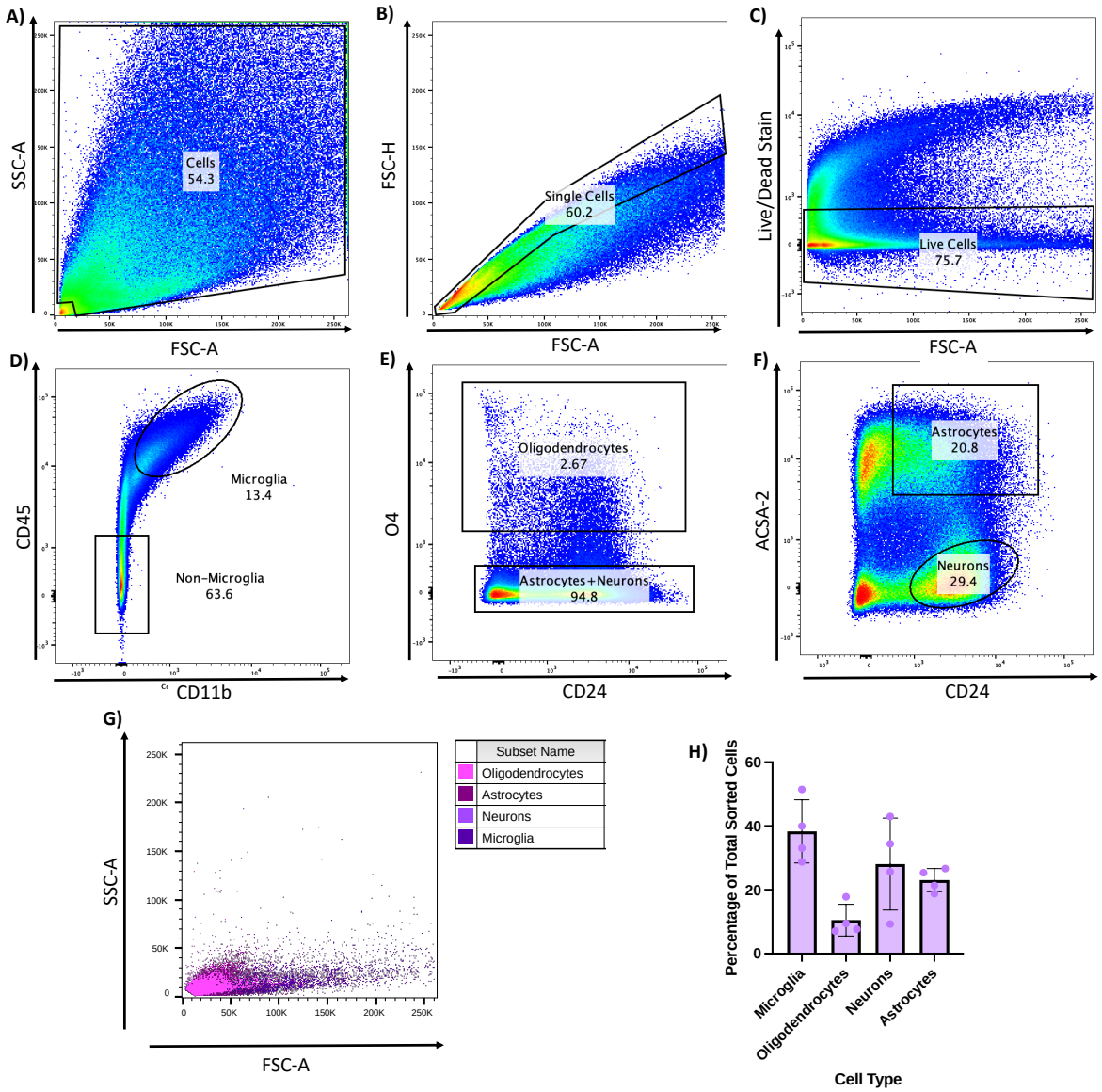


**Figure 5: Flow cytometry gating strategy to generate single cell populations from E17 CNS cultures.** Cells were dissociated using 0.05% trypsin-EDTA and stained with appropriate antibodies then sorted into individual cell populations. A-C) Gating strategy to sort for live, single cells. D) Strategy to select for microglia ($CD45^{+}CD11b^{+}$). E) Strategy to select for oligodendrocytes ($CD45^{-}$ $CD11b^{-}$ $O4^{+}$) cells. F) Strategy to sort for astrocytes ($CD45^{-}$ $CD11b^{-}$ $O4^{-}$ ACSA-$2^{+}$ $CD24^{+}$) and neurons ($CD45^{-}$ $CD11b^{-}$ $O4^{-}$ ACSA-$2^{-}$ $CD24^{+}$). G) Individual cell populations overlaid on each other showing discrete populations. H) Individual cell types as a percentage of the total cells sorted n=4. Error bars are ±SEM.

Around 70% cell viability was obtained from this method, averaging approximately $2x10^6$ viable, single cells per 6 well plate (Figure 5C). In line with the microscopy results (Figure 2N), there were large numbers of microglia, neurons and astrocytes whilst oligodendrocytes were the least abundant.

**DISCUSSION:**

The CNS is a complex network which spans from the brain down to the spinal cord and consists of many cell types, predominantly neurons, oligodendrocytes, astrocytes and microglia[1]. As each cell has an important role in the maintaining homeostasis and generating appropriate responses to challenges in the CNS[8–10] a culture system that contains all these cell types is a useful and versatile tool to investigate how the brain might react to a stimulus. The ability to study these cells, and their interactions, in an *in vitro* context means a great variety of techniques can be employed to investigate various experimental questions easily. We have outlined a quick and efficient method to obtain and culture the main CNS cell types from the prenatal brain which can mimic individual cell populations in the adult mouse brain[11].

Previously established protocols for generating CNS cultures use E13.5 spinal cords[4,5]. In addition to having a suitable model for the spinal cord, it is highly relevant to have a model that recapitulates the brain. Therefore, brains from these E13.5 mice were originally used to generate the CNS cultures described here using the same protocol. However, after DIV14 the cells started to form large aggregates with densely packed neuronal cell bodies. While astrocytes were present it is not clear if they were evenly distributed. It is unclear if the cells in the center of these cell bodies would receive sufficient nutrients and oxygen from the culture medium as the cells outside would. Neurons, when suffering from oxygen and nutrient deprivation, are liable to go through apoptosis and release stress signals to glial cells[12] which might lead to a proinflammatory phenotype[13]. Neurogenesis was thought to be a likely cause of these densely packed aggregates, and this phase subsides by E17[14]. When brains from E17 mouse embryos were used the cells still formed networks but did not cluster into the large aggregates seen in E13.5 and were therefore regarded as a more suitable age for the brain cultures to be generated from.

Our technique also results in a greater number of cells obtained from one pregnancy (averaging $1x10^7$ cells/brain compared to 3-$4x10^6$ cells/spinal cord)[7]. For an average

pregnant mouse with 8-10 embryos, this correlate to up to 54 different experimental conditions in the 6 well plate format, or 150 experimental conditions for microscopy (compared to 19 and 64 respectively from spinal cord). As such, these CNS cultures are a great tool to reduce the required number of mice[15]. Especially the 96-well format can be easily used for high throughput assays, for instance enabling screening of drug candidates prior to testing in animals, vastly reducing the number of required animals for such studies. Hopefully, this will contribute to improving the low success rate of CNS drugs tested in animals prior to clinical trials in humans[16,17].

The cultures reach peak maturity by DIV21. Cell counts increase up until this timepoint, after which the cells start to degenerate with decreasing numbers of each type of cell. This was measured both by looking at the quantified cell numbers (Figure 2N) as well as the quantity of pyknotic nuclei (dense DAPI stains) (Figure 2M). While the developmental markers Nestin and NG2 are still expressed on DIV14 (Figure 2G) and DIV21 (Figure 2J), this is due to some of the astrocytes going through astrogliosis which upregulates nestin[18] while some of the oligodendrocytes are not fully mature and therefore still express some NG2[19]. Based on our microscopy validation, only a small portion of the cells still express developmental markers compared to the fully mature cells by DIV21 (Figure 2I, L) and therefore by this time the cultures are largely mature. Of note, *in vivo* the density of microglia is highly variable across the murine CNS. The level of microglia as defined by Iba1 expression using microscopy is at the high end of this density in our cultures[20]. The high percentage of microglia that survive the flow cytometry procedure is likely due to microglia being more robust than other CNS cells, which generally have delicate extensions and are therefore more likely to be damaged during flow cytometry preparation.

It only takes 3 weeks following dissection until the cells are ready for experimentation which is shorter than most human-based *in vitro* methods such as organoids or iPSC derived models[21]. As long as *in vivo* research is required to ensure the safety of new therapeutics, using *in vitro* cell culturing methods such as ours will aid testing toxicity and efficacy efficiently before testing in animals, reducing the requirement for animals and enhance the translation of research from *in vitro* to *in vivo.* Hopefully this will eventually lead to more efficient translation to human based clinical trials as well. Ultimately these cultures were created to allow the study of the CNS. While *in vitro* systems cannot fully

express the complexity of the CNS, primary cell derived cultures more accurately represent *in vivo* CNS properties[22,23]. *In vitro* approaches can allow for a more reductive approach to investigate the CNS in the absence of infiltrating immune cells[24] and the blood brain barrier integrity[25]. Removing this layer of complexity can make it easier to unravel mechanisms. As such, our culturing system is a useful tool to answer research questions that complements *in vivo* animal research.

The ability to harvest, isolate, and culture CNS cells has already resulted in great advances in our understanding of the innate CNS[15]. This protocol and video demonstrate the dissection of E17 mouse brains and the resulting trituration and culturing of the cells to generate a cell culture system containing all the main cell types of the CNS. Multiple molecular techniques have been employed on these cultures showcasing the effectiveness these cultures have for investigating the CNS.

**ACKNOWLEDGMENTS:**
We would like to thank members of the Edgar and Linington labs, particularly Chris Linington, Diana Arseni and Katja Muecklisch, for their advice, helpful comments, and assistance with feeding the cultures while we set up these cultures. Particular thanks go to Dr Muecklisch for providing the starting points for the Cell Profiler pipelines.

This work was supported by the MS Society (grant 122) and the Yuri and Lorna Chernajovsky foundation to MP; University of Glasgow funding to JC and MP; Wellcome Trust (217093/Z/19/Z) and Medical Research Council (MRV0109721) to GJG.

**DISCLOSURES:**
Authors have nothing to disclose.

**MATERIALS**:

| Name of Material/ Equipment | Company | Catalogue Number | Comments/Description |
|---|---|---|---|
| Boric Acid | Sigma | B6768-500G | For boric acid buffer |
| Sodium Tetraborate | Sigma | 221732-100G | For boric acid buffer |

| | | | |
|---|---|---|---|
| Poly-L-Lysinehydrobromide | Sigma | P1274 | For Boric acid / poly-L-lysine solution to coat coverslips |
| HBSS w/o Ca Mg | Sigma | H9394-500ML | For brains to be added to |
| 10x Trypsin | Sigma | T4549-100ML | To digest tissue |
| Leibovitz L-15 | GIbco | 11415-049 | For SD Inhibitor |
| Trypsin inhibitor from soybean | Sigma | T9003-100MG | For SD Inhibitor |
| DNase I | Thermofisher | 18047019 | For SD Inhibitor, can use this or the other Dnase from sigma |
| DNase I | Sigma | D4263 | For SD Inhibitor, can use this or the other Dnase from thermofisher |
| BSA Fraction V | Sigma | A3059-10G | For SD Inhibitor |
| DMEM High glucose, sodium pyruvate, L-Glutamine | Gibco | 21969-035 | For DM+/-, and for plating media |
| Pen/Strep | Sigma | P0781-100ML | For DM+/-, and for plating media |
| Horse Serum | Gibco | 26050-070 | For plating media |
| HBSS w Ca Mg | Sigma | H9269-500ML | For plating media |
| Hydrocortisone | Sigma | H0396 | For DM+/- |
| Biotin | Sigma | B4501 | For DM+/- |
| N1 media supplement | Sigma | N6530-5ML | For DM+/- |
| Insulin | Sigma | I1882 | For DM+ |
| Coverslip | VWR | 631-0149 | To plate out cells for microscopy |
| 35mm TC Dish | Corning | 430165 | Plate out 3 PLL coated coverslips per 1 35mm dish |
| 140mm TC Dish | Fisher | 11339283 | Put 8 35mm dishes per 1 140mm dish |
| Angled forceps | Dumont | 0108-5/45-PO | For dissection |
| Dissection Scissors | Sigma | S3146-1EA | For dissection |
| Fine forceps | Dumont | 0102-SS135-PO | For dissection |
| 7mL Bijoux | Fisher | DIS080010R | To put brains intp |
| 5mL syringe | Fisher | 15869152 | For trituration of sample |

| | | | |
|---|---|---|---|
| 18G needle | Henke Sass Wolf | 4710012040 | For trituration of sample |
| 21G needle | BD | 304432 | For trituration of sample |
| 23G needle | Henke Sass Wolf | 4710006030 | For trituration of sample |
| 15mL Falcon | Sarstedt | 62554502 | To collect cells into pellet for resuspension in plating media |
| 6 well plate | Corning | 3516 | To plate out cells for RT-qPCR, and flow cytometry |
| 96 well plate | Corning | 3596 | To plate out cells for high-throughput testing |
| NG2 | Sigma | AB5320 | Immature oligodendrocytes |
| Nestin | Merck | MAB353 | Neuronal stem/progenitor cells |
| SMI31 | BioLegend | 801601 | Axons |
| MBP | Bio-Rad | MCA409S | Myelin |
| NeuN | Thermofisher | PA578499 | Neuronal cell body |
| CNP | Abcam | AB6319 | Mature oligodendrocytes |
| GFAP | Invitrogen | 13-0300 | Astrocytes |
| Iba1 | Alpha-Laboratories | 019-1971 | Microglia |
| eBioscience Fixable Viability Dye eFluor 780 | Thermofisher | 65-0865-14 | Live / Dead stain |
| Trizol | Thermofisher | 15596026 | For lysing cells for RT-qPCR |

**REFERENCES for Gamble et al:**


1. Kovacs, G. G. Cellular reactions of the central nervous system. in *Handbook of Clinical Neurology* vol. 145 13–23 (Elsevier B.V., 2018).
2. Russell, W. M. S. & Burch, R. L. *The Principles of Humane Experimental Techniques*. vol. 1 (1959).
3. Hubrecht, R. C. & Carter, E. The 3Rs and humane experimental technique: Implementing change. *Animals* **9**, (2019).
4. Thomson, C. E. *et al.* Myelinated, synapsing cultures of murine spinal cord - Validation as an in vitro model of the central nervous system. *European Journal of Neuroscience* **28**, 1518–1535 (2008).
5. Bijland, S. *et al.* An in vitro model for studying CNS white matter: Functional properties and experimental approaches. *F1000Res* **8**, (2019).
6. Fragkoudis, R. *et al.* Neurons and oligodendrocytes in the mouse brain differ in their ability to replicate Semliki Forest virus. *J Neurovirol* **15**, 57–70 (2009).
7. Hayden, L. *et al.* Lipid-specific IgMs induce antiviral responses in the CNS: Implications for progressive multifocal leukoencephalopathy in multiple sclerosis. *Acta Neuropathol Commun* **8**, 1–16 (2020).
8. Yin, J., Valin, K. L., Dixon, M. L. & Leavenworth, J. W. The Role of Microglia and Macrophages in CNS Homeostasis, Autoimmunity, and Cancer. *Journal of Immunology Research* vol. 2017 Preprint at https://doi.org/10.1155/2017/5150678 (2017).
9. Gee, J. R. & Keller, J. N. Astrocytes: Regulation of brain homeostasis via apolipoprotein E. *International Journal of Biochemistry and Cell Biology* vol. 37 1145–1150 Preprint at https://doi.org/10.1016/j.biocel.2004.10.004 (2005).
10. Madeira, M. M., Hage, Z. & Tsirka, S. E. Beyond Myelination: Possible Roles of the Immune Proteasome in Oligodendroglial Homeostasis and Dysfunction. *Frontiers in Neuroscience* vol. 16 Preprint at https://doi.org/10.3389/fnins.2022.867357 (2022).
11. Keller, D., Erö, C. & Markram, H. Cell densities in the mouse brain: A systematic review. *Frontiers in Neuroanatomy* vol. 12 Preprint at https://doi.org/10.3389/fnana.2018.00083 (2018).
12. Wang, Y. X. *et al.* Oxygenglucose deprivation enhancement of cell death/apoptosis in PC12 cells and hippocampal neurons correlates with changes in neuronal excitatory amino acid neurotransmitter signaling and potassium currents. *Neuroreport* **27**, 617–626 (2016).
13. Rock, K. L. & Kono, H. The inflammatory response to cell death. *Annual Review of Pathology: Mechanisms of Disease* vol. 3 99–126 Preprint at https://doi.org/10.1146/annurev.pathmechdis.3.121806.151456 (2008).
14. Chen, V. S. *et al.* Histology Atlas of the Developing Prenatal and Postnatal Mouse Central Nervous System, with Emphasis on Prenatal Days E7.5 to E18.5. *Toxicol Pathol* **45**, 705– 744 (2017).
15. Gordon, J., Amini, S. & White, M. K. General overview of neuronal cell culture. *Methods in Molecular Biology* vol. 1078 1–8 Preprint at https://doi.org/10.1007/978-1-62703-640-5_1 (2013).

16. Kesselheim, A. S., Hwang, T. J. & Franklin, J. M. Two decades of new drug development for central nervous system disorders. *Nature Reviews Drug Discovery* vol. 14 815–816 Preprint at https://doi.org/10.1038/nrd4793 (2015).
17. Gribkoff, V. K. & Kaczmarek, L. K. The need for new approaches in CNS drug discovery: Why drugs have failed, and what can be done to improve outcomes. *Neuropharmacology* vol. 120 11–19 Preprint at https://doi.org/10.1016/j.neuropharm.2016.03.021 (2017).
18. Zamanian, J. L. *et al.* Genomic analysis of reactive astrogliosis. *Journal of Neuroscience* **32**, 6391–6410 (2012).
19. Nishiyama, A., Suzuki, R. & Zhu, X. NG2 cells (polydendrocytes) in brain physiology and repair. *Frontiers in Neuroscience* Preprint at https://doi.org/10.3389/fnins.2014.00133 (2014).
20. Keller, D., Erö, C. & Markram, H. Cell densities in the mouse brain: A systematic review. *Frontiers in Neuroanatomy* vol. 12 Preprint at https://doi.org/10.3389/fnana.2018.00083 (2018).
21. Lee, C. T., Bendriem, R. M., Wu, W. W. & Shen, R. F. 3D brain Organoids derived from pluripotent stem cells: Promising experimental models for brain development and neurodegenerative disorders Julie Y.H. Chan. *Journal of Biomedical Science* vol. 24 Preprint at https://doi.org/10.1186/s12929-017-0362-8 (2017).
22. Asch, B. B., Medina, D. & Brinkley, B. R. Microtubules and Actin-containing Filaments of Normal, Preneoplastic, and Neoplastic Mouse Mammary Epithelial Cells1. *Cancer Res* **39**, 893–907 (1979).
23. Koch, K. S. & Leffertt, H. L. GROWTH CONTROL OF DIFFERENTIATED ADULT RAT HEPATOCYTES IN PRIMARY CULTURE*. *Ann N Y Acad Sci* **349**, 111–127 (1980).
24. Nevalainen, T., Autio, A. & Hurme, M. Composition of the infiltrating immune cells in the brain of healthy individuals: effect of aging. *Immunity and Ageing* **19**, (2022).
25. Daneman, R. & Prat, A. The blood–brain barrier. *Cold Spring Harb Perspect Biol* **7**, (2015).

# References


Abbott, N.J. (2002) Astrocyte-endothelial interactions and blood-brain barrier permeability, *J. Anat*, 200, pp. 629-638

Abbott, N.J., Rönnbäck, L. and Hansson, E. (2006) 'Astrocyte-endothelial interactions at the blood-brain barrier', *Nature Reviews Neuroscience*, 7(jan), pp. 41–53.

Abdulrahman, Z. *et al.* (2022) 'Tumor-specific T cells support chemokine-driven spatial organization of intratumoral immune microaggregates needed for long survival', *Journal for ImmunoTherapy of Cancer*, 10(2).

Ackerman, Sandra. (1992) *Discovering the Brain*. 1st Edition, pp. 13-31.

Adang, L. and Berger, J. (2015) 'Progressive Multifocal Leukoencephalopathy', *F1000Research*, 4(2), pp. 193–200.

Afrough, B., Dowall, S. and Hewson, R. (2019) 'Emerging viruses and current strategies for vaccine intervention', *Clinical and Experimental Immunology*. 196, pp. 157–166.

Ahmad, A. and Menezes, J. (1996) 'Antibody-dependent cellular cytotoxicity in HIV', *FASEB*, 10, pp. 258–266.

Alberts, B. *et al.* (2002) *Molecular Biology of the Cell*. 4th edn

Aleksander, S.A. *et al.* (2023) 'The Gene Ontology knowledgebase in 2023', *GENETICS*. 224(1), iyad031

All, O.D.H. *et al.* (1998) failure of cytarabine in progressive multifocal leukoencephalopathy associated with hiv infection failure of cytarabine in progressive multifocal leukoencephalopathy associated with human immunodeficiency virus infection. 338(19), pp. 1345-1351.

Allsopp, T.E. *et al.* (1998) Virus infection induces neuronal apoptosis: A comparison with trophic factor withdrawal. 5, pp. 50-59

Angelova, D.M. and Brown, D.R. (2019) 'Microglia and the aging brain: are senescent microglia the key to neurodegeneration?', *Journal of Neurochemistry*., pp. 676–688.

Arellano, G. *et al.* (2017) 'Th1 and Th17 cells and associated cytokines discriminate among clinically isolated syndrome and multiple sclerosis phenotypes', *Frontiers in Immunology*, 8(JUN).

Arimoto, K.I. *et al.* (2017) 'STAT2 is an essential adaptor in USP18-mediated suppression of type i interferon signaling', *Nature Structural and Molecular Biology*, 24(3), pp. 279–289.

Ariza, A. *et al.* (1992) 'Accumulation of Wild-Type p53 protein in progressive multifocal leukoencephalopathy: A flow cytometry and DNA sequencing study', *Journal of Neuropathology and Experimental Neurology*, 55(2), pp. 144–149.

Arnold, D. *et al.* (2021) 'Slowly expanding lesions are a marker of progressive MS – No', *Multiple Sclerosis Journal - Experimental, Translational and Clinical*, 27(11), pp. 1681–1683.

Aronson, J.K. (2016) *Meyler's Side Effects of Drugs*: Macrophage colony-stimulating factor (M-CSF). 16th Edn.

Arrambide, G. *et al.* (2018) 'The value of oligoclonal bands in the multiple sclerosis diagnostic criteria', *Brain*, 141(4), pp. 1075–1084.

Ashburner, M. *et al.* (2000) 'Gene ontology: Tool for the unification of biology', *Nature Genetics*, 25(1), pp. 25–29.

Atif, S.M. *et al.* (2018) 'Immune surveillance by natural IgM is required for early neoantigen recognition and initiation of adaptive immunity', *American Journal of Respiratory Cell and Molecular Biology*, 59(5), pp. 580–591.

Atkins, G.J., Sheahan, B.J. and Liljestro, P. (1999) 'The molecular pathogenesis of Semliki Forest virus : a model virus made useful?', *Journal of General Virology*, 80, pp. 2287–2297.

Austermann, J., Roth, J. and Barczyk-Kahlert, K. (2022) 'The Good and the Bad: Monocytes' and Macrophages' Diverse Functions in Inflammation', *Cells*. 11(1979).

Au-Yeung, N., Mandhana, R. and Horvath, C.M. (2013) 'Transcriptional regulation by STAT1 and STAT2 in the interferon JAK-STAT pathway', *JAK-STAT*, 2(3), p. e23931.

Ayala-Nunez, N.V. and Gaudin, R. (2020) 'A viral journey to the brain: Current considerations and future developments', *PLoS Pathogens*, 16(5).

Azouz, R. and Gray, C.M. (1999) 'Cellular Mechanisms Contributing to Response Variability of Cortical Neurons In Vivo', *Journal of Neuroscience*, 16(6), pp. 2209–2223.

Babetto, E. and Beirowski, B. (2022) 'Of axons that struggle to make ends meet: Linking axonal bioenergetic failure to programmed axon degeneration', *Biochimica et Biophysica Acta - Bioenergetics*, 1863(5).

Balasingam, V. and Wee Yong, V. (1996) *Attenuation of Astroglial Reactivity by Interleukin-10*.16(9), pp. 2945-2955.

Balka, K.R. *et al.* (2020) 'TBK1 and IKKε Act Redundantly to Mediate STING-Induced NF-κB Responses in Myeloid Cells', *Cell Reports*, 31(1).

Bandow, K. *et al.* (2012) 'LPS-induced chemokine expression in both MyD88-dependent and -independent manners is regulated by Cot/Tpl2-ERK axis in macrophages', *FEBS Letters*, 586(10), pp. 1540–1546.

Baranzini, S.E. and Oksenberg, J.R. (2017) 'The Genetics of Multiple Sclerosis: From 0 to 200 in 50 Years', *Trends in Genetics*., 33(12), pp. 960–970.

Barnaba, V. (2022) 'T Cell Memory in Infection, Cancer, and Autoimmunity', *Frontiers in Immunology*. 12, pp. 1-12.

Barnes, S.A. *et al.* (2022) 'Type I interferon subtypes differentially activate the anti-leukaemic function of natural killer cells', *Frontiers in Immunology*, 13.

Barr, T.A. *et al.* (2012) 'B cell depletion therapy ameliorates autoimmune disease through ablation of IL-6-producing B cells', *Journal of Experimental Medicine*, 209(5), pp. 1001–1010.

Batiuk, M.Y. *et al.* (2020) 'Identification of region-specific astrocyte subtypes at single cell resolution', *Nature Communications*, 11(1).

Beck, E.S. and Cortese, I. (2020) 'Checkpoint inhibitors for the treatment of JC virus-related progressive multifocal leukoencephalopathy', *Current Opinion in Virology*, 40, pp. 19–27.

Begitt, A. *et al.* (2014) 'STAT1-cooperative DNA binding distinguishes type 1 from type 2 interferon signaling', *Nature Immunology*, 15(2), pp. 168–176.

Bekele Feyissa, Y. *et al.* (2021) 'The Role of CXCL13 in Antibody Responses to HIV-1 Infection and Vaccination', *Frontiers in Immunology*. 12(638872).

Bellizzi, A. *et al.* (2011) 'Polyomavirus JC reactivation and noncoding control region sequence analysis in pediatric Crohn's disease patients treated with infliximab', *Journal of NeuroVirology*, 17(4), pp. 303–313.

Bénard, A. *et al.* (2018) 'B cells producing type i IFN modulate macrophage polarization in tuberculosis', *American Journal of Respiratory and Critical Care Medicine*, 197(6), pp. 801–813.

Bennett, M.L. *et al.* (2016) 'New tools for studying microglia in the mouse and human CNS', *Proceedings of the National Academy of Sciences of the United States of America*, 113(12), pp. E1738–E1746.

Berger, J.R. *et al.* (2013) 'PML diagnostic criteria', *American Academy of Neurology*, 80, pp. 1430–1438.

Berger, J.R. (2017) 'Classifying PML risk with disease modifying therapies', *Multiple Sclerosis and Related Disorders*, pp. 59–63.

Berger, J.R. and Major, E. 0 (1999) Progressive Multifocal Leukoencephalopathy, *seminars in neurology*.19(2), pp. 193-200.

Betancor, G. *et al.* (2021) 'MX2-mediated innate immunity against HIV-1 is regulated by serine phosphorylation', *Nature Microbiology*, 6(8), pp. 1031–1042.

Bethesda (MD) (2004a) *Adamts6 [Internet]*, *National Library of Medicine (US), National Center for Biotechnology Information*. Available at: https://www.ncbi.nlm.nih.gov/gene/108154 (Accessed: 18 September 2023).

Bethesda (MD) (2004b) *Aoah [Internet]*, *National Library of Medicine (US), National Center for Biotechnology Information*. Available at: https://www.ncbi.nlm.nih.gov/gene/27052 (Accessed: 18 September 2023).

Bethesda (MD) (2004c) *Drd4 [Internet]*, *National Library of Medicine (US), National Center for Biotechnology Information*. Available at: https://www.ncbi.nlm.nih.gov/gene/13491 (Accessed: 18 September 2023).

Bethesda (MD) (2004d) *Erap1 [Internet]*, *National Library of Medicine (US), National Center for Biotechnology Information*. Available at: https://www.ncbi.nlm.nih.gov/gene/80898 (Accessed: 18 September 2023).

Bethesda (MD) (2004e) *Gsdmd [Internet]*, *National Library of Medicine (US), National Center for Biotechnology Information*. Available at: https://www.ncbi.nlm.nih.gov/gene/69146 (Accessed: 18 September 2023).

Bethesda (MD) (2004f) *Il10ra [Internet]*, *National Library of Medicine (US), National Center for Biotechnology Information*. Available at: https://www.ncbi.nlm.nih.gov/gene/16154 (Accessed: 18 September 2023).

Bethesda (MD) (2004g) *Lck [Internet]*, *National Library of Medicine (US), National Center for Biotechnology Information*. Available at: https://www.ncbi.nlm.nih.gov/gene/16818 (Accessed: 18 September 2023).

Bethesda (MD) (2004h) *Rnf225 [Internet]*, *National Library of Medicine (US), National Center for Biotechnology Information*. Available at: https://www.ncbi.nlm.nih.gov/gene/381845 (Accessed: 18 September 2023).

Bethesda (MD) (2004i) *Trim12c [Internet]*, *National Library of Medicine (US), National Center for Biotechnology Information*. Available at: https://www.ncbi.nlm.nih.gov/gene/?term=trim12c+mus (Accessed: 18 September 2023).

Bethesda (MD) (2004j) *Trim56 [Internet]*, *National Library of Medicine (US), National Center for Biotechnology Information*. Available at: https://www.ncbi.nlm.nih.gov/gene/384309 (Accessed: 18 September 2023).

Bettini, M., Rosenthal, K. and Evavold, B.D. (2009) 'Pathogenic MOG-reactive CD8+ T cells require MOG-reactive CD4+ T cells for sustained CNS inflammation during chronic EAE', *Journal of Neuroimmunology*, 213(1–2), pp. 60–68.

Bidgood, S.R. *et al.* (2014) 'Translocalized IgA mediates neutralization and stimulates innate immunity inside infected cells', *Proceedings of the National Academy of Sciences of the United States of America*, 111(37), pp. 13463–13468.

Bitar, M. *et al.* (2019) 'Evaluating STAT5 phosphorylation as a mean to assess T cell proliferation', *Frontiers in Immunology*, 10(APR),

Bitto, A. *et al.* (2010) 'Stress-induced senescence in human and rodent astrocytes', *Experimental Cell Research*, 316(17), pp. 2961–2968.

Björkström, N.K., Strunz, B. and Ljunggren, H.G. (2022) 'Natural killer cells in antiviral immunity', *Nature Reviews Immunology*., 22(Feb), pp. 112–123.

Boccazzi, M. *et al.* (2021) 'The immune-inflammatory response of oligodendrocytes in a murine model of preterm white matter injury: the role of TLR3 activation', *Cell Death and Disease*, 12(2).

Boehncke, W.H. and Brembilla, N.C. (2019) 'Autoreactive T-lymphocytes in inflammatory skin diseases', *Frontiers in Immunology*. 10(May), Article 1198.

Boes, M. *et al.* (1998) 'A critical role of natural immunoglobulin M in immediate defense against systemic bacterial infection', *Journal of Experimental Medicine*, 188(12), pp. 2381–2386.

Bommhardt, U., Schraven, B. and Simeoni, L. (2019) 'Beyond TCR signaling: Emerging functions of Lck in cancer and immunotherapy', *International Journal of Molecular Sciences*. 20, article 3500.

Booll-Mas, õlvia and Girones, R. (2001) Excretion and transmission of JCV in human populations, *Journal of NeuroVirology*. 7(4), pp. 345-349.

Boraschi, D. (2022) 'What Is IL-1 for? The Functions of Interleukin-1 Across Evolution', *Frontiers in Immunology*, 13.

Bose, S. and Cho, J. (2013) 'Role of chemokine CCL2 and its receptor CCR2 in neurodegenerative diseases', *Archives of Pharmacal Research*, 36, pp. 1039–1050.

Boulakirba, S. *et al.* (2018) 'IL-34 and CSF-1 display an equivalent macrophage differentiation ability but a different polarization potential', *Scientific Reports*, 8(1).

Brambilla, R. *et al.* (2005) 'Inhibition of astroglial nuclear factor κB reduces inflammation and improves functional recovery after spinal cord injury', *Journal of Experimental Medicine*, 202(1), pp. 145–156.

Brambilla, R. *et al.* (2009) 'Transgenic inhibition of astroglial NF-κB leads to increased axonal sparing and sprouting following spinal cord injury', *Journal of Neurochemistry*, 110(2), pp. 765–778.

Brandstadter, R. and Sand, I.K. (2017) 'The use of natalizumab for multiple sclerosis', *Neuropsychiatric Disease and Treatment*, 13, pp. 1691–1702.

Braun, M. *et al.* (2023) 'Levels of inflammatory cytokines MCP-1, CCL4, and PD-L1 in CSF differentiate idiopathic normal pressure hydrocephalus from neurodegenerative diseases', *Fluids and Barriers of the CNS*, 20(1).

Brod, S.A. *et al.* (1966) Interferon-plb treatment decreases tumor necrosis factor-a and increases interleukin-6 production in multiple sclerosis. 46(June), pp. 1633-1638.

ten Broeke, T., Wubbolts, R. and Stoorvogel, W. (2013) 'MHC class II antigen presentation by dendritic cells regulated through endosomal sorting', *Cold Spring Harbor Perspectives in Biology*, 5(12)

Broggi, A. and Granucci, F. (2015) 'Microbe- and danger-induced inflammation', *Molecular Immunology*, 63(2), pp. 127–133.

Bromberg, J.F. *et al.* (1996) Transcriptionally active Statl is required for the antiproliferative effects of both interferon a and interferon y. *Proc. Natl Acad. Sci. USA.* 93(July), pp.7673-7678.

Bromley, S.K., Mempel, T.R. and Luster, A.D. (2008) 'Orchestrating the orchestrators: Chemokines in control of T cell traffic', *Nature Immunology*, 9(9), pp. 970–980.

Broome, S.T. *et al.* (2020) 'Dopamine: An immune transmitter', *Neural Regeneration Research*, 15(2), pp. 2173–2185.

Bryda, E.C. (2013) 'The mighty mouse: the impact of rodents on advances in biomedical research', *Missouri Medicine*, 110(3), pp. 207–211.

Bryden, S.R. *et al.* (2020) Pan-viral protection against arboviruses by activating skin macrophages at the inoculation site, *Sci. Transl. Med*. 12(Jan), eeax2421.

Buhelt, S. *et al.* (2019) 'Relationship between multiple sclerosis-associated IL2RA risk allele variants and circulating T cell phenotypes in healthy genotype-selected controls', *Cells*, 8(6).

Buller R M L *et al.* (1987) 'Induction of cytotoxic T-cell responses in vivo in the absence of CD4 helper cells', *Nature*, 328(2), pp. 77–79.

Burmeister, A.R. and Marriott, I. (2018) 'The interleukin-10 family of cytokines and their role in the CNS', *Frontiers in Cellular Neuroscience*. 12, article 458.

Burrell, C.J., Howard, C.R. and Murphy, F.A. (2017) 'Adaptive Immune Responses to Infection', in *Fenner and White's Medical Virology*., 4th Edn. pp. 65–76.

Buttmann, M. *et al.* (2007) 'Interferon-β is a potent inducer of interferon regulatory factor-1/2-dependent IP-10/CXCL10 expression in primary human endothelial cells', *Journal of Vascular Research*, 44(1), pp. 51–60.

Cabezas, R. *et al.* (2014) 'Astrocytic modulation of blood brain barrier: Perspectives on Parkinson's disease', *Frontiers in Cellular Neuroscience*. 8, article 211.

Cai, W. *et al.* (2023) 'LDC7559 inhibits microglial activation and GSDMD-dependent pyroptosis after subarachnoid hemorrhage', *Frontiers in Immunology*, 14.

Capobianchi, M.R. *et al.* (2015) 'Type I IFN family members: Similarity, differences and interaction', *Cytokine and Growth Factor Reviews*, 26(2), pp. 103–111.

Chan, I.S. and Ewald, A.J. (2022) 'The changing role of natural killer cells in cancer metastasis', *Journal of Clinical Investigation*. 132(6), e143762.

Chang, T.-H., Yoshimi, R. and Ozato, K. (2015) 'Tripartite Motif (TRIM) 12c, a Mouse Homolog of TRIM5, Is a Ubiquitin Ligase That Stimulates Type I IFN and NF-κB Pathways along with TNFR-Associated Factor 6', *The Journal of Immunology*, 195(11), pp. 5367–5379.

Channer, B. *et al.* (2023) 'Dopamine, Immunity, and Disease', *Pharmacological Reviews*, 75(1), pp. 62–158.

Chaplin, D.D. (2010) 'Overview of the immune response', *Journal of Allergy and Clinical Immunology*, 125(2 SUPPL. 2).

Chauhan, M.B. and Chauhan, N.B. (2015) 'Brain Uptake of Neurotherapeutics after Intranasal versus Intraperitoneal Delivery in Mice', *J Neurol Neurosurg*, 2(1), pp. 1–20.

Chen, C., Wu, N. and Watson, C. (2018) 'Multiple sclerosis patients who are stable on interferon therapy show better outcomes when staying on same therapy than patients who switch to another interferon', *ClinicoEconomics and Outcomes Research*, 10, pp. 723–730.

Chen, D. *et al.* (2021) 'Interleukin-7 Biology and Its Effects on Immune Cells: Mediator of Generation, Differentiation, Survival, and Homeostasis', *Frontiers in Immunology*. 12, article 747324.

Chen, S.H., Oyarzabal, E.A. and Hong, J.S. (2013) 'Preparation of rodent primary cultures for neuron-glia, mixed glia, enriched microglia, and reconstituted cultures with microglia', *Methods in Molecular Biology*, 1041, pp. 231–240.

Chen, Z. and Li, G. (2021) 'Immune response and blood–brain barrier dysfunction during viral neuroinvasion', *Innate Immunity*, 27(2), pp. 109–117.

Chhatbar, C. and Prinz, M. (2021) 'The roles of microglia in viral encephalitis: from sensome to therapeutic targeting', *Cellular and Molecular Immunology*, 18, pp. 250–258.

Chisari, C.G. *et al.* (2021) 'Rituximab for the treatment of multiple sclerosis: a review', *Journal of Neurology*, 1(0123456789).

Chiu, S. and Bharat, A. (2016) 'Role of monocytes and macrophages in regulating immune response following lung transplantation', *Current Opinion in Organ Transplantation*, 21(3), pp. 239–245.

Choi, U.Y. *et al.* (2015) 'Oligoadenylate synthase-like (OASL) proteins: dual functions and associations with diseases', *Experimental and Molecular Medicine*. 47(3).

Chomarat, P. *et al.* (2000) 'IL-6 switches the differentiation of monocytes from dendritic cells to macrophages', *Nature immunology*, 1, pp. 510–514.

Christensen, J.E. *et al.* (2009) Fulminant Lymphocytic Choriomeningitis Virus-Induced Inflammation of the CNS Involves a Cytokine-Chemokine-Cytokine-Chemokine Cascade 1, *The Journal of Immunology*, 182(2), pp. 1079-1087.

Chun, J. and Hartung, H.P. (2010) 'Mechanism of action of oral fingolimod (FTY720) in multiple sclerosis', *Clinical Neuropharmacology*, 33(2), pp. 91–101.

Clarke, P. *et al.* (2019) Interferon Beta Contributes to Astrocyte Activation in the Brain following Reovirus Infection, *Journal of Virology*, 93(10).

Clifford, D.B. (2015) 'Neurological IRIS: riding the tide of immune-recovery', *Current Opinion in Neurology*, 28(3), pp. 295–301.

Co, J.K.G. *et al.* (2007) 'Interferon-α and -β restrict polyomavirus JC replication in primary human fetal glial cells: Implications for progressive multifocal leukoencephalopathy therapy', *Journal of Infectious Diseases*, 196(5), pp. 712–718.

Coerver, E.M.E. *et al.* (2023) 'Discontinuation of first-line disease-modifying therapy in relapse onset multiple sclerosis', *Multiple Sclerosis and Related Disorders*, 74.

Cohen, J. and Torres, C. (2019) 'Astrocyte senescence: Evidence and significance', *Aging Cell*. 18, e12937.

Colombo, E. and Farina, C. (2016) 'Astrocytes: Key Regulators of Neuroinflammation', *Trends in Immunology*, 37(9), pp. 608–620.

Colucci, F., Caligiuri, M.A. and Di Santo, J.P. (2003) 'What does it take to make a natural killer?', *Nature Reviews Immunology*, 3(May), pp. 413–425.

Comi, G. *et al.* (2021) 'Role of B Cells in Multiple Sclerosis and Related Disorders', *Annals of Neurology*, 89(1), pp. 13–23.

Cordeiro, J. V. and Jacinto, A. (2013) 'The role of transcription-independent damage signals in the initiation of epithelial wound healing', *Nature Reviews Molecular Cell Biology*, 14(Apr), pp. 249–262.

Costello, D.A. and Lynch, M.A. (2013) 'Toll-like receptor 3 activation modulates hippocampal network excitability, via glial production of interferon-β', *Hippocampus*, 23(8), pp. 696–707.

Courtney, A.H., Lo, W.L. and Weiss, A. (2018) 'TCR Signaling: Mechanisms of Initiation and Propagation', *Trends in Biochemical Sciences*, 43(2), pp. 108–123.

Creemers, P.C. *et al.* (1986) Increased interleukin-2 receptor expression after mitogen stimulation on CD4-and CD8-positive lymphocytes and decreased interleukin-2 production in HTLV-III antibody-positive symptomatic individuals, *Immunology*, 59, 627-629.

Cronk, J.C. *et al.* (2018) 'Peripherally derived macrophages can engraft the brain independent of irradiation and maintain an identity distinct from microglia', *Journal of Experimental Medicine*, 215(6), pp. 1627–1647.

Crotty, S. (2015) 'A brief history of T cell help to B cells', *Nature Reviews Immunology*, 15(3), pp. 185–189.

Cuadros, M.A. *et al.* (2022) 'Microglia and Microglia-Like Cells: Similar but Different', *Frontiers in Cellular Neuroscience*, 16, article 816439.

Cui, X. and Eyles, D.W. (2022) 'Vitamin D and the Central Nervous System: Causative and Preventative Mechanisms in Brain Disorders', *Nutrients*, 14, 4353.

Cumberbatch, M., and Kimber, I. (1992). "Dermal tumour necrosis factor-alpha induces dendritic cell migration to draining lymph nodes, and possibly provides one stimulus for Langerhans' cell migration." *Immunology,* 75(2), pp. 257-63.

Culley, F.J. *et al.* (2006) 'Role of CCL5 (RANTES) in Viral Lung Disease', *Journal of Virology*, 80(16), pp. 8151–8157.

Cunill, V. *et al.* (2018) 'Relapsing-remitting multiple sclerosis is characterized by a T follicular cell pro-inflammatory shift, reverted by dimethyl fumarate treatment', *Frontiers in Immunology*, 9(MAY).

Dahm, R., Kiebler, M. and Macchi, P. (2007) 'RNA localisation in the nervous system', *Seminars in Cell and Developmental Biology*, 18 pp. 216–223.

Dalianis, T. and Hirsch, H.H. (2013) 'Human polyomaviruses in disease and cancer', *Virology*, 437, pp. 63–72.

Daniels, M.A. *et al.* (2001) 'CD8 Binding to MHC Class I Molecules Is Influenced by T Cell Maturation and Glycosylation', *Immunity*, 15, pp. 1051–1061.

Decout, A. *et al.* (2021) 'The cGAS–STING pathway as a therapeutic target in inflammatory diseases', *Nature Reviews Immunology*, 21, pp. 548–569.

DeGiosio, R.A. *et al.* (2022) 'More than a marker: potential pathogenic functions of MAP2', *Frontiers in Molecular Neuroscience*, 15.

Detje, C.N. *et al.* (2015) 'Upon Intranasal Vesicular Stomatitis Virus Infection, Astrocytes in the Olfactory Bulb Are Important Interferon Beta Producers That Protect from Lethal Encephalitis', *Journal of Virology*, 89(5), pp. 2731–2738.

Dixon, H. *et al.* (2006) 'The role of Th2 cytokines, chemokines and parasite products in eosinophil recruitment to the gastrointestinal mucosa during helminth infection', *European Journal of Immunology*, 36(7), pp. 1753–1763.

Dixon, M.A. *et al.* (2021) 'The Contribution of Microglia to the Development and Maturation of the Visual System', *Frontiers in Cellular Neuroscience*, 15.

Domachowske, J.B. *et al.* (2000) The Chemokine Macrophage-Inflammatory Protein-1 and Its Receptor CCR1 Control Pulmonary Inflammation and Antiviral Host Defense in Paramyxovirus Infection, *The Journal of Immunology*, 165(5), pp. 2677-2682.

Dong, C. (2021) 'Cytokine Regulation and Function in T Cells'. *Annual Review of Immunology*, 39, pp. 51-76.

Dorries, K. and Ter Meulen, V. (1983) Progressive MuItifocal Leucoencephalopathy : Detection of Papovavirus JC in Kidney Tissue, *Journal of Medical Virology,* 11, pp. 307-317.

Dubey, D. *et al.* (2018) 'Autoimmune encephalitis epidemiology and a comparison to infectious encephalitis', *Annals of Neurology*, 83(1), pp. 166–177.

Durafourt, B.A. *et al.* (2013) 'Isolating, Culturing, and Polarizing Primary Human Adult and Fetal Microglia', *Microglia: Methods and Protocols*., 1st Edn. pp. 199–211.

Durali, D. *et al.* (2015) 'B cells and progressive multifocal leukoencephalopathy: Search for the missing link', *Frontiers in Immunology*, 15, article 241.

Durfee, L.A. *et al.* (2010) 'The ISG15 Conjugation System Broadly Targets Newly Synthesized Proteins: Implications for the Antiviral Function of ISG15', *Molecular Cell*, 38(5), pp. 722–732.

Dyck, S. *et al.* (2018) 'Perturbing chondroitin sulfate proteoglycan signaling through LAR and PTPσ receptors promotes a beneficial inflammatory response following spinal cord injury', *Journal of Neuroinflammation*, 15(1).

Eberlein, J. *et al.* (2020) 'Chemokine Signatures of Pathogen-Specific T Cells I: Effector T Cells', *The Journal of Immunology*, 205(8), pp. 2169–2187.

Edgar, J.M. *et al.* (2021) 'Río-Hortega's drawings revisited with fluorescent protein defines a cytoplasm-filled channel system of CNS myelin', *Journal of Anatomy*, 239(6), pp. 1241–1255.

Efendi, H. (2015) 'Clinically isolated syndromes: Clinical characteristics, differential diagnosis, and management', *Noropsikiyatri Arsivi*. 52(Suppl 1), pp. S1–S11.

Egea, L., Hirata, Y. and Kagnoff, M.F. (2010) 'GM-CSF: A role in immune and inflammatory reactions in the intestine', *Expert Review of Gastroenterology and Hepatology*, 4(6), pp. 723–731.

Eisele, P. *et al.* (2021) 'Characterization of chronic active multiple sclerosis lesions with sodium (23Na) magnetic resonance imaging—preliminary observations', *European Journal of Neurology*, 28(7), pp. 2392–2395.

Elphick, G.F. et al (2004) 'The human polyomavirus, JCV, uses serotonin receptors to infect cells', *Science*, 306, pp. 1380–1383.

Van Erp, E.A. *et al.* (2019) 'Viral infection of human natural killer cells', *Viruses*. 11(3):243.

Estevao, C. *et al.* (2021) 'CCL4 induces inflammatory signalling and barrier disruption in the neurovascular endothelium', *Brain, Behavior, and Immunity - Health*, 18.

Falcão, A.M. *et al.* (2018) 'Disease-specific oligodendrocyte lineage cells arise in multiple sclerosis', *Nature Medicine*, 24(12), pp. 1837–1844.

Fazakerley, J.K. *et al.* (2006) 'Virus tropism, distribution, persistence and pathology in the corpus callosum of the Semliki Forest virus-infected mouse brain: A novel system to study virus-oligodendrocyte interactions', *Neuropathology and Applied Neurobiology*, 32(4), pp. 397–409.

Fazakerley, J.K. and Webb, H.E. (1987) 'Semliki Forest virus induced, immune mediated demyelination: the effect of irradiation', *Br. J. exp. Path*, 68, p. 3.

Ferrari, G. *et al.* (2011) 'An HIV-1 gp120 Envelope Human Monoclonal Antibody That Recognizes a C1 Conformational Epitope Mediates Potent Antibody-Dependent Cellular Cytotoxicity (ADCC) Activity and Defines a Common ADCC Epitope in Human HIV-1 Serum', *Journal of Virology*, 85(14), pp. 7029–7036.

Ferreira, J.E. *et al.* (2019) 'Molecular characterization of viruses associated with encephalitis in São Paulo, Brazil', *PLoS ONE*, 14(1).

Field, R. *et al.* (2010) 'Systemic challenge with the TLR3 agonist poly I: C induces amplified IFNα/β and IL-1β responses in the diseased brain and exacerbates chronic neurodegeneration', *Brain, Behavior, and Immunity*, 24(6), pp. 996–1007.

Filipi, M. and Jack, S. (2020) 'Interferons in the treatment of multiple sclerosis: A clinical efficacy, safety, and tolerability update', *International Journal of MS Care*, 22(4), pp. 165–172.

Filipi, M.L. *et al.* (2014) 'Nurses' perspective on approaches to limit flu-like symptoms during interferon therapy for multiple sclerosis', *International Journal of MS Care*, 16(1), pp. 55–60.

Fine, N. *et al.* (2020) 'The Neutrophil: Constant Defender and First Responder', *Frontiers in Immunology*, 11, article 571085.

Fitzgerald, K.A., McWhirter, S.M., *et al.* (2003) 'IKKE and TBKI are essential components of the IRF3 signalling pathway', *Nature Immunology*, 4(5), pp. 491–496.

Fitzgerald, K.A., Rowe, D.C., *et al.* (2003) 'LPS-TLR4 signaling to IRF-3/7 and NF-κB involves the toll adapters TRAM and TRIF', *Journal of Experimental Medicine*, 198(7), pp. 1043–1055.

Fletcher, J.M. *et al.* (2010) 'T cells in multiple sclerosis and experimental autoimmune encephalomyelitis', *Clinical and Experimental Immunology*, 162, pp. 1–11.

Forthal, D.N. (2014) 'Functions of Antibodies', *Microbiol Spectr*, 2(4), pp. 1–17.

Fournier, A. *et al.* (2017) 'Immune reconstitution inflammatory syndrome unmasking or worsening aids-related progressive multifocal leukoencephalopathy: A literature review', *Frontiers in Immunology*. 23(8), article 00577.

Fragkoudis, R. *et al.* (2009) 'Neurons and oligodendrocytes in the mouse brain differ in their ability to replicate Semliki Forest virus', *Journal of NeuroVirology*, 15(1), pp. 57–70.

Frattaroli, P. *et al.* (2021) 'Immune reconstitution inflammatory syndrome with recurrent paradoxical cerebellar hiv-associated progressive multifocal leukoencephalopathy', *Pathogens*, 10(7).

Frauwirth, K.A. and Thompson, C.B. (2002) 'Activation and inhibition of lymphocytes by costimulation', *Journal of Clinical Investigation*, 109(3), pp. 295–299.

Fresegna, D. *et al.* (2020) 'Re-Examining the Role of TNF in MS Pathogenesis and Therapy', *Cells*. 9, 2290.

Fu, L. *et al.* (2023) 'The Functions of TRIM56 in Antiviral Innate Immunity and Tumorigenesis', *International Journal of Molecular Sciences*, 24, 5046.

Fu, X.-Y. *et al.* (1990) ISGF3, the transcriptional activator induced by interferon a, consists of multiple interacting polypeptide chains, *Proc. Natl. Acad. Sci. USA*, 87, pp, 8555-8559.

Fu, Z. *et al.* (2021) 'In vivo self-assembled small RNAs as a new generation of RNAi therapeutics', *Cell Research*, 31(6), pp. 631–648.

Fujii, S.I. *et al.* (2002) 'Prolonged IFN-γ-producing NKT response induced with α-galactosylceramide-loaded DCs', *Nature Immunology*, 3(9), pp. 867–874.

G. Kantzer, C. *et al.* (2017) 'Anti-ACSA-2 defines a novel monoclonal antibody for prospective isolation of living neonatal and adult astrocytes', *GLIA*, 65(6), pp. 990–1004.

Gadani, S.P. *et al.* (2012) 'IL-4 in the Brain: A Cytokine To Remember', *The Journal of Immunology*, 189(9), pp. 4213–4219.

Gajofatto, A. and Benedetti, M.D. (2015) 'Treatment strategies for multiple sclerosis: When to start, when to change, when to stop?', *World Journal of Clinic]al Cases*, 3(7), p. 545.

Galea, I. (2021) 'The blood–brain barrier in systemic infection and inflammation', *Cellular and Molecular Immunology*, 18, pp. 2489–2501.

Galiano, M.R. *et al.* (2006) 'Myelin basic protein functions as a microtubule stabilizing protein in differentiated oligodendrocytes', *Journal of Neuroscience Research*, 84(3), pp. 534–541.

Gamble, A. *et al.* (2023) 'Establishing Mixed Neuronal and Glial Cell Cultures from Embryonic Mouse Brains to Study Infection and Innate Immunity', *Journal of Visualized Experiments*, 2023(196).

Gangaplara, A. *et al.* (2018) 'Type I interferon signaling attenuates regulatory T cell function in viral infection and in the tumor microenvironment', *PLoS Pathogens*, 14(4).

Garré, J.M. and Yang, G. (2018) 'Contributions of monocytes to nervous system disorders', *Journal of Molecular Medicine*., 96(9), pp. 873–883.

Gauthier, M. *et al.* (2021) 'Natural Killer cells and monoclonal antibodies: Two partners for successful antibody dependent cytotoxicity against tumor cells', *Critical Reviews in Oncology/Hematology*. 160(Apr).

Gauzzi, M.C. *et al.* (1996) Interferon-dependent Activation of Tyk2 Requires Phosphorylation of Positive Regulatory Tyrosines by Another Kinase, *biological chemistry*, 271(34), pp. 20494-20500.

Gavin, C. *et al.* (2019) 'The Complement System Is Essential for the Phagocytosis of Mesenchymal Stromal Cells by Monocytes', *Frontiers in Immunology*, 10.

Ge, L. *et al.* (2020) 'LCK expression is a potential biomarker for distinguishing primary central nervous system lymphoma from glioblastoma multiforme', *FEBS Open Bio*, 10(5), pp. 904–911.

Geisberger, R., Lamers, M. and Achatz, G. (2006) 'The riddle of the dual expression of IgM and IgD', *Immunology*, 118, pp. 429–437.

Geisert, E.E. *et al.* (1990) Expression of microtubule-associated protein 2 by reactive astrocytes, *Proc. Nadl. Acad. Sci. USA*. 87(10), pp. 3967-3971.

Gelfand, J.M., Cree, B.A.C. and Hauser, S.L. (2017) 'Ocrelizumab and Other CD20+ B-Cell-Depleting Therapies in Multiple Sclerosis', *Neurotherapeutics*, 14, pp. 835–841

Geloso, M.C. and D'ambrosi, N. (2021) 'Microglial pruning: Relevance for synaptic dysfunction in multiple sclerosis and related experimental models', *Cells*, 10(3), ,pp. 1–17.

Gemma, C. and Bachstetter, A.D. (2013) 'The role of microglia in adult hippocampal neurogenesis', *Frontiers in Cellular Neuroscience*. 7, article 229.

Gengatharan, A., Bammann, R.R. and Saghatelyan, A. (2016) 'The role of astrocytes in the generation, migration, and integration of new neurons in the adult olfactory bulb', *Frontiers in Neuroscience*. 10, article 149.

Ghasemi, N., Razavi, S. and Nikzad, E. (2017) 'Multiple sclerosis: Pathogenesis, symptoms, diagnoses and cell-based therapy', *Cell Journal*, 19(1), pp. 1–10.

Gheuens, S. *et al.* (2011) ' Role of CD4 + and CD8 + T-Cell Responses against JC Virus in the Outcome of Patients with Progressive Multifocal Leukoencephalopathy (PML) and PML with Immune Reconstitution Inflammatory Syndrome ', *Journal of Virology*, 85(14), pp. 7256–7263.

Ghosh, A. *et al.* (2019) 'Oligoadenylate-Synthetase-Family Protein OASL Inhibits Activity of the DNA Sensor cGAS during DNA Virus Infection to Limit Interferon Production', *Immunity*, 50(1), pp. 51-63.e5.

Gill, N. *et al.* (2011) 'NK cells require type I IFN receptor for antiviral responses during genital HSV-2 infection', *Cellular Immunology*, 269(1), pp. 29–37.

Gillespie, M. *et al.* (2022) 'The reactome pathway knowledgebase 2022', *Nucleic Acids Research*, 50(D1), pp. D687–D692.

Ginhoux, F. *et al.* (2010) 'Fate mapping analysis reveals that adult microglia derive from primitive macrophages', *Science*, 330(6005), pp. 841–845.

Ginhoux, F. and Prinz, M. (2015) 'Origin of microglia: Current concepts and past controversies', *Cold Spring Harbor Perspectives in Biology*, 7(8).

Giovannoni, F. and Quintana, F.J. (2020) 'The Role of Astrocytes in CNS Inflammation', *Trends in Immunology*., 41(9), pp. 805–819.

Glim, J.E. *et al.* (2010) 'The release of cytokines by macrophages is not affected by myelin ingestion', *GLIA*, 58(16), pp. 1928–1936.

Goaillard, J.M. *et al.* (2020) 'Diversity of Axonal and Dendritic Contributions to Neuronal Output', *Frontiers in Cellular Neuroscience*. 13, article 570.

Godin, I. and Cumano, A. (2002) 'The hare and the tortoise: An embryonic haematopoietic race', *Nature Reviews Immunology*. European Association for Cardio-Thoracic Surgery, 2(august), pp. 593–604.

Gold, R. and Lühder, F. (2008) 'Interleukin-17 - Extended features of a key player in multiple sclerosis', *American Journal of Pathology*.172(1),, pp. 8–10.

Goldenberg, M.M. (2012) 'Multiple Sclerosis Review', *P&T*, 37(3), pp. 175–184.

Goldmann, T. *et al.* (2015) ' USP 18 lack in microglia causes destructive interferonopathy of the mouse brain ', *The EMBO Journal*, 34(12), pp. 1612–1629.

Gómez-Nicola, D. *et al.* (2013) 'Regulation of microglial proliferation during chronic neurodegeneration', *Journal of Neuroscience*, 33(6), pp. 2481–2493.

Gosert, R. *et al.* (2010) 'Rearranged JC Virus Noncoding Control Regions Found in Progressive Multifocal Leukoencephalopathy Patient Samples Increase Virus Early Gene Expression and Replication Rate', *Journal of Virology*, 84(20), pp. 10448–10456.

Gravel, M. *et al.* (1996) Overexpression of 2',3,-Cyclic Nucleotide 3'-Phosphodiesterase in Transgenic Mice Alters Oligodendrocyte Development and Produces Aberrant Myelination, *Molecular and Cellular Neuroscience*. 7, pp. 453-466.

Greenbaum, D. *et al.* (2003) Comparing protein abundance and mRNA expression levels on a genomic scale, *Genome Biology*. 4(117), pp. 117.1-117.8

Greenberg, B.M. *et al.* (2022) 'A double-blind, placebo-controlled, single-ascending-dose intravenous infusion study of rHIgM22 in subjects with multiple sclerosis immediately following a relapse', *Multiple Sclerosis Journal - Experimental, Translational and Clinical*, 8(2).

Greenfeder, S. *et al.* (2001) 'Th2 cytokines and asthma The role of interleukin-5 in allergic eosinophilic disease', *Respir Res*, (2), pp. 71–79.

Greenfield, A.L. and Hauser, S.L. (2018) 'B-cell Therapy for Multiple Sclerosis: Entering an era', *Annals of Neurology*, 83(1), pp. 13–26.

Griffin, D.E. (1991) Therapy of viral infections of the central nervous system, *Antiviral Research*. 15, pp. 1-10

Griss, J. *et al.* (2020) 'ReactomeGSA - Efficient Multi-Omics Comparative Pathway Analysis', *Molecular and Cellular Proteomics*, 19(12), pp. 2115–2124.

Gruber, C. *et al.* (2020) 'Homozygous STAT2 gain-of-function mutation by loss of USP18 activity in a patient with type I interferonopathy', *Journal of Experimental Medicine*, 217(5).

Guo, D., Hu, H. and Pan, S. (2020) 'Oligodendrocyte dysfunction and regeneration failure: A novel hypothesis of delayed encephalopathy after carbon monoxide poisoning', *Medical Hypotheses*, 136.

Guo, X. *et al.* (2021) 'Interferon-Induced Transmembrane Protein 3 Blocks Fusion of Diverse Enveloped Viruses by Altering Mechanical Properties of Cell Membranes Interferon-Induced Transmembrane Protein 3 Blocks Fusion of Diverse Enveloped Viruses by Altering Mechanical Properties of Cell Membranes HHS Public Access', *ACS Nano*, 15(5), pp. 8155–8170.

Gygi, S.P. *et al.* (1999) Correlation between Protein and mRNA Abundance in Yeast, *molecular and cellular biology*, 19(3), pp. 1720-1730.

Haley, S.A. *et al.* (2015) 'Human Polyomavirus Receptor Distribution in Brain Parenchyma Contrasts with Receptor Distribution in Kidney and Choroid Plexus', *American Journal of Pathology*, 185(8), pp. 2246–2258.

Hall, C.L. and Munford, R.S. (1983) Enzymatic deacylation of the lipid A moiety of Salmonella typhimurium lipopolysaccharides by human neutrophils , *Proc. Nati. Acad. Sci. USA*. 80, pp. 6671-6675.

Haller, O. *et al.* (2015) 'Mx GTPases: Dynamin-like antiviral machines of innate immunity', *Trends in Microbiology*, 23(3), pp. 154–163.

Hammer, G.E., Kanaseki, T. and Shastri, N. (2007) 'The Final Touches Make Perfect the Peptide-MHC Class I Repertoire', *Immunity*, 26, pp. 397–406.

Hanaei, S. *et al.* (2020) 'Prevalence of anti-jc virus antibody seropositivity in patients with multiple sclerosis: A systematic review and meta-Analysis', *Intervirology*, 62 pp. 169–173.

Hanamsagar, R., Hanke, M.L. and Kielian, T. (2012) 'Toll-like receptor (TLR) and inflammasome actions in the central nervous system', *Trends in Immunology*,33(7), pp. 333–342.

Handschin, J. *et al.* (2020) 'Technical Considerations and Confounders for Urine CXCL10 Chemokine Measurement', *Transplantation Direct*, 6(1), p. E519.

Harper, E.G. *et al.* (2009) 'Th17 cytokines stimulate CCL20 expression in keratinocytes in vitro and in vivo: Implications for psoriasis pathogenesis', *Journal of Investigative Dermatology*, 129(9), pp. 2175–2183.

Harrington, E.P. *et al.* (2023) 'MHC class i and MHC class ii reporter mice enable analysis of immune oligodendroglia in mouse models of multiple sclerosis', *eLife*, 12.

Hato, T. and Dagher, P.C. (2015) 'How the innate immune system senses trouble and causes trouble', *Clinical Journal of the American Society of Nephrology*, 10(8), pp. 1459–1469.

Haugen, M., Frederiksen, J.L. and Degn, M. (2014) 'B cell follicle-like structures in multiple sclerosis-With focus on the role of B cell activating factor', *Journal of Neuroimmunology*, pp. 1–7.

Hauser, S.L. and Cree, B.A.C. (2020) 'Treatment of Multiple Sclerosis: A Review', *American Journal of Medicine*, 133(12), pp. 1380-1390.e2.

Häusser-Kinzel, S. and Weber, M.S. (2019) 'The role of B cells and antibodies in multiple sclerosis, neuromyelitis optica, and related disorders', *Frontiers in Immunology*, 10, article 201.

Havenar-Daughton, C., Kolumam, G.A. and Murali-Krishna, K. (2006) Cutting Edge: The Direct Action of Type I IFN on CD4 T Cells Is Critical for Sustaining Clonal Expansion in Response to a Viral but Not a Bacterial Infection 1, *Immunology*, 176(6), pp. 3315-3319.

Havla, J. and Hohlfeld, R. (2022) 'Antibody Therapies for Progressive Multiple Sclerosis and for Promoting Repair', *Neurotherapeutics*. 19, pp. 774–784.

Hawley, T.S., Hawley, R.G. and Telford, W.G. (2017) 'Fluorescent proteins for flow cytometry', *Current Protocols in Cytometry*, 2017, pp. 9.12.1-9.12.20.

Hayden, L. *et al.* (2020) 'Lipid-specific IgMs induce antiviral responses in the CNS: Implications for progressive multifocal leukoencephalopathy in multiple sclerosis', *Acta Neuropathologica Communications*, 8(135), pp. 1–16.

Heine, S. *et al.* (2006) 'Effects of interferon-beta on oligodendroglial cells', *Journal of Neuroimmunology*, 177(1–2), pp. 173–180.

Helbig, K.J. *et al.* (2005) 'Analysis of ISG expression in chronic hepatitis C identifies viperin as a potential antiviral effector', *Hepatology*, 42(3), pp. 702–710.

Heufler, C. *et al.* (1996) Interleukin-l2 is produced by dendritic cells and mediates T helper 1 development as well as interferon-y production by T helper 1 cells *Eur. J. Immunol*, 26, pp. 659-668

Hewitt, E.W. (2003) 'The MHC class I antigen presentation pathway: strategies for viral immune evasion', *Immunology*, 110, pp. 163–169.

Hiramoto, E. *et al.* (2018) The IgM pentamer is an asymmetric pentagon with an open groove that binds the AIM protein, *Sci. Adv*, 4, eaau1199.

Hiyoshi, H. *et al.* (2018) 'Mechanisms to Evade the Phagocyte Respiratory Burst Arose by Convergent Evolution in Typhoidal Salmonella Serovars', *Cell Reports*, 22(7), pp. 1787–1797.

Hoeffel, G. and Ginhoux, F. (2018) 'Fetal monocytes and the origins of tissue-resident macrophages', *Cellular Immunology*, 330, pp. 5–15.

Hollen, C. *et al.* (2020) 'The Future of Progressive Multiple Sclerosis Therapies', *Federal Practicioner Special Issue*, (April), pp. S43–S49.

Hollenbach, J.A. and Oksenberg, J.R. (2015) 'The immunogenetics of multiple sclerosis: A comprehensive review', *Journal of Autoimmunity*. 64, pp. 13–25.

Holloman, J.P. *et al.* (2021) 'The Role of B Cells in Primary Progressive Multiple Sclerosis', *Frontiers in Neurology*, 12, article 680581.

Horiuchi, M. *et al.* (2006) 'MEK-ERK signaling is involved in interferon-γ-induced death of oligodendroglial progenitor cells', *Journal of Biological Chemistry*, 281(29), pp. 20095–20106.

Horiuchi, M. *et al.* (2011) 'Cooperative contributions of Interferon regulatory factor 1 (IRF1) and IRF8 to interferon-γ-mediated cytotoxic effects on oligodendroglial progenitor cells', *Journal of Neuroinflammation*, 8.

Hornung, V. *et al.* (2004) Replication-Dependent Potent IFN-Induction in Human Plasmacytoid Dendritic Cells by a Single-Stranded RNA Virus 1, *The Journal of Immunology*, 173(10), pp. 5935-5943.

Hou, Y., Jia, Y. and Hou, J. (2018) 'Natural Course of Clinically Isolated Syndrome: A Longitudinal Analysis Using a Markov Model', *Scientific Reports*, 8(1).

Hovanessian, A.G. and Justesen, J. (2007) 'The human 2'-5'oligoadenylate synthetase family: Unique interferon-inducible enzymes catalyzing 2'-5' instead of 3'-5' phosphodiester bond formation', *Biochimie*, 89(6–7), pp. 779–788.

Huang, Y. *et al.* (2014) 'Met-CCL5 represents an immunotherapy strategy to ameliorate rabies virus infection', *Journal of Neuroinflammation*, 11(1).

Huber, J.P. and David Farrar, J. (2011) 'Regulation of effector and memory T-cell functions by type I interferon', *Immunology*, 132, pp. 466–474.

Hulshof, S. *et al.* (2002) 'Cellular localization and expression patterns of interleukin-10, interleukin-4, and their receptors in multiple sclerosis lesions', *GLIA*, 38(1), pp. 24–35.

Hwang, M. and Bergmann, C.C. (2018) 'Alpha/Beta Interferon (IFN-α/β) Signaling in Astrocytes Mediates Protection against Viral Encephalomyelitis and Regulates IFN-γ-Dependent Responses', *Journal of Virology*, 92(10).

Imai, Y. *et al.* (1996) 'A Novel Gene iba1 in the Major Histocompatibility Complex Class III Region Encoding an EF Hand Protein Expressed in a Monocytic Lineage 1', *Biochemical and biophysical research communications*, 224(1112), pp. 855–862.

Imai, Y. *et al.* (2008) 'Identification of Oxidative Stress and Toll-like Receptor 4 Signaling as a Key Pathway of Acute Lung Injury', *Cell*, 133(2), pp. 235–249.

Ishige, K. *et al.* (2001) *The Activation of Dopamine D4 Receptors Inhibits Oxidative Stress-Induced Nerve Cell Death*, 21(16), pp. 6069-6076.

Ito, D. *et al.* (1988) *Microglia-specific localisation of a novel calcium binding protein, Iba1*, *Molecular Brain Research*. 57, pp. 1-7.

Ivashkiv, L.B. and Donlin, L.T. (2014) 'Regulation of type i interferon responses', *Nature Reviews Immunology*, 14(1), pp. 36–49.

Iwasaki, A. and Medzhitov, R. (2004) 'Toll-like receptor control of the adaptive immune responses', *Nature Immunology*, 5(10), pp. 987–995.

Izzy, S. *et al.* (2019) 'Time-Dependent Changes in Microglia Transcriptional Networks Following Traumatic Brain Injury', *Frontiers in Cellular Neuroscience*, 13.

Jack, C.S. *et al.* (2005) 'TLR Signaling Tailors Innate Immune Responses in Human Microglia and Astrocytes', *The Journal of Immunology*, 175(7), pp. 4320–4330.

Jafari, M. *et al.* (2013) 'Distorted expression of dopamine receptor genes in systemic lupus erythematosus', *Immunobiology*, 218(7), pp. 979–983.

Jakimovski, D. *et al.* (2018) 'Interferon β for Multiple Sclerosis', *Cold Spring Harbor perspectives in medicine*. 8, a032003.

James, S.H., Kimberlin, D.W. and Whitley, R.J. (2009) 'Antiviral therapy for herpesvirus central nervous system infections: Neonatal herpes simplex virus infection, herpes simplex encephalitis, and congenital cytomegalovirus infection', *Antiviral Research*, 83(3), pp. 207–213.

Janeway, C.J., Travers, P. and Walport, M. (2001) 'The complement system and innate immunity', in *Immunobiology: The immune system in health and disease*. 5th edn.

Jelčić, Ilijas *et al.* (2013) ' T Cell Epitope Mapping of JC Polyoma Virus-Encoded Proteome Reveals Reduced T Cell Responses in HLA-DRB1*04:01 + Donors ', *Journal of Virology*, 87(6), pp. 3393–3408.

Jia, G.-Q. *et al.* (1996) Distinct Expression and Function of the Novel Mouse Chemokine Monocyte Chemotactic Protein-5 in Lung Allergic Inflammation. *J. exp med.* 184, pp. 1939-1951.

Jiang, Z.G. *et al.* (2010) 'Hexadecyloxypropyl-cidofovir (CMX001) suppresses JC virus replication in human fetal brain SVG cell cultures', *Antimicrobial Agents and Chemotherapy*, 54(11), pp. 4723–4732.

Jorgovanovic, D. *et al.* (2020) 'Roles of IFN-γin tumor progression and regression: A review', *Biomarker Research*. 8(49).

Jung, H.E., Oh, J.E. and Lee, H.K. (2019) 'Cell-penetrating Mx1 enhances anti-viral resistance against mucosal influenza viral infection', *Viruses*, 11(2).

Jung, S. and Schwartz, M. (2012) 'Non-identical twins - microglia and monocyte-derived macrophages in acute injury and autoimmune inflammation', *Frontiers in Immunology*. 3, article 89.

Kadir, L.A., Stacey, M. and Barrett-Jolley, R. (2018) 'Emerging roles of the membrane potential: Action beyond the action potential', *Frontiers in Physiology*. 9, article 1661.

Kahn, R.A., Der, C.J. and Bokoch, G.M. (1992) The ras superfamily of GTP-binding proteins: guidelines on nomenclature, *Faseb*, 6(8), pp. 2512-2513.

Kallfass, C. *et al.* (2012) 'Visualizing Production of Beta Interferon by Astrocytes and Microglia in Brain of La Crosse Virus-Infected Mice', *Journal of Virology*, 86(20), pp. 11223–11230.

Kalló, G. *et al.* (2022) 'Chemical Barrier Proteins in Human Body Fluids', *Biomedicines*. 10(7), pp. 1472.

Kamma, E. *et al.* (2022) 'Central nervous system macrophages in progressive multiple sclerosis: relationship to neurodegeneration and therapeutics', *Journal of Neuroinflammation*. 19(45).

Kanehisa, M. (2019) 'Toward understanding the origin and evolution of cellular organisms', *Protein Science*. Blackwell Publishing Ltd, 28, pp. 1947–1951.

Kanehisa, M. *et al.* (2023) 'KEGG for taxonomy-based analysis of pathways and genomes', *Nucleic Acids Research*, 51(D1), pp. D587–D592.

Kanehisa, M. and Goto, S. (2000) *KEGG: Kyoto Encyclopedia of Genes and Genomes*, *Nucleic Acids Research*. Available at: http://www.genome.ad.jp/kegg/.

Kang, J.S. *et al.* (2018) 'OASL1 traps viral RNAs in stress granules to promote antiviral responses', *Molecules and Cells*, 41(3), pp. 214–223.

Kapellos, T.S. *et al.* (2019) 'Human monocyte subsets and phenotypes in major chronic inflammatory diseases', *Frontiers in Immunology*. 30(Aug), pp. 2010-2035.

Kaskow, B.J. and Baecher-Allan, C. (2018) 'Effector t cells in multiple sclerosis', *Cold Spring Harbor Perspectives in Medicine*, 8(4).

Kasper, L.H. and Reder, A.T. (2014) 'Immunomodulatory activity of interferon-beta', *Annals of Clinical and Translational Neurology*. Wiley-Blackwell, 1(8), pp. 622–631.

Kato, A. *et al.* (2004) 'Detection of the archetypal regulatory region of JC virus from the tonsil tissue of patients with tonsillitis and tonsilar hypertrophy', *Journal of NeuroVirology*, 10(4), pp. 244–249.

Katz Sand, I. (2018) 'The Role of Diet in Multiple Sclerosis: Mechanistic Connections and Current Evidence', *Current Nutrition Reports*, 7(3), pp. 150–160.

Katze, M.G., He, Y. and Gale, M. (2002) 'Viruses and interferon: A fight for supremacy', *Nature Reviews Immunology*, 2(Sep), pp. 675–687.

Kaul, M., Garden, G.A. and Lipton, S.A. (2001) 'Pathways to neuronal injury and apoptosis in HIV-associated dementia', *Nature*, 410, pp. 988–994.

Kaur, M. and Esau, L. (2015) 'Two-step protocol for preparing adherent cells for high-throughput flow cytometry', *BioTechniques*, 59(3), pp. 119–126.

Kaveri, S. V., Silverman, G.J. and Bayry, J. (2012) 'Natural IgM in Immune Equilibrium and Harnessing Their Therapeutic Potential', *The Journal of Immunology*, 188(3), pp. 939–945.

Kebir, H. *et al.* (2007) 'Human TH17 lymphocytes promote blood-brain barrier disruption and central nervous system inflammation', *Nature Medicine*, 13(10), pp. 1173–1175.

Keele, B.F. *et al.* (2008) Identification and characterization of transmitted and early founder virus envelopes in primary HIV-1 infection, *PNAS*, 105(21), pp. 7552-7557.

Kelwick, R. *et al.* (2015) 'The ADAMTS (A Disintegrin and Metalloproteinase with Thrombospondin motifs) family', *Genome Biology*, 16(1).

Kenway-Lynch, C.S. *et al.* (2014) ' Cytokine/Chemokine Responses in Activated CD4 + and CD8 + T Cells Isolated from Peripheral Blood, Bone Marrow, and Axillary Lymph Nodes during Acute Simian Immunodeficiency Virus Infection ', *Journal of Virology*, 88(16), pp. 9442–9457.

Keyt, B.A. *et al.* (2020) 'Structure, Function, and Therapeutic Use of IgM Antibodies', *Antibodies*, 9(4), p. 53.

Kiefer, K. *et al.* (2012) 'Role of type i interferons in the activation of autoreactive B cells', *Immunology and Cell Biology*, 90(5), pp. 498–504.

Kigerl, K.A. *et al.* (2014) 'Pattern recognition receptors and central nervous system repair', *Experimental Neurology*. 258, pp. 5–16.

Kim, H.-S. (2013) 'Role of insulin-like growth factor binding protein-3 in glucose and lipid metabolism', *Annals of Pediatric Endocrinology & Metabolism*, 18(1), p. 9.

Kim, N.D. and Luster, A.D. (2015) 'The role of tissue resident cells in neutrophil recruitment', *Trends in Immunology*, pp. 547–555.

Kirby, L. *et al.* (2019) 'Oligodendrocyte precursor cells present antigen and are cytotoxic targets in inflammatory demyelination', *Nature Communications*, 10(1).

Kirby, L. and Castelo-Branco, G. (2021) 'Crossing boundaries: Interplay between the immune system and oligodendrocyte lineage cells', *Seminars in Cell and Developmental Biology*, 116, pp. 45–52.

Klineova, S. and Lublin, F.D. (2018) 'Clinical course of multiple sclerosis', *Cold Spring Harbor Perspectives in Medicine*, 8(9).

Knowles, W.A. *et al.* (2003) 'Population-based study of antibody to the human polyomaviruses BKV and JCV and the simian polyomavirus SV40', *Journal of Medical Virology*, 71(1), pp. 115–123.

Kolb, H. *et al.* (2022) 'From pathology to MRI and back: Clinically relevant biomarkers of multiple sclerosis lesions', *NeuroImage: Clinical*, 36.

Kolls, J.K. and Lindé, A. (2004) Interleukin-17 Family Members and Inflammation, *Immunity*, 21, pp. 467-476.

Kolumam, G.A. *et al.* (2005) 'Type I interferons act directly on CD8 T cells to allow clonal expansion and memory formation in response to viral infection', *Journal of Experimental Medicine*, 202(5), pp. 637–650.

Kondo, Y. *et al.* (2014) 'Human glial chimeric mice reveal astrocytic dependence of JC virus infection', *Journal of Clinical Investigation*, 124(12), pp. 5323–5336.

Kopitar-Jerala, N. (2017) 'The role of interferons in inflammation and inflammasome activation', *Frontiers in Immunology*. 8, article 873.

Korn, T. *et al.* (2009) 'IL-17 and Th17 cells', *Annual Review of Immunology*, 27, pp. 485–517.

Koronyo-Hamaoui, M. *et al.* (2009) 'Attenuation of AD-like neuropathology by harnessing peripheral immune cells: Local elevation of IL-10 and MMP-9', *Journal of Neurochemistry*, 111(6), pp. 1409–1424.

Koudriavtseva, T. and Mainero, C. (2016) 'Neuroinflammation, neurodegeneration and regeneration in multiple sclerosis: Intercorrelated manifestations of the immune response', *Neural Regeneration Research*, 11(11), pp. 1727–1730.

Kovacs, G.G. (2018) 'Cellular reactions of the central nervous system', in *Handbook of Clinical Neurology*. 145, pp. 13–23.

Kowarik, M.C. *et al.* (2012) CXCL13 is the major determinant for B cell recruitment to the CSF during neuroinflammation, *Neuroinflammation*, 9(93), pp. 1-11.

Koyuncu, O.O., Hogue, I.B. and Enquist, L.W. (2013) 'Virus infections in the nervous system', *Cell Host and Microbe*. pp. 379–393.

Krammer, F. (2019) 'The human antibody response to influenza A virus infection and vaccination', *Nature Reviews Immunology*. 19(June), pp. 383–397.

Kraus, J. *et al.* (2008) 'Interferon-β stabilizes barrier characteristics of the blood-brain barrier in four different species in vitro', *Multiple Sclerosis*, 14(6), pp. 843–852.

Kreit, M. *et al.* (2014) 'Inefficient Type I Interferon-Mediated Antiviral Protection of Primary Mouse Neurons Is Associated with the Lack of Apolipoprotein L9 Expression', *Journal of Virology*, 88(7), pp. 3874–3884.

Kress, G.J. and Mennerick, S. (2009) 'Action potential initiation and propagation: Upstream influences on neurotransmission', *Neuroscience*, 158(1), pp. 211–222.

Kuchroo, V.K. and Weiner, H.L. (2022) 'How does Epstein-Barr virus trigger MS?', *Immunity*. 55, pp. 390–392.

Kujala, P. *et al.* (2001) 'Biogenesis of the Semliki Forest Virus RNA Replication Complex', *Journal of Virology*, 75(8), pp. 3873–3884.

Kulakauskienė, D. *et al.* (2021) 'Virus mimetic poly (I:C)-primed airway exosome-like particles enter brain and induce inflammatory cytokines and mitochondrial reactive oxygen species in microglia', *Biology*, 10(12).

Kulcsar, K.A. *et al.* (2014) 'Interleukin 10 modulation of pathogenic Th17 cells during fatal alphavirus encephalomyelitis', *Proceedings of the National Academy of Sciences of the United States of America*, 111(45), pp. 16053–16058.

Kumar, V. and McNerney, M.E. (2005) 'A new self: MHC-class-I-independent natural-killer-cell self-tolerance', *Nature Reviews Immunology*,5(Apr), pp. 363–374.

Lacy, P. and Stow, J.L. (2011) 'Cytokine release from innate immune cells: Association with diverse membrane trafficking pathways', *Blood*. 118(1), pp. 9–18.

Lambrianides, S. *et al.* (2019) 'Prevalence of Anti-JC Virus (JCV) Antibodies in the Multiple Sclerosis (MS) Population in Cyprus: A Retrospective Study', *Neurology Research International*, 2019.

Lanfranco, M.F. *et al.* (2018) 'Glial- and neuronal-specific expression of CCL5 mRNA in the rat brain', *Frontiers in Neuroanatomy*, 11.

Lang, R. *et al.* (2022) 'Expression and mechanisms of interferon-stimulated genes in viral infection of the central nervous system (CNS) and neurological diseases', *Frontiers in Immunology*. 13, 1008072.

van Langelaar, J. *et al.* (2020) 'B and T Cells Driving Multiple Sclerosis: Identity, Mechanisms and Potential Triggers', *Frontiers in Immunology*. 11, article 760.

Lassmann, H. (2018) 'Multiple sclerosis pathology', *Cold Spring Harbor Perspectives in Medicine*. 8, a028936.

Lauver, M.D. and Lukacher, A.E. (2020) 'JCPyV VP1 Mutations in Progressive Multifocal Leukoencephalopathy: Altering Tropism or Mediating Immune Evasion?', *Viruses*. 12(1156).

Lawson, L.J. *et al.* (1990) Heterogeneity in the distribution and morphology of microglia in the normal adult mouse brain. *Neuroscience*, 39(1), pp. 151-170.

Lazear, H.M., Schoggins, J.W. and Diamond, M.S. (2019) 'Shared and Distinct Functions of Type I and Type III Interferons', *Immunity*. 50(4), pp. 907–923.

Lee, E.Y., Lee, Z.H. and Song, Y.W. (2009) 'CXCL10 and autoimmune diseases', *Autoimmunity Reviews*, 8(5), pp. 379–383.

Lee, J.Y., Oh, T.H. and Yune, T.Y. (2011) 'Ghrelin inhibits hydrogen peroxide-induced apoptotic cell death of oligodendrocytes via ERK and p38MAPK signaling', *Endocrinology*, 152(6), pp. 2377–2386.

Lee, M.S. *et al.* (2013) 'Negative Regulation of Type I IFN Expression by OASL1 Permits Chronic Viral Infection and CD8+ T-Cell Exhaustion', *PLoS Pathogens*, 9(7).

Lee, S.J. *et al.* (2023) 'Seasonal Trends in the Prevalence and Incidence of Viral Encephalitis in Korea (2015–2019)', *Journal of Clinical Medicine*, 12(5).

Lee, W.L., Harrison, R.E. and Grinstein, S. (2003) 'Phagocytosis by neutrophils', *Microbes and Infection*. 5, pp. 1299–1306.

Leong, C.R. *et al.* (2016) Interferon-stimulated gene of 20 kDa protein (ISG20) degrades RNA of hepatitis B virus to impede the replication of HBV in vitro and in vivo. 7(42), pp. 68179-68193,

Lesch, S. *et al.* (2021) 'T cells armed with C-X-C chemokine receptor type 6 enhance adoptive cell therapy for pancreatic tumours', *Nature Biomedical Engineering*, 5(11), pp. 1246–1260.

Letunic, I., Khedkar, S. and Bork, P. (2021) 'SMART: Recent updates, new developments and status in 2020', *Nucleic Acids Research*, 49(D1), pp. D458–D460.

Leviyang, S. (2021) 'Interferon stimulated binding of ISRE is cell type specific and is predicted by homeostatic chromatin state', *Cytokine: X*, 3(4).

Levy, D.E. and García-Sastre, A. (2001) The virus battles: IFN induction of the antiviral state and mechanisms of viral evasion, *Cytokine & Growth Factor Reviews*. 12, pp. 143-156.

Li, C.-J. *et al.* (2022) 'Neutralizing Monoclonal Antibodies Inhibit SARS-CoV-2 Infection through Blocking Membrane Fusion', *Microbiology Spectrum*, 10(2).

Li, D. and Wu, M. (2021) 'Pattern recognition receptors in health and diseases', *Signal Transduction and Targeted Therapy*. 6(291).

Li, F., Jiang, D. and Samuel, M.A. (2019) 'Microglia in the developing retina', *Neural Development*. 14(12).

Li, H.H. *et al.* (2017) 'Effect of dopamine on bone morphogenesis protein-2 expression in human retinal pigment epithelium', *International Journal of Ophthalmology*, 10(9), pp. 1370–1373.

Li, J. *et al.* (2017) 'Pro-inflammatory effects of the Th1 chemokine CXCL10 in acquired aplastic anaemia', *Cytokine*, 94, pp. 45–51.

Li, L. *et al.* (2021) 'Role of astroglial toll-like receptors (TLRs) in central nervous system infections, injury and neurodegenerative diseases', *Brain, Behavior, and Immunity*. 91, pp. 740–755.

Li, M.M.H., MacDonald, M.R. and Rice, C.M. (2015) 'To translate, or not to translate: Viral and host mRNA regulation by interferon-stimulated genes', *Trends in Cell Biology*. 25(6), pp. 320–329.

Li, M.Z. *et al.* (2022) 'LPS-Induced Activation of the cGAS-STING Pathway is Regulated by Mitochondrial Dysfunction and Mitochondrial DNA Leakage in Endometritis', *Journal of Inflammation Research*, 15, pp. 5707–5720.

Li, Q.Z. *et al.* (2010) 'Interferon signature gene expression is correlated with autoantibody profiles in patients with incomplete lupus syndromes', *Clinical and Experimental Immunology*, 159(3), pp. 281–291.

Li, W. *et al.* (2018) 'Microglia have a more extensive and divergent response to interferon-α compared with astrocytes', *GLIA*, 66(10), pp. 2058–2078.

Li, X. *et al.* (1996) Formation of STAT1-STAT2 Heterodimers and Their Role in the Activation of IRF-1 Gene Transcription by Interferon. 271(10), pp. 5790-5794.

Libbey, J.E. and Fujinami, R.S. (2014) 'Adaptive immune response to viral infections in the central nervous system', in *Handbook of Clinical Neurology*. 123, pp. 225–247.

Liff, I. *et al.* (2020) 'Modulation of IL10 and Its Receptor Subunits in Normal and Progesterone-Prolonged Gestation in the Mouse', *Reproductive Sciences*, 27(2), pp. 555–560.

Lim, J.J., Grinstein, S. and Roth, Z. (2017) 'Diversity and versatility of phagocytosis: Roles in innate immunity, tissue remodeling, and homeostasis', *Frontiers in Cellular and Infection Microbiology*, 7(MAY).

Limanaqi, F. *et al.* (2022) 'Dopamine Reduces SARS-CoV-2 Replication In Vitro through Downregulation of D2 Receptors and Upregulation of Type-I Interferons', *Cells*, 11(10).

Lin, M. miao *et al.* (2022) 'Mitochondrial-derived damage-associated molecular patterns amplify neuroinflammation in neurodegenerative diseases', *Acta Pharmacologica Sinica*. 271(10), pp. 2439–2447.

Lin, Y.S. *et al.* (2016) 'Neuronal splicing regulator RBFOX3 (NeuN) regulates adult hippocampal neurogenesis and synaptogenesis', *PLoS ONE*, 11(10).

Linnerbauer, M., Wheeler, M.A. and Quintana, F.J. (2020) 'Astrocyte Crosstalk in CNS Inflammation', *Neuron*. 108(4), pp. 608–622.

Liour, S.S. and Yu, R.K. (2003) 'Differentiation of radial glia-like cells from embryonic stem cells', *GLIA*, 42(2), pp. 109–117.

Liu, C.K., Wei, G. and Atwood, W.J. (1998) Infection of Glial Cells by the Human Polyomavirus JC Is Mediated by an N-Linked Glycoprotein Containing Terminal (2-6)-Linked Sialic Acids, *journal of virology*. 72(6), pp. 4643-4649.

Liu, C.Y. *et al.* (2018) 'Emerging roles of astrocytes in neuro-vascular unit and the tripartite synapse with emphasis on reactive gliosis in the context of alzheimer's disease', *Frontiers in Cellular Neuroscience*. 12, article 193.

Liu, H. *et al.* (2017) 'Variants in the IL7RA gene confer susceptibility to multiple sclerosis in Caucasians: Evidence based on 9734 cases and 10436 controls', *Scientific Reports*, 7(1).

Liu, H. *et al.* (2022) 'Endoplasmic Reticulum Aminopeptidase 1 Is Involved in Anti-viral Immune Response of Hepatitis B Virus by Trimming Hepatitis B Core Antigen to Generate 9-Mers Peptides', *Frontiers in Microbiology*, 13.

Liu, H., Leak, R.K. and Hu, X. (2016) 'Neurotransmitter receptors on microglia', *Stroke and Vascular Neurology*, 1, p. 12.

Liu, J. *et al.* (2019) 'Role of the IgM Fc receptor in immunity and tolerance', *Frontiers in Immunology*. 10, article 529.

Liu, M.T. *et al.* (2001) Expression of Mig (Monokine Induced by Interferon-) Is Important in T Lymphocyte Recruitment and Host Defense Following Viral Infection of the Central Nervous System 1, *The Journal of Immunology*. 166(3), pp. 1790-1795.

Liu, S. *et al.* (2018) 'Nuclear RNF2 inhibits interferon function by promoting K33-linked STAT1 disassociation from DNA article', *Nature Immunology*, 19(1), pp. 41–50.

Liu, T. *et al.* (2017) 'NF-κB signaling in inflammation', *Signal Transduction and Targeted Therapy*. 2, e17023.

Liu, Y. *et al.* (2017) 'Interferon-inducible ribonuclease ISG20 inhibits hepatitis B virus replication through directly binding to the epsilon stem-loop structure of viral RNA', *PLoS Pathogens*, 13(4).

Lively, S. and Schlichter, L.C. (2018) 'Microglia responses to pro-inflammatory stimuli (LPS, IFNγ+TNFα) and reprogramming by resolving cytokines (IL-4, IL-10)', *Frontiers in Cellular Neuroscience*, 12.

Lopes, C.C.B. *et al.* (2019) 'Progressive multifocal leukoencephalopathy: A challenging diagnosis established at autopsy', *Autopsy and Case Reports*, 9(1).

Lu, L.L. *et al.* (2018) 'Beyond binding: Antibody effector functions in infectious diseases', *Nature Reviews Immunology*. 18(1), pp. 46–61.

Luan, Y.Y. *et al.* (2015) 'Effect of regulatory T cells on promoting apoptosis of t lymphocyte and its regulatory mechanism in sepsis', *Journal of Interferon and Cytokine Research*, 35(12), pp. 969–980.

Lukacs, G.L., Rotstein, O.D. and Grinstein, S. (1991) 'Determinants of the phagosomal pH in macrophages: In situ assessment of vacuolar H+-ATPase activity, counterion conductance, and H+ "'leak'"', *Journal of Biological Chemistry*, 266(36), pp. 24540–24548.

Lun, M.P., Monuki, E.S. and Lehtinen, M.K. (2015) 'Development and functions of the choroid plexus-cerebrospinal fluid system', *Nature Reviews Neuroscience*. 16(Aug), pp. 445–457.

Lund, H. *et al.* (2018) 'Competitive repopulation of an empty microglial niche yields functionally distinct subsets of microglia-like cells', *Nature Communications*, 9(1).

Lundström, W. and Gustafsson, R. (2022) 'Human Herpesvirus 6A Is a Risk Factor for Multiple Sclerosis', *Frontiers in Immunology*. 13, article 840753.

Ma, W. *et al.* (2023) 'Type I interferon response in astrocytes promotes brain metastasis by enhancing monocytic myeloid cell recruitment', *Nature Communications*, 14(1).

Ma, A. *et al.* (1992) Surface IgM mediated regulation of RAG gene expression in Elt-N-myc B cell lines, *The EMBO Journal*. 11(7), 2727-2734.

Macaron, G. and Ontaneda, D. (2019) 'Diagnosis and management of progressive multiple sclerosis', *Biomedicines*. 7(56).

Mackenzie, I.S. *et al.* (2014) 'Incidence and prevalence of multiple sclerosis in the UK 1990-2010: A descriptive study in the General Practice Research Database', *Journal of Neurology, Neurosurgery and Psychiatry*, 85(1), pp. 79–84.

Magliozzi, R. *et al.* (2007) 'Meningeal B-cell follicles in secondary progressive multiple sclerosis associate with early onset of disease and severe cortical pathology', *Brain*, 130(4), pp. 1089–1104.

Mah, A.Y. and Cooper, M.A. (2016) 'Metabolic regulation of natural killer cell IFN-γ production', *Critical Reviews in Immunology*, 36(2), pp. 131–147.

Majoros, A. *et al.* (2017) 'Canonical and non-canonical aspects of JAK-STAT signaling: Lessons from interferons for cytokine responses', *Frontiers in Immunology*. 8(29).

Mallery, D.L. *et al.* (2010) 'Antibodies mediate intracellular immunity through tripartite motif-containing 21 (TRIM21)', *Proceedings of the National Academy of Sciences of the United States of America*, 107(46), pp. 19985–19990.

Mangi, M.H. and Newland, A.C. (1998) 'Interleukin-3: Promises and perspectives', *Hematology*. 3(1), pp. 55–66.

Manivasagam, S. and Klein, R.S. (2021) 'Type III Interferons: Emerging Roles in Autoimmunity', *Frontiers in Immunology*. 12, article 764062.

Mantlo, E. *et al.* (2020) 'Antiviral activities of type I interferons to SARS-CoV-2 infection', *Antiviral Research*, 179.

Marone, G. *et al.* (2019) 'The intriguing role of interleukin 13 in the pathophysiology of asthma', *Frontiers in Pharmacology*, 10.

Marques, R.E. *et al.* (2013) 'Targeting CCL5 in inflammation', *Expert Opinion on Therapeutic Targets*, 17(12), pp. 1439–1460.

Marra, C.M. *et al.* (2002) 'A pilot study of cidofovir for progressive multifocal leukoencephalopathy in AIDS', *Lippincott Williams & Wilkins AIDS*, 16, pp. 1791–1797.

Marsh, M. and Heleniust, A. (1989) Virus entry into animal cells, *Advances in virus research.* 36, pp. 107-151.

Marshall, J.S. *et al.* (2018) 'An introduction to immunology and immunopathology', *Allergy, Asthma and Clinical Immunology,* 14(49).

Martin, S.J., Henry, C.M. and Cullen, S.P. (2012) 'A Perspective on Mammalian Caspases as Positive and Negative Regulators of Inflammation', *Molecular Cell*, 46(May), pp. 387–397.

Marzocchetti, A. *et al.* (2008) 'Rearrangement of the JC virus regulatory region sequence in the bone marrow of a patient with rheumatoid arthritis and progressive multifocal leukoencephalopathy', *Journal of NeuroVirology*, 14(5), pp. 455–458.

Mathews, E.S. and Appel, B. (2016) 'Oligodendrocyte differentiation', *Methods in Cell Biology*, 134, pp. 69–96.

Mathy, N.L. *et al.* (2000) 'Interleukin-16 stimulates the expression and production of pro-inflammatory cytokines by human monocytes', *Immunology*, (100), pp. 63–69.

Matsudaira, T. *et al.* (2014) 'Mirtazapine treatment ceased the progression of progressive multifocal leukoencephalopathy associated with systemic sarcoidosis', *Neurology and Clinical Neuroscience*, 2(5), pp. 158–160.

Matsumiya, T. and Stafforini, D.M. (2010) Function and Regulation of Retinoic Acid-Inducible Gene-I, *Cris Rev Immunol*, 30(6), pp. 489-453.

Mattorre, B. *et al.* (2022) 'The emerging multifunctional roles of ERAP1, ERAP2 and IRAP between antigen processing and renin-angiotensin system modulation', *Frontiers in Immunology*. 13(1002375).

McDonald, J.W., Belegu, V. and Becker, D. (2013) 'Spinal Cord', in *Principles of Tissue Engineering: Fourth Edition*. Elsevier Inc., pp. 1353–1373.

McGavern, D.B. and Kang, S.S. (2011) 'Illuminating viral infections in the nervous system', *Nature Reviews Immunology*, pp. 318–329.

McNamara, N.B. *et al.* (2023) 'Microglia regulate central nervous system myelin growth and integrity', *Nature*, 613(7942), pp. 120–129.

Mead, T.J. (2022) 'ADAMTS6: Emerging roles in cardiovascular, musculoskeletal and cancer biology', *Frontiers in Molecular Biosciences*. 9(1023511).

Meinl, E. and Hohlfeld, R. (2002) 'Immunopathogenesis of multiple sclerosis: MBP and beyond', *Clin Exp Immunol*, (128), pp. 395–397.

Melief, J. *et al.* (2016) 'Characterizing primary human microglia: A comparative study with myeloid subsets and culture models', *GLIA*, 64(11), pp. 1857–1868.

Meneguzzi, G. *et al.* (1978) 'Minichromosome from BK virus as a template for transcription in vitro', *Proc. Natl. Acad. Sci. USA*, 75(3), pp. 1126–1130.

De Mercanti, S.F. *et al.* (2020) 'Atypical Multiple Sclerosis Lesions or Progressive Multifocal Leukoencephalopathy Lesions: That Is the Question', *Journal of Investigative Medicine High Impact Case Reports*, 8.

Merle, N.S. *et al.* (2015) 'Complement system part II: Role in immunity', *Frontiers in Immunology*. 6(257).

Meuwissen, M.E.C. *et al.* (2016) 'Human USP18 deficiency underlies type 1 interferonopathy leading to severe pseudo-TOR CH syndrome', *Journal of Experimental Medicine*, 213(7), pp. 1163–1174.

Meyding-Lamadé, U., Craemer, E. and Schnitzler, P. (2019) 'Emerging and re-emerging viruses affecting the nervous system', *Neurological Research and Practice* [Preprint]. 1(20).

Meyerson, N.R. *et al.* (2017) 'Nuclear TRIM25 Specifically Targets Influenza Virus Ribonucleoproteins to Block the Onset of RNA Chain Elongation', *Cell Host and Microbe*, 22(5), pp. 627-638.e7.

Meyts, I. and Casanova, J.L. (2021) 'Viral infections in humans and mice with genetic deficiencies of the type I IFN response pathway', *European Journal of Immunology*. 51(5), pp. 1039–1061.

Michalski, J.P. and Kothary, R. (2015) 'Oligodendrocytes in a nutshell', *Frontiers in Cellular Neuroscience*. 9(340).

Michlmayr, D. and McKimmie, C.S. (2014) 'Role of CXCL10 in central nervous system inflammation', *International Journal of Interferon, Cytokine and Mediator Research*. 6, pp. 1–18.

Mielke, D. *et al.* (2019) 'Antibody-Dependent Cellular Cytotoxicity (ADCC)-Mediating Antibodies Constrain Neutralizing Antibody Escape Pathway', *Frontiers in Immunology*, 10.

Mildner, A. *et al.* (2009) 'CCR2+Ly-6Chi monocytes are crucial for the effector phase of autoimmunity in the central nervous system', *Brain*, 132(9), pp. 2487–2500.

Miller, S.J. (2018) 'Astrocyte heterogeneity in the adult central nervous system', *Frontiers in Cellular Neuroscience*. 12(401).

Mills, E.A. *et al.* (2018) 'Emerging understanding of the mechanism of action for dimethyl fumarate in the treatment of multiple sclerosis', *Frontiers in Neurology*. 9(5).

Mitrovic, B. *et al.* (1995) Nitric oxide induces necrotic but not apoptotic cell death in oligodendrocytes, *Neuroscience*. 65(2), pp. 531-539.

Mitrović, M. *et al.* (2012) ' The NK Cell Response to Mouse Cytomegalovirus Infection Affects the Level and Kinetics of the Early CD8 + T-Cell Response ', *Journal of Virology*, 86(4), pp. 2165–2175.

Miyagi, T. *et al.* (2007) 'High basal STAT4 balanced by STAT1 induction to control type 1 interferon effects in natural killer cells', *Journal of Experimental Medicine*, 204(10), pp. 2383–2396.

Miyamoto, A. *et al.* (2016) 'Microglia contact induces synapse formation in developing somatosensory cortex', *Nature Communications*, 7.

Mizee, M.R., van der Poel, M. and Huitinga, I. (2018) 'Purification of cells from fresh human brain tissue: primary human glial cells', in *Handbook of Clinical Neurology*. 150, pp. 273–283.

Mogensen, T.H. (2009) 'Pathogen recognition and inflammatory signaling in innate immune defenses', *Clinical Microbiology Reviews*, 22(2), pp. 240–273.

Molina-Holgado, E. *et al.* (2001) 'LPS/IFN-g cytotoxicity in oligodendroglial cells: role of nitric oxide and protection by the anti-in¯ammatory cytokine IL-10', *European Journal of Neuroscience*, 13, pp. 493–502.

Monzani, E. *et al.* (2019) 'Dopamine, OxidativeStress and Protein–Quinone Modifications in Parkinsons and Other Neurodegenerative Diseases', *Angewandte Chemie*, 131(20), pp. 6580–6596.

Morales-Núñez, J.J. *et al.* (2021) 'Overview of neutralizing antibodies and their potential in COVID-19', *Vaccines*. 9(1376).

Morikawa, Y., K. *et al*. (1995). "Different migration patterns of antigen-presenting cells correlate with Th1/Th2- type responses in mice." *Immunology.* 85(4), pp. 575-81.

Moser, T. *et al.* (2020) 'The role of TH17 cells in multiple sclerosis: Therapeutic implications', *Autoimmunity Reviews*. 19(102647).

Moyon, S. *et al.* (2015) 'Demyelination causes adult CNS progenitors to revert to an immature state and express immune cues that support their migration', *Journal of Neuroscience*, 35(1), pp. 4–20.

Mulero, P., Midaglia, L. and Montalban, X. (2018) 'Ocrelizumab: a new milestone in multiple sclerosis therapy', *Therapeutic Advances in Neurological Disorders*. 11.

Müller, L., Aigner, P. and Stoiber, D. (2017) 'Type I interferons and natural killer cell regulation in cancer', *Frontiers in Immunology*. 8(304).

Müller, M. *et al.* (2010) 'Review: The chemokine receptor CXCR3 and its ligands CXCL9, CXCL10 and CXCL11 in neuroimmunity - A tale of conflict and conundrum', *Neuropathology and Applied Neurobiology*. 36, pp. 368–387.

Müller, R. *et al.* (1997) Expression of microtubule-associated proteins MAP2 and tau in cultured rat brain oligodendrocytes. *Cell and tissue research*. 288, pp. 239-249.

Mullin, A.P. *et al.* (2017) 'rHIgM22 enhances remyelination in the brain of the cuprizone mouse model of demyelination', *Neurobiology of Disease*, 105, pp. 142–155.

Mullins, C. *et al.* (2017) 'The Benefit of Mirtazapine in the Treatment of Progressive Multifocal Leukoencephalopathy in a Young HIV-positive Patient: A Case Report', *Innov Clin Neurosci*, 15(1–2), pp. 33–35.

Munford, R.S. *et al.* (2003) Acyloxyacyl hydrolase: studies on its regulation and function in mus musculus, *The University of Texas Southwestern Medical Center at Dallas,* Dissertation for doctor of philosophy.

Nagasawa, T. *et al.* (1996) 'Defects of B-cell lymphopoiesis and bone-marrow myelopoiesis in mice lacking the CXC chemokine PBSF/SDF-1', *Nature*, 382, pp. 635–638.

Nahvi, A., Barrick, J.E. and Breaker, R.R. (2004) 'Coenzyme B12 riboswitches are widespread genetic control elements in prokaryotes', *Nucleic Acids Research*, 32(1), pp. 143–150.

Nair, S. and Diamond, M.S. (2015) 'Innate immune interactions within the central nervous system modulate pathogenesis of viral infections', *Current Opinion in Immunology*. 36, pp. 47–53.

Najafi, M.R. *et al.* (2012) Vitamin B 12 Deficiency and Multiple Sclerosis; Is there Any Association?, *Original Article International Journal of Preventive Medicine*. 3(4), pp. 3-6.

Nakayama, T. *et al.* (2004) 'Selective Induction of Th2-Attracting Chemokines CCL17 and CCL22 in Human B Cells by Latent Membrane Protein 1 of Epstein-Barr Virus', *Journal of Virology*, 78(4), pp. 1665–1674.

Nauseef, W.M. and Borregaard, N. (2014) 'Neutrophils at work', *Nature Immunology*. 15(7), pp. 602–611.

Nemazee, D. (2017) 'Mechanisms of central tolerance for B cells', *Nature Reviews Immunology*. 17(May), pp. 281–294.

Nevalainen, T., Autio, A. and Hurme, M. (2022) 'Composition of the infiltrating immune cells in the brain of healthy individuals: effect of aging', *Immunity and Ageing*, 19(1).

Newton, K. and Dixit, V.M. (2012) 'Signaling in innate immunity and inflammation', *Cold Spring Harbor Perspectives in Biology*, 4(3).

Nguyen, K.B. *et al.* (2002) 'Critical Role for STAT4 Activation by Type 1 Interferons in the Interferon-✐ Response to Viral Infection', *Science*, 297(5589), pp. 2063–2066.

Nishiyama, A. *et al.* (2021) 'Life-long oligodendrocyte development and plasticity', *Seminars in Cell and Developmental Biology*, 116, pp. 25–37.

Noh, J.Y. *et al.* (2020) 'Toll-Like Receptors in Natural Killer Cells and Their Application for Immunotherapy', *Journal of Immunology Research*. 2045860.

Van Norman, G.A. (2019) 'Limitations of Animal Studies for Predicting Toxicity in Clinical Trials: Is it Time to Rethink Our Current Approach?', *JACC: Basic to Translational Science*, 4(7), pp. 845–854.

Novick, K.E. *et al.* (1992) 'Polyreactive IgM antibodies generated from autoimmune mice and selected for histone-binding activity', *International Immunology*, 4(10), pp. 1103–1111.

Nussenzweig, M. C, *et al*. (1980). "Dendritic cells are accessory cells for the development of anti- trinitrophenyl cytotoxic T lymphocytes." *J Exp Med,* 152(4), pp. 1070-84.

O'Hara, B.A. *et al.* (2020) 'JC Virus infected choroid plexus epithelial cells produce extracellular vesicles that infect glial cells independently of the virus attachment receptor', *PLoS Pathogens*, 16(3).

O'Hara, B.A. and Atwood, W.J. (2008) 'Interferon β1-a and selective anti-5HT2a receptor antagonists inhibit infection of human glial cells by JC Virus', *Virus Res*, 132(1–2), pp. 97–103.

Okada, K. *et al.* (2005) 'Effects of interferon-β on the cytokine production of astrocytes', *Journal of Neuroimmunology*, 159(1–2), pp. 48–54.

Omidian, Z. *et al.* (2019) 'IL-17 and limits of success', *Cellular Immunology*, 339, pp. 33–40.

Ontaneda, D. and Fox, R.J. (2015) 'Progressive multiple sclerosis', *Current Opinion in Neurology,* 28(3), pp. 237–243.

Orduz, D. *et al.* (2019) 'Developmental cell death regulates lineage-related interneuron-oligodendroglia functional clusters and oligodendrocyte homeostasis', *Nature Communications*, 10(1).

Orton, S.-M. *et al.* (2011) Association of UV radiation with multiple sclerosis prevalence and sex ratio in France, *Neurology*, 76, pp. 425-431.

Osanai, Y. *et al.* (2022) 'Heterogeneity and regulation of oligodendrocyte morphology', *Frontiers in Cell and Developmental Biology*. 10(1030486).

Ota, Y., Zanetti, A.T. and Hallock, R.M. (2013) 'The role of astrocytes in the regulation of synaptic plasticity and memory formation', *Neural Plasticity*. 185463.

Ottoboni, L. *et al.* (2013) Clinical relevance and functional consequences of the TNFRSF1A multiple sclerosis locus. *Neurology*, 81, pp. 1891-1899.

Padgett, B.L. *et al.* (1971) 'Cultivation of Papova-like Virus from Human Brain with Progressive Multifocal Leucoencephalopathy', *The Lancet*, June 19(24), pp. 1257–1260.

Palm, A.K.E. and Henry, C. (2019) 'Remembrance of Things Past: Long-Term B Cell Memory After Infection and Vaccination', *Frontiers in immunology*. 10(1787).

Pan, J. *et al.* (2004) 'Interferon-γ is an autocrine mediator for dendritic cell maturation', *Immunology Letters*, 94(1–2), pp. 141–151.

Pan, R. *et al.* (2020) 'Oligodendrocytes that survive acute coronavirus infection induce prolonged inflammatory responses in the CNS', *PNAS*, 117(27), pp. 15902–15910.

Pan, Z. *et al.* (2022) 'Role of the CXCL13/CXCR5 Axis in Autoimmune Diseases', *Frontiers in Immunology*. 13(850998).

Du Pasquier, R.A. *et al.* (2004) 'A prospective study demonstrates an association between JC virus-specific cytotoxic T lymphocytes and the early control of progressive multifocal leukoencephalopathy', *Brain*, 127(9), pp. 1970–1978.

Patabendige, A. and Janigro, D. (2023) 'The role of the blood-brain barrier during neurological disease and infection', *Biochemical Society Transactions*51, pp. 613–626.

Pavlovic, D. *et al.* (2015) 'Progressive multifocal leukoencephalopathy: Current treatment options and future perspectives', *Therapeutic Advances in Neurological Disorders*, 8(6), pp. 255–273.

Pavlovic, D. *et al.* (2018) 'T cell deficiencies as a common risk factor for drug associated progressive multifocal leukoencephalopathy', *Immunobiology,* 223, pp. 508–517.

Payne, S.L. *et al.* (2018) 'Central Nervous System', in *Principles of Regenerative Medicine*. Elsevier, 1st Edn, pp. 1199–1221

Paysan-Lafosse, T. *et al.* (2023) 'InterPro in 2022', *Nucleic Acids Research*, 51(D1), pp. D418–D427.

Pegram, H.J. *et al.* (2011) 'Activating and inhibitory receptors of natural killer cells', *Immunology and Cell Biology*, 89, pp. 216–224.

Pelletier, M. *et al.* (2010) 'Evidence for a cross-talk between human neutrophils and Th17 cells'. 115(2), pp. 335-343.

Pereira, C.P.M. *et al.* (2023) 'Microglial depletion exacerbates motor impairment and dopaminergic neuron loss in a 6-OHDA model of Parkinson's disease', *Journal of Neuroimmunology*, 375.

Pestka, S. *et al.* (2004) 'Interferons, interferon-like cytokines, and their receptors', *Immunological Reviews*, 202, pp. 8–32.

Pfefferkorn, C. *et al.* (2016) 'Abortively Infected Astrocytes Appear To Represent the Main Source of Interferon Beta in the Virus-Infected Brain', *Journal of Virology*, 90(4), pp. 2031–2038.

Phares, T.W. *et al.* (2013) 'Astrocyte-Derived CXCL10 Drives Accumulation of Antibody-Secreting Cells in the Central Nervous System during Viral Encephalomyelitis', *Journal of Virology*, 87(6), pp. 3382–3392.

Piersma, S.J. *et al.* (2020) 'Virus infection is controlled by hematopoietic and stromal cell sensing of murine cytomegalovirus through sting', *eLife*, 9, pp. 1–21.

Pilzecker, B. and Jacobs, H. (2019) 'Mutating for good: DNA damage responses during somatic hypermutation', *Frontiers in Immunology*. 10(438).

Pittaluga, A. (2017) 'CCL5-glutamate cross-talk in astrocyte-neuron communication in multiple sclerosis', *Frontiers in Immunology*. 8(1079).

Pittman, K. and Kubes, P. (2013) 'Damage-associated molecular patterns control neutrophil recruitment', *Journal of Innate Immunity*, 5, pp. 315–323.

Platanias, L.C. (2005) 'Mechanisms of type-I- and type-II-interferon-mediated signalling', *Nature Reviews Immunology*, 5(May), pp. 375–386.

Platanitis, E. *et al.* (2019) 'A molecular switch from STAT2-IRF9 to ISGF3 underlies interferon-induced gene transcription', *Nature Communications*, 10(1).

Polman, C. and Uitdehaag, B.M.J. (2000) 'Drug treatment of multiple sclerosis', *Medicine Cabinet*, 173(December), pp. 398–402.

Power, C., Kong, P.-A. and Trapp, B.D. (1996) Major Histocompatibility Complex Class I Expression in Oligodendrocytes Induces Hypomyelination in Transgenic Mice, *Journal of Neuroscience Research*. 44, p. 165-173.

Pradhan, S. *et al.* (2022) 'Viral Aggregation: The Knowns and Unknowns', *Viruses*. 14(438).

Prajeeth, C.K. *et al.* (2017) 'Effectors of Th1 and Th17 cells act on astrocytes and augment their neuroinflammatory properties', *Journal of Neuroinflammation*, 14(1).

Prineas, J.W. and Connell, F. (1978) 'Remyelination in Multiple Sclerosis', *Ann Neurol*, 5, pp. 22–31.

Prior, H. *et al.* (2020) 'Opportunities for use of one species for longer-term toxicology testing during drug development: A cross-industry evaluation', *Regulatory Toxicology and Pharmacology*, 113.

Ptáček, R. *et al.* (2011) 'Dopamine D4 receptor gene DRD4 and its association with psychiatric disorders', *Med Sci Monit*, 17(9), pp. 215–220.

Ptáček, R. *et al.* (2011) Dopamine D4 receptor gene DRD4 and its association with psychiatric disorders. *Med sci monit*, 17(9), pp. 215-220.

Pugliese, A. *et al.* (2005) 'Phagocytic activity in human immunodeficiency virus type 1 infection.', *Clinical and diagnostic laboratory immunology*, 12(18), pp. 889–895.

Raftery, N. and Stevenson, N.J. (2017) 'Advances in anti-viral immune defence: revealing the importance of the IFN JAK/STAT pathway', *Cellular and Molecular Life Sciences*. 74, pp. 2525–2535.

Rahman-Enyart, A. *et al.* (2022) 'Acyloxyacyl hydrolase regulates microgliamediated pelvic pain', *PLoS ONE*, 17(8 August).

Raine, C.S. and Wu, E. (1993) 'Multiple Sclerosis: Remyelination in Acute Lesions', *Journal of Neuropathology and Experimental Neurology*, 5(3), pp. 199–204.

Rasband, M.N. and Peles, E. (2021) 'Mechanisms of node of Ranvier assembly', *Nature Reviews Neuroscience*. 22(Jan), pp. 7–20.

Rasley, A. *et al.* (2006) 'Murine glia express the immunosuppressive cytokine, interleukin-10, following exposure to Borrelia burgdorferi or Neisseria meningitidis', *GLIA*, 53(6), pp. 583–592.

Ratajczak, W. *et al.* (2018) 'Immunological memory cells', *Central European Journal of Immunology*. 43(2)., pp. 194–203.

Raúl, V. *et al.* (2012) Antibody-Dependent Cellular Cytotoxicity (ADCC).

Reeves, E. and James, E. (2018) 'The role of polymorphic ERAP1 in autoinflammatory disease', *Bioscience Reports*. 38(4).

Reich, N.C. (2013) 'A death-promoting role for ISG54/IFIT2', *Journal of Interferon and Cytokine Research*, 33(4), pp. 199–205.

Reiling, L. *et al.* (2019) 'Targets of complement-fixing antibodies in protective immunity against malaria in children', *Nature Communications*, 10(1).

Reinert, L.S. *et al.* (2012) 'TLR3 deficiency renders astrocytes permissive to herpes simplex virus infection and facilitates establishment of CNS infection in mice', *Journal of Clinical Investigation*, 122(4), pp. 1368–1376.

Rivera-Serrano, E.E. *et al.* (2020) 'Annual Review of Virology Viperin Reveals Its True Function', *Annu. Rev. Virol*, 7, pp. 421–446.

Robertson, D. and Moreo, N. (2016) *Disease-Modifying Therapies in Multiple Sclerosis: Overview and Treatment Considerations*. June, pp. 28-34.

Rosales, C. (2018) 'Neutrophil: A cell with many roles in inflammation or several cell types?', *Frontiers in Physiology*. 9(113).

Rouault, C. *et al.* (2013) 'Roles of chemokine ligand-2 (CXCL2) and neutrophils in influencing endothelial cell function and inflammation of human adipose tissue', *Endocrinology*, 154(3), pp. 1069–1079.

Rouse, B.T. and Sehrawat, S. (2010) 'Immunity and immunopathology to viruses: What decides the outcome?', *Nature Reviews Immunology*, 10(7), pp. 514–526.

Rovaris, M. *et al.* (2006) 'Secondary progressive multiple sclerosis: current knowledge and future challenges', *Lancet Neurol*, 5, pp. 343–354.

Rozenberg, F. (2013) 'Acute viral encephalitis', in *Handbook of Clinical Neurology*. 3rd Edition, pp. 1171–1181.

Rubio, A.J., Porter, T. and Zhong, X. (2020) 'Duality of B Cell-CXCL13 Axis in Tumor Immunology', *Frontiers in Immunology*. 11(521110).

Rusakov, D.A. *et al.* (2011) 'Shaping the synaptic signal: Molecular mobility inside and outside the cleft', *Trends in Neurosciences*, 34(7), pp. 359–369.

Russo, R.C. *et al.* (2014) 'The CXCL8/IL-8 chemokine family and its receptors in inflammatory diseases', *Expert Review of Clinical Immunology*. Early Online,, pp. 593–619.

Rustenhoven, J. *et al.* (2016) 'Isolation of highly enriched primary human microglia for functional studies', *Scientific Reports*, 6.

Sallusto, F. (2016) 'Heterogeneity of Human CD4+ T Cells Against Microbes', *Annual Review of Immunology*. 34, pp. 317–334.

Sallusto, F. and Lanzavecchia, A. (1994) 'Efficient Presentation of Soluble Antigen by Cultured Human Dendritic Cells Is Maintained by Granulocyte/Macrophage Colony-stimulating Factor Plus Iuterleukin 4 and Downregulated by Tumor Necrosis Factor c~', *J Exp. Med*, 179, pp. 1109–1118.

Santos, C. de O. *et al.* (2021) 'Blocking IL-10 signaling with soluble IL-10 receptor restores in vitro specific lymphoproliferative response in dogs with leishmaniasis caused by Leishmania infantum', *PLoS ONE*, 16(1 January).

Saribaş, A.S. *et al.* (2010) 'JC virus-induced progressive multifocal leukoencephalopathy', *Future Virology*, 5(3) pp. 313–323.

Sato, M. *et al.* (1998) 'Positive feedback regulation of type I IFN genes by the IFN-inducible transcription factor IRF-7', *FEBS Letters*, 441(1), pp. 106–110.

Saul, S. *et al.* (2015) 'Differences in Processing Determinants of Nonstructural Polyprotein and in the Sequence of Nonstructural Protein 3 Affect Neurovirulence of Semliki Forest Virus', *Journal of Virology*, 89(21), pp. 11030–11045.

Sauter, C. and Wolfensberger, C. (1980) 'Interferon in human serum after injection of endotoxin', *The Lancet*, October(18), pp. 852–853.

Savarin, C., Dutta, R. and Bergmann, C.C. (2018) 'Distinct gene profiles of bone marrow-derived macrophages and microglia during neurotropic coronavirus-induced demyelination', *Frontiers in Immunology*, 9(JUN).

Saveanu, L. *et al.* (2005) 'Concerted peptide trimming by human ERAP1 and ERAP2 aminopeptidase complexes in the endoplasmic reticulum', *Nature Immunology*, 6(7), pp. 689–697.

Saverio, L.T. and Retta, F. (2014) Ras Signaling *Methods and Protocols Methods in Molecular Biology*. 1st Edn.

Sawant, K. V. *et al.* (2016) 'Chemokine CXCL1 mediated neutrophil recruitment: Role of glycosaminoglycan interactions', *Scientific Reports*, 6.

El Sayed, S. *et al.* (2022) 'CCR2 promotes monocyte recruitment and intestinal inflammation in mice lacking the interleukin-10 receptor', *Scientific Reports*, 12(1).

Scapini, P. and Cassatella, M.A. (2014) 'Social networking of human neutrophils within the immune system', *Blood*, 124(5), pp. 710–719.

Schildge, S. *et al.* (2013) 'Isolation and culture of mouse cortical astrocytes.', *Journal of visualized experiments : JoVE* [Preprint], (71).

Schneider, W.M., Chevillotte, M.D. and Rice, C.M. (2014) 'Interferon-stimulated genes: A complex web of host defenses', *Annual Review of Immunology*. 32., pp. 513–545.

Schoggins, J.W. (2014) 'Interferon-stimulated genes: Roles in viral pathogenesis', *Current Opinion in Virology*. 6, pp. 40–46.

Schoggins, J.W. (2019) 'Interferon-Stimulated Genes: What Do They All Do?', *Annual Review of Virology*, 14(1).

Schott, B.H. *et al.* (2022) 'Single-cell genome-wide association reveals that a nonsynonymous variant in ERAP1 confers increased susceptibility to influenza virus', *Cell Genomics*, 2(11).

Schulz, C. *et al.* (2012) 'A Lineage of Myeloid Cells Independent of Myb and Hematopoietic Stem Cells', *Science*, 335(6077), pp. 86–90.

Seidl, A.H. (2014) 'Regulation of conduction time along axons', *Neuroscience*. 0, pp. 126–134.

Selewski, D.T. *et al.* (2010) 'Natalizumab (Tysabri)', *American Journal of Neuroradiology*, 31((9), pp. 1588–1590.

Seo, Y. and Hahm, B. (2010) 'Type I interferon modulates the battle of host immune system against viruses', in *Adv Appl Microbiol*, 73, pp. 83–101.

Serwold, T. *et al.* (2002) Competing interests statement ERAAP customizes peptides for MHC class I molecules in the endoplasmic reticulum. *Nature*, 419(Oct), pp. 480-483.

de Sèze, J. *et al.* (2023) 'Anti-CD20 therapies in multiple sclerosis: From pathology to the clinic', *Frontiers in Immunology*. 23(Mar), 1004795.

Shang, X.-Z. *et al.* (2002) Eosinophil Recruitment in Type-2 Hypersensitivity Pulmonary Granulomas Source and Contribution of Monocyte Chemotactic Protein-3 (CCL7). *American J. path.* 161(1), pp. 257-266.

Shannon, L.A. *et al.* (2012) 'CCR7/CCL19 controls expression of EDG-1 in T cells', *Journal of Biological Chemistry*, 287(15), pp. 11656–11664.

Shao, R. *et al.* (2022) 'Review: the role of GSDMD in sepsis', *Inflammation Research*. 71, pp. 1191–1202.

Sharma, S.K. *et al.* (2013) 'Progressive multifocal leucoencephalopathy in HIV/AIDS: Observational study from a tertiary care centre in northern India', *Indian J Med Res*, 138(July), pp. 72–77.

Shaw, A.E. *et al.* (2017) 'Fundamental properties of the mammalian innate immune system revealed by multispecies comparison of type I interferon responses', *PLoS Biology*, 15(12).

Shedlock, D.J. *et al.* (2003) Role of CD4 T Cell Help and Costimulation in CD8 T Cell Responses During Listeria monocytogenes Infection 1, *The Journal of Immunology*. 170(4), pp. 2053-2063.

Shemer, A. *et al.* (2018) 'Engrafted parenchymal brain macrophages differ from microglia in transcriptome, chromatin landscape and response to challenge', *Nature Communications*, 9(1).

Shemesh, A. *et al.* (2022) 'Differential IL-12 signaling induces human natural killer cell activating receptor-mediated ligand-specific expansion', *Journal of Experimental Medicine*, 219(8).

Sheng, J., Ruedl, C. and Karjalainen, K. (2015) 'Most Tissue-Resident Macrophages Except Microglia Are Derived from Fetal Hematopoietic Stem Cells', *Immunity*, 43(2), pp. 382–393.

Sherry, M.M. *et al.* (2009) 'STAT3 is required for proliferation and maintenance of multipotency in glioblastoma stem cells', *Stem Cells*, 27(10), pp. 2383–2392.

Shi, J. *et al.* (2015) 'Cleavage of GSDMD by inflammatory caspases determines pyroptotic cell death', *Nature*, 526(7575), pp. 660–665.

Shields, D.C., Haque, A. and Banik, N.L. (2020) 'Neuroinflammatory responses of microglia in central nervous system trauma', *Journal of Cerebral Blood Flow and Metabolism*. 40(1S), pp. S25–S33.

Shih, J. and Dulla, C.G. (2018) 'The THIK and Thin of Microglia Dynamics', *Neuron*. 97(2), pp. 253–255.

Shouval, D.S. *et al.* (2014) 'Interleukin-10 receptor signaling in innate immune cells regulates mucosal immune tolerance and anti-inflammatory macrophage function', *Immunity*, 40(5), pp. 706–719.

Sidiropoulou, K., Pissadaki, E.K. and Poirazi, P. (2006) 'Inside the brain of a neuron', *EMBO Reports*, 7(9), pp. 886–892.

Silva, M.J.A. *et al.* (2023) 'The Association between CCL5/RANTES SNPs and Susceptibility to HIV-1 Infection: A Meta-Analysis', *Viruses*. 15(9).

Silva, R.A. and Appelberg, R. (2001) 'Blocking the receptor for interleukin 10 protects mice from lethal listeriosis', *Antimicrobial Agents and Chemotherapy*, 45(4), pp. 1312–1314.

Silva, T. *et al.* (2021) 'The Chemokine CCL5 Inhibits the Replication of Influenza A Virus Through SAMHD1 Modulation', *Frontiers in Cellular and Infection Microbiology*, 11.

Simons, M. and Nave, K.A. (2016) 'Oligodendrocytes: Myelination and axonal support', *Cold Spring Harbor Perspectives in Biology*. 8(a020479).

Sintzel, M.B., Rametta, M. and Reder, A.T. (2018) 'Vitamin D and Multiple Sclerosis: A Comprehensive Review', *Neurology and Therapy*. 7, pp. 59–85.

Smart, T.G. and Paoletti, P. (2012) 'Synaptic neurotransmitter-gated receptors', *Cold Spring Harbor Perspectives in Biology*, 4(3).

Smith, D.R. *et al.* (2020) 'Polycistronic Delivery of IL-10 and NT-3 Promotes Oligodendrocyte Myelination and Functional Recovery in a Mouse Spinal Cord Injury Model', *Tissue Engineering - Part A*, 26(11–12), pp. 672–682.

Soares, J.B. *et al.* (2010) ‘The role of lipopolysaccharide/toll-like receptor 4 signaling in chronic liver diseases’, *Hepatology International*, 4(4), pp. 659–672.

Sofroniew, M. V. (2015) ‘Astrogliosis’, *Cold Spring Harbor Perspectives in Biology*, 7(2).

Soldan, S.S. and Lieberman, P.M. (2023) ‘Epstein–Barr virus and multiple sclerosis’, *Nature Reviews Microbiology*. 21(Jan), pp. 51–64.

Soltani, M.H. *et al.* (2005) Tumorigenesis and Neoplastic Progression Microtubule-Associated Protein 2, a Marker of Neuronal Differentiation, Induces Mitotic Defects, Inhibits Growth of Melanoma Cells, and Predicts Metastatic Potential of Cutaneous Melanoma, *Am J Pathol*. 166(6), pp. 1841-1850.

Sorce, S., Myburgh, R. and Krause, K.H. (2011) ‘The chemokine receptor CCR5 in the central nervous system’, *Progress in Neurobiology*, 93, pp. 297–311.

Speaks, S. *et al.* (2023) ‘Gasdermin D promotes influenza virus-induced mortality through neutrophil amplification of inflammation’, *BioRxiv Preprint* [Preprint].

Spindler, K.R. and Hsu, T.H. (2012) ‘Viral disruption of the blood-brain barrier’, *Trends in Microbiology*, 20(6), pp. 282–290.

Stanifer, M.L., Pervolaraki, K. and Boulant, S. (2019) ‘Differential regulation of type I and type III interferon signaling’, *International Journal of Molecular Sciences*. 20(1445).

Stanton, G.J. *et al.* (1987) ‘Interferon Review’, *Investigative Radiology*, 22(3).

Steigbigel, R.T., Lambert, L.H. and Remington, J.S. (1974) ‘Phagocytic and Bactericidal Properties of Normal Human Monocytes’, *Journal of Clinical Investigation*, 53(January), pp. 131–142.

Steinman, R. M *et al.* (1979). "Identification of a novel cell type in peripheral lymphoid organs of mice. V. Purification of spleen dendritic cells, new surface markers, and maintenance in vitro." *J Exp Med.* 149(1), pp. 1-16.

Stephens, L.A., Malpass, K.H. and Anderton, S.M. (2009) ‘Curing CNS autoimmune disease with myelin-reactive Foxp3+ Treg’, *European Journal of Immunology*, 39(4), pp. 1108–1117.

Sterlin, D. *et al.* (2020) ‘The antibody/microbiota interface in health and disease’, *Mucosal Immunology*. Springer Nature, pp. 3–11.

Stiles, L.N. *et al.* (2006) ‘Differential roles for CXCR3 in CD4+ and CD8+ T cell trafficking following viral infection of the CNS’, *European Journal of Immunology*, 36(3), pp. 613–622.

Strauss, J.H. and Strauss, E.G. (1994) The Alphaviruses: Gene Expression, Replication, and Evolution, *Microbiological reviews*. 58(3), 491-562.

Subramanian Iyer, S. and Cheng, G. (2012) Role of Interleukin 10 Transcriptional Regulation in Inflammation and Autoimmune Disease. *Crit Rev Immunol.* 32(1), pp. 23-61.

Sun, L. *et al.* (2023) ‘T cells in health and disease’, *Signal Transduction and Targeted Therapy*. 8(253).

Suzuki, N. *et al.* (2017) ‘Differentiation of Oligodendrocyte Precursor Cells from Sox10-Venus Mice to Oligodendrocytes and Astrocytes’, *Scientific Reports*, 7(1).

Szakal, A. K., Holmes, K. L., and Tew, J. G. (1983). "Transport of immune complexes from the subcapsular sinus to lymph node follicles on the surface of nonphagocytic cells, including cells with dendritic morphology." *J Immunol,* 131(4), pp. 1714-27.

Szpakowski, P. *et al.* (2022) 'Human Primary Astrocytes Differently Respond to Pro- and Anti-Inflammatory Stimuli', *Biomedicines*, 10(8).

Takahashi, K. *et al.* (1992) Detection of lipopolysaccharide (LPS) and identification of its serotype by an enzyme-linked immunosorbent assay (ELISA) using poly-L-lysine, *Journal of Immunological Methods*. 253, pp. 67-71.

Takatsu', K. (1997) 'MINI R EVI EW Cytokines Involved in B-Cell Differentiation and Their Sites of Action (44119)', p. 2151.

Takeuchi, O. and Akira, S. (2009) 'Innate immunity to virus infection', *Immunological Reviews*, 227(1), pp. 75–86.

Tamberg, N. *et al.* (2007) 'Insertion of EGFP into the replicase gene of Semliki Forest virus results in a novel, genetically stable marker virus', *Journal of General Virology*, 88(4), pp. 1225–1230.

Tan, C.S. *et al.* (2013) 'Detection of JC Virus-Specific Immune Responses in a Novel Humanized Mouse Model', *PLoS ONE*, 8(5).

Tanabe, Y. *et al.* (2005) 'Cutting Edge: Role of STAT1, STAT3, and STAT5 in IFN-αβ Responses in T Lymphocytes', *The Journal of Immunology*, 174(2), pp. 609–613.

Tanaka, T., Narazaki, M. and Kishimoto, T. (2014) 'Il-6 in inflammation, Immunity, And disease', *Cold Spring Harbor Perspectives in Biology*, 6(10).

Tang, Y. *et al.* (2020) 'Dendritic cells promote treg expansion but not th17 generation in response to Talaromyces marneffei yeast cells', *Infection and Drug Resistance*, 13, pp. 805–813.

Tapia-Maltos, M.A. *et al.* (2021) 'Identification of regulatory T cell molecules associated with severity of multiple sclerosis', *Multiple Sclerosis Journal*, 27(11), pp. 1695–1705.

Tay, M.Z., Wiehe, K. and Pollara, J. (2019) 'Antibody dependent cellular phagocytosis in antiviral immune responses', *Frontiers in Immunology*, 10(FEB).

Taylor, M.P. and Enquist, L.W. (2015) 'Axonal spread of neuroinvasive viral infections', *Trends in Microbiology*. 23(5), pp. 283–288.

Tecchio, C. and Cassatella, M.A. (2016) 'Neutrophil-derived chemokines on the road to immunity', *Seminars in Immunology*. 28, pp. 119–128.

Teijaro, J.R. *et al.* (2013) 'Persistent LCMV infection is controlled by blockade of type I interferon signaling', *Science*, 340(6129), pp. 207–211.

Telikani, Z. *et al.* (2022) 'Antiviral response within different cell types of the CNS', *Frontiers in Immunology*. 13(1044721).

Thapa, P. and Farber, D.L. (2019) 'The Role of the Thymus in the Immune Response', *Thoracic surgery clinics* 29(2), pp. 123–131.

Théry, C. and Amigorena, S. (2001) 'The cell biology of antigen presentation in dendritic cells', *Current Opinion in Immunology*, (13), pp. 45–51.

Thompson, K.K. and Tsirka, S.E. (2017) 'The diverse roles of microglia in the neurodegenerative aspects of central nervous system (CNS) autoimmunity', *International Journal of Molecular Sciences*. 18(504).

Tian, H. *et al.* (2023) 'RNF213 modulates γ-herpesvirus infection and reactivation via targeting the viral Replication and Transcription Activator', *Proceedings of the National Academy of Sciences of the United States of America*, 120(12).

van Tilborg, E. *et al.* (2018) 'Origin and dynamics of oligodendrocytes in the developing brain: Implications for perinatal white matter injury', *GLIA*. 66, pp. 221–238.

Toda, G. *et al.* (2021) 'Preparation and culture of bone marrow-derived macrophages from mice for functional analysis', *STAR Protocols*, 2(1).

Tolsá-García, M.J. *et al.* (2023) 'Worldwide transmission and infection risk of mosquito vectors of West Nile, St. Louis encephalitis, Usutu and Japanese encephalitis viruses: a systematic review', *Scientific Reports*, 13(1).

Torres Iglesias, G. *et al.* (2023) 'Dual role of peripheral B cells in multiple sclerosis: emerging remote players in demyelination and novel diagnostic biomarkers', *Frontiers in Immunology*, 14.

Tran, V. *et al.* (2020) 'Influenza virus repurposes the antiviral protein IFIT2 to promote translation of viral mRNAs', *Nature Microbiology*, 5(12), pp. 1490–1503.

Tremlett, H., Zhao, Y. and Devonshire, V. (2008) 'Natural history of secondary-progressive multiple sclerosis', *Multiple Sclerosis*, 14(3), pp. 314–324.

Trifilo, M.J. *et al.* (2004) 'CXC Chemokine Ligand 10 Controls Viral Infection in the Central Nervous System: Evidence for a Role in Innate Immune Response through Recruitment and Activation of Natural Killer Cells', *Journal of Virology*, 78(2), pp. 585–594.

Tsai, D.Y. *et al.* (2019) 'Regulatory mechanisms of B cell responses and the implication in B cell-related diseases', *Journal of Biomedical Science*, 26(1).

Tsuji, K. *et al.* (2017) 'Effects of different cell-detaching methods on the viability and cell surface antigen expression of synovial mesenchymal stem cells', *Cell Transplantation*, 26(6), pp. 1089–1102

Turnley, A.M., Miller, J.F.A.P. and Bartlett, P.F. (1991) Regulation of MHC molecules on MBP positive oligodendrocytes in mice by IFN-γ and TNF, *Neuroscience Letters*. 123, pp. 45-48.

Tyner, J.W. *et al.* (2004) 'Chemokine CCL5 Signals Required for Survival During Viral Infection', *J allergy clin immunol*, 113(2).

Uematsu, S. and Akira, S. (2007) 'Toll-like receptors and type I Interferons', *Journal of Biological Chemistry*, 282(21), pp. 15319–15324.

Upadhyay, R.K. (2014) 'Drug delivery systems, CNS protection, and the blood brain barrier', *BioMed Research International*. 2014(869269).

Vanderven, H.A. *et al.* (2017) 'Antibody-dependent cellular cytotoxicity and influenza virus', *Current Opinion in Virology*. 22, pp. 89–96.

Vavasour, I.M. *et al.* (2022) 'Characterization of multiple sclerosis neuroinflammation and neurodegeneration with relaxation and diffusion basis spectrum imaging', *Multiple Sclerosis Journal*, 28(3), pp. 418–428.

Veldman, C.M., Cantorna, M.T. and DeLuca, H.F. (2000) 'Expression of 1,25-dihydroxyvitamin D3 receptor in the immune system', *Archives of Biochemistry and Biophysics*, 374(2), pp. 334–338.

Verhelst, J. *et al.* (2012) 'Interferon-Inducible Protein Mx1 Inhibits Influenza Virus by Interfering with Functional Viral Ribonucleoprotein Complex Assembly', *Journal of Virology*, 86(24), pp. 13445–13455.

Viengkhou, B. and Hofer, M.J. (2023) 'Breaking down the cellular responses to type I interferon neurotoxicity in the brain', *Frontiers in Immunology*. 14(1110593).

Villalón, E. *et al.* (2018) 'Internode length is reduced during myelination and remyelination by neurofilament medium phosphorylation in motor axons', *Experimental Neurology*, 306, pp. 158–168.

Villar, L.M. *et al.* (2002) 'Intrathecal IgM synthesis predicts the onset of new relapses and a worse disease course in MS', *Neurology*, 59(4), pp. 555–559.

Villar, L.M. *et al.* (2005) 'Intrathecal synthesis of oligoclonal IgM against myelin lipids predicts an aggressive disease course in MS', *Journal of Clinical Investigation*, 115(1), pp. 187–194.

Villar, L.M. *et al.* (2015) 'Lipid-specific immunoglobulin M bands in cerebrospinal fluid are associated with a reduced risk of developing progressive multifocal leukoencephalopathy during treatment with natalizumab', *Annals of Neurology*, 77(3), pp. 447–457.

Wack, A., Terczyńska-Dyla, E. and Hartmann, R. (2015) 'Guarding the frontiers: The biology of type III interferons', *Nature Immunology*. Nature Publishing Group, pp. 802–809.

Walton, C. *et al.* (2020) 'Rising prevalence of multiple sclerosis worldwide: Insights from the Atlas of MS, third edition', *Multiple Sclerosis Journal*, 26(14), pp. 1816–1821.

Wang, H., Peters, N. and Schwarze, J. (2006) 'Plasmacytoid Dendritic Cells Limit Viral Replication, Pulmonary Inflammation, and Airway Hyperresponsiveness in Respiratory Syncytial Virus Infection', *The Journal of Immunology*, 177(9), pp. 6263–6270.

Wang, J. *et al.* (2011) 'TRIM56 Is a Virus- and Interferon-Inducible E3 Ubiquitin Ligase That Restricts Pestivirus Infection', *Journal of Virology*, 85(8), pp. 3733–3745.

Wang, J. and Campbell, I.L. (2005) 'Innate STAT1-Dependent Genomic Response of Neurons to the Antiviral Cytokine Alpha Interferon', *Journal of Virology*, 79(13), pp. 8295–8302.

Wang, J., Campbell, I.L. and Zhang, H. (2008) 'Systemic interferon-α regulates interferon-stimulated genes in the central nervous system', *Molecular Psychiatry*, 13(3), pp. 293–301.

Wang, S. *et al.* (2016) 'TRIM14 inhibits hepatitis C virus infection by SPRY domain-dependent targeted degradation of the viral NS5A protein', *Scientific Reports*, 6.

Wang, W.Y. *et al.* (2015) 'Role of pro-inflammatory cytokines released from microglia in Alzheimer's disease', *Annals of Translational Medicine*. 3(10):136.

Wang, X., Hinson, E.R. and Cresswell, P. (2007) 'The Interferon-Inducible Protein Viperin Inhibits Influenza Virus Release by Perturbing Lipid Rafts', *Cell Host and Microbe*, 2(2), pp. 96–105.

Wang, Y. *et al.* (2023) 'Regulatory T cells alleviate myelin loss and cognitive dysfunction by regulating neuroinflammation and microglial pyroptosis via TLR4/MyD88/NF-κB pathway in LPC-induced demyelination', *Journal of Neuroinflammation*, 20(1).

Wang, Z. *et al.* (2008) Regulation of innate immune responses by DAI (DLM-1/ZBP1) and other DNA-sensing molecules, *PNAS April*. 105(14), pp. 5477-5482.

Weber, B. and Barros, L.F. (2015) 'The astrocyte: Powerhouse and recycling center', *Cold Spring Harbor Perspectives in Biology*, 7(12).

De Weerd, N.A. and Nguyen, T. (2012) 'The interferons and their receptors-distribution and regulation', *Immunology and Cell Biology*, 90, pp. 483–491.

Weinstein, J.R. *et al.* (2008) 'Lipopolysaccharide is a frequent and significant contaminant in microglia-activating factors', *GLIA*, 56(1), pp. 16–26.

Welsh, R.M. *et al.* (2012) 'Type 1 interferons and antiviral CD8 T-Cell responses', *PLoS Pathogens*, 8(1).

Wensveen, F.M., Jelenčić, V. and Polić, B. (2018) 'NKG2D: A master regulator of immune cell responsiveness', *Frontiers in Immunology*. 9(441).

West, E.E., Kolev, M. and Kemper, C. (2018) 'Complement and the Regulation of T Cell Responses', *Annual Review of Immunology*. 36, pp. 309–338.

Wharton, K.A. *et al.* (2016) 'JC polyomavirus abundance and distribution in progressive multifocal leukoencephalopathy (PML) brain tissue implicates myelin sheath in intracerebral dissemination of infection', *PLoS ONE*, 11(5).

Wheeler, N.A. and Fuss, B. (2016) 'Extracellular cues influencing oligodendrocyte differentiation and (re)myelination', *Experimental Neurology*. 283, pp. 512–530.

Williamson, E.M.L. and Berger, J.R. (2017) 'Diagnosis and Treatment of Progressive Multifocal Leukoencephalopathy Associated with Multiple Sclerosis Therapies', *Neurotherapeutics*, 14(4), pp. 961–973.

Wilson, H.L. (2012) 'B cells contribute to MS pathogenesis through antibody-dependent and antibody-independent mechanisms', *Biologics: Targets and Therapy*. 6, pp. 117–123.

Wingerchuk, D.M. (2012) 'Smoking: Effects on multiple sclerosis susceptibility and disease progression', *Therapeutic Advances in Neurological Disorders*, 5(1), pp. 13–22.

Wollebo, H.S. *et al.* (2011) 'Role for tumor necrosis factor-alpha in JC virus reactivation and progressive multifocal leukoencephalopathy', *Journal of Neuroimmunology*, 233(1–2), pp. 46–53.

Woodburn, S.C., Bollinger, J.L. and Wohleb, E.S. (2021) 'The semantics of microglia activation: neuroinflammation, homeostasis, and stress', *Journal of Neuroinflammation*. 18(258).

Wu, C.H. *et al.* (2003) 'The protein information resource', *Nucleic Acids Research*, 31(1), pp. 345–347.

Wu, G., Nie, L. and Zhang, W. (2008) 'Integrative analyses of posttranscriptional regulation in the yeast Saccharomyces cerevisiae using transcriptomic and proteomic data', *Current Microbiology*, 57(1), pp. 18–22.

Wuest, T.R. and Carr, D.J.J. (2009) Dysregulation of CXCR3 Signaling due to CXCL10 Deficiency Impairs the Anti-Viral Response to HSV-1 Infection 1. *J. Immunol.* 181(11), pp. 7985-7993.

Yanai, H., Negishi, H. and Taniguchi, T. (2012) 'The IRF family of transcription factors inception, impact and implications in oncogenesis', *OncoImmunology*, 1(8), pp. 1376–1386.

Yang, E. and Li, M.M.H. (2020) 'All About the RNA: Interferon-Stimulated Genes That Interfere With Viral RNA Processes', *Frontiers in Immunology*. 11(605024).

Yang, I. *et al.* (2010) 'The role of microglia in central nervous system immunity and glioma immunology', *Journal of Clinical Neuroscience*, 17(1), pp. 6–10.

Yang, S. *et al.* (2005) 'Characterization of the Elements and Proteins Responsible for Interferon-Stimulated Gene Induction by Human Cytomegalovirus', *Journal of Virology*, 79(8), pp. 5027–5034.

Yang, W. *et al.* (2020) 'To TRIM the Immunity: From Innate to Adaptive Immunity', *Frontiers in Immunology*. 11(02157).

Yang, Y. and Rosenberg, G.A. (2011) 'Blood-brain barrier breakdown in acute and chronic cerebrovascular disease', *Stroke*, 42(11), pp. 3323–3328.

Yang, Z. and Wang, K.K.W. (2015) 'Glial fibrillary acidic protein: From intermediate filament assembly and gliosis to neurobiomarker', *Trends in Neurosciences*. 38(6), pp. 364–374.

Yao, V., Platell, C. and Hall, J.C. (2002) 'Dendritic cells', *ANZ Journal of Surgery*, 72(7), pp. 501–506.

Yin, X. *et al.* (1997) CNP Overexpression Induces Aberrant Oligodendrocyte Membranes and Inhibits MBP Accumulation and Myelin Compaction, *J. Neurosci. Res*. 50, pp. 238-247.

Yoo, J.K. *et al.* (2002) IL-12 Provides Proliferation and Survival Signals to Murine CD4 T Cells Through Phosphatidylinositol 3-Kinase/Akt Signaling Pathway 1, *The Journal of Immunology*, 169(7), pp. 3637-3643.

Yu, G., Shu, Y. and McCormick, D.A. (2008) 'Cortical action potential backpropagation explains spike threshold variability and rapid-onset kinetics', *Journal of Neuroscience*, 28(29), pp. 7260–7272.

Zahid, M. *et al.* (2011) 'Formation of dopamine quinone-DNA adducts and their potential role in the etiology of Parkinson's disease', *IUBMB Life*, 63(12), pp. 1087–1093.

Zenobia, C. and Hajishengallis, G. (2015) 'Basic biology and role of interleukin-17 in immunity and inflammation', *Periodontology 2000*, 69(1), pp. 142–159.

Zhang, B. *et al.* (2008) 'CXCR3 Mediates Region-Specific Antiviral T Cell Trafficking within the Central Nervous System during West Nile Virus Encephalitis', *The Journal of Immunology*, 180(4), pp. 2641–2649.

Zhang, W. *et al.* (2011) 'Neuromelanin activates microglia and induces degeneration of dopaminergic neurons: Implications for progression of parkinson's disease', *Neurotoxicity Research*, 19(1), pp. 63–72.

Zhao, C. *et al.* (2016) 'Influenza B virus non-structural protein 1 counteracts ISG15 antiviral activity by sequestering ISGylated viral proteins', *Nature Communications*, 7.

Zheng, M. *et al.* (2020) 'Impaired NLRP3 inflammasome activation/pyroptosis leads to robust inflammatory cell death via caspase-8/RIPK3 during coronavirus infection', *Journal of Biological Chemistry*, 295(41), pp. 14040–14052.

Zhou, L.-J., Tedder, T.F. and Amos, B. (1996) CD14+ blood monocytes can differentiate into functionally mature CD83+ dendritic cells*, Immunology,* 93, pp. 2588-2592.

Zhou, Y.-Q. *et al.* (2019) 'The Role of CXCR3 in Neurological Diseases', *Current Neuropharmacology*, 17(2), pp. 142–150.

Zhu, J. *et al.* (2014) 'Antiviral Activity of Human OASL Protein Is Mediated by Enhancing Signaling of the RIG-I RNA Sensor', *Immunity*, 40(6), pp. 936–948.

Zhu, S. *et al.* (2017) 'Nlrp9b inflammasome restricts rotavirus infection in intestinal epithelial cells', *Nature*, 546(7660), pp. 667–670.

Zhu, S. *et al.* (2019) ‘Tir domain-containing adaptor-inducing interferon-β (TRIF) participates in antiviral immune responses and hepatic lipogenesis of large yellow croaker (larimichthys crocea)’, *Frontiers in Immunology*, 10(OCT).

Zinkernagel, R. M., and P. C. Doherty. (1975). "H-2 compatability requirement for T-cell-mediated lysis of target cells infected with lymphocytic choriomeningitis virus. Different cytotoxic T-cell specificities are associated with structures coded for in H-2K or H-2D." *J Exp Med.* 141(6), pp. 1427-36.

Ziv, Y. *et al.* (2006) ‘Immune cells contribute to the maintenance of neurogenesis and spatial learning abilities in adulthood’, *Nature Neuroscience*, 9(2), pp. 268–275.

Zorina, Y. *et al.* (2018) ‘Human IgM antibody rHIgM22 promotes phagocytic clearance of myelin debris by microglia’, *Scientific Reports*, 8(1).

Zou, B. *et al.* (2017) ‘Acyloxyacyl hydrolase promotes the resolution of lipopolysaccharide-induced acute lung injury’, *PLoS Pathogens*, 13(6).

Zuo, Y. *et al.* (2020) ‘Regulation of the linear ubiquitination of STAT1 controls antiviral interferon signaling’, *Nature Communications*, 11(1).